

## Topical Report

---

# A PRELIMINARY EVALUATION OF THE ROCK MASS DISTURBANCE RESULTING FROM SHAFT, TUNNEL, OR BOREHOLE EXCAVATION

P.C. Kelsall  
J.B. Case  
C.R. Chabannes

---

Battelle Memorial Institute  
Project Management Division  
Office of Nuclear Waste Isolation  
Columbus, Ohio

## Topical Report

# A PRELIMINARY EVALUATION OF THE ROCK MASS DISTURBANCE RESULTING FROM SHAFT, TUNNEL, OR BOREHOLE EXCAVATION

P.C. Kelsall  
J.B. Case  
C.R. Chabannes

D'Appolonia Consulting Engineers, Inc.  
Albuquerque, New Mexico

This report was prepared as an account of work sponsored by the United States Government. Neither the United States nor the Department of Energy, nor any of their employees, nor any of their contractors, sub contractors, or their employees, makes any warranty, express or implied, or assumes any legal liability or responsibility for the accuracy, completeness, or usefulness of any information, apparatus, product, or process disclosed, or represents that its use would not infringe privately-owned rights.

**D'APPOLONIA**

## ACKNOWLEDGEMENTS

The authors wish to acknowledge the assistance of several of their colleagues in preparing this report, notably W. E. Coons, R. D. Ellison, J. J. Holcomb, H. Janzon, J. W. Nelson, C. E. Schubert, and D. E. Stephenson.

## ABSTRACT

The isolation of nuclear wastes in deep, mined repositories will require the sealing of all penetrations such as shafts, tunnels, or boreholes, into or nearby the repository. An important consideration in penetration sealing is the disturbed zone, or zone of increased permeability, which may be created in the rock mass adjacent to the penetration as a result of excavation. Disturbed zone characteristics for shafts, tunnels, and boreholes are evaluated by analysis and by review of previous laboratory and field tests. Consideration is given also to test methods for characterizing the disturbed zone in situ, and to methods for treating the disturbed zone in seal construction.

Laboratory tests indicate that the disturbed zone associated with small-diameter boreholes is probably insignificant. In contrast, the disturbed zone is potentially a significant pathway for flow through seals placed in shafts and tunnels. Because a major mechanism for disturbance is believed to be stress relief acting across fractures, much of the disturbance occurs regardless of the excavation method used. Various test methods are proposed for disturbed zone characterization in shafts and tunnels, with seismic refraction identified as a promising index test. A proposed method for treating the disturbed zone uses cutoffs constructed as a series of overlapping boreholes. Each hole is filled with concrete which is allowed to cure before the adjacent holes are drilled.

## TABLE OF CONTENTS

	<u>PAGE</u>
EXECUTIVE SUMMARY	1
1.0 INTRODUCTION	11
1.1 BACKGROUND	11
1.2 SIGNIFICANCE TO SEAL AND REPOSITORY DESIGN	13
1.2.1 Seal Design	13
1.2.2 Repository Design	18
1.3 MECHANISMS FOR CREATION OF A DISTURBED ZONE	18
1.3.1 Disturbance Due to Stress Changes	18
1.3.2 Damage by the Excavation Process	20
1.3.3 Weathering and Rock-Ground Water Interaction	21
2.0 DISTURBANCE ASSOCIATED WITH BOREHOLES	23
2.1 LABORATORY STUDIES OF BOREHOLE DISTURBED ZONE CHARACTERISTICS	23
2.2 DISCUSSION	26
3.0 DISTURBANCE ASSOCIATED WITH SHAFTS AND TUNNELS IN FRACTURED ROCK	29
3.1 ANALYTICAL ASSESSMENT OF DISTURBANCE RESULTING FROM STRESS REDISTRIBUTION	29
3.1.1 Rock Mass Behavior	29
3.1.2 Fracturing of Intact Rock	30
3.1.3 Effects of Stress on Pre-existing Fractures	34
3.2 PREVIOUS INVESTIGATIONS OF DISTURBED ZONE CHARACTERISTICS IN SHAFTS AND TUNNELS	49
3.2.1 Colorado School of Mines Investigations	50
3.2.2 Stripa Investigations	52
3.2.3 Other Disturbed Zone Investigations in Fractured Rock	59
3.3 DAMAGE DUE TO BLASTING	75
3.3.1 Review of Field Investigations	75
3.3.2 Permeability Changes Due to Blasting	79
3.4 CONCLUSIONS REGARDING DISTURBED ZONE EXTENT IN FRACTURED ROCK	79

## TABLE OF CONTENTS

(Cont'd)

	<u>Page</u>
4.0 DISTURBANCE ASSOCIATED WITH SHAFTS AND TUNNELS IN SALT	85
4.1 ANALYSIS OF DISTURBANCE DUE TO STRESS RELIEF	85
4.2 EVIDENCE FROM PREVIOUS FIELD INVESTIGATIONS	89
4.3 SIGNIFICANCE TO SEAL PERFORMANCE	91
5.0 RECOMMENDED METHODS FOR DISTURBED ZONE INVESTIGATIONS	93
5.1 TEST METHODS FOR SHAFTS AND TUNNELS	93
5.1.1 Hydrological Tests	94
5.1.2 Geologic Tests and Observations	97
5.1.3 Geophysical Methods	98
5.1.4 Mechanical Methods	105
5.1.5 Test Program for Fractured Rock	105
5.1.6 Test Program for Salt	109
5.2 TEST METHODS FOR DEEP BOREHOLES	110
6.0 METHODS FOR TREATMENT OF THE DISTURBED ZONE	111
6.1 ROCK SUPPORT	111
6.2 GROUTING	113
6.3 REDUCTION OF PERMEABILITY BY PRECIPITATION OF SECONDARY MINERALS	116
6.3.1 Formation of Secondary Minerals	116
6.3.2 Secondary Mineralization at Hanford	117
6.3.3 Concepts for Inducing Secondary Mineralization	117
6.3.4 Conclusions and Recommendations	119
6.4 BULKHEADS	119
6.5 DRILLED CUTOFFS	122
6.6 CONCLUSIONS	122
REFERENCES	
APPENDIX A - FRACTURING OF INTACT ROCK	
APPENDIX B - STRESS AND DISPLACEMENT ANALYSES	

## LIST OF TABLES

<u>Table No.</u>	<u>Title</u>	<u>PAGE</u>
3-1	Approximate Temperatures for a Repository in Basalt as a Function of Time	47
6-1	Groutability of Fractured Rock	115

## LIST OF FIGURES

<u>Figure No.</u>	<u>Title</u>	<u>PAGE</u>
1-1	Seal Zone Components	12
1-2	Influence of Disturbed Zone Characteristics on Seal Performance	14
1-3	Relative Importance of Plug Zone, Interface, and Disturbed Zone Flow as a Function of Penetration Radius	17
3-1	Idealized Scheme of Elastic, Plastic, and Fracture Zones Around a Shaft Opening in a Strong Rock Formation	31
3-2	Extent of Plastic Zone (a) and Predicted Displacements (b) for a Shaft in Basalt with Hydrostatic Initial Stress Condition	32
3-3	Maximum Tangential Boundary Stress for a Circular Opening Related to Depth and In Situ Stress Ratio (K)	33
3-4	Permeability of an Artificial Fracture in Basalt as a Function of Effective Normal Stress	36
3-5	Predicted Disturbed Zone Permeability Based on Elastic Stress Distribution and Cubic Law Permeability-Stress Relationship for Fractured Basalt - Isotropic Initial Stress Condition	39
3-6	Predicted Disturbed Zone Permeability Based on Elasto-Plastic Stress Analysis and Cubic Law Permeability-Stress Relationship for Fractured Basalt -Isotropic Initial Stress Conditions	40
3-7	Effect of Fracture Orientation on Extent of Disturbed Zone	42
3-8	Notation for Considering Effects of Anisotropic Stress Field	44
3-9	Macropermeability Test, Stripa	54
3-10	Comparison of Hydraulic Conductivities Predicted by Analysis and Inferred from Field Measurements, Stripa Macropermeability Test	57
3-11	Comparison of Water Heads Predicted by Finite Element Analysis Using Disturbed Zone Model and Field Measurements, Stripa Macropermeability Test	58
3-12	Predicted Disturbed Zone Hydraulic Conductivities for the Stripa Macropermeability Test	60

## LIST OF FIGURES

(Cont'd)

<u>Figure No.</u>	<u>Title</u>	<u>PAGE</u>
3-13	Disturbed Zone Permeability in Coal Pillars Measured by Methane Inflow Between Packers	62
3-14	Fracture Index in a Coal Pillar Measured by Air-Injection	62
3-15	Typical Seismic Velocity Profile Obtained From Seismic Refraction, Belledonne Tunnel, France	65
3-16	Disturbed Zone Indicated by Seismic Velocity in Circular Tunnel in Limestone - Rama Hydroelectric Plant, Yugoslavia	66
3-17	Thickness of Disturbed Zone (Low Velocity Layer) as a Function of Rock Quality and Seismic Velocity of the Undisturbed Rock, Straight Creek Tunnel Pilot Bore, Colorado	69
3-18	Typical Modulus and Rock Quality Designation (RQD) Profiles in Pillar Between Two Drifts, Climax Granite, Nevada Test Site	71
3-19	Elastic Recovery as Percentage of Total Deformation Observed in Radial Jacking Tests, Churchill Falls, Canada	73
3-20	Typical Displacement Profiles in Excavated Caverns at the Nevada Test Site	74
3-21	Comparison of Fracture Patterns resulting from Smooth Blasting and Conventional Blasting	77
3-22	Method for Estimating Thickness of Blast-Damaged Zone in Relation to Explosive Charge Density	78
3-23	Preliminary Disturbed Zone Permeability Model for 3 m Radius Shaft in Basalt at 1000 m Depth (Elastoplastic Analysis and Isotropic Initial Stress Condition)	81
4-1	Permeability of Rock Salt as a Function of Hydrostatic Confining Pressure	86
4-2	Predicted Disturbed Zone Permeability for Salt Based on Steady State Stress Distribution	87
5-1	Test Concept for Disturbed Zone Evaluation Using Tracer Injection and Cross-Hole Seismic	95
5-2	Macropermeability Test Concept for Disturbed Zone Evaluation in Rock Above Water Table	95

## LIST OF FIGURES

(Cont'd)

<u>Figure No.</u>	<u>Title</u>	<u>PAGE</u>
5-3	Seismic Methods for Delineating Disturbed Zone Extent	99
5-4	Variation of Shear Wave Frequency with Confining Stress for Laboratory Tests on Marble	101
5-5	Resistivity Method for Delineating Disturbed Zone Extent	104
5-6	Approach for Disturbed Zone Characterization-Stage 1	107
5-7	Approach for Disturbed Zone Characterization-Stage 2	108
6-1	Effect of Support Pressure on Predicted Extent of Disturbed Zone (Isotropic Initial Stress Condition, Elasto-Plastic Analysis)	112
6-2	Concept for Forming Impermeable or Sorptive Barriers in the Disturbed Zone Using Overlapping Boreholes	123

## EXECUTIVE SUMMARY

Introduction

The isolation of nuclear wastes in deep, mined repositories will require the sealing of all penetrations into or nearby the underground facility. These penetrations include the shafts and tunnels used to gain access to the repository, plus any boreholes which are drilled for site exploration or which exist from previous investigations at the site.

Seal designs must address three potential pathways for fluid flow: the plug (i.e., the seal material placed within the penetration), the interface between the seal and the host rock, and a disturbed zone that may exist in the host rock (Figure 1-1). Laboratory tests conducted by Terra Tek (described below) indicate that the disturbed zone associated with boreholes is insignificant and that the dominant pathway for flow through a typical borehole seal is likely to be the interface. For shafts and tunnels, however, the disturbed zone is likely to be the dominant pathway. Accordingly, information regarding disturbed zone characteristics, specifically disturbed zone permeability, is vital to proper seal design.

Eventually, information regarding the disturbed zone must be obtained from site-specific in situ testing. Meanwhile, information is required for use in conceptual seal design, performance assessment, and planning of field tests. This report is a preliminary evaluation of disturbed zone characteristics, considering:

- factors influencing disturbed zone characteristics, especially permeability;
- likely disturbed zone characteristics indicated by analysis and review of previous investigations;
- test methods for characterizing the disturbed zone in the field;
- methods for "treatment" of the disturbed zone.

### Mechanisms for Creation of a Disturbed Zone

Three processes may contribute to formation of a disturbed zone around a penetration:

- stress redistribution,
- damage by the excavation process,
- weathering and rock-ground water interaction.

Of the three processes, only one is directly related to the excavation method. Also, the effects of stress redistribution apply to all penetrations and excavation methods although the magnitude of the effects depends greatly on site specific conditions. Accordingly, it is not appropriate to consider the disturbed zone solely as a blast-damaged zone that does not exist if mechanical excavation methods are used. Weathering and rock-ground water interaction are considered to be relatively insignificant mechanisms for disturbance.

When a penetration is excavated, there is a redistribution of the original in situ stresses around the opening. The nature of this redistribution depends on the original in situ stresses, on rock properties, and on the shape of the opening. Adjacent to the penetration, stresses in a radial direction are relieved, whereas stresses in a tangential direction may be increased or reduced depending on the rock properties. Disturbance to the rock mass might arise in one of three ways:

- by fracturing of originally intact rock due to excessive compressive or tensile stresses,
- by opening or closing of pre-existing fractures due to changes in the normal stresses acting across the fractures or to shearing along the fractures,
- by loosening of the crystal structure in response to reduced confining stresses (particularly in salt).

The relative influence of these three processes on disturbed zone permeability will vary according to parameters such as the size of the opening relative to the fracture spacing, the strength of the intact rock, the in situ stress field, and the shape of the opening.

Fracturing of intact rock due to stress redistribution is unlikely in most conditions (excluding strongly anisotropic stress fields) for rocks such as basalt, granite, or welded tuff. In these same rock types, however, fracture permeability is known to be highly stress-dependent so that rock mass permeability is expected to increase in zones around a penetration where stresses are relieved. In salt, which is generally unfractured at repository depths, the most likely response to stress relaxation is a loosening of the crystal structure with a corresponding increase in permeability.

It is to be expected that blasting will cause greater damage to the walls of a shaft or tunnel than will excavation by mechanical methods. The degree of damage associated with blasting can be greatly reduced by the use of a controlled blasting method such as smooth-wall blasting where the perimeter holes in the round are lightly charged. As discussed later, it appears likely that the increases in permeability due to controlled blasting may be approximately equal to, or less than, the increases due to stress relief which will occur regardless of the excavation method.

Discussion of mechanisms for creating a disturbed zone leads to the observation that the mechanism is likely to be different for boreholes than for shafts and tunnels because of an important scale effect. For boreholes, the penetration diameter is similar to the typical fracture spacing in many rock masses, and stress relief around the hole is unlikely to affect fracture permeability on a significant scale. Little disturbance of any type is likely in most rock types at repository depths because the stresses developed around the borehole will not exceed the intact rock strength. For shafts and tunnels in fractured rock, where the penetration diameter is typically much greater than the fracture spacing, the influence on rock mass permeability of opening or closing of fractures is likely to be much more significant than effects due to fracturing of intact rock.

#### Disturbance Associated with Boreholes

Direct evidence that the disturbance associated with boreholes is relatively minor has been obtained from laboratory tests conducted at Terra Tek and the University of Arizona. At Terra Tek, 20cm diameter boreholes were drilled in 50cm diameter cylindrical specimens enclosed in an apparatus which simulates in situ pressure conditions. Five rock types have been tested, anhydrite, salt, granite, basalt and tuff, with the holes drilled with diamond or roller cone bits and various flushing media. Detailed examination of the borehole walls has shown that the drilling-induced disturbance is minor. In all cases, the thickness of the disturbed zone was less than 3% of the borehole radius and the disturbance effects were intergranular. At the University of Arizona, 12.7mm diameter holes were drilled in quartz diorite and granite using percussion and rotary methods under ambient laboratory conditions. As in the case of the Terra Tek tests, the damaged zone was found to be very thin.

The laboratory tests described above have used unfractured (intact) rock samples. The applicability of the results to the field may be judged by considering the relative scales of the observed disturbance and the in situ fracture spacing. Typically, the thickness of the damaged zone due to drilling is of the order of a few millimeters, whereas the fracture spacing is likely to be in the range 10cm - 1m. Thus, although boreholes will intersect fractures, most of the surface area will consist of essentially intact rock, and the damage due to drilling in situ should be comparable to that observed in the laboratory.

#### Disturbance Associated with Shafts and Tunnels in Fractured Rock

There have been few field studies of the changes in rock mass permeability associated with excavation of shafts and tunnels. In the National Waste Terminal Storage program, some indication of permeability changes in the walls of a tunnel has been obtained from the macropermeability test at Stripa, and a comprehensive series of tests designed to investigate disturbed zone characteristics is in progress at the

Colorado School of Mines test mine. In other civil and mining projects there have been investigations which define the extent of the disturbed zone by changes in mechanical properties but few studies which have measured permeability.

In the present study, disturbed zone characteristics have been evaluated by combining analytical assessments with a review of previous investigations. The analytical approach used first considers the redistribution of stresses around a circular opening excavated in an initially hydrostatic stress field. Two models are evaluated, one for a rock mass which responds elastically, and one for a rock mass which responds elasto-plastically, i.e. where there is permanent deformation by slippage along fractures in a "failed" zone adjacent to the penetration. Permeability changes along fractures are related to stress changes using the relationship that fracture permeability is proportional to the cubic power of the fracture aperture. Parameters for fracture deformability are obtained from laboratory tests on basalt and granite reported in the literature. All analyses conservatively assume that fractures exist normal to the directions of maximum stress change.

A major conclusion of the analytical study is that significant disturbance (permeability increased by at least an order of magnitude) may be contained within 1 to 1.5 radii of the excavation face. A good quality rock mass at relatively shallow depth (approximately less than 300 m) will respond to stress changes essentially elastically, in which case stresses adjacent to the penetration walls will be reduced in the radial direction and increased in the tangential direction. Consequently, the permeability of any fractures that occur in a parallel or subparallel direction to the penetration axis should be increased, whereas the permeability of any fractures that occur in the radial direction should be reduced (Figure 3-5). This result was partially confirmed by the Stripa macropermeability test which found permeability reduced in the radial direction close to the tunnel wall. At greater depths, the same rock mass will exhibit a plastic zone close to the

penetration wall in which both the radial and tangential stresses are reduced. In this case, permeability will be increased in both the radial and axial directions (Figure 3-6).

Results from disturbed zone investigations where parameters other than permeability have been measured vary according to the method used and how the disturbed zone is defined, as well as according to variation in site parameters. Seismic measurements and modulus determinations at several sites indicate a disturbed zone thickness typically in the range 0.3 to 0.7 times the excavation radius. In these cases the disturbed zone is defined as a distressed zone with no indication of the magnitude of permeability increases. Other examples may be found where the disturbed zone extends greater than one radius. In practice, the extent of the disturbed zone will depend on many factors related to site geology, excavation method, depth, and penetration geometry.

Few disturbed zone studies specifically distinguish blast damage and stress relaxation effects. Available data from cases where controlled blasting methods were used indicate that significant blast damage (creation of new fractures) may be limited to a zone 1 m or less thick. The extent of blast damage will be greatly influenced by blasting technique but may be more or less independent of excavation size within the probable limits for shafts and tunnels. More severe disturbance may occur in a thin zone immediately adjacent to the face. This zone can probably be removed by machine excavation and may not be a consequence to sealing.

The analyses and reviews described above have been used to construct a model of the disturbed zone likely to be associated with a circular shaft or tunnel excavated in fractured basalt at 1000m depth assuming a hydrostatic initial stress condition. In this model the zone in which the permeability is increased by one order of magnitude or greater extends to about one penetration radius (Figure 3-23). The magnitude of the disturbance rapidly reduces away from the penetration. For a 3m

radius shaft excavated by blasting, for example, up to 80% of the potential increase in flow due to the disturbed zone is predicted to occur within 1m from the penetration wall.

Most of the analyses presented in the report refer to a circular opening with hydrostatic initial stresses and idealized fracture geometries, and with no consideration given to temperature effects. It is believed that the conclusions drawn will apply generally to repository shafts and tunnels, although additional site-specific analyses are required to confirm the predicted trends.

#### Disturbance Associated with Shafts and Tunnels in Salt

The most likely mechanism for disturbance in salt is loosening of the crystal fabric in response to stress relief. Additional damage may be in the form of fractures caused by blasting or by slabbing. Analysis of the effects of crystal loosening, using laboratory data relating stress and permeability, indicates that the increase in permeability is unlikely to exceed one order of magnitude. Review of field studies conducted in salt mines indicates that blast damage is generally confined to within 1 to 1.5m of a tunnel face.

An important consideration regarding the disturbed zone in salt is the ability of salt to heal fractures when subjected to confining stress. If a relatively rigid structure such as a concrete plug is placed in a shaft or tunnel in salt, the stresses acting on the plug and in the adjacent disturbed zone will build rapidly in response to salt creep. Analyses for salt from southeastern New Mexico (which creeps relatively slowly) show that the radial stress acting on a plug will build to greater than 50% of lithostatic (13.8 MPa) in less than 10 years. Preliminary laboratory test results indicate that fractures should be significantly healed at this stress level. This being the case, the disturbed zone in salt may be insignificant with respect to long-term seal performance, at least at repository depths. Fracture healing will be slower at shallower depths in repository shafts.

### Recommended Methods For Disturbed Zone Characterization

This report provides a preliminary model for shaft or tunnel disturbed zone characteristics that can be used in schematic seal design and performance assessment. This model can be refined by more rigorous, site-specific modeling but eventually it must be validated by in situ testing. Various test methods are proposed for this purpose. In a test facility, a test program should include a combination of tests conducted at one or more test locations representative of the geology of the repository and the excavation methods to be used. The intention would be to establish correlations among various rock mass properties in order to select index tests that could be used rapidly and inexpensively throughout the repository.

A comprehensive test program for disturbed zone characterization in fractured rocks should include the following tests:

- macropermeability
- piezometers installed in boreholes at varying distances from excavation
- injection tests in boreholes
- cross-hole tracer flow
- integral sampling in boreholes, and borescope or impression packer logging
- seismic refraction (petite sismique) surveys
- resistivity surveys
- cross-hole acoustic surveys
- radar profiling
- borehole deformation jack
- plate loading
- multiple-point borehole extensometers.

A candidate index test is seismic refraction profiling assuming that firm correlations can be established between seismic parameters and permeability.

A similar test program may be applied in salt for disturbed zone characterization in shafts and tunnels. Either the borescope or integral sampling should be particularly valuable for detecting fractures.

Many of the test methods listed above are inappropriate for boreholes because of limited accessibility. Moreover, it is unlikely that geophysical logs can be used to detect either fine fractures or a relatively thin disturbed zone. Fortunately, as described above, laboratory tests can be used for evaluating the disturbance associated with boreholes. Methods that can be used to evaluate larger-scale sidewall characteristics and to locate major fractures in deep boreholes include downhole television, the borehole televiewer, and the impression packer.

#### Methods for Treatment of the Disturbed Zone in Fractured Rock

Disturbed zone effects may be reduced by a combination of careful excavation and properly constructed cutoffs. A suggested method for constructing cutoffs involves drilling a series of overlapping boreholes from the shaft or tunnel through the disturbed zone into the undisturbed rock. Each hole is filled with a low-permeability, expansive material (e.g. concrete) which is allowed to cure before the adjacent holes are drilled. In this way, only a small volume of the rock mass is stress-relieved at any one time. Grouting might be considered as an alternative method for treating the disturbed zone. However, if the hydraulic conductivity of the repository host rock is in the range  $10^{-8}$  to  $10^{-10}$  cm/sec, and if the disturbed zone is only one to two orders of magnitude more permeable, it is unlikely that grouting will be effective. Possibly, fractures in the disturbed zone might be sealed by natural precipitation of silica or other secondary minerals. Such precipitation might occur as ground water saturated in silica flows from the storage areas towards cooler areas.

### Conclusions and Recommendations

The disturbed zone is potentially a significant pathway for flow through seals placed in shafts and tunnels. Because a significant mechanism for disturbance is believed to be stress relief acting across fractures, much of the disturbance is independent of the excavation method used. Based on available information, the increases in permeability resulting from controlled blasting may approximately double the increases that will occur in response to stress relief if mechanical excavation methods are used. Permeability changes due to blasting are likely to be confined within a depth of 1m from a shaft or tunnel face, however, whereas changes due to stress relief may extend to several penetration radii. Laboratory tests indicate that the disturbed zone associated with small-diameter boreholes is probably insignificant.

Further work is required to extend analyses and design concepts presented in this report. Further analyses must be site-specific, taking into account planned opening shapes and excavation methods, anticipated in situ stress ratios, and actual rock mass characteristics. As soon as possible within the schedule for developing at depth test facilities at candidate repository sites, these models must be validated by in situ testing. Testing, combined with further analyses, is also required to evaluate concepts such as drilled cutoffs for treatment of the disturbed zone.

## 1.0 INTRODUCTION

### 1.1 BACKGROUND

The isolation of nuclear wastes in deep, mined repositories will require the sealing of all penetrations into or nearby the underground facility. These penetrations include the shafts and tunnels used to gain access to the repository, plus any boreholes which are drilled for site exploration or which exist from previous activities at the site. Seals will also be placed within the repository to isolate separate waste storage panels, and the storage rooms will be backfilled primarily with the mined-out rock. The design program for penetration seals is being conducted by D'Appolonia Consulting Engineers, Inc. (D'Appolonia) for the Office of Nuclear Waste Isolation (ONWI).

Seal designs must address three potential pathways for fluid flow: the plug (or seal material); the interface between the seal material and the host rock; and a disturbed zone that may exist in the host rock (Figure 1-1). As discussed in Section 1.2.1, the disturbed zone is potentially the dominant pathway for shafts and tunnels, and information regarding disturbed zone characteristics is vital to proper seal design. Eventually, information regarding the disturbed zone must be obtained from site-specific in situ testing. Meanwhile, there is a necessity for preliminary data for use in schematic seal design, performance assessment, and planning of field tests. This report is a preliminary evaluation of disturbed zone characteristics, and methods for treatment of the disturbed zone. Consideration is given to:

- factors influencing disturbed zone characteristics in salt and fractured rock,
- likely disturbed zone characteristics indicated by analysis and review of previous field investigations,
- techniques which may be used to evaluate disturbed zone characteristics in the field,
- methods for "treatment" of the disturbed zone in seal design and construction.

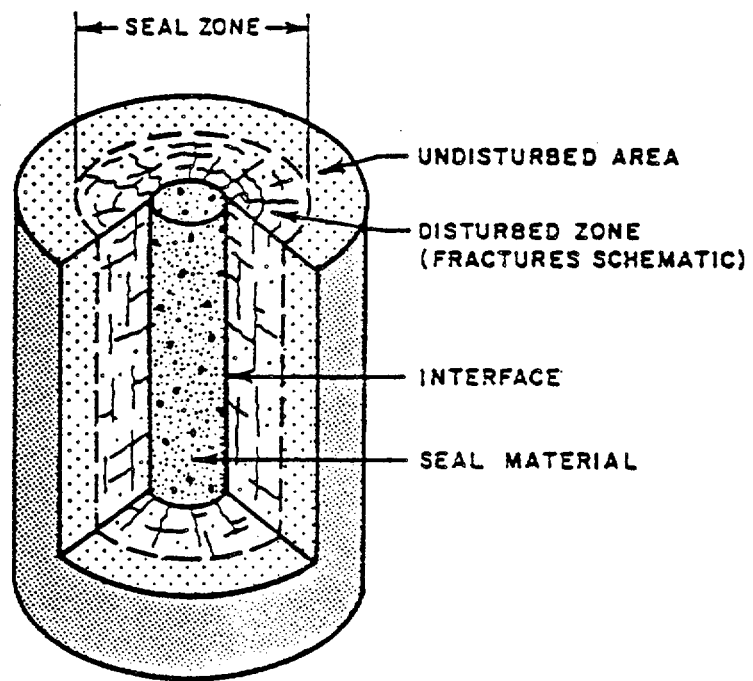


Figure 1-1. Seal Zone Components

For the most part, emphasis is given to disturbed zone characteristics for shafts and tunnels. Consideration to boreholes is given in Section 2.0 showing that the degree of disturbance associated with boreholes is less significant to seal performance than is the case for shafts or tunnels.

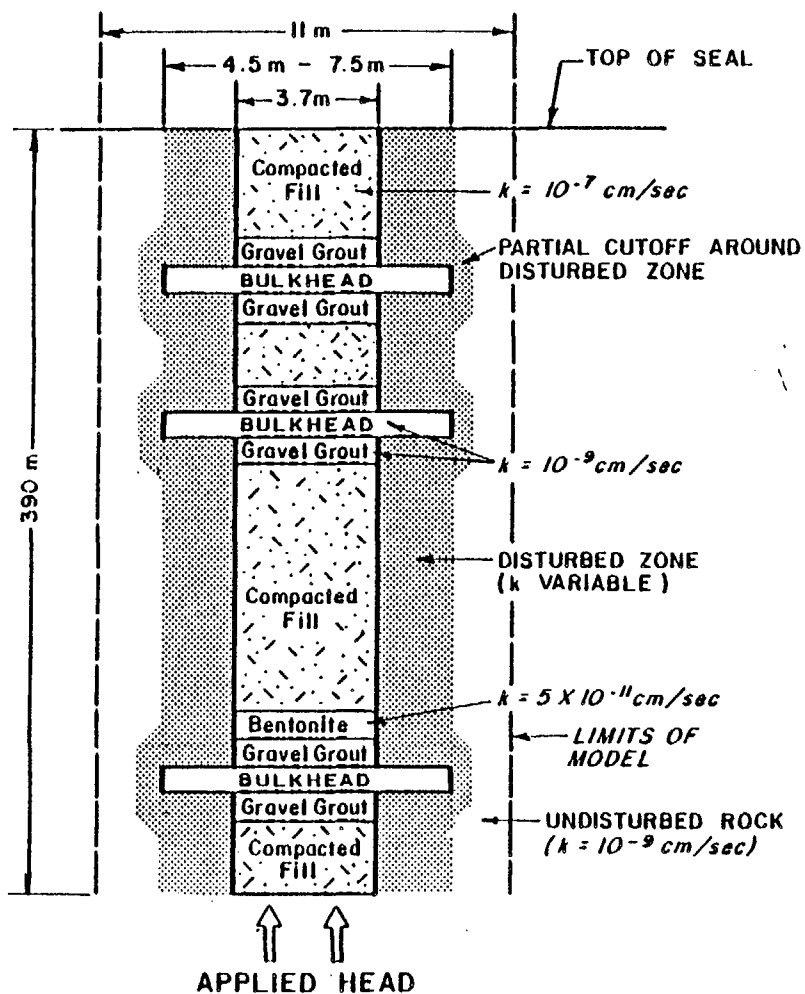
In the context of this report, the disturbed zone is that part of the rock mass adjacent to a shaft, tunnel or borehole which is affected in some manner by the presence of the penetration, and which may influence seal performance. As discussed below, the major mechanisms for this disturbance are damage by the excavation process and effects due to redistribution of stresses around the opening. This disturbance will occur relatively quickly following excavation, before the waste is emplaced. Subsequently, the heat generated by the waste may modify the properties of the disturbed zone further, particularly in the repository rooms. This report does not evaluate disturbance to the rock mass and ground water system surrounding the overall repository resulting from heat generation from the waste.

## 1.2 SIGNIFICANCE TO SEAL AND REPOSITORY DESIGN

### 1.2.1 Seal Design

A disturbed zone adjacent to a penetration provides a pathway for fluid flow to bypass a seal placed within the penetration. With respect to seal performance, the critical disturbed zone characteristic is the permeability contrast between the disturbed zone and the undisturbed host rock. Figure 1-2 illustrates a model used to evaluate the impact of disturbed zone characteristics on ground water flow through a shaft seal. The shaft seal modeled is 390m long with various seal components as illustrated. Bulkheads (cutoff collars) are included to reduce disturbed zone flow, but it is assumed that the cutoff itself results in some disturbance so that the effective areal cutoff relative to the original disturbed zone is only 50 percent. Ground water flow and travel time are calculated for an arbitrary 30m head and for various

### SHAFT SEAL MODEL



### ANALYSIS FOR 30 M HEAD

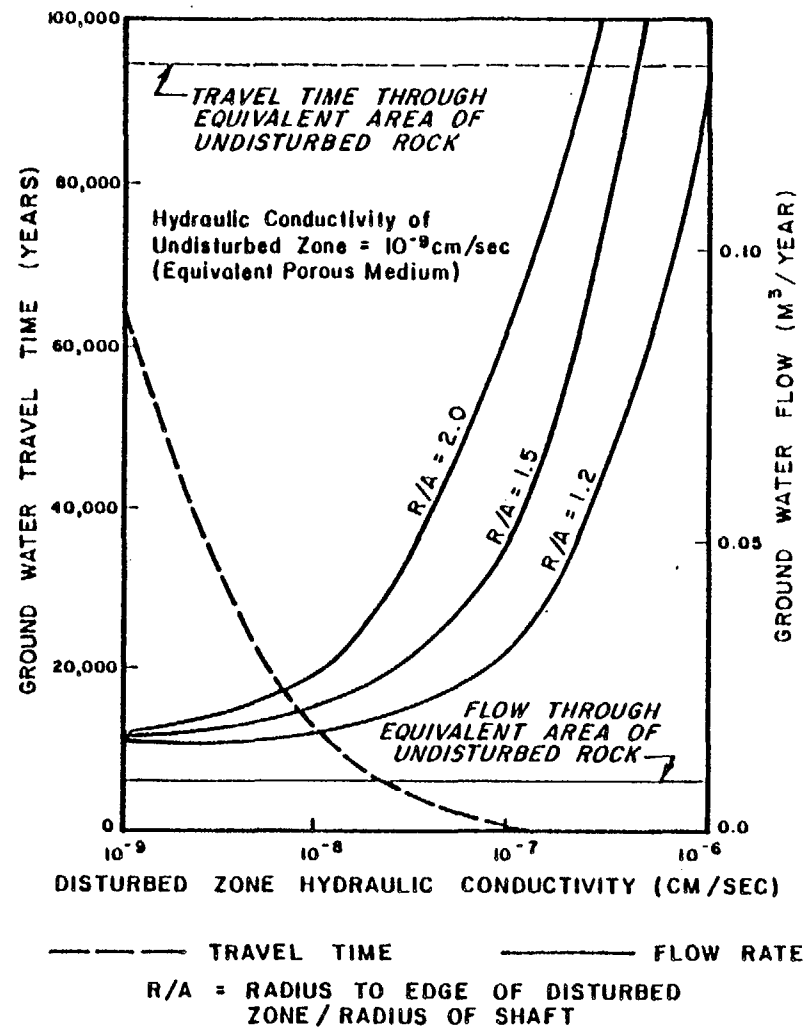


Figure 1-2. Influence of Disturbed Zone Characteristics on Seal Performance

thicknesses and hydraulic conductivities\* of the disturbed zone. Complete details of the model and the analytical method will be given in a subsequent report.

The results from the analyses show that flow rate is strongly affected by the hydraulic conductivity of the disturbed zone and, to a lesser degree, by the extent of the disturbed zone. For hydraulic conductivities in the range of one to two orders of magnitude greater than the host rock, the flow is in the range of three to ten times the rate through the equivalent area of undisturbed rock. Ground water travel times are also strongly affected by disturbed zone conductivity reducing from greater than 60,000 years, where there is no disturbed zone, to about 1,000 years, where the disturbed zone hydraulic conductivity is 100 times that of the undisturbed zone. Because the bulkheads do not achieve 100 percent cutoff in the disturbed zone, the lateral extent of the disturbed zone has negligible effect on travel times.

These analyses confirm that seal performance is sensitive to disturbed zone characteristics. For purposes of performance assessment, it is particularly important to have some knowledge of at least the order of magnitude contrast between the hydraulic conductivity of the disturbed zone and that of the undisturbed rock. For the design of measures to mitigate the effects of the disturbed zone, it is important to have some evidence of the thickness of that zone. The results also show that ground water flow is relatively insensitive to disturbed zone hydraulic conductivity when the contrast with the conductivity of the undisturbed rock is less than one order of magnitude. This is noteworthy in that it is probably impracticable to distinguish a contrast of less than one order of magnitude by field testing. For practical purposes, therefore, the disturbed zone may be considered as a zone in which the permeability is at least an order of magnitude greater than that of the undisturbed rock.

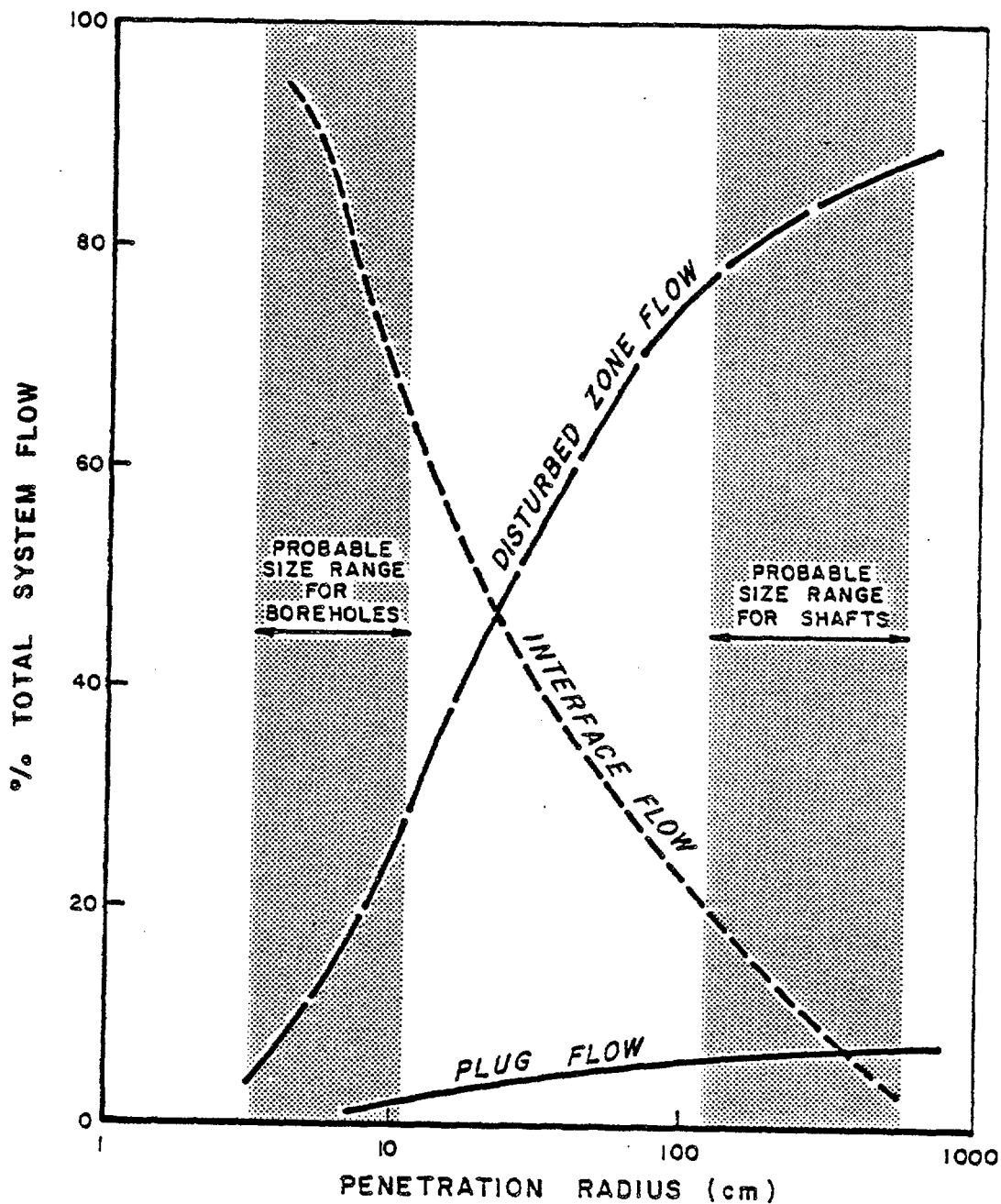
---

\*Throughout this report "permeability" is used to denote an intrinsic rock property (dimensions  $L^2$ ). "Hydraulic conductivity" is used where water flow is specified (dimensions  $L/T$ ).

Further simplified analyses have been conducted to compare the relative significance of plug zone, disturbed zone, and interface flow for various sizes of excavation. Two basic assumptions are made:

- Interface flow is due to a zone of closely-spaced circumferential cracks, the thickness of the zone being largely independent of excavation size. Interface flow thus increases in linear proportion to the circumference (and consequently the radius) of the excavation. Interface flow is then proportioned from the results of the Bell Canyon Test in which a flow test was performed on a cement plug set in a 20cm diameter borehole (Christensen & Peterson, 1981).
- Plug zone and disturbed zone flow are proportional to area, and hence the second power of the radius of the excavation. Disturbed zones with varying extents and permeabilities relative to the host rock are considered.

A number of parametric analyses were performed for nominal seal lengths and applied hydraulic heads using the above assumptions. Figure 1-3 shows the proportions of flow attributed to the plug, interface, and disturbed zones for one set of conditions in which the disturbed zone extent is 0.5 times the penetration radius and the disturbed zone permeability ten times that of the plug. For boreholes, the interface is found to be the dominant flow path. In contrast, for shafts or tunnels, the disturbed zone is found to be the dominant flow path. These results are based on simplified analyses and largely assumed parameters. Nonetheless, experimental and analytical data presented later in this report tend to support the assumptions made. For example, laboratory tests on borehole plugs (Section 2.2) show that interface flow is much more significant than disturbed zone flow. Analysis and review of disturbed zone characteristics for shafts and tunnels (Section 3.0) indicate that there is likely to be a zone up to one penetration radius wide in which the permeability is significantly increased. Collectively, the parametric analyses and the available test results indicate that borehole sealing studies should emphasize the interface whereas shaft and tunnel studies should emphasize the disturbed zone.



EXTENT OF DISTURBED ZONE =  $0.5 \times$  PENETRATION RADIUS  
 DISTURBED ZONE PERMEABILITY =  $10 \times$  PLUG PERMEABILITY  
 INTERFACE FLOW PROPORTIONAL TO BELL CANYON TEST

Figure 1-3. Relative Importance of Plug Zone, Interface, and Disturbed Zone Flow as a Function of Penetration Radius

### 1.2.2 Repository Design

One concept for waste disposal in a geologic repository is to place the waste in boreholes drilled either in the floors or the walls of storage rooms. If this concept is adopted, it will be advantageous to place the waste canisters beyond the disturbed zone associated with the storage room. This will help to avoid a direct communication between the canisters and the storage room backfill which in most repositories will be a preferred pathway for fluid flow. A further consideration is that the waste emplacement hole may itself create a disturbed zone. In the proposed design for a repository in basalt, the diameter of the emplacement holes is 1.2m (Rockwell Hanford, 1981) which is probably large enough that the hole should be considered more as a small shaft than as a borehole (Figure 1-3).

### 1.3 MECHANISMS FOR CREATION OF A DISTURBED ZONE

Three processes may contribute to formation of a disturbed zone around a penetration:

- stress redistribution,
- damage by the excavation process,
- weathering and rock-ground water interaction.

Of the three processes, only one is directly related to the excavation method. Also, the effects of stress distribution apply to all penetrations and excavation methods although the magnitude of the effects depends greatly on site specific conditions. Accordingly, it is not appropriate to consider the disturbed zone solely as a "blast-damaged" zone that does not exist if mechanical excavation methods are used.

#### 1.3.1 Disturbance Due to Stress Changes

When a penetration is excavated there is a redistribution of the original in situ stresses around the opening. The nature of this redistribution depends on the original in situ stresses, on rock properties, and on the shape of the opening. Adjacent to the penetration, stresses in a radial direction are relieved, whereas stresses in a tangential direction may be increased or reduced depending on the rock properties. Disturbance to the rock mass might arise in one of three ways:

- by fracturing of originally-intact rock due to excessive compressive or tensile stresses,
- by opening or closing of pre-existing fractures due to changes in the normal stresses acting across the fractures or to shearing along the fractures,
- by loosening of the crystal structure in response to reduced confining stresses (particularly in salt).

The relative influence of these three processes on disturbed zone permeability will vary according to parameters such as the size of the opening relative to the fracture spacing, the strength of the intact rock, the in situ stress field, and the shape of the opening. For shafts and tunnels in fractured rock (as discussed in Section 3.0), the influence of opening or closing of pre-existing fractures is likely to be much more significant than effects due to fracturing of intact rock. Fracturing of intact rock around an opening is unlikely to occur in most conditions for rocks such as basalt, granite, or welded tuff. Some fracturing may occur if the in situ stress field is strongly anisotropic but the fractures created should be localized and should not add greatly to the overall degree of fracturing in the rock mass. As noted in Section 3.1.3.1, permeability in a fractured rock mass is much more sensitive to changes in fracture aperture than to the number of fractures.

For boreholes, fracturing of intact rock may have a more significant effect on increased flow potential because the size of the opening is small relative to the fracture spacing. Conveniently, the disturbance resulting from drilling small-diameter boreholes can be investigated in the laboratory. Laboratory tests at Terra Tek and the University of Arizona (Section 2.0) indicate that the disturbed zone for boreholes is very small but these tests have not addressed the full range of rock types and in situ stress fields that may be encountered at candidate repository sites. It may be concluded that fracturing of intact rock is not likely to be a major cause of disturbance around boreholes in

basalt, granite, or welded tuff, at least if the stress field is isotropic. Further site-specific evaluation is required to evaluate whether significant fracturing could occur in anisotropic stress fields.

The mechanisms for creation of a disturbed zone in salt will differ from the mechanisms applying in rocks such as basalt or granite. At repository depths, salt is not generally fractured so that there should be no effect of opening of pre-existing fractures due to stress relaxation. The most likely cause of disturbance in salt is a loosening of the crystal fabric due to stress relaxation, evidence for which is obtained from laboratory tests which show that the permeability of salt is strongly dependent on confining stress. A further possibility is that salt may fracture in response to stress relaxation. Disturbance effects in salt are considered in Section 4.0.

#### 1.3.2 Damage by the Excavation Process

It is well known that blasting causes some degree of damage to the rock mass outside the excavation perimeter. This damage may be in the form of new fractures created by excessive explosive energy, propagation of existing fractures by high pressure gases produced by the blast, or a general loosening of a fractured rock mass due to excessive ground vibration. The degree of damage may be greatly reduced, though not eliminated, by the use of controlled blasting methods (Holmberg & Persson, 1980; Hoek & Brown, 1980). For example, smooth blasting employs a ring of closely-spaced and carefully-aligned drill holes at the intended perimeter of the excavation. These holes are lightly charged and are fired as the last delay in the round. Fractures propagated between the perimeter holes result in a much smoother excavation contour than would be obtained by conventional blasting methods. Also, damage to the adjacent rock mass is reduced by the low explosive charges used in the perimeter holes and by the low burden resulting from prior breakage of the rock within the perimeter. Based on visual observation of the excavation walls, and on the obvious improvements gained in the stability of the excavation, the degree of disturbance to the remaining rock mass is significantly less with smooth blasting than with

conventional drill and blast methods. As reviewed in Section 3.3, however, there have been few studies to compare the extent of the disturbed zone associated with different blasting methods.

Some degree of damage may result also from excavation by mechanical (tunnel boring machine) methods. This might be in the form of loosening of a surface zone of fractured rock due to vibration or possibly a plucking action, depending on the type of machine used. Nonetheless, machine excavation is known to have improved stability conditions in many underground excavations where blasting had been used previously. Minor disturbance due to machine excavation is likely to be obscured by disturbance due to stress redistribution.

### 1.3.3 Weathering and Rock-Ground Water Interaction

In general terms "weathering" includes a large number of chemical or physical effects. In the context of this report weathering may be significant only in clay-bearing rocks and may result from swelling due to contact with water or slaking due to cyclic changes in moisture content. A contributing factor in these processes in shales may be expansion or rebound due to stress relief. Such changes would be readily discernible and the disturbed zone could be removed prior to placing a seal.

A special case concerns swelling of clay fillings in fractures which could lead to loosening of the rock mass. If expandable clay fillings are present in the rock mass, swelling could be prevented in key seal locations by shotcreting immediately following excavation.

Effects due to interaction between rock and ground water might include washing out of fracture infillings by flowing ground water or precipitation of minerals in fractures. The latter process has been suggested as an explanation for the zone of reduced permeability observed in the Stripa macropermeability test (Section 3.2.2), although an alternate explanation postulated by this report is that the reduced permeability is due to increased tangential stresses close to the tunnel wall.

## 2.0 DISTURBANCE ASSOCIATED WITH BOREHOLES

Section 1.3 noted three mechanisms that result in disturbance adjacent to a penetration: stress redistribution effects, damage by the excavation process, and weathering or rock-ground water interaction. Of these, weathering and rock-ground water interaction are considered to be less significant (or at least more easily detected and treated) and are not given further consideration. For boreholes, the effects of damage due to drilling and to stress redistribution are conveniently studied in the laboratory.

### 2.1 LABORATORY STUDIES OF BOREHOLE DISTURBED ZONE CHARACTERISTICS

Laboratory studies of borehole disturbance are being conducted at the Drilling Research Laboratory operated by Terra Tek, Inc., in Salt Lake City. The facility includes a drilling rig and three well-drilling simulator pressure vessels designed to simulate in situ drilling conditions. Cylindrical rock samples up to 50cm in diameter and 2.1m in length can be placed in the simulator and subjected to confining pressures to 138 MPa (20,000 psi) and wellbore pressures up to 34.5 MPa (5,000 psi).

Five rock types have been tested and examined in the current study (Lingle et al, 1981):

- anhydrite - Winnfield salt dome, Louisiana
- salt - Avery Island salt mine, Louisiana
- granite - Cold Springs, Minnesota
- basalt - Columbia River, Washington
- tuff - Kamas, Utah

Samples placed in the drilling simulator were cored from large blocks transported from the field. A total of 19 samples have been drilled in the simulator with combinations of bit-type and drilling fluid as follows:

<u>Rock type</u>	<u>Drill bit</u>	<u>Drilling fluid</u>			
		<u>air</u>	<u>water</u>	<u>mud</u>	<u>mud &amp; flush</u>
anhydrite	roller cone	x		x	x
	diamond		x	x	x
salt	roller cone	x		x	x
granite	roller cone	x		x	x
basalt	roller cone	x		x	x
tuff	roller cone	x		x	x

All samples were drilled with a bit weight of 20,000 lbf (89KN) at 60 rpm. For samples drilled with mud or water, the well-bore pressure was 13.8 MPa, the confining pressure 20.7 MPa, and the overburden pressure 34.5 MPa. For samples drilled with air, the bore pressure was 0.3 MPa, the confining pressure 3.5 MPa, and the overburden pressure 10.3 MPa. The bit diameter for all tests was 20cm.

The disturbance due to drilling has been evaluated on core samples obtained from the sidewalls of the 20cm diameter holes drilled under simulated conditions. Inspection procedures included dye-penetrant visual examination, microscopic examination, and permeability tests on small cores. Generally, microscopic examination was found to be the most successful method. In the permeability tests, any variations due to disturbance were found to be obscured by variations also present in the undisturbed rock. Results for the five rock types were as follows:

- Anhydrite: There were detectable drilling-induced disturbance effects up to 2.5mm in thickness affecting up to 80% of the anhydrite grains in that thickness. Diamond bit-water was found to be the least damaging drilling method, and roller-cone-mud the most damaging. All damage was on an intergranular scale consisting of intergranular fracturing along cleavage planes, scintillation (changes in optical properties), and flow gliding (translational displacement of fractured grains). Other effects observed were removal of surface particles by etching or plucking, and softening of the borehole wall as a result of gypsification.

- Salt: Damage due to drilling could not be distinguished from damage due to sample preparation.
- Granite and Basalt: A damaged zone was detected but was limited to two to three grain depths from the borehole wall. The observed disturbance mechanisms were the same as for anhydrite, with grain plucking the most prominent.
- Tuff: Damage due to drilling could not be distinguished from natural variation in the samples.

It is noted that the drilling-induced disturbance observed in the Terra Tek tests is relatively minor. The thickness of the disturbed zone is less than three percent of the borehole radius and the disturbance effects are intergranular. Greater disturbance might be found with higher horizontal stresses, or if the horizontal stresses are unequal, and this deserves additional attention.

Disturbed zone studies are being conducted also at the University of Arizona (Daemen et al, 1981). The following table summarizes results for the thickness of the disturbed zone for 12.7mm diameter holes drilled with a percussion or diamond drill. The thickness of the disturbed zone is the extent of cracking indicated by fluorescent dye penetration.

<u>Rock Type</u>	<u>Drilling Method</u>	<u>No. Samples</u>	<u>Average Damage Zone Thickness (mm)</u>
Quartz diorite	percussion	8	1.9 (1.8)*
	diamond	9	1.1 (0.2)
Granite	percussion	13	2.1 (0.3)
	diamond	18	1.2 (0.3)

\*standard deviation

Microscope examination showed that the cracking pattern around diamond-drilled holes was more regular than for percussion-drilled holes. The surface of percussion-drilled holes appeared to be much rougher. The University of Arizona results are in agreement with the Terra Tek results in that the disturbed zone is very thin, although in the former case the thickness is a greater percentage of the borehole radius.

## 2.2 DISCUSSION

The laboratory tests described in the previous section have been conducted on intact rock specimens. The applicability of the results to the field may be judged by considering the relative scales of the observed disturbance and the in situ fracture spacing. Typically, the thickness of the damaged zone due to drilling is of the order of a few mm, whereas the fracture spacing is likely to be in the range 10cm - 1m. Thus, although boreholes will intersect fractures, most of the surface area will consist of essentially intact rock, and the damage due to drilling in situ should be comparable to that observed in the laboratory.

Similarly, the response of the rock adjacent to the borehole to stress redistribution will be governed by the relative scales of the borehole diameter and the fracture spacing. Typically, the borehole diameter will be approximately the same or somewhat less than the fracture spacing so that the volume of rock likely to be affected by stress changes should contain few, if any, fractures. In that case, the response to stress redistribution should be governed largely by intact rock properties. Analyses discussed later (Section 3.1.2 and Appendix A) indicate that stress changes around circular openings are unlikely to result in fracturing of intact rock at proposed repository depths. Some fractures might be affected by stress changes, but the effect should be limited because fractures are unlikely to be continuous through the disturbed zone.

It is concluded that the disturbance associated with boreholes is likely to be relatively minor. Evidence regarding the significance of the

interface on flow through borehole seals is obtained from another test at Terra Tek in which a cement plug was set in a borehole drilled in a block of anhydrite. A flow test was conducted using dyes to highlight the fluid flow path. Following the test, the plug was sectioned revealing a concentration of flow at the interface (Lingle et al, 1981). This test appears to support the concept presented in Section 1.2.1 that the interface is likely to be the dominant component of flow through borehole seals.

### 3.0 DISTURBANCE ASSOCIATED WITH SHAFTS AND TUNNELS IN FRACTURED ROCK

This section evaluates the changes in rock mass permeability associated with the excavation of shafts and tunnels in a fractured rock such as basalt, granite or welded tuff. Section 3.1 presents an analytical approach for predicting changes in permeability due to stress redistribution based on laboratory derived, stress-permeability relationships. Previous field investigations of disturbed zone characteristics are reviewed in Section 3.2, emphasizing studies at the Colorado School of Mines and Stripa. Damage attributed specifically to blasting is considered in Section 3.3. Conclusions regarding disturbed zone characteristics in fractured rock are given in Section 3.4.

#### 3.1 ANALYTICAL ASSESSMENT OF DISTURBANCE RESULTING FROM STRESS REDISTRIBUTION

##### 3.1.1 Rock Mass Behavior

Section 1.3 identified three possible mechanisms for creation of a disturbed zone: changes due to stress redistribution, damage due to the excavation process, and weathering or rock-ground water interaction. This section provides an analytical approach for evaluating the effects of stress redistribution for specified rock conditions.

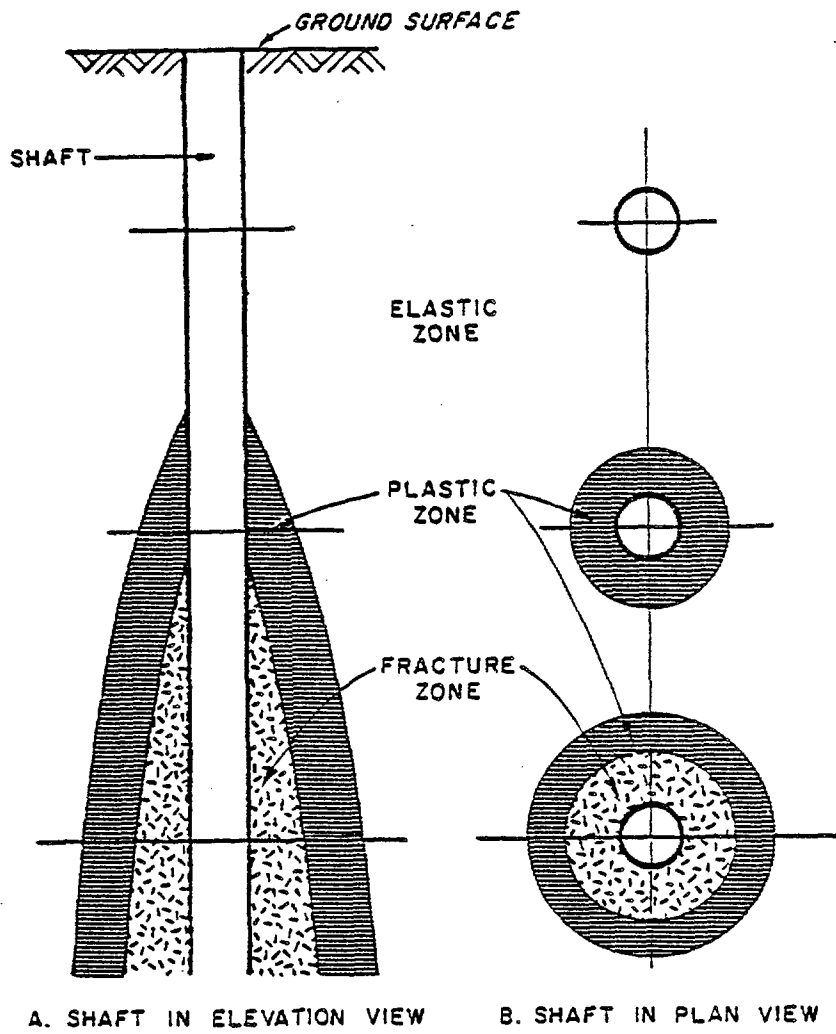
The response of a rock mass to stress changes around an underground opening is determined by the properties of the rock mass and by the magnitudes of the induced stresses. Relatively strong rocks at shallow depths behave essentially elastically whereby deformations are reversible and there is no failure. At greater depths the same rock might respond with proportionately greater deformations due to slippage along fractures. In this case, there is again no significant failure of intact rock material, but deformations in the "plastic" zone adjacent to the opening may be nonreversible. The depth (stress level) at which the plastic behavior is first observed, and at progressively greater stress levels the extent of the plastic zone, depend on the rock mass strength. At even greater depths, the stresses may be high enough to induce failure of the intact rock.

The succession of idealized elastic, plastic, and fracture zones associated with a shaft is shown in Figure 3-1. Simple calculations can be performed to estimate the depths at which the plastic and fracture zones will be first observed for given rock conditions. For example, for basalt with typical rock mass properties (Appendix B) and a hydrostatic initial stress condition, plastic behavior would be observed at depths below about 300m (Figure 3-2a). Fracture of intact rock would not occur above a depth of about 2500m for the hydrostatic initial stress condition. Figure 3-2b shows predicted displacements plotted against depth for the same rock conditions. The figure illustrates that rock mass behavior can be characterized readily as elastic or plastic by comparing measured displacements against the displacements predicted by elastic analysis.

In the following sections, analyses are presented for both elastic and elasto-plastic rock behavior. According to Figure 3-2a, the expected behavior for basalt at repository depths (in a shaft or tunnel) is elasto-plastic with the plastic zone extending approximately one radius. Section 3.1.2 first considers more specifically the stress conditions necessary to induce failure of intact rock.

### 3.1.2 Fracturing of Intact Rock

The discussion presented above indicates that fracturing of intact rock in response to stress redistribution should not occur at depths shallower than 2500m given typical basalt properties and a hydrostatic initial stress condition. Figure 3-3 summarizes a more detailed analysis (See Appendix A) of the general conditions in which failure of intact rock could occur around a circular shaft or tunnel opening. Considering a conservative lower bound (150MPa) for the strength of intact basalt, fracturing at a depth of 1000m is likely only if the ratio of the maximum to minimum in situ stresses is greater than 2.0. Even if fracturing did occur (for example, in response to a slightly higher in situ stress ratio), it would be limited to a thin zone and would not extend around the complete perimeter. This indicates that fracturing of intact rock is not a significant mechanism for disturbance



*After Ostrawski (1972)*

Figure 3-1. Idealized Scheme of Elastic, Plastic, and Fracture Zones Around a Shaft Opening in a Strong Rock Formation

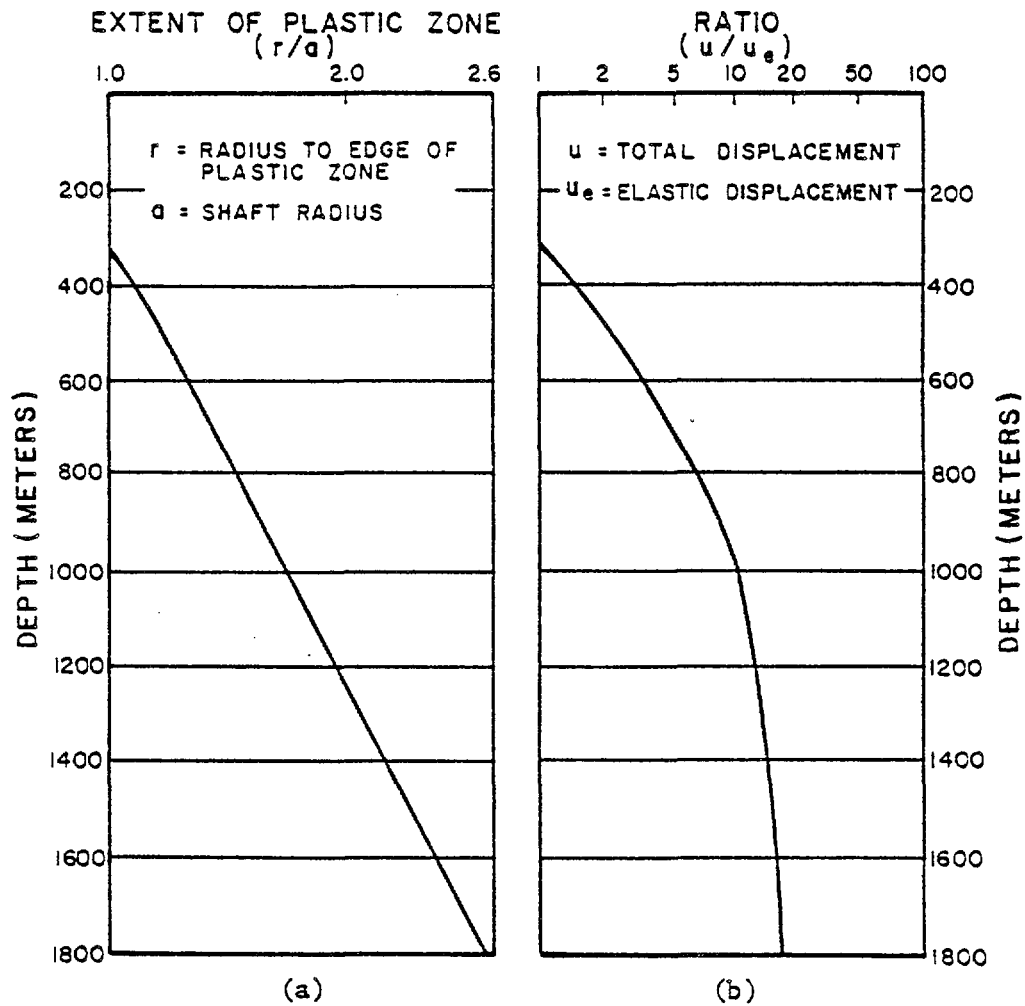


Figure 3-2. Extent of Plastic Zone (a) and Predicted Displacements (b) For a Shaft In Basalt With Hydrostatic Initial Stress Condition

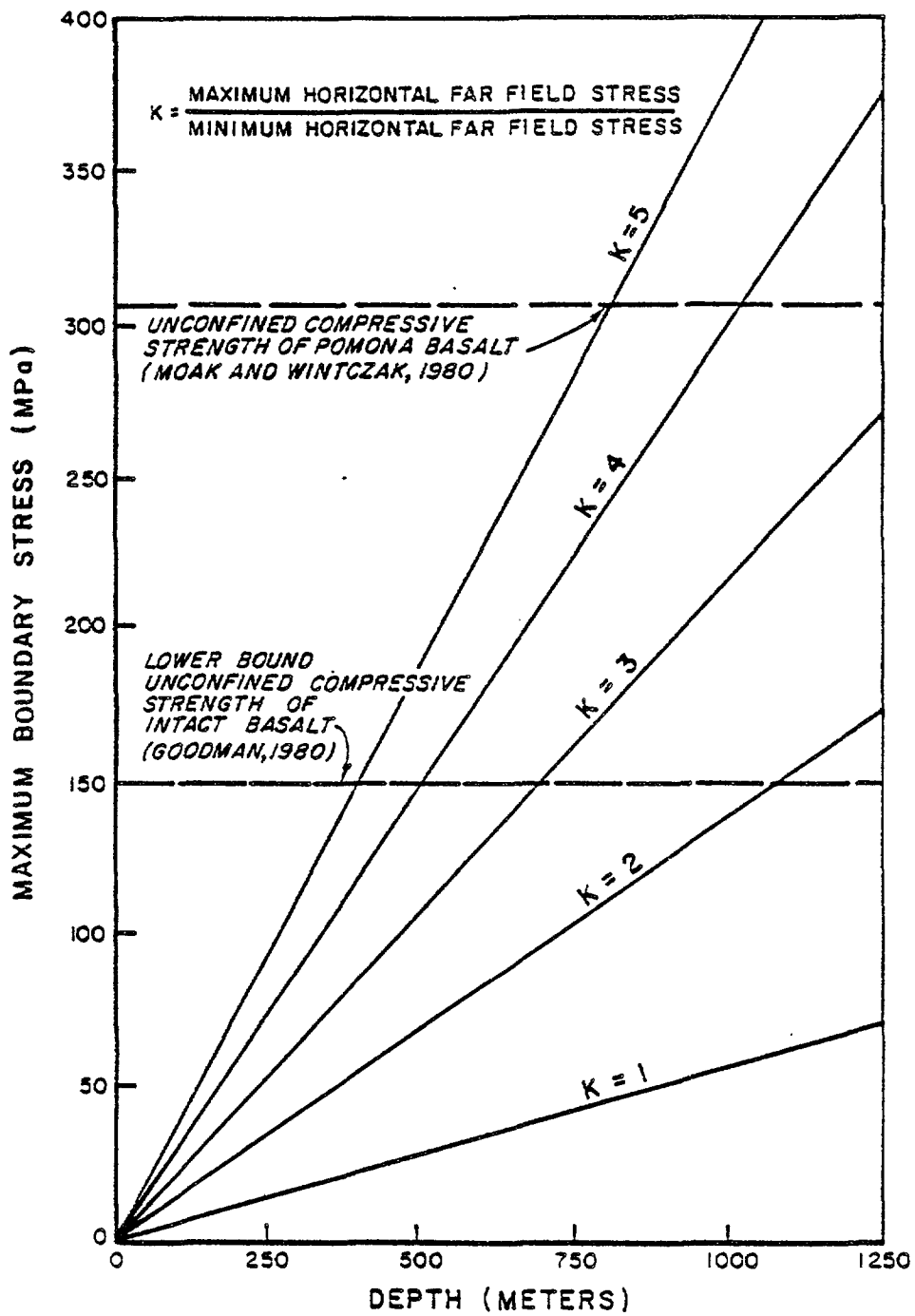


Figure 3-3. Maximum Tangential Boundary Stress for a Circular Opening Related to Depth and In-Situ Stress Ratio (K)

in relatively strong rocks such as basalt, granite or welded tuff. The effect of stress on pre-existing fractures, considered in the following section, is by comparison more important.

### 3.1.3 Effects of Stress on Pre-existing Fractures

The following sections present a number of analyses of the effects of stress redistribution on the permeability of pre-existing fractures. Section 3.1.3.1 first reviews basic relationships for the effect of stress on fracture permeability. Section 3.1.3.2 then considers simplified analyses for an initially hydrostatic stress field in which the effects of pore pressure and temperature are ignored. The effects of anisotropic stresses, pore pressures, and temperatures are then considered in Sections 3.1.3.3 through 3.1.3.5.

#### 3.1.3.1 Effects of Stress on Fracture Permeability

The permeability ( $k$ ) of a planar array of parallel smooth cracks is given by Hoek & Bray (1977, after others) as:

$$k = \frac{ge^3}{12vb} \quad (3.1)$$

where  $g$  = gravitational acceleration  
 $e$  = fracture aperture (opening)  
 $b$  = spacing between fractures  
 $v$  = coefficient of kinematic viscosity

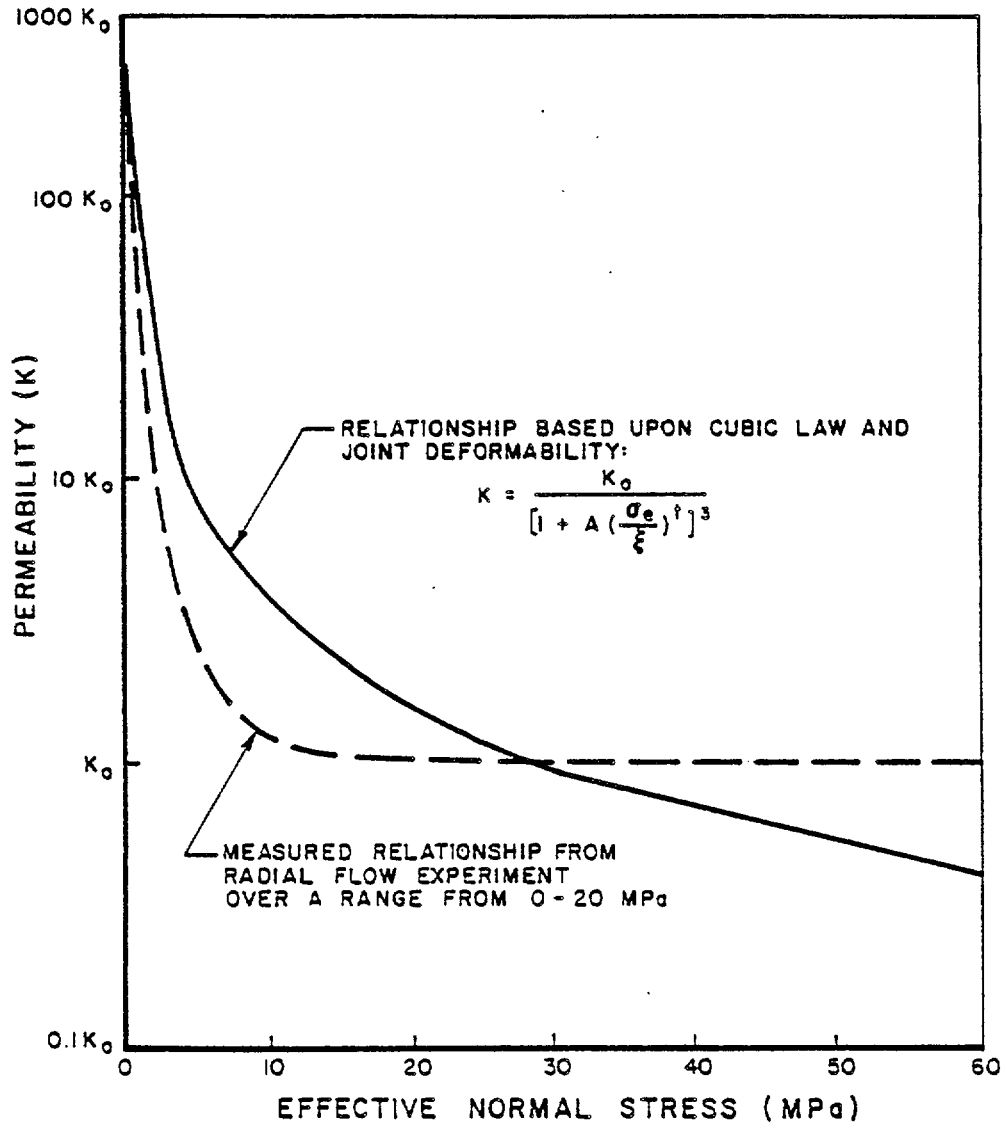
It will be noted that permeability is related to the cubic power of fracture aperture but only the first power of fracture spacing. Accordingly, it is to be expected that the permeability of a fractured rock mass should be strongly affected by the normal stress acting across the fractures and by the stiffness of the fractures.

The validity of the "cubic law" (equation 3.1) to natural, nonplanar fractures is the subject of much continuing research. This research has included laboratory testing (e.g., Iwai, 1976; Krantz et al, 1979), field testing of jointed blocks (Pratt et al, 1977; Voegele et al, 1981), and phenomenological modeling (Gangi, 1978; Tsang and Witherspoon, 1981). Recent reviews of the subject are given by Witherspoon et al (1980) and

Witherspoon (1981). Generally, this work has concluded that the cubic law is valid provided that it is based on a real aperture which takes into account the roughness and tortuosity of the fracture. The permeability-stress relationship is then determined by a number of factors which influence the fracture stiffness, including fracture roughness, fracture wall compressive strength, and the initial aperture. It follows that the relationship will differ according to the rock type, roughness and weathering of the fracture surface, and any infillings that are present. The relationship will also depend on the stress history of the fracture, and on whether displacements are purely normal or whether shearing occurs. There may be a scale effect also related to the fracture roughness. In most cases, actual flow is likely to be less than the flow predicted from an idealized cubic law relationship.

It is not the purpose of this report to present a detailed evaluation of the validity of the cubic law. For purposes of the analyses presented below, it appears that an idealized cubic law relationship provides a reasonably valid, and probably conservative, means for predicted permeability changes in response to changes in normal stress. Figure 3-4 (solid curve) shows such a relationship between permeability and effective normal stress developed for fractures in basalt using an approach suggested by Iwai (1976). In this relationship, fracture aperture is determined according to the model for nonlinear fracture deformability proposed by Goodman (1976). The constants  $A$  and  $t$  are empirically derived from tests of fracture deformability and are dependent on rock properties, fracture surface characteristics, and stress history. In Figure 3-4,  $A$  and  $t$  are derived from Iwai's tests on basalt and permeabilities are normalized to an effective stress of 28 MPa (approximately the lithostatic stress at a depth of 1000m in basalt).

The solid curve in Figure 3-4 can be used to determine relative permeabilities for any effective stress normal to the fracture in the range 0-60 MPa. This relationship has been used for all the basalt analyses presented subsequently. (A similar relationship has been used for



*After Iwai (1976)*

Figure 3-4. Permeability of an Artificial Fracture in Basalt as a Function of Effective Normal Stress

granite using different values for A and t also obtained from Iwai.) For comparison, Figure 3-4 also shows the permeability-stress relationship derived by Iwai directly from flow tests on the same basalt sample. The difference between the two curves represents a deviation from the idealized cubic law relationship attributed mainly to roughness effects. It can be seen that the idealized relationship obtained from deformability data is more conservative in the sense that it predicts less reduction in permeability as the normal stress is reduced below the 28 MPa reference value. Also, the relationship obtained from deformability data predicts that permeability should be further reduced at stresses above 28 MPa; by comparison, the flow tests indicate that there is effectively no further reduction in permeability above stresses of about 20 MPa. A point to note is that Iwai's test data were obtained from fractures that were formed at low stress and subsequently subjected to higher stresses. Different stress-permeability relationships might apply to fractures around a tunnel formed at high stress levels and subsequently subjected to lower stresses. For purposes of the analyses presented herein, Iwai's data are considered adequate.

#### 3.1.3.2 Analyses for Circular Opening with Isotropic Initial Stress Condition

The permeability-stress relationship derived in the previous section can be used to predict the changes in permeability around an underground opening. The basic method is to calculate the changes in stresses occurring in response to excavation and then to relate stress changes to permeability changes given the relationship shown in Figure 3-4. A number of simplifying assumptions must be made:

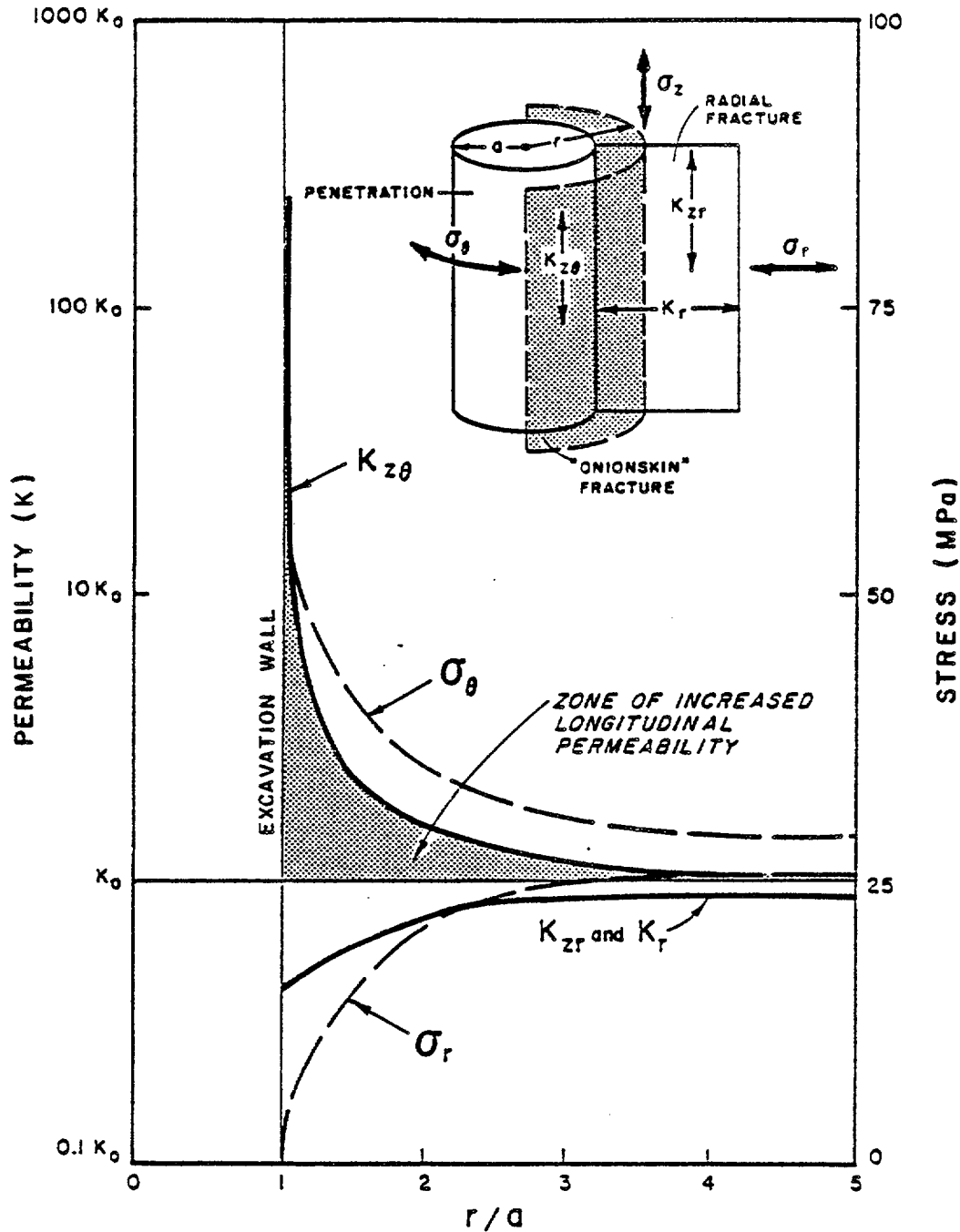
- fracture aperture and spacing are statistically uniform throughout the rock mass prior to excavation,
- there is no change in fracture spacing or continuity in response to excavation,
- stress changes can be calculated using elastic or elasto-plastic solutions,

- permeability is determined by fractures perpendicular to specified stress orientations.

In the analyses presented in this section, the initial stress condition is defined by two equal principal stresses acting in a plane normal to the penetration axis. In a sense this isotropic model is a hydrostatic stress condition although the stress in the direction of the penetration axis is ignored. The analyses are equally applicable to shafts or tunnels provided that the effects of gravity loosening of the rock mass in a tunnel roof are ignored. Also, the effects of pore pressures and temperature changes are presently ignored. Figure 3-5 shows the stress distributions in the radial and tangential directions around a circular opening for the elastic case. Corresponding permeabilities are obtained from Figure 3-4 with  $K_0$  established at 28 MPa. It will be noted that the axial (vertical for a shaft) permeability is increased close to the excavation whereas the radial permeability is reduced. The analysis assumes that the axial permeability is determined by continuous circumferential (or "onionskin") fractures normal to the radial stress, and that the radial permeability is determined by fractures normal to the tangential stress.

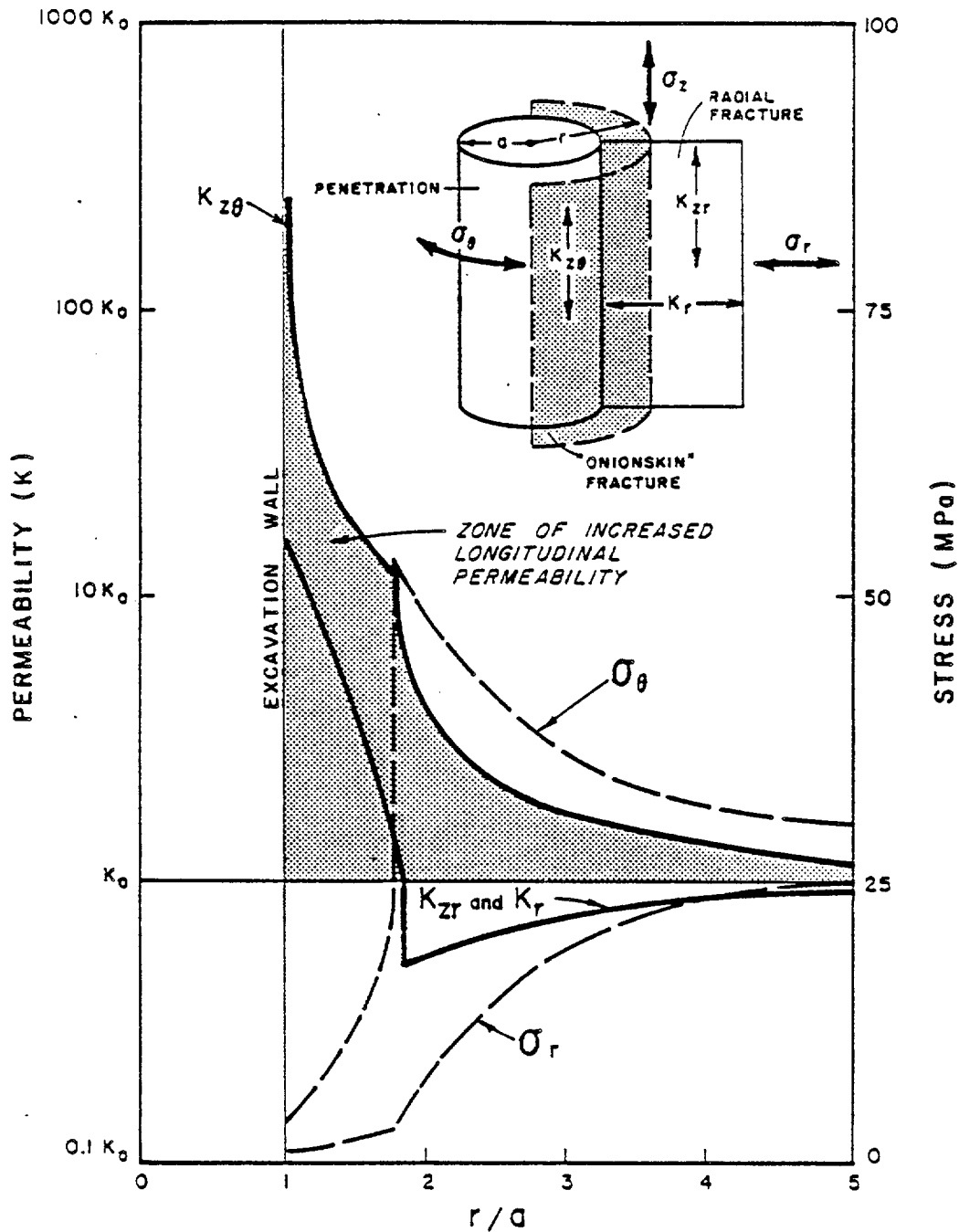
Figure 3-6 shows the same analysis for the elasto-plastic case again assuming hydrostatic in situ stresses. The stress distribution is obtained using an analytical solution which predicts the extent of a failed (plastic) zone around a circular opening as a function of stress and rock properties. Analytical solutions developed by Bray (1967), Jaeger and Cook (1969), and Hoek and Brown (1980) were found to yield similar results. Details of one of the solutions and of the rock strength parameters used are given in Appendix B.

In the elasto-plastic case, both the tangential and radial stresses are reduced in the plastic zone close to the excavation so that the corresponding radial and axial permeabilities are both increased. The maximum value of the axial permeability is the same as for the elastic case but the thickness of the disturbed zone is greater. Also, both components of axial flow (corresponding to radial and circumferential fractures)



- $K_{zr}$  = PERMEABILITY OF RADIAL FRACTURES IN THE VERTICAL DIRECTION  
 $K_{z\theta}$  = PERMEABILITY OF ONIONSKIN FRACTURES IN THE VERTICAL DIRECTION  
 $K_z$  = TOTAL PERMEABILITY IN THE VERTICAL DIRECTION:  $K_{zr} + K_{z\theta}$   
 $K_r$  = PERMEABILITY IN THE RADIAL DIRECTION  
 $K_0$  = PERMEABILITY IN THE UNDISTURBED ROCK (ISOTROPIC)

Figure 3-5. Predicted Disturbed Zone Permeability Based on Elastic Stress Analysis and Cubic Law Permeability-Stress Relationship for Fractured Basalt - Isotropic Initial Stress Condition



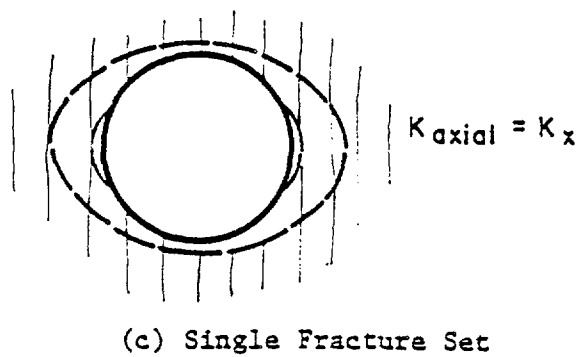
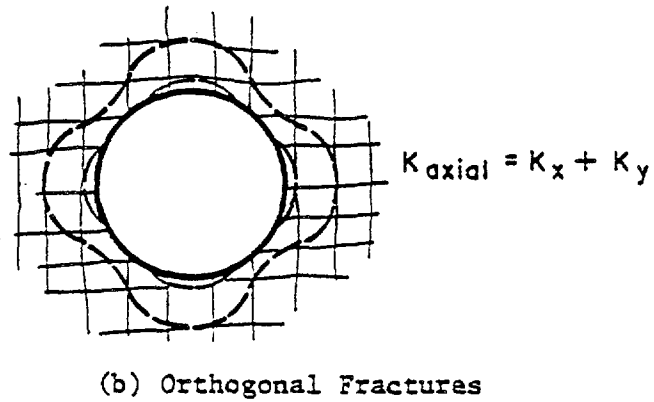
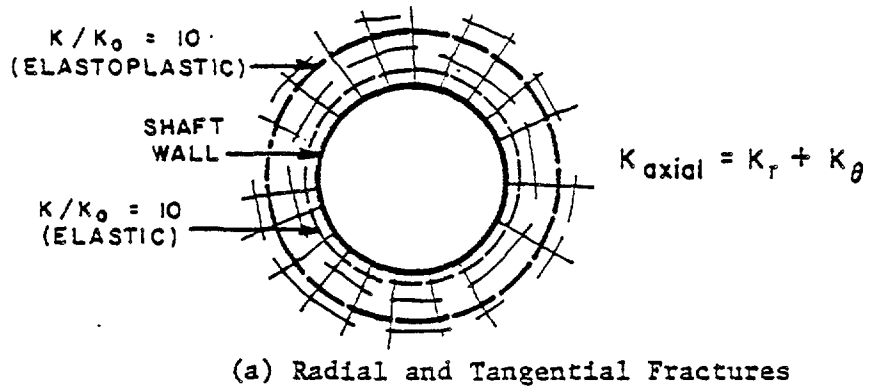
- $K_{zr}$  = PERMEABILITY OF RADIAL FRACTURES IN THE VERTICAL DIRECTION  
 $K_{z\theta}$  = PERMEABILITY OF ONIONSKIN FRACTURES IN THE VERTICAL DIRECTION  
 $K_z$  = TOTAL PERMEABILITY IN THE VERTICAL DIRECTION:  $K_{zr} + K_{z\theta}$   
 $K_r$  = PERMEABILITY IN THE RADIAL DIRECTION  
 $K_0$  = PERMEABILITY IN THE UNDISTURBED ROCK (ISOTROPIC)

Figure 3-6. Predicted Disturbed Zone Permeability Based on Elasto-Plastic Stress Distribution and Cubic Law Permeability-Stress Relationship for Fractured Basalt - Isotropic Initial Stress Condition

are increased. If the elasto-plastic case exists in reality, it is of major significance that axial permeability will be increased in the disturbed zone if either radial or circumferential fractures exist. If the elastic case is more relevant, the disturbed zone permeability is increased only if circumferential fractures exist, since the tangential stress concentration will tend to close radial fractures.

In one sense, the analyses performed are conservative in that they assume the existence of continuous fractures oriented in the least favorable direction, i.e., normal to the direction(s) in which stresses are reduced. Actual fracture patterns will be more complex but as a first approximation, real cases can be modeled reasonably well as idealized radial or circumferential sets. Figure 3-7 illustrates the effect of fracture orientation on the extent of the zone in which the original, undisturbed permeability in the axial direction around a circular opening is increased by a factor of 10 or more. The extent of the disturbed zone with radial and tangential fractures, as considered previously, is compared against the extent of the disturbed zone with orthogonal fractures oriented parallel to the far-field in situ stresses and with a single fracture set oriented parallel to one of the far-field stresses. With an elastic stress distribution, it is anticipated that axial permeability will be increased only where fractures are tangential to the surface of the opening. With an elasto-plastic stress distribution, permeability is increased all around the opening with the disturbed zone more extensive where there are fractures tangential to the surface of the opening. With the elasto-plastic stress distribution, there is essentially little difference between the cases with radial and tangential fractures and orthogonal fractures.

The significance of the permeability distributions obtained with either the elastic or elasto-plastic analyses is that the permeability reduces rapidly away from the excavation. With the more conservative elasto-plastic case, the permeability is five to ten times greater than the undisturbed permeability at a distance of about one radius from the excavation and only two times greater at two radii. In a locally



NOTE: ALL FIGURES SHOW CONTOURS OF  $K/K_0 = 10$  FOR ELASTIC AND ELASTO-PLASTIC STRESS DISTRIBUTIONS, ISOTROPIC INITIAL STRESS CONDITION.

Figure 3-7. Effect of Fracture Orientation on Extent of Disturbed Zone

variable, fractured rock mass, permeability differences of less than one order of magnitude are not considered to be highly significant. As noted previously, the analyses are conservative in that conducting fractures are assumed to occur in the direction normal to the minimum stress. On the other hand, there is no allowance for any increases in fracture frequency or continuity close to the opening. On balance, the analyses may offer a reasonable approximation of actual disturbed zone characteristics.

### 3.1.3.3 Circular Opening With Anisotropic Initial Stress Condition

The elastic and elasto-plastic analyses discussed in the previous sections assumed that the initial stress condition is defined by two equal principal stresses acting in a plane normal to the penetration axis. Although detailed analyses have not been conducted, it is possible to evaluate the effects of unequal principal stresses conceptually. Figure 3-8 shows a circular opening in a stress field in which the principal stresses in the plane normal to the penetration axis are  $2P$  and  $P$ . At the points A and A', the tangential stresses close to the surface of the opening will be lower than the tangential stresses that would act at the same points if the far-field stresses were  $P$  in all directions. Conversely, at the points B and B' the tangential stresses will be higher than for the isotropic stress case. It is thus postulated that the extent of the disturbed zone will be greater at A and A' than at B and B'. In a highly anisotropic stress field it is possible that tension could develop at A and A' in which case fracture permeability would be significantly increased close to the surface of the opening.

The effects of anisotropic initial stresses will depend on several factors including stress ratio, absolute stress level (as determined by depth), rock properties, and the orientation of fractures with respect to the principal stress orientations. Detailed analyses beyond the scope of this preliminary report are required to evaluate these factors. Until these analyses are conducted, the analyses in this report should be considered applicable only to isotropic (or nearly isotropic) stress fields.

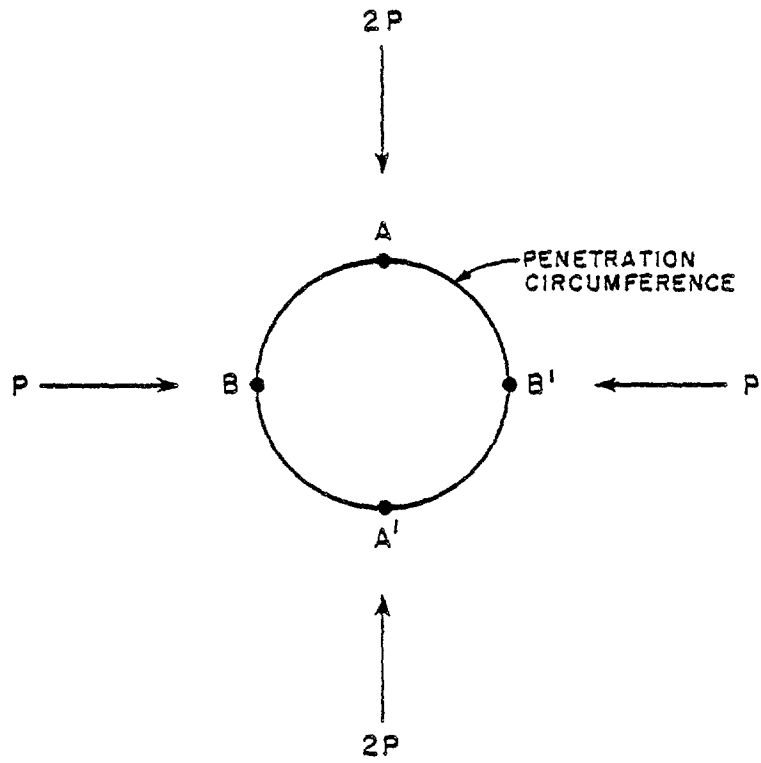


Figure 3-8. Notation for Considering Effects of Anisotropic Initial Stress Field

#### 3.1.3.4 Effects of Pore Pressure

The analyses presented in the previous two sections have ignored the possible influence of pore pressures. Effective stresses acting across joints have been calculated from the overburden load and the in situ stress ratio, with pore pressures assumed to be zero. As discussed in this section, pore pressures might have a significant influence on disturbed zone characteristics. Rigorous evaluation of these effects, however, would require a sophisticated coupled model considered beyond the scope of this report.

Conceptually, pore pressures might influence disturbed zone characteristics in two ways. First, pore pressures acting in fractures will increase the fracture permeability because permeability is determined by the effective normal stress acting across the fracture. It appears reasonable to ignore this effect for two reasons. In the near field, close to the penetration, the pore pressures will be reduced by drawdown and the normal stresses acting across fractures will be essentially those determined by the rock load. In the far-field, away from the influence of the drawdown, the pore pressures may be high (possibly as much as 40 percent of the total stresses), but for a deep shaft or tunnel their effect will be relatively minor because permeability is relatively insensitive to stress changes at high stress levels (Figure 3-4).

The second means by which pore pressure may affect disturbed zone characteristics concerns the reduction in rock mass strength that arises in response to reduced effective stresses. Reduced rock mass strength could result in an extension of the plastic zone developed around a penetration. For example, consider a shaft excavated in basalt at a depth of 1000m with a pore pressure of 12 MPa (approximately equivalent to a 1000m head). A simplified analysis shows that the extent of the plastic zone (measured from the shaft wall) is increased from approximately 0.8 shaft radii for the case with no pore pressure (as shown in Figure 3-6) to approximately 2.0 radii for the case with 12 MPa pore pressure. It must be noted, however, that this is a worst-case analysis

which ignores dissipation of pore pressures due to drawdown. A second simplified analytical approach is to model effective stresses in terms of steady state drawdown of pore pressures in the region surrounding the shaft. This indicates the extent of the plastic zone to be about 1.3 shaft radii. In practice, the extent of the plastic zone would fall between these two bounding analyses. Drawdown around the shaft would occur but probably simultaneously with the plastic deformations.

Rigorous analysis of the extent of the plastic zone would require a coupled model to account for the interaction of rock mass deformation, drawdown, and permeability changes. Such an analysis is considered beyond the scope of this report and is possibly not justified at present given the uncertainty regarding in situ rock properties. Conceptual consideration of the effects of pore pressure indicates that the elasto-plastic analysis presented in Section 3.1.3.2 may underestimate the extent of the plastic zone. In this sense, the analysis may underestimate the extent of the disturbed zone in which permeability is significantly increased. On the other hand, the analysis is considered conservative in that it is based on an idealized cubic law relationship between stress and permeability.

#### 3.1.3.5 Effects of Temperature on Disturbed Zone Characteristics

The analyses described previously have assumed constant temperature conditions. In a repository, however, the rock mass will be heated by decay of the waste. Approximate temperatures at a number of points in the repository and the shaft pillar for a repository in basalt are shown in Table 3-1. These temperatures are calculated for the geometry of the proposed BWIP repository (Rockwell Hanford, 1981) in which the shafts are located in a central shaft pillar between two main storage panels. The horizontal separation between a storage panel and the central shaft is 350 m. The temperatures presented are based on simplified calculations and probably over-estimate actual temperatures. They are presented to illustrate the contrast between different parts of the repository.

Table 3-1. Approximate Temperatures for a Repository in Basalt as a Function to Time

<u>Location</u>	<u>Time</u>		
	100 years	1000 years	10,000 years
Access tunnel in storage area	70	78	70
Tunnel in shaft pillar 100m from edge of storage area	63	68	65
Base of shaft	62	62	65

temperatures in °C  
ambient temperature = 62°C

In evaluating the effects of increased temperatures on disturbed zone characteristics, it is instructive to first review test results from the jointed block test at the Colorado School of Mines (CSM) test mine, and from tests at the Stripa mine in Sweden. In the CSM test (Voegele et al, 1981), fracture permeability was studied as a function of stress and temperature. In one series of tests the normal stress acting across the fracture was first increased from 0 to 3.1 MPa with a constant temperature of 12°C. This stress increase reduced the effective fracture aperture from about 47 to 30 microns. The temperature was then increased under constant stress and the aperture was further reduced to 18 microns at 41°C and 9 microns at 74°C. The temperature increase thus reduced the fracture permeability from 75 to 7 darcys. This effect was attributed to improved mating of the opposing fracture surfaces in conditions which progressively better matched the temperature and pressure environment in which the fracture was formed. In contrast to this result, a second experiment was conducted where the temperature was increased with no applied stress. In this case the aperture was found to increase from 42 microns at 17°C to 48 microns at 51°C. This effect was attributed to thermal expansion of the roughness profile. A point to note regarding these tests is that temperatures were relatively constant throughout the block.

At Stripa, evidence for temperature effects was obtained from heater tests and the macropermeability test. The heater tests included ultrasonic velocity measurements between boreholes located adjacent to the heater (Paulsson and King, 1980). One set of measurements showed that P-wave velocities increased from 5,850 m/sec before the heater was turned on to about 6,020 m/sec 150 days after turn-on. Similar increases were observed for S-wave velocities. These increases may be attributed to joint closure in response to thermal stresses established by the steep temperature gradient away from the heater. A second effect noted from the heater test (Hood, 1979) was that extensometers emplaced on opposite sides of the main heater hole indicated a net outward displacement (i.e., that the hole expanded). The significance of this observation is discussed below. The macropermeability test conducted at Stripa is described in Section 3.2.2. At this point it is sufficient to note that the rock mass permeability immediately adjacent to a tunnel was observed to be reduced slightly as the temperature was raised from 20°C to 30°C (Nelson and Wilson, 1980). This result is also believed to be due to temperature gradients away from the room which establish thermal stresses and close fractures.

These examples have been included to show that the effects of temperature on disturbed zone permeability will depend greatly on boundary conditions. In the storage rooms, there are likely to be significant thermal gradients away from the waste canisters emplaced in the floor. In this case, both the radial and tangential stresses around the room will be increased relative to the unheated case. Permeabilities in both the radial and axial directions will thus be reduced relative to the unheated case for at least the period while the high temperatures are maintained. Even during this period, however, it is likely that there will be an increase in permeability relative to the undisturbed case. For one reason, joint deformations are seldom completely reversible. For another, stresses in the radial direction must reduce to zero at the excavation (assuming an open hole) so that permeabilities in the axial direction must be correspondingly increased (assuming that fractures occur in the axial direction).

Away from the storage rooms, for example in the shafts and the tunnels joining the shafts to the repository, the temperatures will be lower and will be more uniform. In this case thermal stresses will be low and the effects of temperature will be related to expansion of the rock mass. Theoretically, the nature of this expansion adjacent to the tunnel or shaft is determined by the boundary conditions applied. If the boundary condition is one of constant stress, the excavation will expand outwards. If the boundary condition is one of constant displacement, the excavation will contract inwards. As noted above, test results from Stripa indicate that the constant stress condition appears to apply in that the excavation was observed to expand outwards. This expansion results in a circumferential expansion and an increase in the permeability of radial fractures. Simultaneously, there would be compression in the radial direction and a reduction in the permeability of axial fractures.

The discussion above indicates that increased temperature should tend to reduce permeabilities in the disturbed zone at least in the axial direction. In the storage rooms the temperature rise will occur rapidly after waste emplacement but temperatures decline in the period 100 to 1,000 years following emplacement. In the shafts, and tunnels close to the shafts, the temperature rise is not very great and it does not occur for about 1,000 years following waste emplacement. At present it is concluded that no reliance should be placed on temperature increases to alleviate disturbance effects. As discussed in Section 5.1.5, further disturbed zone studies should include more rigorous modeling of the rock mass. This modeling should include temperature changes in order to confirm the effects postulated herein.

### 3.2 PREVIOUS INVESTIGATIONS OF DISTURBED ZONE CHARACTERISTICS IN SHAFTS AND TUNNELS

Valuable information regarding disturbed zone characteristics may be obtained from a review of previous investigations. If sufficient data were available it might be possible to identify general trends for use in design prior to site-specific testing, relating for example a

disturbed zone thickness and permeability to penetration radius and excavation method. A literature review reveals that many studies have been conducted to evaluate the disturbed zone but these usually emphasize mechanical rock characteristics rather than permeability which is of major significance to penetration sealing. Important exceptions, where permeability has been measured directly, include tests conducted for the NWTS Program at the Stripa Mine in Sweden, and at the Colorado School of Mines test mine. Sections 3.2.1 and 3.2.2 review these two tests in detail while Section 3.2.3 reviews results from other sites. Section 3.2.3 is not intended to be a complete literature review. It is included to illustrate the variability in the results obtained, and to give examples of techniques that might be used in disturbed zone investigations at repository sites.

### 3.2.1 Colorado School of Mines Investigations

The Colorado School of Mines (CSM) has established a mining technology research facility at the Edgar Mine located at Idaho Springs, Colorado. A mining technology research program sponsored by ONWI is directed specifically toward evaluating the structural damage caused by various types of blasting and toward measuring permeability in the disturbed zone (Hustrulid et al, 1980). ONWI is also sponsoring a heated block test conducted at the same site by Terra Tek (Voegelé et al, 1981).

The disturbed zone and heated block tests are being conducted in an experimental room excavated specifically for the tests. The room is 5 m wide, 3 m high and 30 m long and was excavated using 10 different blasting patterns. Variations of a Swedish, smoothwall technique were used for seven rounds and variations of the Livingstone blasting method, developed in the U.S., for the other three. The rock cover above the experimental room is about 100 m and the room is located above the water table.

The principal rock type in the experimental room is a varyingly-banded, biotite gneiss which is intruded and recrystallized by granitic

migmatites and pegmatites. Fracture patterns have been mapped in detail in the experimental room and in adjacent drifts and raises. At least 10 structural trends have been recognized but in practical terms there are 3 main fracture sets each steeply dipping or vertical. In the heated block, fracture spacing varies from 60 to 100 cm for the 3 major sets (Voegele et al, 1981).

The damage zone evaluation is being made using boreholes drilled from the tunnel. Three 30 m long holes were drilled parallel to the tunnel axis and a pattern of 6.5 and 7.0 m long radial holes was drilled at each of 6 different blast round locations. The techniques used for disturbed zone assessment include:

- core logging,
- borescope and/or TV logging,
- cross-hole ultrasonic measurements,
- single-packer, air-injection permeability measurements,
- guarded-packer, water-injection permeability measurements,
- borehole deformation measurements using the CSM Cell and the Goodman Jack.

Other tests in the mine include roof to floor and wall to wall convergence measurements using convergence meters and tape extensometers, and in situ stress measurements using the CSIRO and USBM gages, as well as the heated block test referenced above. Currently, only preliminary results are available from the CSM studies (Montazer & Hustrulid, 1981), from which the following tentative conclusions can be drawn:

- the blast damaged zone is estimated to be less than 1 m wide;
- tangential stresses close to the excavation are approximately 6 MPa compared with an undisturbed value of about 2.1 MPa; the total width of the zone of stress increase is about 9 m, i.e., 1.8 times the tunnel width;

- radial permeability (as measured in boreholes parallel to the tunnel axis) is reduced by 1 to 2 orders of magnitude within about 2 m from the tunnel face;
- axial permeabilities (as measured in the radial boreholes) close to the tunnel walls are typically several orders of magnitude greater than the radial permeabilities; these results may be affected by communication between the packed-off zone and the tunnel face, and by leakage around the packers which were difficult to seal close to the tunnel face;

Generally, the results from the permeability tests tend to confirm the predictions for an elastic stress distribution (Section 3.1.3.2) that axial permeabilities should increase, and radial permeabilities decrease close to an excavation. Results from the ultrasonic tests are not yet available.

### 3.2.2 Stripa Investigations

A comprehensive investigation of fracture system geometry and the coupled interactions of heat flow, fluid flow and fracture deformation in crystalline rock has been conducted by Lawrence Berkeley Laboratory and the Swedish Nuclear Fuel Supply Company at the Stripa iron ore mine in Sweden (Witherspoon et al, 1981). The Stripa investigations provide direct evidence of a disturbed zone and can be used for a comparison between observed and predicted disturbed zone characteristics.

#### 3.2.2.1 Test Program and Results

The in situ tests at Stripa were conducted in a number of experimental drifts excavated in 1977 using smooth-blasting techniques (Andersson and Halen, 1978). The drift of particular interest herein regarding disturbed zone assessment, the "ventilation drift" (see below), is arch-shaped 4 m high and 4 m wide at the floor.

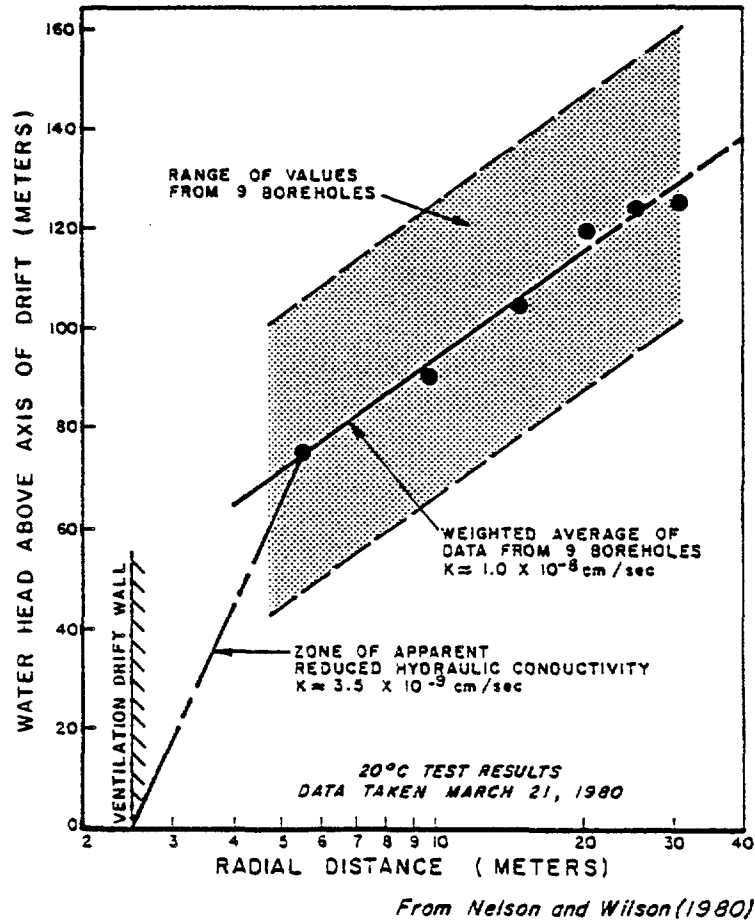
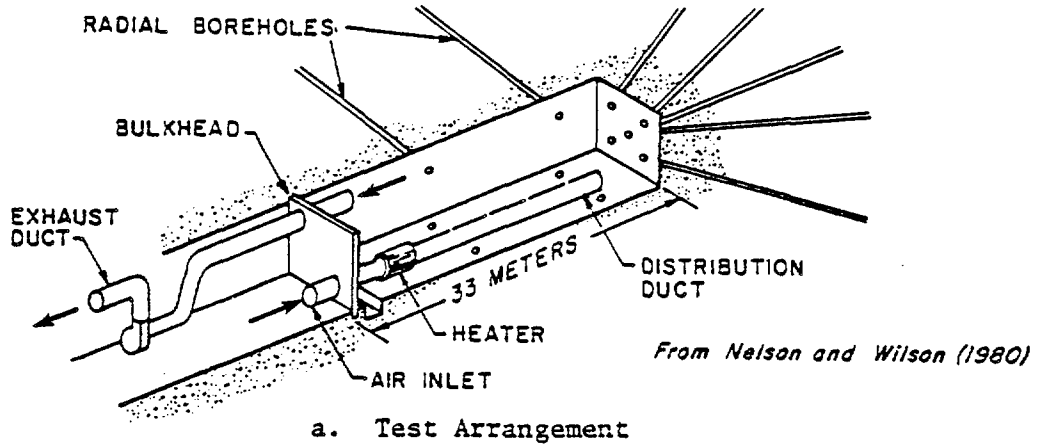
The experimental rooms are located in a medium-grained granite intruded by pegmatite and aplite dykes. Detailed fracture mapping showed that four major joint sets exist in the test area, one approximately

horizontal and three roughly orthogonal sets dipping in the range 45 to 70°. In the ventilation drift two major joint sets strike obliquely to the drift axis (Olkiewicz et al, 1979). Fracture frequency measured in holes drilled from the drift is on average 4.5 joints/m in inclined holes and 2.9 joints/m in vertical holes.

The tests conducted at Stripa have included:

- heater tests to evaluate near-field rock mass thermomechanical behavior (using thermocouples, extensometers, and USBM borehole deformation gages);
- borehole logging methods for fracture detection, including: core logging, borescope and television inspection, and various geophysical logs (neutron, gamma ray, gamma-gamma, resistivity, sonic, differential resistance, caliper);
- cross-hole ultrasonic measurements for fracture detection;
- packer injection tests for measuring permeability in boreholes;
- in situ stress measurements (using IRAD vibrating wire stressmeters);
- macropermeability test.

The macropermeability test is of particular interest to disturbed zone assessment. This was a test designed to measure the permeability of a large volume of low permeability, fractured rock by monitoring water inflow into a 33 m long section of the ventilation drift (Nelson and Wilson, 1980). Water inflow was monitored as the net moisture pick-up of the ventilation system inside a sealed portion of the drift. Hydraulic gradients around the drift were determined by monitoring water pressures in piezometers installed in a total of 90 isolated intervals in 15 radial boreholes drilled from the drift. Figure 3-9 is a plot of head measured in the boreholes versus radial distance from the wall of the drift. Using this plot, an average rock mass hydraulic conductivity may be calculated from the observed gradient (the slope of the head-distance plot) and the water inflow monitored in the tunnel. If the



b. Distance-Drawdown Plot at End of 20°C Temperature Experiment

Figure 3-9. Macropermeability Test, Stripa

weighted average line shown in Figure 3-9 is projected to the drift wall, it indicates a higher water head than can exist in practice. This indicates that there is a zone, approximately 2.5 m thick adjacent to the walls of the drift, in which the hydraulic conductivity is reduced by a factor of approximately three.

Other disturbed zone assessments at Stripa were made by direct inspection of fractures produced by blasting and by borehole logging. A detailed inspection of the smooth-blasted tunnel walls showed that 10 percent of the outer ring holes had wavy fractures along their length (Andersson and Halen, 1978). The fractures were caused by blasting and their length ranged from 0.1 to 1.0 m. The extent of these fractures perpendicular to the tunnel walls was investigated by drilling a number of short core holes each intended to follow a particular fracture. The average extent of fractures was found to be about 0.3 m. Considering an average explosive charge for the contour holes of about 0.3 kg/m, Andersson and Halen report that the Stripa results appear to correspond to a general rule developed in Sweden that the extent of fracturing caused by blasting measured in meters roughly corresponds numerically with the charge measured in kg/m (see Section 3.3).

#### 3.2.2.2 Evaluation of Results

Nelson and Wilson (1980) suggested that the permeability reduction close to the tunnel wall observed in the macropermeability test might be related to thermal expansion of the rock or to chemical precipitation as the water evaporates into the tunnel. Although these explanations may be at least partly valid, an alternative explanation offered herein is that the permeability is reduced in response to the tangential stress concentration around the opening. As discussed in Section 3.1.3.2, considering a rock mass which deforms elastically, the expected stress changes around an underground opening are that the radial stresses are reduced close to the opening whereas the tangential stresses are increased. One theoretical result is that the permeability of fractures oriented radially to the axis of the opening should be reduced. The Stripa test was conducted in a good quality rock mass at relatively

shallow depth where the deformational behavior is probably close to elastic. Also, the macropermeability test is largely a measure of radial flow and is likely to be affected by changes in permeability along fractures conducting flow in a radial direction.

The hypothesis that the observed reduction in hydraulic conductivity is related to stress changes is tested by comparing the observed changes with those predicted using the analytical approach described in Section 3.1.3.2. The predicted hydraulic conductivity is based on the cubic law for fracture flow and on empirical data for fracture deformability (for a granite specimen) obtained by Iwai (1976). The far-field hydraulic conductivity away from the influence of the room is set as  $1 \times 10^{-8}$  cm/sec, the value inferred from the 20°C macropermeability test (Figure 3-9).

As noted previously, the macropermeability test revealed a constant hydraulic conductivity beyond a radial distance of 2.5 m from the tunnel wall. Closer to the wall, the conductivity appeared to be reduced but, because no head measurements were obtained within this zone, only an average hydraulic conductivity could be assigned. Consequently, the macropermeability test provides only two averaged data points to compare against the continuous hydraulic conductivity versus radial distance plot obtained by analysis. As shown by Figure 3-10, the predicted zone of reduced hydraulic conductivity extends further from the excavation wall than does the observed zone of reduced conductivity. Nonetheless, the two methods are in close agreement as regards the average conductivity of the zone within about 3 to 4 m of the tunnel wall.

The comparison between predicted and observed disturbance can also be made on the basis of predicted versus observed head distributions. Figure 3-11 shows head distributions calculated using a finite element solution for radial flow towards a circular opening. The head distribution is calculated for the hydraulic conductivity profile shown in Figure 3-9 by specifying the far-field head, the head at the tunnel wall, and the flow volume. As shown, there is close agreement between the

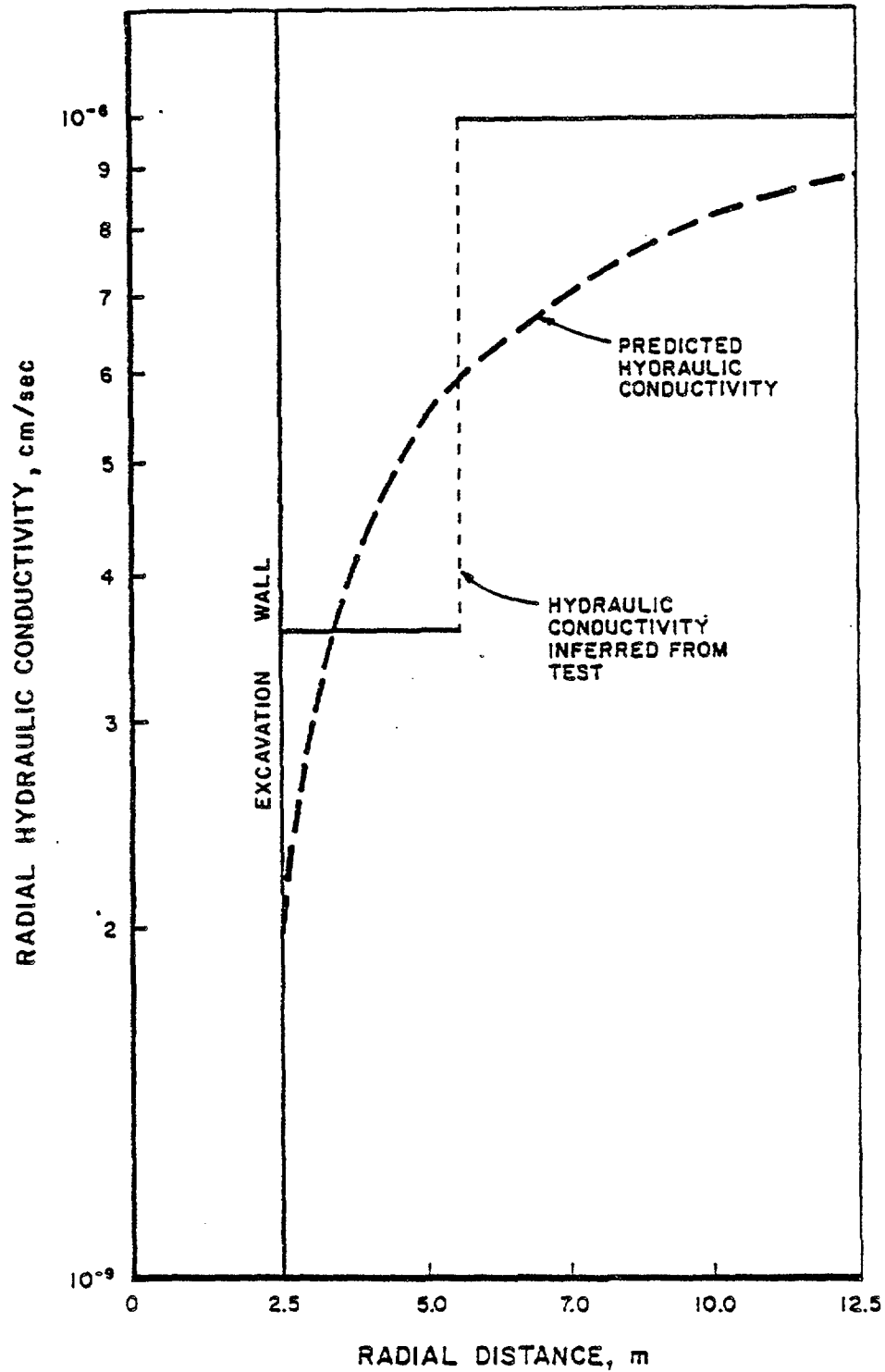
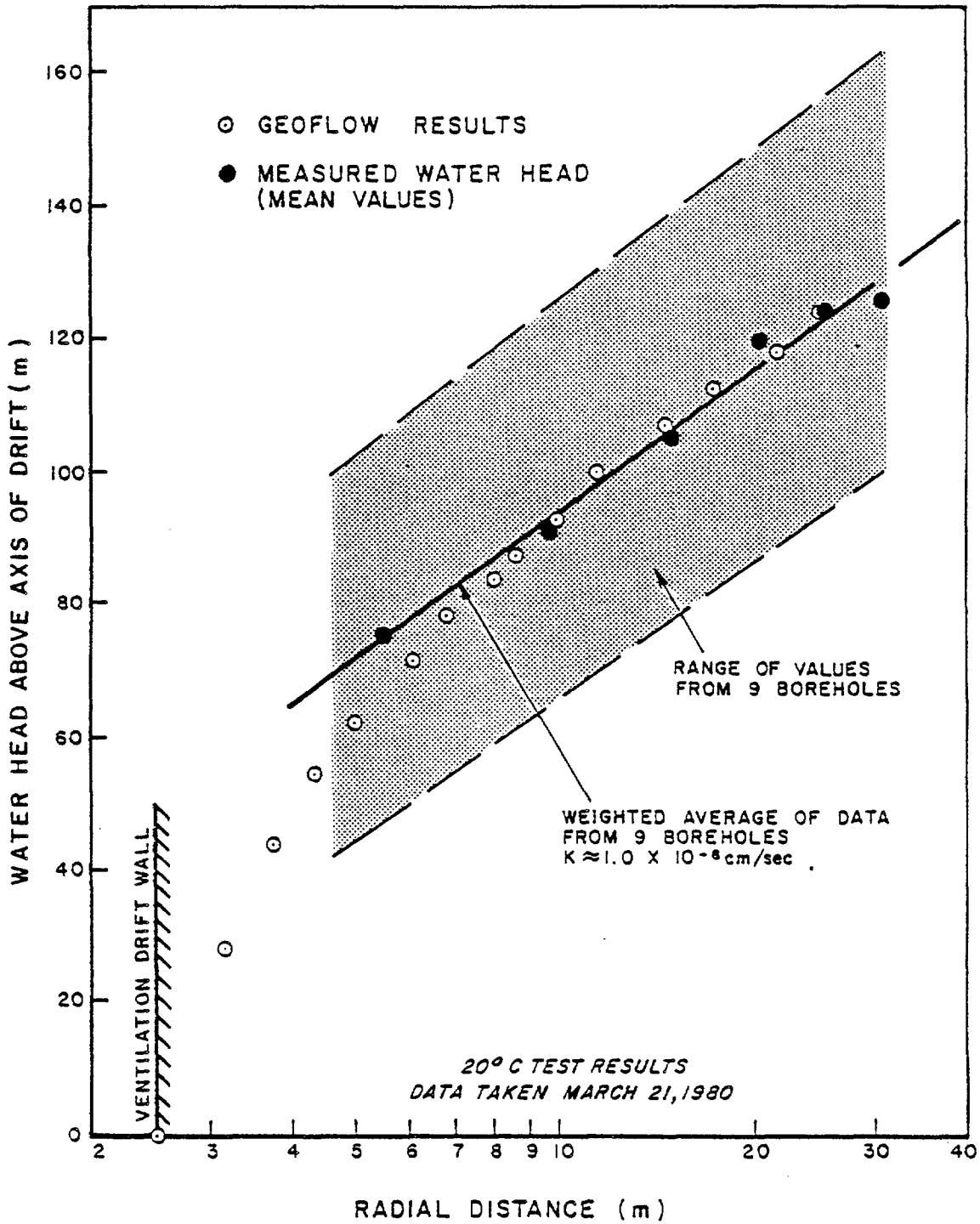


Figure 3-10. Comparison of Hydraulic Conductivities Predicted by Analysis and Inferred from Field Measurements, Stripa Macropermeability Test



Test results from Nelson and Wilson (1980)

Figure 3-11. Comparison of Water Heads Predicted by Finite Element Analysis Using Disturbed Zone Model and Field Measurements, Stripa Macroporosity Test

predicted and observed distributions. This agreement is due in part to restrictions imposed by the specified boundary conditions but is also considered to be partial validation of the analytical approach used.

The good comparison between observed and predicted disturbance obtained for the Stripa case is taken to be a validation of the analytical approach used and of the stress-permeability relationship based on fracture deformability data. The good comparison is especially interesting in view of some of the assumptions involved in the analysis. For example, the laboratory fracture deformability data obtained by Iwai (1976) was for an artificially induced fracture in a granite specimen not obtained from Stripa. Also, the analysis assumes the existence of radial fractures. The correspondence between predicted and observed effects thus obtained may indicate that such fractures do control flow toward the drift; the analysis would not hold if flow was controlled, for example, by a single set of fractures oriented normal to the drift axis.

As described, the effect of a tangential stress concentration around the ventilation drift is to reduce the permeability in the radial direction. Conversely, the radial stresses adjacent to the drift wall are reduced so that the permeability of any fractures parallel to the walls of the drift should be increased. Figure 3-12 compares radial and longitudinal hydraulic conductivities calculated using the method previously described. Because of the non-linear relationship between stress and fracture permeability, the increase in hydraulic conductivity in the longitudinal direction is greater than the reduction in the radial direction.

### 3.2.3 Other Disturbed Zone Investigations in Fractured Rock

As noted previously, a literature review has revealed few cases (other than CSM and Stripa) where disturbed zone permeability has been measured. There are many case histories in the general rock mechanics literature where the extent of the disturbed zone is indicated by variation in geophysical or mechanical properties.

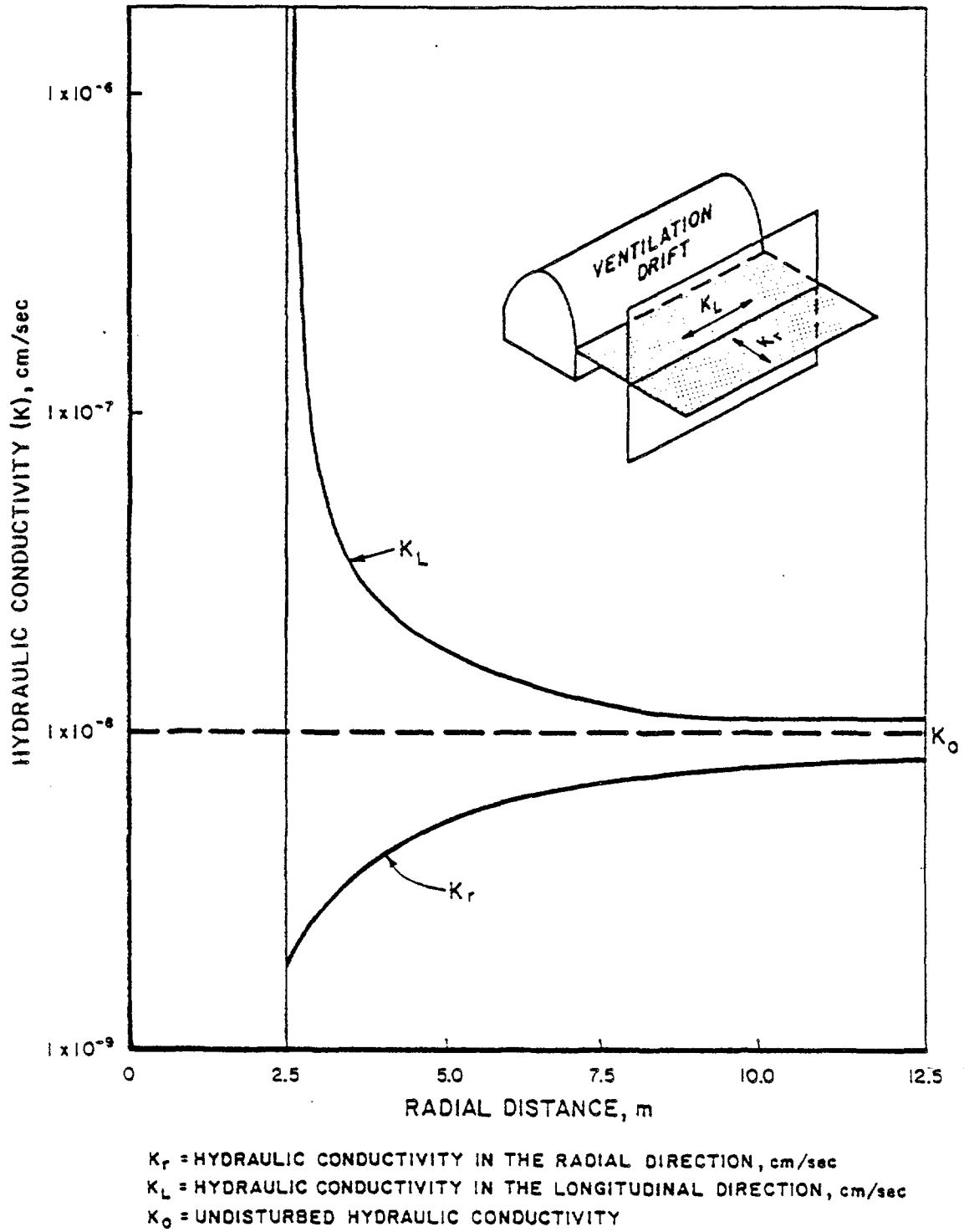


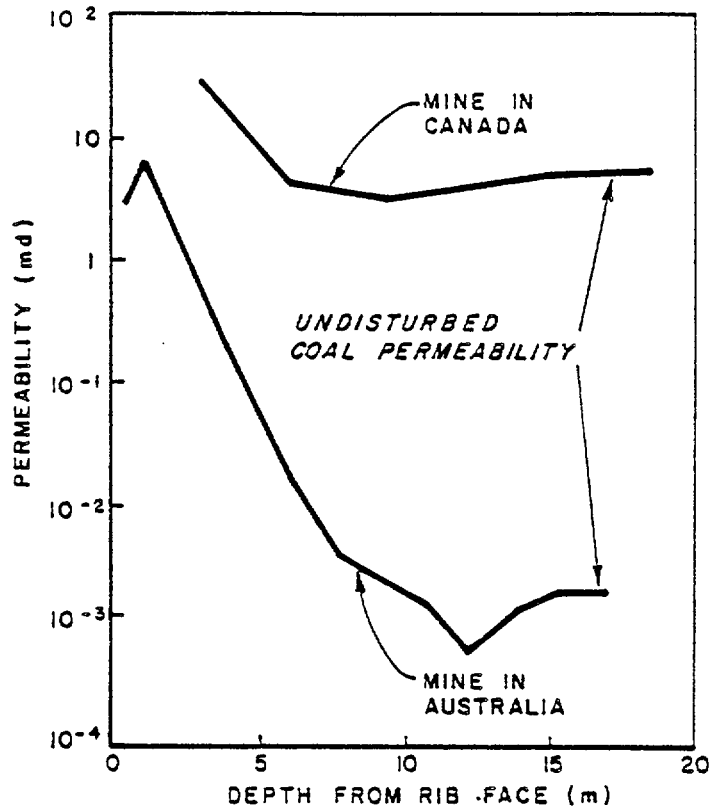
Figure 3-12. Predicted Disturbed Zone Hydraulic Conductivities for the Stripa Macropermeability Test

### 3.2.3.1 Permeability Measurements

Fisekci & Barron (1975) measured permeability as a function of depth in coal pillars at mines in Canada and Australia. The investigations were related to methane-inflow problems and permeability was evaluated from the rate of pressure increase due to methane inflow in packed-off sections of boreholes. Figure 3-13 shows permeability as a function of depth into the pillar face at the two sites. In one case the permeability increases by nearly three orders of magnitude near to the edge of the rib but in the other case the increase is much less dramatic. This difference may be attributed to the greater depth of cover, and correspondingly lower undisturbed permeability, at the site displaying the greater change in permeability.

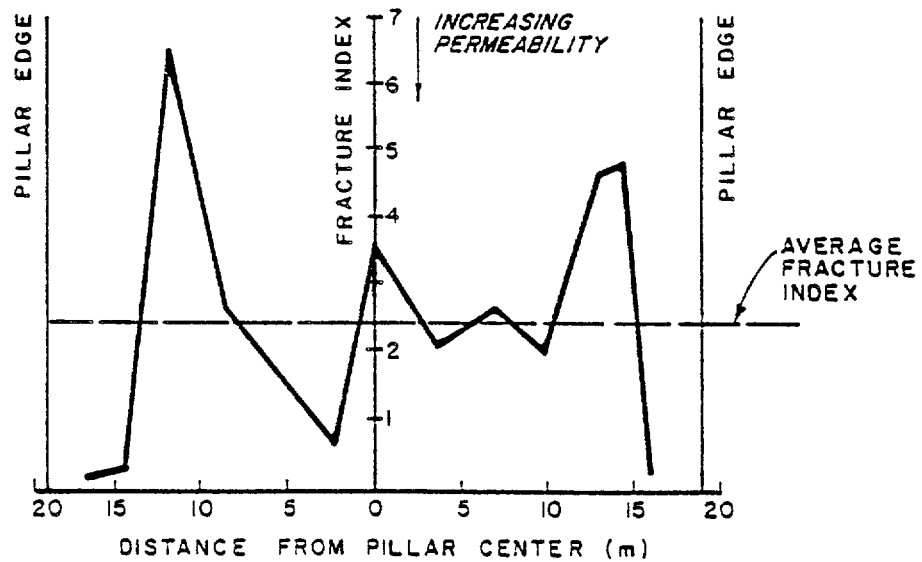
Barron (1978) used an air-injection method to investigate the degree of fracturing in coal pillars. In this case the air inflow in a packed-off section of a borehole was related to a fracture index which is inversely proportional to permeability. Figure 3-14 shows the variation in permeability observed across the complete width of a pillar. These results are interesting in that the variation in permeability closely matches the theoretical stress distribution across the pillar. Higher permeabilities close to the pillar edge correspond to a destressed zone, whereas lower permeabilities within the pillar correspond to increased stresses in abutment zones.

An air-injection method has also been used by the U.S. Geological Survey to study the intensity of fracturing around a 3m (10-foot) diameter tunnel in volcanic rocks at the Nevada Test Site (Miller et al, 1974). Injection tests were run at 0.3 m intervals in 17 boreholes drilled from the tunnel. Characteristically, the flow rates obtained were either very low (indicating no fractures present) or relatively high (indicating fractures present in the test interval), with ninety percent of the high flow rates recorded within 1.7 m of the tunnel face. Observations in the tunnel revealed many induced fractures attributed to blasting or stresses exceeding the rock strength. These induced fractures are probably responsible for the marked increase in permeability



From Fisekci and Barron (1975)

Figure 3-13. Disturbed Zone Permeability in Coal Pillars Measured by Methane Inflow Between Packers



From Barron (1978)

Figure 3-14. Fracture Index in a Coal Pillar Measured by Air-Injection

within 1.7 m of the tunnel face. The opening of pre-existing fractures in response to stress relief might be expected to produce a more gradual increase in permeability.

Miller et al's, air injection method has been used by the U.S. Bureau of Mines to investigate fracturing around a shaft in the Coeur d'Alene mining district (Miller and Skinner, 1980). As at the Nevada Test Site, the flow rates obtained were typically very low away from the opening and much higher (6 orders of magnitude) in a surface zone extending 0.6 to 1.2 m from the shaft wall. Again as at the Nevada Test Site, the marked increase in permeability results from the creation of fractures by blasting and stress relief. Miller and Skinner report that the air injection method can be used to detect permeabilities as low as 1 micro-darcy. They also note previous work by the USBM (Chan et al, 1974) which showed that the air-injection method could be used to indicate chemical grouting feasibility.

#### 3.2.3.2 Geophysical Methods

Seismic methods have been used in many cases to delineate the "loosened" or distressed zone in the walls of structures such as underground powerhouses or tunnels. Two methods have been used, seismic refraction and cross-hole acoustical surveying. The following sections provide examples of these methods where a disturbed zone has been delineated. A further discussion of the techniques involved is given in Section 5.1.3.1.

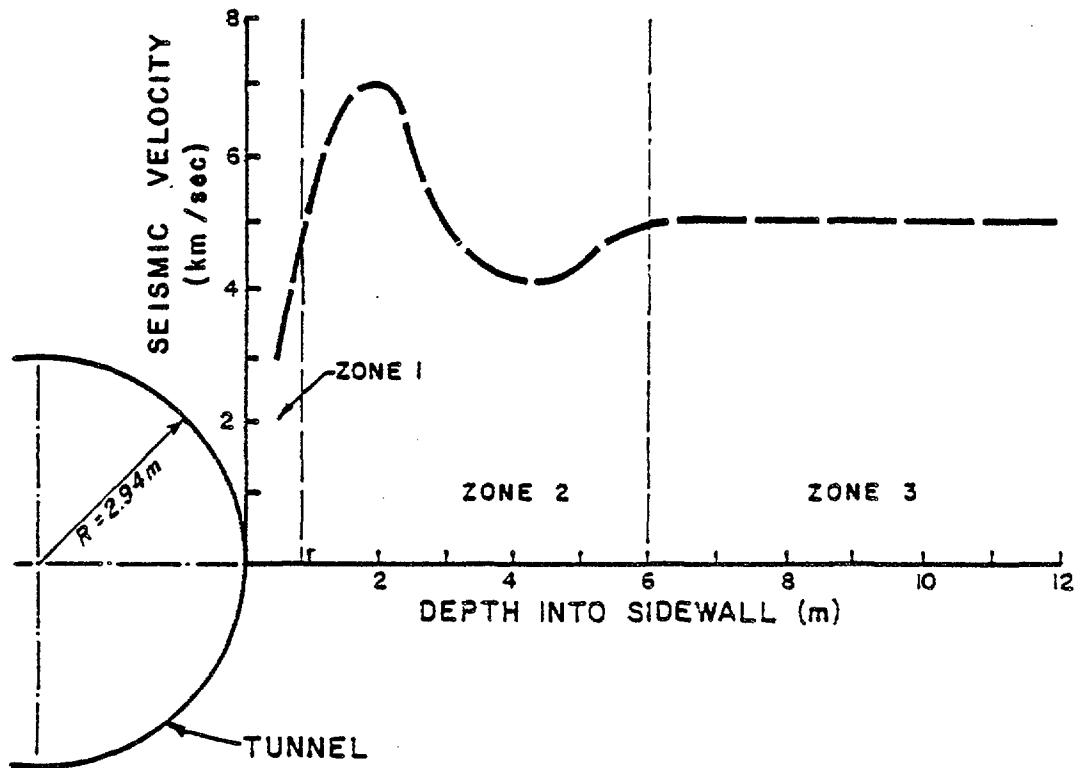
Seismic refraction was used at the Belledonne water-supply tunnel in France (Plichon, 1980). This is a circular tunnel, 5.88 m in diameter and 18,200 m long, driven in part by drill-and-blasting and in part using a full-face tunnel boring machine. The tunnel is driven through granite and granite-gneiss with a cover of greater than 2000 m in the central part. Measurements of seismic velocity in the tunnel walls made using the "petite sismique" method (see Section 5.1.3.1) typically revealed an inner decompressed zone of reduced velocity immediately adjacent to the tunnel wall, and an outer compressed zone of increased

velocity (Figure 3-15). The thickness of the decompressed zone was found to vary from 1.0 to 1.8 m and the velocity varied from 65 to 87 percent of the velocity in the undisturbed zone. The thickness of the decompressed zone was found to be greatest in one of the stations in the machine-bored section of the tunnel but there are too few measurements to attach much significance to this observation. There is no evidence that the disturbed zone is any thicker or any more fractured in sections excavated by drill-and-blast than in machine-bored sections.

Seismic refraction was used also in a pressure tunnel at the Tavera project in the Dominican Republic (Murphy, 1972). This approximately 3m diameter tunnel was driven through conglomerate, siltstone, and shale, presumably by drill-and-blast methods. In a conglomerate section, two layers were found within the disturbed zone, with velocities approximately 30 percent and 70 percent of the velocity in the undisturbed rock. The combined thickness of the two layers was about 2.4 m. Similar trends were measured in a shale and siltstone zone of the tunnel.

A third seismic refraction case history is given by Brizzolari (1981) from investigations in a mine access tunnel excavated in shale. Seismic profiles were run at four 36 m long test zones revealing a loosened zone (velocity reduced by approximately 30 percent) ranging in thickness from less than 0.5m to 1.5m. Unfortunately, the diameter of the tunnel is not given. The results are interesting, however, in that the loosened zone appeared to be only half as thick at one station where a tunneling machine had been used compared with the other stations where blasting was used. Also, repeated surveys showed that the loosening was progressive over a period of up to three years. (This progressive loosening may indicate swelling of the shale; loosening in hard rock should occur much more rapidly.)

Figure 3-16 is an example of disturbed zone extent indicated by cross-hole seismic methods from the Rama Tunnel in Yugoslavia (Kujundzic et al, 1970). The measurements were made longitudinally along the tunnel



*From Plichon (1980)*

- ZONE 1 - DECOMPRESSED AREA NEAR TUNNEL WALL
- ZONE 2 - INTERMEDIATE AREA AFFECTED BY TUNNEL CONSTRUCTION
- ZONE 3 - UNAFFECTED ROCK MASS

Figure 3-15. Typical Seismic Velocity Profile Obtained from Seismic Refraction, Belledonne Tunnel, France



between two sets of radial boreholes drilled 1.2 m apart. The tunnel, 5.0 m in diameter, was driven in steeply-dipping dolomites by drill-and-blast methods. As shown by the figure, the loosened zone adjacent to the tunnel was found to be less than 1 m thick. Surrounding the loosened zone is a compressed zone indicated by increased velocities.

A similar cross-hole method was used in an exploratory tunnel at the Turlough Hill power plant in Ireland (O'Donoghue and O'Flaherty, 1974). This 2.5 x 2.5 m tunnel was driven by blasting through variably jointed and decomposed granite. The results indicated that the depth of loosening was related to the intensity of jointing and decomposition in the undisturbed rock. In "almost unjointed" granite the depth of loosening was 0.5 to 1.25 m, whereas in "very intensely" jointed rock the depth increased to 2.5 m.

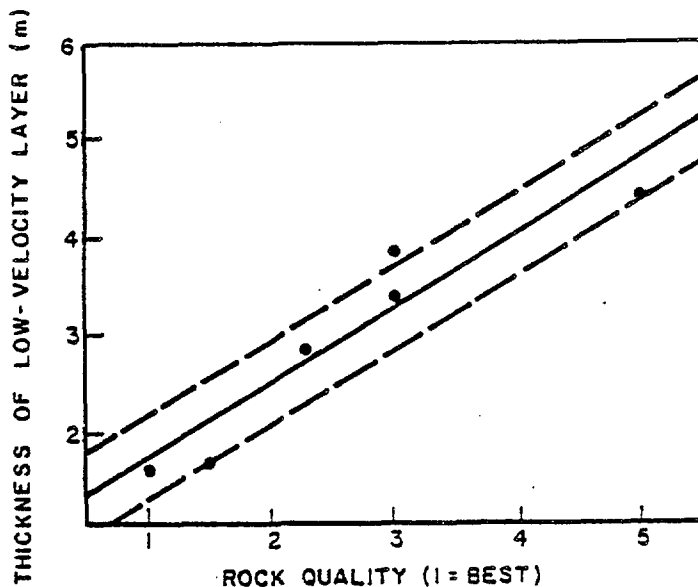
Seismic refraction and electrical resistivity methods were used to measure the disturbed zone around the Straight Creek Tunnel (now named the Eisenhower Tunnel) pilot bore in Colorado (Scott et al, 1968). The pilot bore was 4 m in diameter, 2,500 m long, excavated using drill-and-blast methods. The bore was driven through granite, gneiss, schist, and migmatite which were extensively faulted and sheared and locally altered. Cover ranged up to 430 m. Seismic refraction measurements were made by positioning 10 high frequency detectors along the tunnel walls (spacing of 1.5 to 7.6 meters) and setting small explosive charges in shallow drill holes at the end and near the midpoint of each array. A low-velocity layer was identified adjacent to the tunnel walls, varying in thickness from less than 1 m in more competent sections of rock to about 5 m in severely fractured sections of rock. The low-velocity layer was attributed to two mechanisms, blast damage, and adjustment of stresses due to excavation. Blast damage was estimated to extend probably only a "few feet" into the rock.

Electrical resistivity measurements were made using electrodes positioned horizontally in the Wenner configuration along the walls of the tunnel, using spacings of up to 9 m. A layer of high-resistivity rock

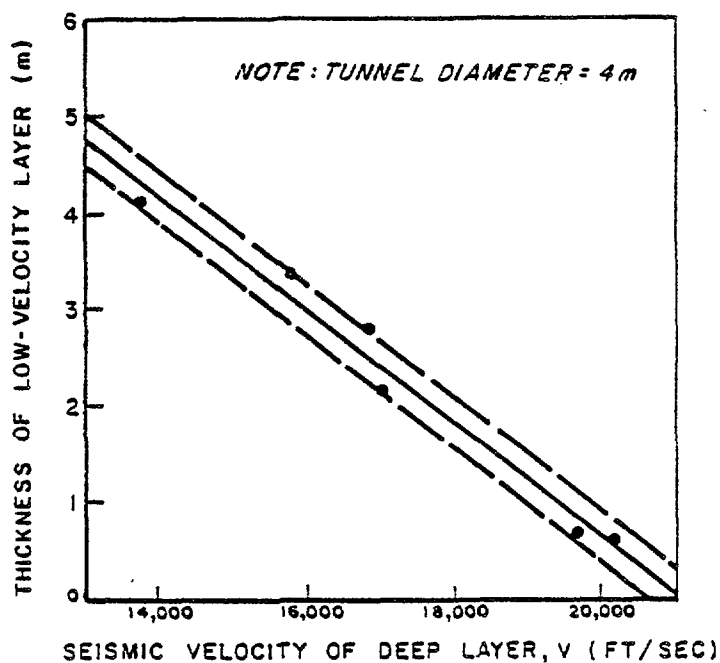
was identified adjacent to the tunnel walls, ranging in thickness from 0.3 to 3 m. It was concluded that the high resistivity layer thickness was an upper bound on the depth to which blast damage occurred. A detailed comparison of the depth of the "disturbed" rock layer measured by the two different methods (seismic and resistivity) is not possible from the data presented; however, in all cases, it appears that seismic refraction measured a larger disturbed zone than the resistivity method.

Extensometers were installed in the pilot bore and Scott et al found a good correlation between the thickness of the low-velocity layer and the height of the "tension arch" developed above the tunnel. The height of the tension arch was defined as the transition point between zones of compression and tension in the rock above the bore as indicated by extensometer measurements (or estimated from load cell measurements). Rock within the tension arch was observed to move toward the excavation; rock outside the tension arch was observed to move away from the excavation. Scott et al also found a close correlation between the thickness of the low-velocity layer and rock quality (Figure 3-17a). Rock quality was evaluated from observations of the fracture spacing, mineral alteration, faulting, foliation, and schistosity, and was assigned an index rating from 5 (worst) to 1 (best). A similar close correlation was established between the thickness of the low-velocity layer and the seismic velocity of the deep, undisturbed zone (Figure 3-17b).

Resistivity measurements have also been used by the U.S. Bureau of Mines (unpublished) to measure zones of fractured rock surrounding tunnels in the Climax Mine in Colorado. The purpose of these measurements was to establish an index of caveability for the block caving mining method used at the mine. The tunnels were approximately square in cross section, 2.2 m high, excavated using drill and blast methods in a relatively competent granitic gneiss. A Wenner electrode configuration was applied to the tunnel walls, similar to the procedure used at Straight Creek. A high resistivity layer approximately 1.2 to 1.5 m thick was identified. No other observations or indirect measurements of the disturbance around the tunnel were made with which to correlate these results.



(a)



(b)

*From Scott et al (1968)*

Figure 3-17. Thickness of Seismic Low-Velocity Layer as a Function of Rock Quality and Seismic Velocity of the Undisturbed Rock, Straight Creek Tunnel Pilot Bore, Colorado

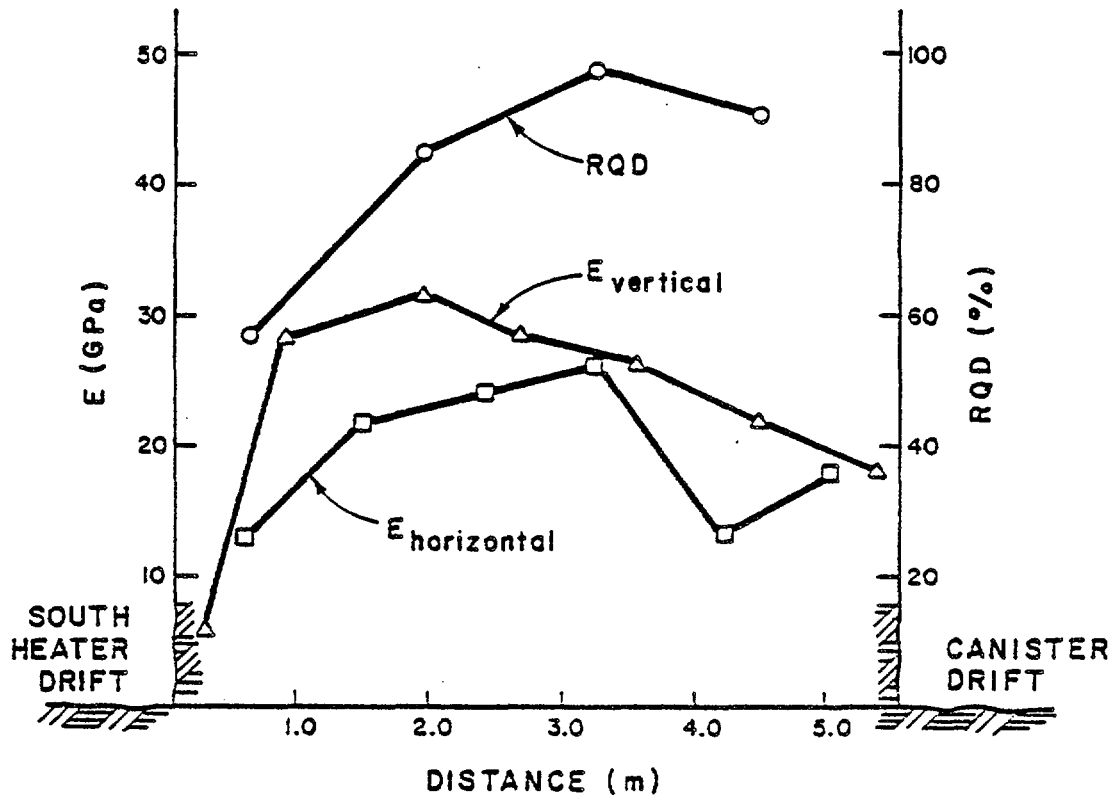
These examples have been included to illustrate that geophysical (mostly seismic) methods have been used to delineate a disturbed zone in a variety of rock types. In some cases, seismic surveys appear to indicate a two-layer disturbed zone with both destressed and compressed (high velocity) zones. In other cases there may be only a destressed zone. Section 5.1.3.1 considers the possibility that this distinction may be related to the direction (longitudinal or radial) in which the seismic waves are transmitted. Section 5.1.3.1 also considers the possibility for estimating permeability from velocities.

### 3.2.3.3 Mechanical Methods

Other methods which have been used to delineate a disturbed zone include fracture logging, borehole extensometers (which indicate displacement toward the excavation), and various techniques for measuring rock mass deformability as a function of distance from the excavation face.

Figure 3-18 shows the variation of in situ modulus and Rock Quality Designation (RQD) measured in the pillar between two parallel tunnels in the Climax Granite at the Nevada Test Site (Heuze et al, 1981a). The moduli were measured using an NX-borehole jack (Goodman Jack) and the RQD was determined from conventional core logging. In hard, unweathered rock, RQD is an expression of fracture frequency. The south heater drift has dimensions 3.3 m high by 3.4 m wide, whereas the canister drift is 6.2 m high by 5 m wide. Both drifts were excavated by blasting.

The Climax results generally show a reduction in modulus of about 50 to 75 percent in a zone adjacent to the tunnel walls about 1.0 to 1.5 m thick. The pattern of the variations across the pillars is similar to the variation in vertical pillar stress obtained from numerical modeling (Heuze et al, 1981b). No clear trend is apparent from the variation in RQD values (particularly when considering other profiles not shown in Figure 3-18). A tentative conclusion from these results is that the disturbed zone results more from stress relaxation (which opens fractures and reduces modulus) than from creation of new fractures by blasting.

**NOTE**

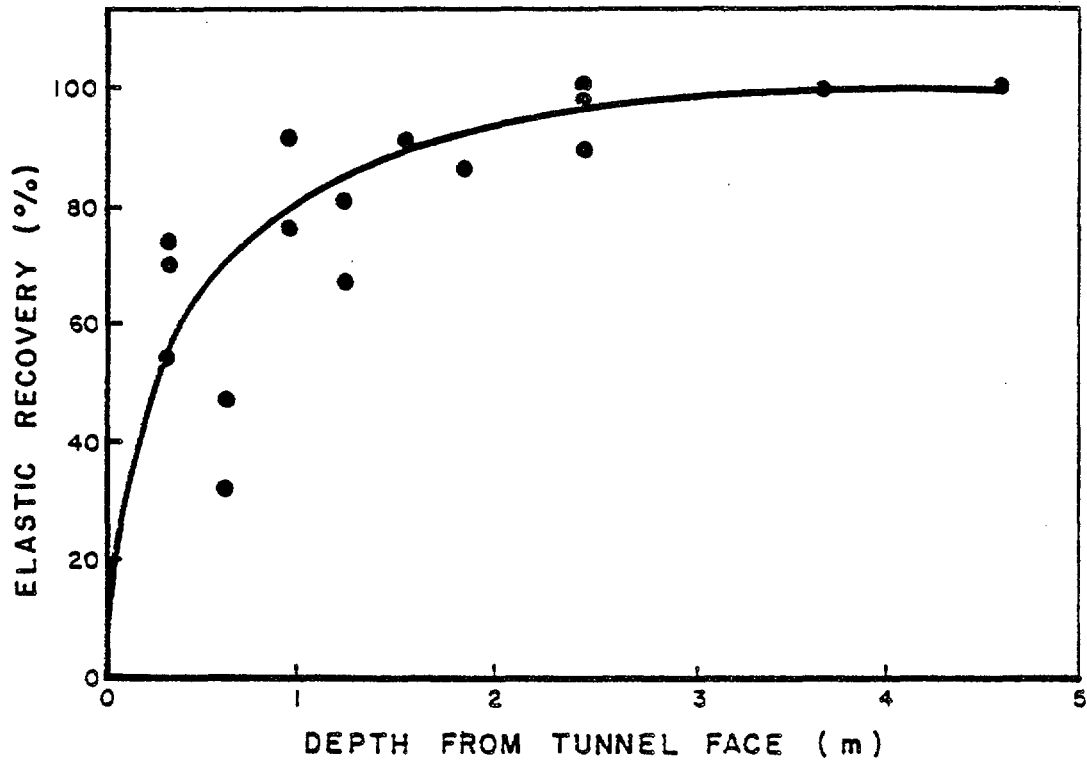
MODULUS DETERMINED BY GOODMAN JACK  
HOLE MBI-7, STATION 2 + 87

*From Heuze (1981a)*

Figure 3-18. Typical Modulus and Rock Quality Designation (RQD) Profiles in Pillar Between Two Drifts, Climax Granite, Nevada Test Site

Plate-jacking tests were used to determine the extent of the disturbed zone at the Churchill Falls underground powerhouse in Canada (Benson et al, 1970). Tests were performed in 2.1 by 2.4 m test drifts excavated in gneiss using controlled perimeter blasting. It was found that the damaged zone was less than 1 m thick with the effects most pronounced within 0.3 m of the tunnel walls. Figure 3-19 shows the degree of elastic recovery observed in the tests as a function of depth from the tunnel wall. Within 0.3 m of the tunnel at least half of the deformation is irrecoverable, whereas at depths greater than 1 m more than 80% is recoverable. The damage observed in these tests was attributed to blast damage rather than to stress relaxation. For some of the tests, up to 0.6 m of obviously blast-damaged material was removed from jacking locations using percussion drills and hammers. In these zones, "minute cracks" parallel to the face could still be seen in drill holes within 0.15 to 0.3 m of the excavated surface.

Multiple-point borehole extensometers have been used in many underground excavations to measure displacements induced by excavation. Extensometers installed at the time of excavation could indicate the true extent of the disturbed zone (as the point at which there is no displacement) and provide a direct measure of the dilation of the rock mass, but it is difficult to relate the measurements to permeability changes. Also, extensometer data are valuable for characterizing rock mass deformational behavior as elastic or plastic (Section 3.1.1). Figure 3-20 shows typical displacement-depth profiles obtained from two large cavities constructed in tuff at the Nevada Test Site (Cording et al, 1971). Three types of displacement are clearly distinguished by the extensometer data. Comparisons between measured displacements and those predicted from elastic theory indicate a low-modulus loosened zone about 1 m thick. A disadvantage of extensometers for distinguishing a disturbed zone is that much of the movement can occur before the extensometer is installed. In a test tunnel a more complete displacement history can be obtained by installing extensometers from a small-diameter pilot bore and then enlarging to full size.

**NOTE**

*2.1m X 2.4m TEST DRIFT IN GNEISS EXCAVATION  
BY CONTROLLED PERIMETER BLASTING.*

*From Benson et al (1970)*

Figure 3-19. Elastic Recovery as Percentage of Total Deformation Observed in Radial Jacking Tests, Churchill Falls, Canada

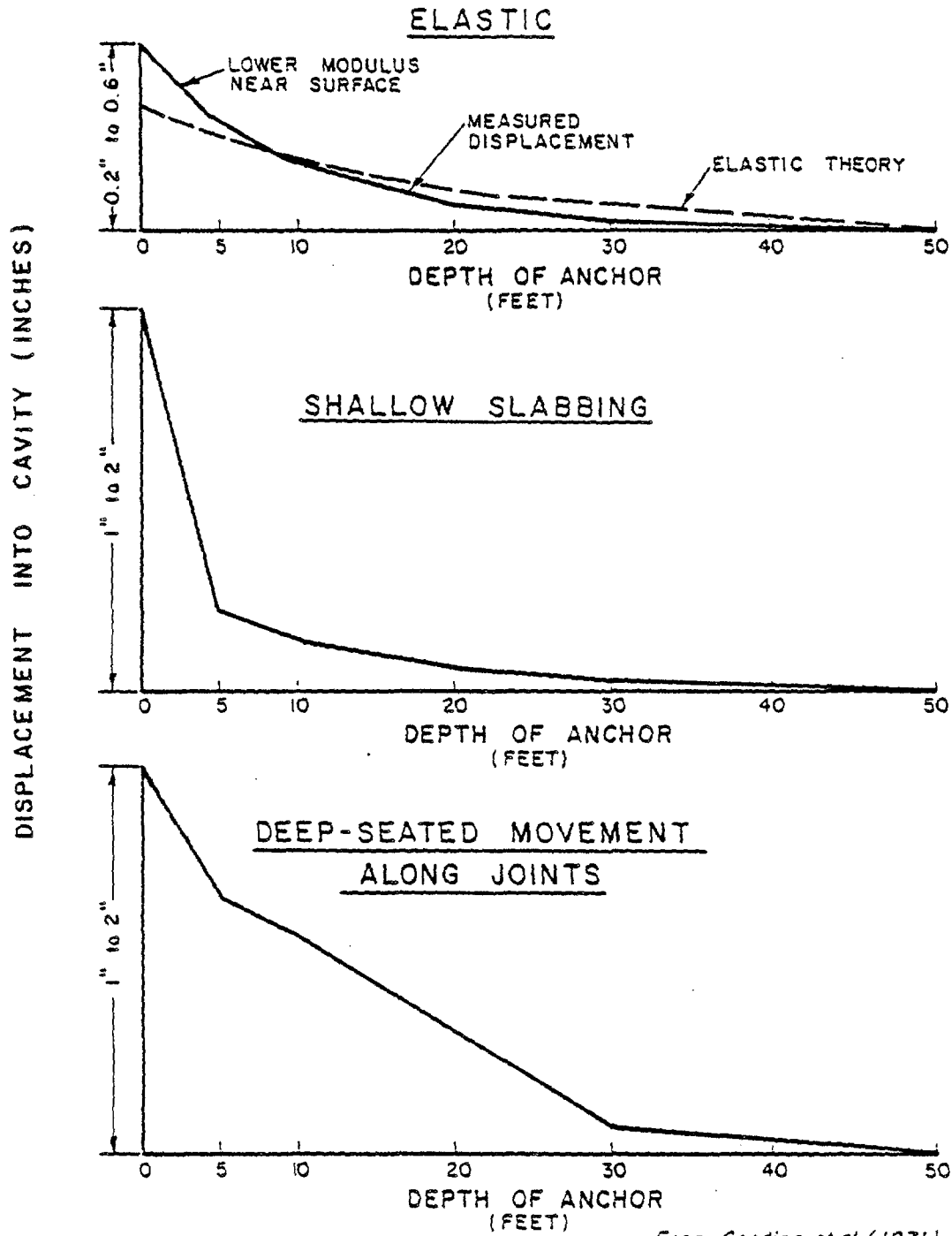


Figure 3-20. Typical Displacement Profiles in Excavated Caverns at the Nevada Test Site

### 3.3 DAMAGE DUE TO BLASTING

#### 3.3.1 Review of Field Investigations

Several of the studies described in the previous sections distinguished damage due to blasting from that due to stress redistribution. At these sites the thickness of the blast-damaged zone ranged from 0.3 m at Stripa to 0.3 to 0.6 m at Churchill Falls, less than 1 m at Colorado School of Mines, and "a few feet" at Straight Creek. Other studies, described below, have evaluated the effects of blasting more specifically.

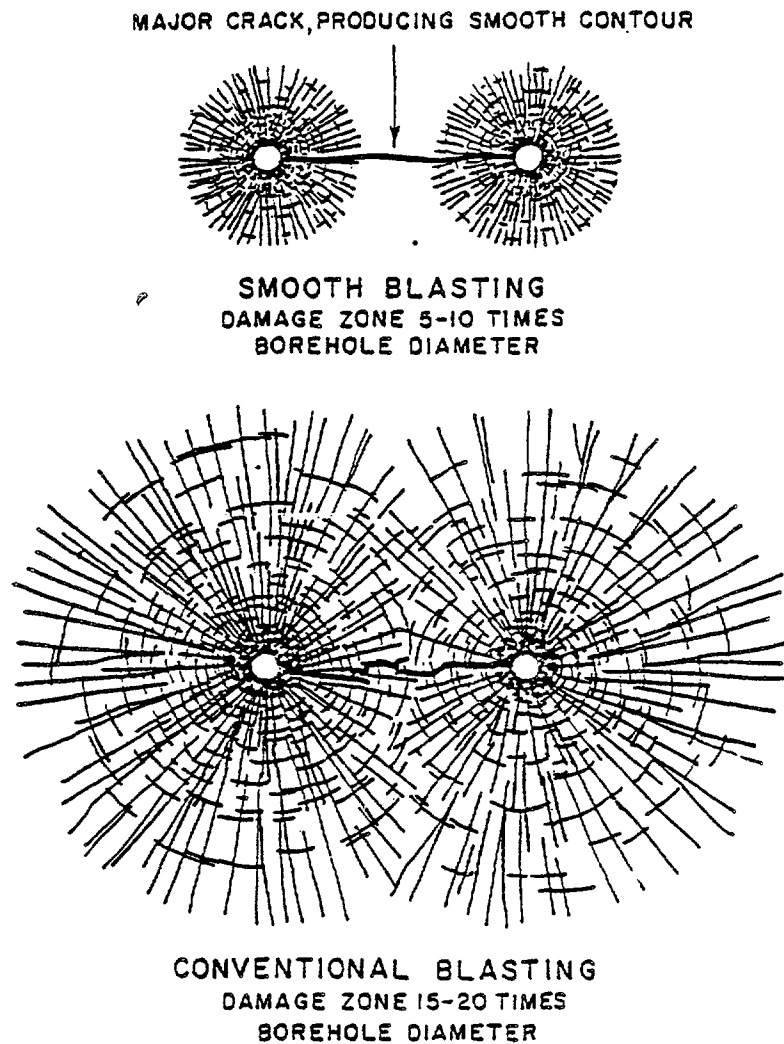
The USBM has conducted experiments to measure blast damage extent around single shot holes in shale (Siskind et al, 1973) and granite (Olson et al, 1973). Although these experiments may not relate directly to tunnel or shaft excavation, they do illustrate general trends. In the granite tests the radius of the damaged zone, estimated from core logging and sonic velocities, was found to increase with increased explosive charge from about 0.25 m for a 0.25 kg charge to 0.77 m for a 2.0 kg charge. Examination of thin sections revealed microfractures extending beyond the damaged zone limit indicated by core logging and velocities. In the shale tests the damaged zone extent was found to be related to charge and to the type of explosive. Approximate radii of the damaged zone for explosive loadings of about 1 kg/m ranged from 1 to 1.3 m for high energy dynamite to 0.3 to 0.5 m for low energy ANFO.

Subsequently, the USBM examined the fracturing produced in the vicinity of large-diameter production blastholes in granite (Siskind and Fumanti, 1974). Damage was assessed by testing cores recovered from the vicinity of the blasthole. Properties determined included porosity, permeability, tensile and compressive strength, Young's modulus and acoustic pulse velocity. The results for a 165 mm diameter hole charged with ANFO indicated that the rock was highly fractured to a radius of 0.65 m (8 blasthole radii), and partly fractured to a radius of 1.14 m (14 blasthole radii). No damage was detected beyond 1.14 m radius. Hocking and St. John (1979) summarized the USBM work and derived a general conclusion that the diameter of blast-damage zones for a high-energy

explosive in hard rock such as granite should range from 15 to 20 charge diameters. For a low-energy explosive, used as a decoupled explosive in smooth wall blasting, the damaged zone should be only 5 to 10 charge diameters. Figure 3-21 shows a comparison between smooth blasting and conventional blasting based on these values. For 35 mm diameter perimeter holes, as used at Stripa (Andersson and Halen, 1978), the predicted damaged zone would extend about 175 to 350 mm. This is in excellent agreement with the observed 0.3 m thick damage zone.

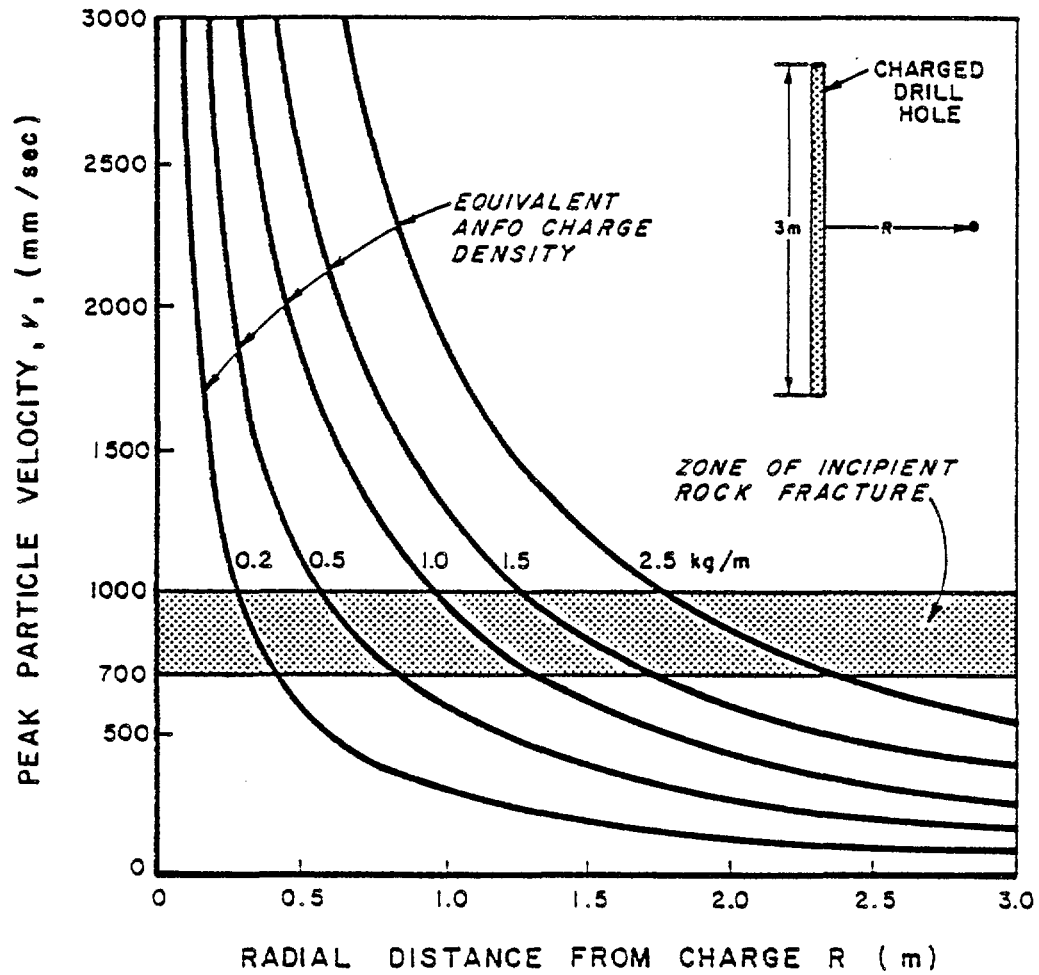
A general relationship between blast damage and charge density for tunnel blasting conditions has been developed from Swedish experience in granitic rocks by Holmberg and Persson (1980). Figure 3-22 shows a series of correlations between peak particle velocity and radial distance from the charge for varying charge densities normalized for explosives with the weight strength of ANFO. The potential extent of the damage zone is indicated by the range of peak particle velocity associated with incipient rock fracture. This shows that a charge density of 1.5 kg/m ANFO should produce a damaged zone of about 1.5 m thickness. If the charge density (in the perimeter holes) is reduced to 0.2 kg/m, the damaged zone extent should be reduced to about 0.3 m. This reduced charge density can be achieved using an explosive with a lower linear charge density than ANFO. For example, GURIT, a special explosive used for smooth blasting in Sweden, has a linear charge density equivalent to 0.2 kg/m ANFO.

Figure 3-22 provides a general guideline for estimating the extent of the damage zone in hard, competent rocks when blasting parameters are known. The data suggest that blast effects are largely independent of excavation size. In practice, the extent of damage, relative to the size of the excavation, may be greater for smaller openings because of the effects of additional confinement. Also, the extent of the damage zone will be influenced by other parameters such as control of blasting procedures and rock conditions.



*After Hocking and St. John, 1979*

Figure 3-21. Comparison of Fracture Patterns Resulting from Smooth Blasting and Conventional Blasting



*From Holmberg and Persson (1980)*

Figure 3-22. Method for Estimating Thickness of Blast-Damaged Zone in Relation to Explosive Charge Density

### 3.3.2 Permeability Changes Due to Blasting

Permeability changes associated with blast damage may be estimated from the increase in fracture frequency that is anticipated within the damaged zone. For example, consider a rock mass in which the natural fracture frequency is 10 fractures/m. Blasting is then assumed to create new fractures such that the frequency increases to 100 fractures/m within 0.3 m of the opening and to 30 fractures/m between 0.3 m and the edge of the blast-damaged zone at 1.0 m depth from the opening. (As a conservative assumption, this increase in fracture frequency is greater than has been observed at Stripa and other sites where controlled blasting has been used; Section 3.3.1.) If the newly-created fractures have similar characteristics to the pre-existing fractures, the increase in permeability due to blasting will be about 10 times in the outer zone and 5 times in the inner blast-damaged zone. These effects would be additional to the effects due to stress relief. The significance of these increases in permeability resulting from blasting, compared with the permeability changes resulting from stress relief, is considered in Section 3.4.

The model used to estimate permeability changes associated with blasting must be regarded as very preliminary. The changes in fracture frequency associated with blasting have not been well documented. Also, the assumption that fractures created by blasting have similar characteristics to natural fractures is presently unsubstantiated. Further field testing, or detailed evaluation of ongoing field tests such as at CSM, is required to add confidence to the model presented.

### 3.4 CONCLUSIONS REGARDING DISTURBED ZONE EXTENT IN FRACTURED ROCK

Data from field tests, supplemented by analytical evaluations, indicate a number of general trends regarding disturbed zone characteristics.

1. There have been few measurements of disturbed zone permeability. Existing measurements show that disturbance may be obscured on a small scale (in borehole tests) by the variability of the undisturbed rock and that permeability may vary in the radial and longitudinal directions (as would be predicted from stress distributions).

2. Analytical studies of the effects of stress redistribution indicate that significant disturbance (permeability increased by at least an order of magnitude) may be contained within 1 to 1.5 radii of the excavation face. Disturbance may be slightly greater where high pore pressures exist prior to excavation and when these are slow to dissipate. High temperatures will tend to reduce permeabilities in the disturbed zone, but these effects will be significant only in the storage rooms and tunnels close to the storage rooms, not in the shafts and tunnels close to the shafts. Most of the analyses conducted have been for an isotropic initial stress field. Highly anisotropic initial stresses may result in greater disturbance, particularly if the major principal stress is parallel to a major fracture set.
3. Results for disturbed zone investigations where parameters other than permeability have been measured vary according to the method used and how the disturbed zone is defined, as well as according to variation in site parameters. Seismic measurements and modulus determinations at several sites indicate a disturbed zone thickness typically in the range 0.3 to 0.7 times the excavation radius. In these cases the disturbed zone is defined as a distressed zone with no indication of the magnitude of permeability increases. Other examples may be found where the disturbed zone extends greater than one radius. In practice the extent of the disturbed zone will depend on many factors related to site geology, excavation method, depth, and penetration geometry.
4. Few disturbed zone studies specifically distinguish blast damage and stress relaxation effects. Available data indicate that significant blast damage (creation of new fractures) may be limited to a zone 1 m or less thick. The extent of blast damage will be greatly influenced by blasting technique but may be more or less independent of excavation size within the probable limits for repository shafts and tunnels. More severe disturbance may occur in a thin zone immediately adjacent to the face. This zone can probably be removed by machine excavation and may not be a consequence to sealing.

These preliminary conclusions are illustrated as a disturbed zone model for a 3 m diameter shaft in basalt (Figure 3-23). Although this model is tentative it is more realistic than a model which assumes a uniform permeability across the disturbed zone. The model used to predict the effects of stress redistribution was developed for basalt at a depth of 1000 m based on an elasto-plastic stress distribution and a hydrostatic initial stress condition. The model is probably conservative for

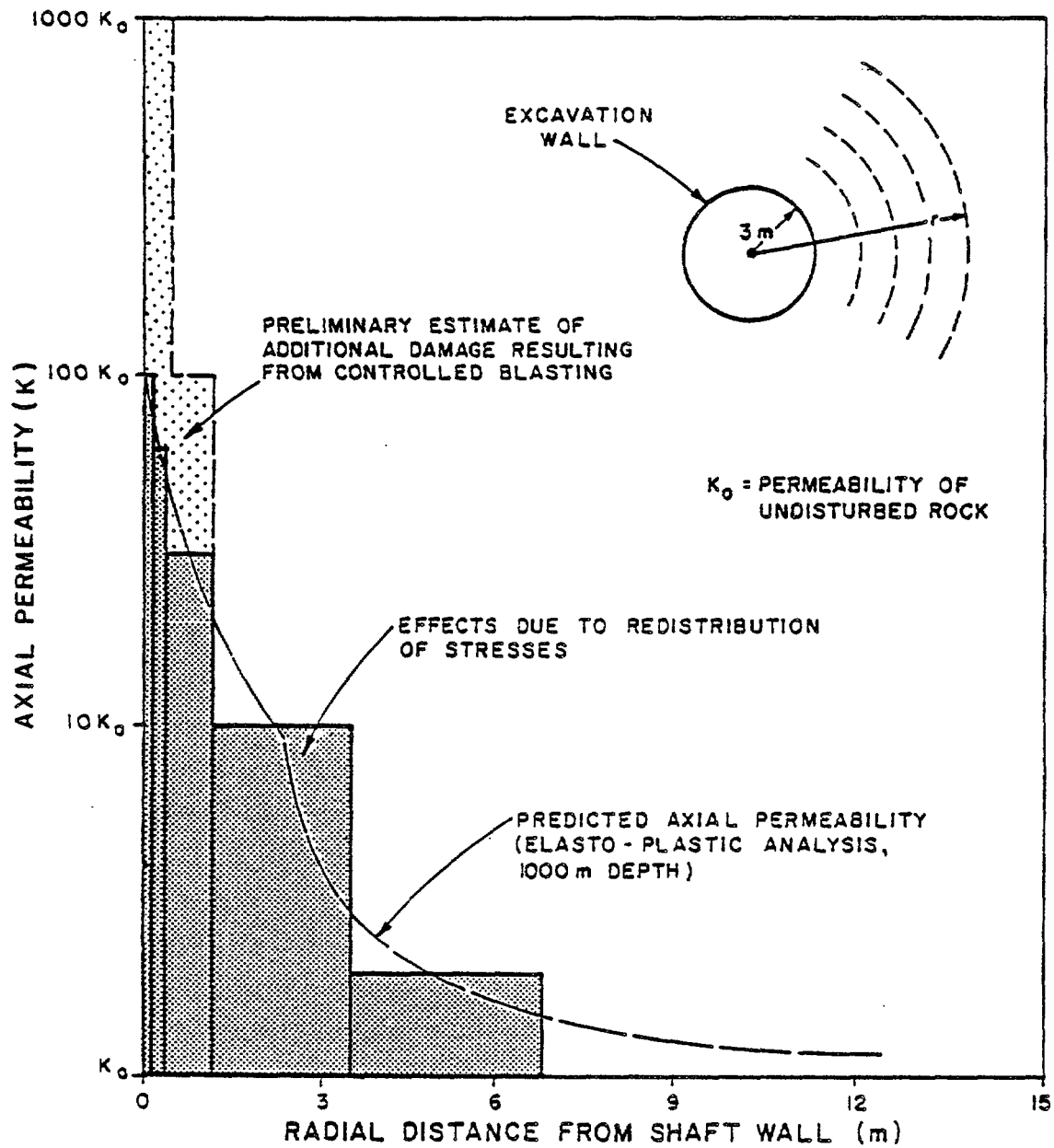


Figure 3-23. Preliminary Disturbed Zone Permeability Model for a 3m Radius Shaft in Basalt at 1000m Depth (Elastoplastic Analysis and Isotropic Initial Stress Condition)

shallower depths. As noted previously, the effects attributed to blast damage are derived from a preliminary estimate and require field confirmation.

The model shown in Figure 3-23 highlights that the increase in permeability due to disturbance diminishes away from the penetration wall. Taking into account the estimated damage due to blasting, approximately 80% of the flow through the disturbed zone would occur within 1 m of the wall of a 3 m radius shaft. Discounting the effects of blasting, approximately 60% of the flow would occur within 1.5 m of the wall. (These analyses assume that the effective edge of the disturbed zone - i.e., where there is no increase in permeability - is at a depth of 12 m from the wall.) Beyond one radius, the flow in successive annuli of equal width is essentially the same in each, because the effects of reduced permeability and increased area with increasing radius are counteracting.

Using on the model in Figure 3-23, it can be shown that blasting accounts for approximately 50 to 70 percent of the increased flow potential through the disturbed zone caused by blasting and stress relief combined. (The proportion due to blasting reduces as the penetration diameter increases because the blast-damaged zone is assumed to have the same depth regardless of the penetration size.) All of the blast damage occurs within 1 m of the penetration face, however, with a substantial proportion within 0.3 m of the face. This damaged "skin" could be removed in critical seal zones by machine excavation. In contrast, it appears that it may not be technically feasible or cost effective to attempt to intercept flow at distances from the excavation much greater than one radius. Also, because of the area effect, there is probably no practical means for restoring the permeability throughout the disturbed zone to that of the undisturbed rock.

The analyses presented in this report are based on several simplifying assumptions and are regarded as preliminary. It is recommended that the analyses be updated to be site-specific to candidate repository sites.

More rigorous analyses should take into account:

- further review of ongoing laboratory and field testing of stress-permeability relationships for fractures,
- stress distributions for proposed tunnel geometries and anticipated in situ stresses,
- further consideration of blasting effects, in particular comparing characteristics of natural and blast-induced fractures,
- continuing review of field tests, especially at Colorado School of Mines.

Eventually, the models presented in this report as well as those developed in the future will be validated by in situ testing at repository sites. Test methods for characterizing the disturbed zone are evaluated in Chapter 5.0.

#### 4.0 DISTURBANCE ASSOCIATED WITH SHAFTS AND TUNNELS IN SALT

As in fractured rock, the most probable mechanisms for disturbance in salt are damage due to blasting and the effects of stress redistribution. The response of salt to stress redistribution is likely to be rather different, however, because there are few if any natural fractures in salt, and because the strength of intact salt is significantly less than that of rocks such as basalt considered previously. Evidence for disturbed zone characteristics may be obtained by analysis and from the results of previous field investigations.

##### 4.1 ANALYSIS OF DISTURBANCE DUE TO STRESS RELIEF

Indirect evidence that the permeability of salt may increase close to an excavation is obtained from laboratory tests which show that permeability is dependent on confining stress. Results from several sources (Figure 4-1) compiled by Isherwood (1981) show permeability reduced by 5 to 6 orders of magnitude as confining stress is increased from zero to 10,000 psi (69 MPa). In these tests the higher permeabilities at low stress levels are probably due to loosening of the crystal structure in response to stress relief and physical sample disturbance. A reasonable assumption is that similar increases in permeability might occur in response to stress relief adjacent to a shaft or tunnel.

Lai (1971) presents laboratory data that relate salt permeability to mean confining stress and octahedral shear stress. Figure 4-1 shows that Lai's data corresponds to results obtained by other workers in the confining stress range of 1000 to 10000 psi. If the stress distribution around a shaft or tunnel is known, Lai's data can be used to predict the variation of permeability with distance from the opening. Figure 4-2 shows the variation in permeability calculated by this method for a shaft or tunnel at a depth of 610 m (2000 feet). The analysis assumes a hydrostatic state of stress and a power law for the secondary creep response of the salt. The stress distribution shown is the steady state

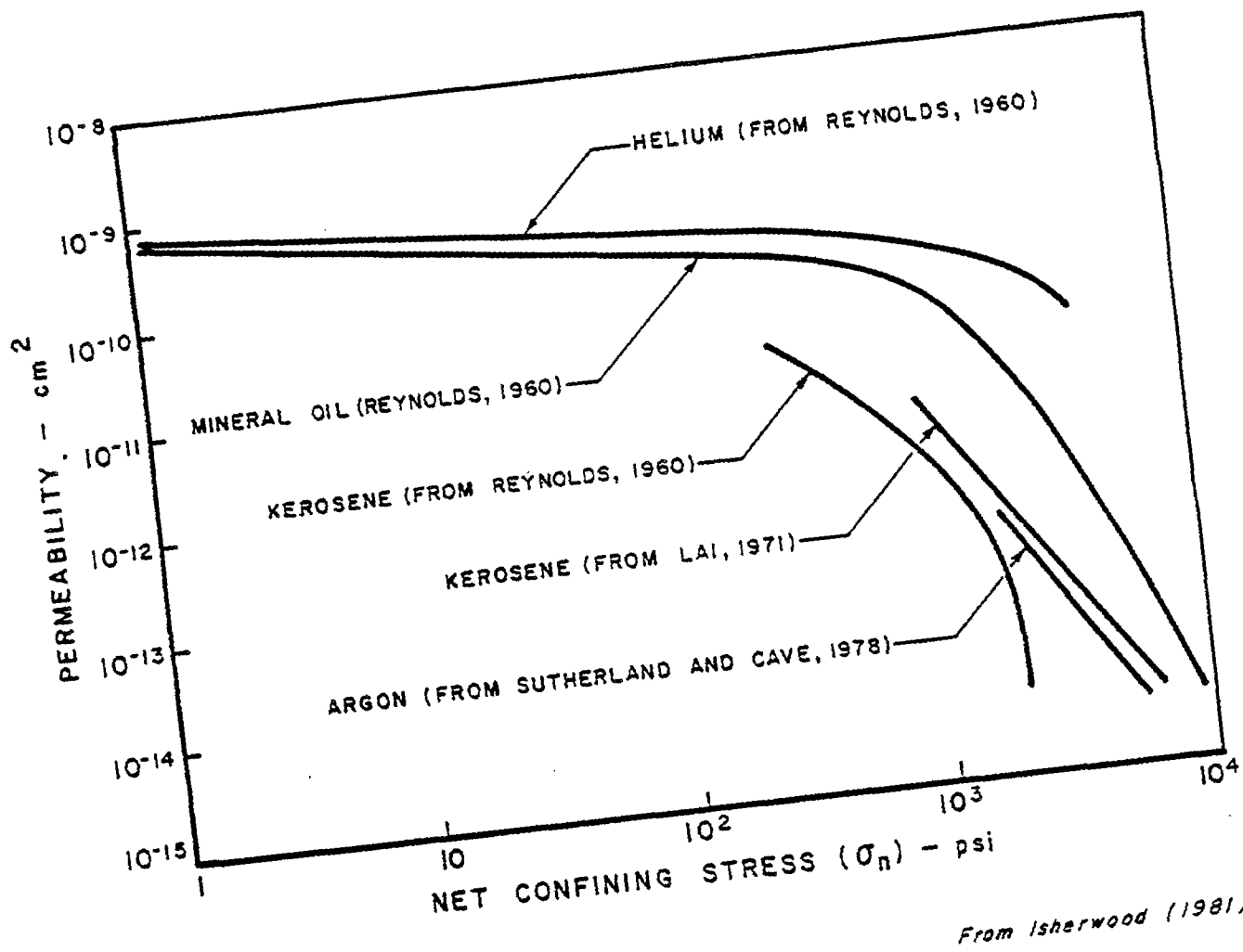
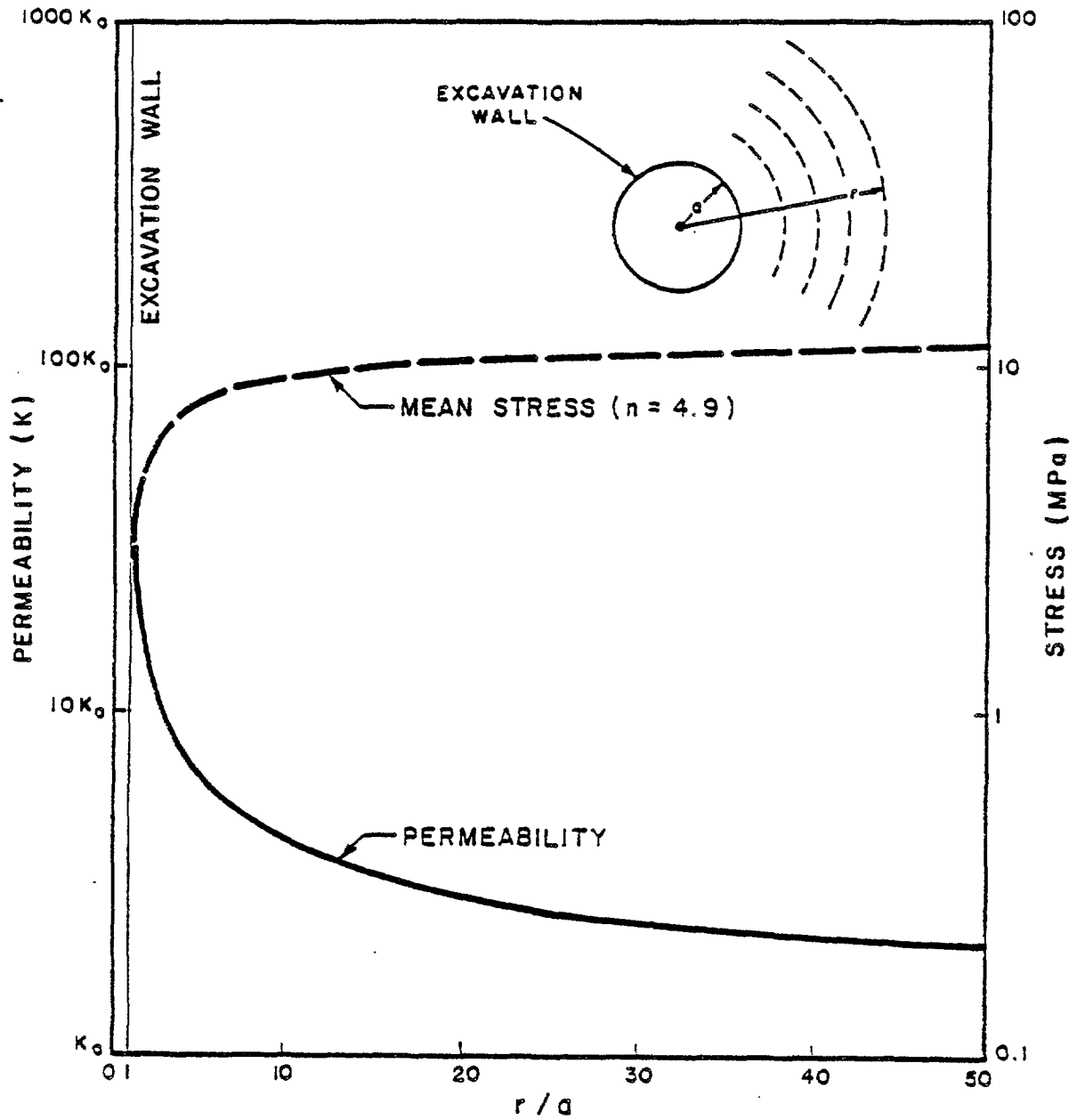


Figure 4-1. Permeability of Rock Salt as a Function of Hydrostatic Confining Pressure



$K_0$  = Permeability in undisturbed salt  
 WIPP stress exponent ( $n$ ) from Herrman et al (1980)

Figure 4-2. Predicted Disturbed Zone Permeability for Salt Based on Steady State Stress Distribution

condition that pertains when the stress relaxation due to creep is complete (Chabannes, 1982). The analytical solution indicates that the final stress distribution is a function only of the stress exponent ( $n$ ) in the constitutive relation for the salt. The time required to reach the steady state condition is inferred to be small relative to the operational life of a repository shaft or tunnel.

The observed increase in permeability close to the wall of the excavation is related primarily to the decrease in mean stress. The maximum increase is relatively small because the mean stress does not reduce to zero. Whereas the magnitude of this increase is less than that predicted for fractured rocks, the lateral extent of the disturbed zone is greater for salt. Provided that the initial stress state is hydrostatic, the effects predicted by this analysis apply to both shafts and tunnels.

The disturbance mechanism discussed above involves loosening of the crystal fabric perhaps combined with some microfracturing. Another possible mechanism for disturbance in salt would involve macroscopic fracturing similar to the slabbing observed in pillars in salt mines (Section 4.2). Nair and Singh (1974) discuss a creep rupture failure criterion for salt whereby failure occurs in response to a critical strain rather than to a critical stress. Considering the state of stress around a shaft or tunnel, the relatively high tangential stresses coupled with low radial stresses in the vicinity of the excavation wall create a state of triaxial extension. Laboratory triaxial extension tests show that rupture can occur in relatively short time periods. Applying these results to the field, it appears that rupture could occur in a shallow zone surrounding an opening, but propagation of the failed zone should be prevented by the increased confinement at greater depths.

#### 4.2 EVIDENCE FROM PREVIOUS FIELD INVESTIGATIONS

Some evidence regarding the extent of a disturbed zone in salt is obtained from geotechnical investigations conducted in Gulf Coast salt mines. In the Cote Blanche Mine there is a visible blast damage zone containing minor fractures extending up to 1 m into the pillars (Golder, 1977). Loose slabs remaining after blasting are removed, but over a period of about one year additional vertical fractures develop in a zone extending 1 to 2 m further into the pillar. These fractures eventually extend the full height of the pillar and large slabs become detached from the pillar. Slabs in 8 m high pillars are typically 1 m thick, whereas slabs in 24 m high pillars are 1.5 to 2 m thick. Except at the corners, the slabs form parallel to the pillar face. Golder examined a number of boreholes drilled into pillars without obvious slabs and found fractures only within 0.6m of the pillar face. These fractures were attributed to blast damage.

Golder postulated that the slabs form in a blast-damaged zone in response to a relatively high uniaxial state of stress that exists near the pillar face. Acres (1977) examined similar slabbing in the Weeks Island Mine and suggested that the slabs might be related to creep rupture (i.e., failure due to excessive strain) as well as to brittle fracture in response to rapid unloading at the pillar edges. At both Cote Blanche and Weeks Island it appears that fracturing in the pillars is restricted to the outer 1 to 2 m. When slabs are removed for safety reasons, it appears that the slabbing process is "rejuvenated" into the pillar, but at a slower rate than the initial slabbing. Similar slabbing phenomena have been observed by the authors in potash mines in New Mexico.

Barron and Toews (1963) used extensometers to measure displacements around a 5.5 m diameter shaft in salt in Saskatchewan at a depth of 939 m. Extensometer anchors were installed at depths of 15 cm, 1.2 m, 2.1 m and 3 m. Measurements at the three outer anchors indicated constant volume creep with the radial displacement inversely proportional to the

radius to the measurement point. Displacement at the anchor closest to the shaft wall was less than would be predicted from the other measurement points assuming constant volume creep extending to the shaft wall. This indicated that there was a surface "skin", up to 1.2 m thick, with material properties different from those of the salt at depths greater than 1.2 m. The displacement measurements indicated that the material within this surface skin was compacting in response to the deeper-seated creep. Barron and Toews considered that the changed properties more likely resulted from blast damage than from failure due to excessive creep.

Aufricht and Howard (1961) performed in situ permeability tests in the Grand Saline and Weeks Island Mines. Tests were run in 3.4-3.7 m boreholes drilled into pillars with a packer sealed in the hole 0.6-1.5 m from the pillar face. Gasoline was injected to the hole at constant pressure and the flow rate observed against time. The permeabilities obtained ranged from 0 to 6 millidarcies with an average of about 0.3 millidarcies. In one test at Weeks Island the packer was set a depth of 1 m and Freon was injected in the hole at 60 psig. After a few minutes, small quantities of Freon were detected escaping from the face of the pillar at distances of up to 4.3 m from the borehole. This result is consistent with the observations of pillar spalling discussed above, although presumably Aufricht and Howard did not perform their tests at locations with obvious slabs. Acres (1977, 1979) conducted similar permeability tests at Weeks Island, but with the packer set 4.5 to 9 m from the collars of the holes, and diesel fuel or nitrogen used as the permeant. Permeabilities obtained ranged from 0.15 to .0001 millidarcies and were thus generally lower than the values obtained by Aufricht and Howard. Because Aufricht and Howard had set their packer at shallower depths, these results may be taken as evidence for a disturbed zone extending a few meters into the pillars.

#### 4.3 SIGNIFICANCE TO SEAL PERFORMANCE

The preceding sections have indicated that a disturbed zone with increased permeability may exist adjacent to underground openings in salt. Because of the ability of salt to "heal" fractures, the significance of this zone to seal performance is considered to be relatively insignificant in the long term.

Figure 4-1 shows permeability reduced by 5 orders of magnitude as stress is increased from zero to several thousand psi. This reduction in permeability is, in effect, reversing the sample disturbance responsible for the higher permeabilities at low stress levels. Sutherland and Cave (1980) found that the permeability of bedded salt from New Mexico was reduced by about a factor of 3 over a period of 200 hours under a confining stress of 13.8 MPa. At the end of the 200 hour period the measured permeability was still reducing.

Tests to evaluate fracture healing in salt are being conducted by Sandia (Costin and Wawersik, 1980). Preliminary results indicate that healing is effective within a few days when samples are heated in the range 22-100°C and subjected to confining stresses of up to 35 MPa. Healing is considered to result from creep and interlocking of asperities rather than from recrystallization. The Sandia tests evaluated fracture healing in terms of fracture toughness, a parameter which indicates the resistance to crack propagation along an existing fracture. They do not indicate permeability directly although it appears likely that permeability should be reduced significantly along fractures which exhibit high values (approaching values for intact specimens) for fracture toughness. Tests to measure permeability of healed fractures are in progress at Sandia.

It is known from the use of salt bricks for cattle feeding that even crushed salt can be reconstituted to an apparently intact material. Wagner (1980) investigated the strength characteristics of crushed salt consolidated under varying confining stress. Tests were conducted on

two grades of salt at temperatures up to 400°F and stress levels up to 17 MPa. At a volumetric consolidation of approximately 35 percent, one sample attained a uniaxial compressive strength of about 50 percent of the strength of undisturbed, intact salt. Although no permeability measurements were made, the increase in strength would indicate that permeability should be greatly reduced by consolidation.

If a relatively rigid seal component such as a concrete bulkhead is placed in a tunnel or shaft in salt, the salt will creep and the stress acting on the seal and throughout the disturbed zone will rise and eventually approach the lithostatic level. Analyses by Kelsall et al (1982) for southeast New Mexico salt indicate that the stress acting on a concrete bulkhead at 610 m depth will attain 50% of the lithostatic stress level within 10 years. These analyses suggest that any fractures in the disturbed zone may completely heal within a period of the order to 10 to 100 years. Additional analyses, as well as laboratory and field tests, are required to confirm these predictions.

## 5.0 RECOMMENDED METHODS FOR DISTURBED ZONE INVESTIGATIONS

This section describes a number of test methods that might be used to investigate disturbed zone characteristics. Some of the methods have been used for this purpose previously and results have been reviewed in Sections 3.0 and 4.0. Other methods have not been evaluated previously and in some cases modifications in test technique may be required before the method can be applied. In practice it is likely that a disturbed zone investigation will include a number of tests used in combination. Test methods applicable to shafts and tunnels (where direct access is possible), and to boreholes (where remote methods must be used), are reviewed separately in Sections 5.1 and 5.2.

### 5.1 TEST METHODS FOR SHAFTS AND TUNNELS

It has been noted that permeability is the disturbed zone characteristic of most interest to repository sealing. Consequently, test methods of greatest interest are those that measure permeability directly. Other test methods may be used as indirect measures of permeability or to determine other properties of interest such as deformability. Test methods reviewed in the following sections include:

- Hydrologic tests
  - packer tests in boreholes
  - tracer tests between boreholes
  - macropermeability tests
- Geologic tests and observations
  - fracture mapping
  - core logging
  - integral sampling/dye penetrant
  - borehole periscope
  - impression packer
- Geophysical methods
  - seismic refraction
  - petite sismique
  - cross-hole seismic
  - resistivity
  - radar
  - borehole logs

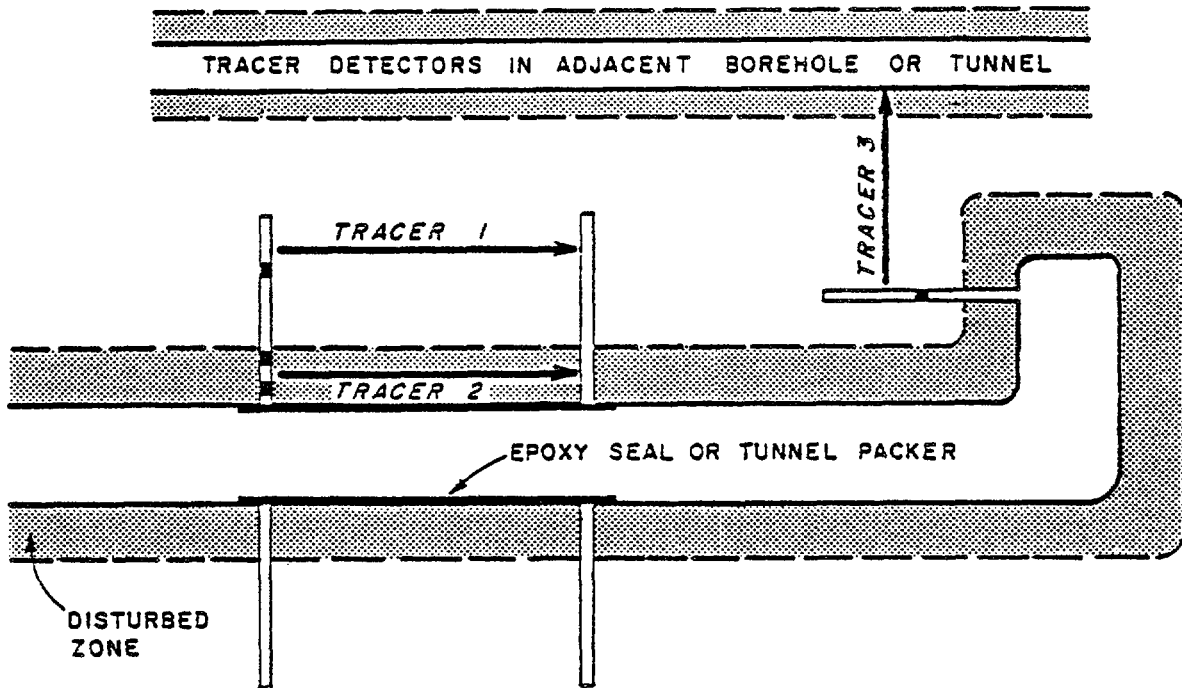
- Mechanical tests
  - plate loading tests
  - borehole deformation jacks
  - extensometers

These tests are reviewed according to their applicability to disturbed zone evaluation in various rock types. Test methods are described in detail only where they are not commonly known.

#### 5.1.1 Hydrological Tests

The most common method for measuring rock permeability in situ is to inject a fluid into a section of a borehole isolated by packers. Several variations of the technique are used, with liquid or gas as the permeant, with two packers or with a guarded system employing four packers, and measuring either steady state flow at constant pressure or a pressure decay after a pressure has been applied. One of these methods (depending on site specific conditions) might be used for disturbed zone investigations by testing in boreholes drilled from a shaft or tunnel to penetrate through the disturbed zone into the undisturbed rock mass. Air permeability and guarded straddle packer tests are being used in the Colorado School of Mines investigations (Section 3.2.1). Test methods for air-injection are described by Chan et al (1974) and Miller et al (1974).

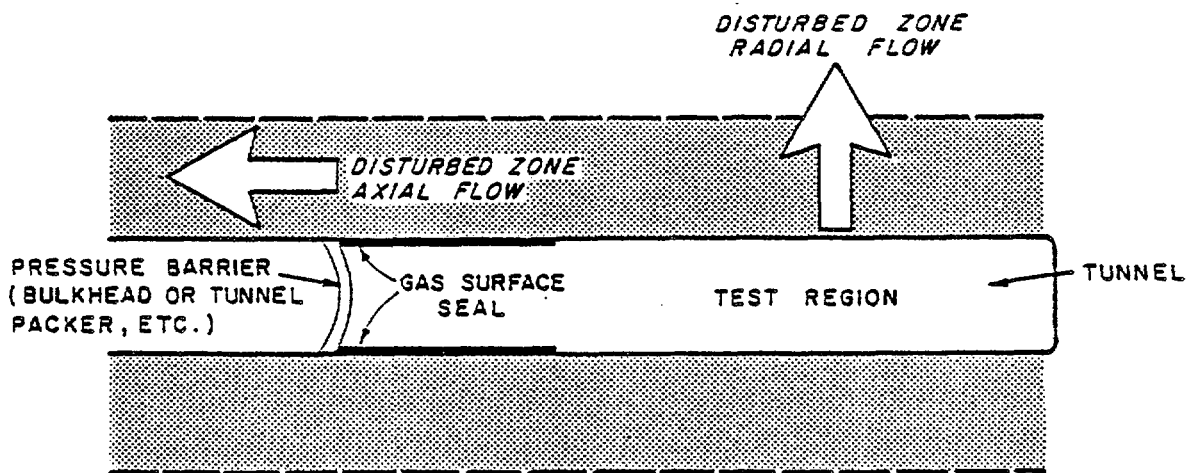
Figure 5-1 shows a conceptual arrangement for disturbed zone characterization using injection tests in boreholes. Cross-hole tests using tracers can be used to determine travel times parallel to the tunnel axis. By testing between adjacent tunnels, it will be possible to obtain travel times in the perpendicular, radial direction. Chan et al (1974) describe a test method using air, whereby both the injected air volume and the air volume entering the monitoring hole(s) are measured. This method may be useful to give some comparison of the interconnection (continuity) of fractures in the disturbed and undisturbed zones. The same boreholes used for permeability testing can be used for fracture logging and cross-hole seismic surveys as discussed below.



**NOTE**

SAME BOREHOLE ARRANGEMENT TO BE USED FOR CROSS-HOLE SEISMIC.

Figure 5-1. Test Concept for Disturbed Zone Evaluation Using Tracer Injection and Cross-Hole Seismic



After Peterson and Lagus (1980)

Figure 5-2. Macropermeability Test Concept for Disturbed Zone Evaluation in Rock Above Water Table

A shortcoming of borehole permeability tests in fractured rocks is that a very small volume of the rock mass is sampled by each test interval. Test results are strongly influenced by the number of fractures intersected by the borehole and if the test intervals are short there is likely to be a considerable scatter in the permeability values obtained. At Hanford, for example, measured permeabilities in 12 tests in columnar Grande Ronde basalt range from  $10^{-7}$  to  $10^{-12}$  cm/sec (Rockwell Hanford, 1979). In a disturbed zone investigation it is likely that disturbance will be at least partly obscured by local variability in the undisturbed rock mass. With borehole testing, it may be difficult also to test in the zone immediately adjacent to the excavation face. This difficulty may be overcome by sealing the excavation face (Figure 5-1).

An alternative to borehole testing is some form of macropermeability test. One such test conducted at Stripa has revealed a zone of reduced permeability around a tunnel. As noted in Section 3.2.2, this type of drainage test induces flow dominantly in the radial direction toward the tunnel and the reduced permeability may result from a tangential (longitudinal) stress concentration. This type of test does not indicate permeability in the longitudinal direction.

For seal design purposes the longitudinal permeability parallel to the penetration axis is of greater interest. A macropermeability test to measure this parameter has been proposed by Systems, Science and Software (Peterson & Lagus, 1980). This test would employ a gas-tight seal to isolate a closed section of tunnel (Figure 5-2). Gas would be injected into the isolated section and the pressure response monitored on both sides of the seal. Any significant disturbed zone that would promote preferential flow longitudinally along the tunnel would be distinguished by a characteristic pressure response. Tracer gas would be used to indicate travel time. This test is conceptual and has not been evaluated in the field. Because low pressure gas is used, the test may be limited to "dry" rocks above the water table. Nonetheless, the method appears highly promising and a field trial is recommended.

## 5.1.2 Geologic Tests and Observations

### 5.1.2.1 Mapping

Detailed geologic mapping of a tunnel or shaft may provide some indication of surface disturbance resulting from the excavation process. Mapping should distinguish spalling effects and cracks obviously formed by blasting. Primarily, however, detailed mapping is required to support other tests by defining the fracture system.

### 5.1.2.2 Core and Borehole Logging

Information regarding fracture characteristics in the disturbed zone may be obtained from core holes drilled radially from the penetration. A disadvantage of logging fractures from cores is that it is often difficult to distinguish natural fractures from breaks in the core induced by drilling. This problem can be overcome using the integral sampling method developed by Rocha (1971). The method consists of first drilling a small diameter borehole into the area to be sampled. A hollow reinforcing bar is then inserted and grouted in the hole and, after the grout has cured, the complete assembly is over-cored.

Integral sampling yields a continuous section of core in which separate blocks of the rock mass are held together in their natural relative positions. In some cases it may be possible to estimate fracture apertures and permeabilities (Rocha & Franciss, 1977). Colored dyes can be used with resin grouts to aid core inspection.

Other methods which may be used in combination with conventional core logging are the borehole periscope (borescope) and impression packers. The borehole periscope, which consists of a rigid tube supporting a system of lenses and prisms, has been used to depths of up to 100 feet in holes drilled from the surface (Krebs, 1967). The impression packer consists of an inflatable packer around which is wrapped a highly inelastic rubber membrane (Baar & Hocking, 1976; Harper & Hinds, 1977). Once positioned in the hole, the packer is inflated and the rubber membrane is pushed into fractures in the wall forming an impression which is retained when the assembly is removed.

A problem common to all borehole methods is that the fracture densities obtained are greatly influenced by local variability and anisotropy. These effects may tend to obscure any variation resulting from penetration disturbance. Also, the methods described may not be sufficiently sensitive to distinguish small changes in fracture aperture which can have a major effect on permeability.

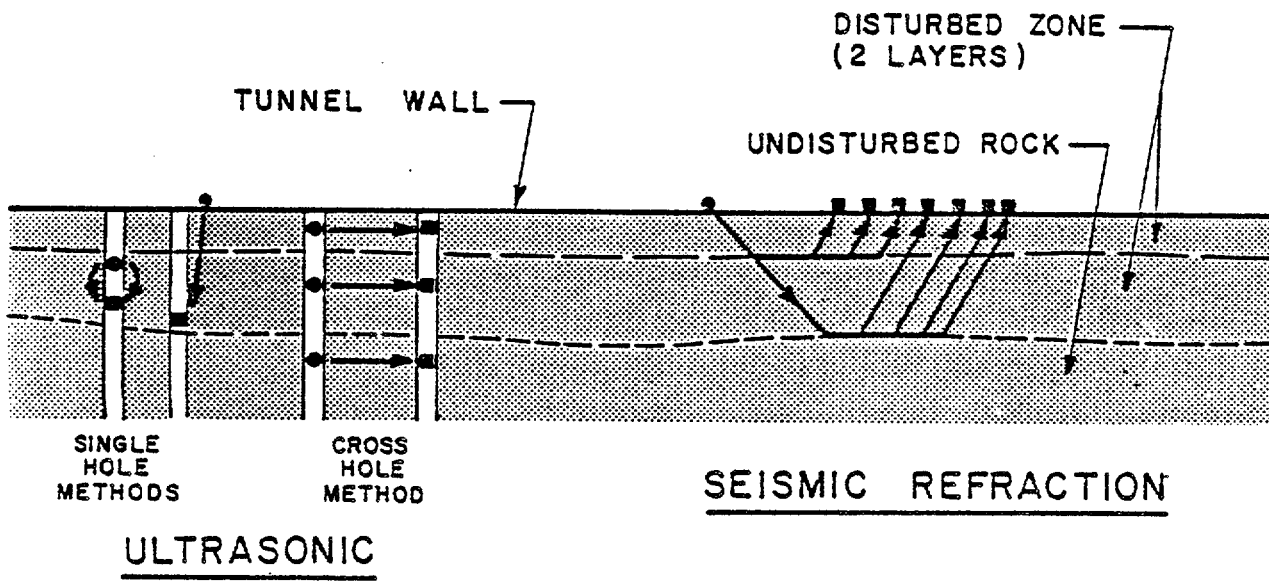
### 5.1.3 Geophysical Methods

#### 5.1.3.1 Seismic Methods

Two types of seismic investigation appear applicable to disturbed zone investigations in shafts and tunnels, seismic refraction and ultrasonic (cross-hole or single-hole) surveying (Figure 5-3). Seismic refraction surveys are conducted by generating a seismic shock at the tunnel face and monitoring wave arrival time at geophones spaced along the tunnel. Explosive charges, sledge-hammer blows, or sparking devices may be used to generate the waves. Interpretation is normally based on the first arrival compressional wave. By plotting arrival times against distance from each geophone to the source, it is possible to distinguish velocity contrasts in the rock mass. Examples of the successful use of seismic refraction to delineate a distressed zone around a tunnel were given in Section 3.2.3.2.

"Petite sismique" is a variation of the seismic refraction method developed in France by Schneider (1967). Bieniawski (1978) provides an updated review of the method. Whereas conventional seismic methods utilize seismic velocities (mostly of compressional waves), the petite sismique method takes into account various shear wave properties such as frequency, attenuation and wavelength, as well as velocity. Bieniawski (after Schneider) has demonstrated a close correlation between shear wave frequency and in situ static modulus of deformation, and has compared moduli values determined by a number of methods including petite sismique.

Cross-hole acoustic methods employ a pulsed high-frequency seismic wave transmitted between boreholes. Both compressional and shear waves are



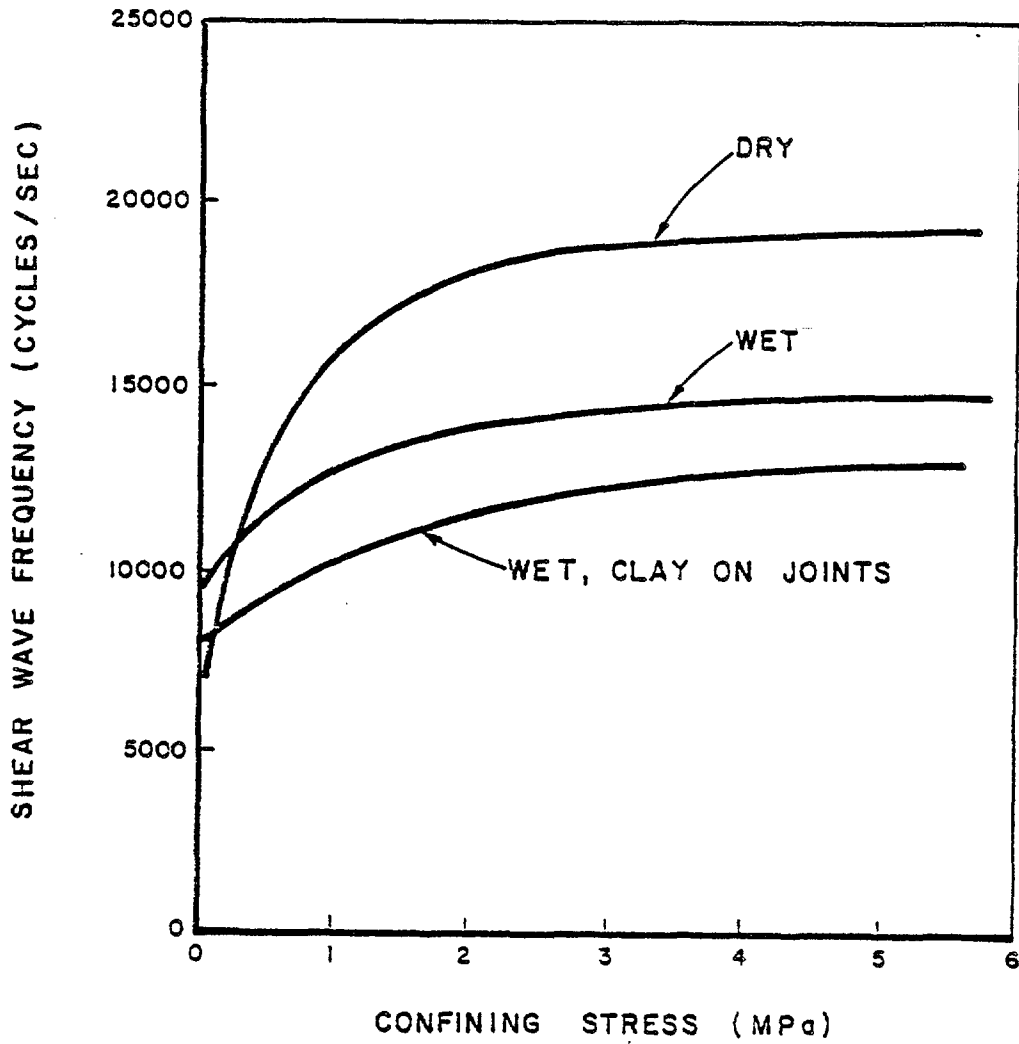
*From Murphy (1972)*

Figure 5-3. Seismic Methods for Delineating Disturbed Zone Extent

utilized, with velocity, frequency and amplitude recorded. Cross-hole methods have been used extensively in rock engineering and the technique is relatively well developed. Extensive instrument development was carried out for tests at Stripa (Nelson et al, 1979; Paulsson & King, 1980).

Seismic velocity is influenced by a number of rock mass characteristics including the density and porosity of the rock material, weathering and alteration, joint spacing and joint opening. In an unaltered rock mass of locally uniform lithology (such as a repository formation), velocity will vary according to joint spacing and opening. Laboratory tests by Stacy (1976) show that other seismic parameters, such as frequency and amplitude of both compressional and shear waves, are in many cases more sensitive indicators of fracture characteristics than velocities. Of particular interest is the effect of confining stress on various parameters, for example shear wave frequency (Figure 5-4). At low confining stress, shear wave frequency is highly sensitive to stress, whereas at higher stress levels the frequency is relatively constant approaching that of the intact rock. Similar results have been reported by New & West (1980) showing that the stress level at which joints become "acoustically closed" depends on rock type and the nature of the joint surface.

The relationship between stress and seismic parameters is very similar in form to the relationship between stress and permeability presented in Section 3.1.3.1 (Figure 3-4). In the case of Stacy's laboratory tests on marble there is a seismic contrast at a stress of about 2 MPa. In the case of the predicted permeability of basalt, permeability increases rapidly at stresses less than 3 to 4 MPa. It appears promising, therefore, that good correlations between permeability and seismic parameters can be established for a particular rock type, and that seismic surveys can be used to estimate disturbed zone permeability. An advantage of seismic methods is that a relatively large volume of the rock mass can be sampled.



*From Stacy (1976)*

Figure 5-4. Variation of Shear Wave Frequency With Confining Stress for Laboratory Tests on Marble

Seismic refraction and cross-hole surveys each have a number of advantages and disadvantages. In the case of refraction, a major advantage is the ease of measurement with little preparation of the measurement location necessary. Surface zones are readily recognized, and the depth of measurement is easily adjusted. A disadvantage is that interpretation requires some subjectivity, and intermediate velocity zones may be misinterpreted or "averaged." In the case of cross-hole measurements, an advantage is that zones of varying velocity parallel to the tunnel wall are readily distinguished. Disadvantages are that it is difficult to characterize surface zones and that drilling is required for measurement. The latter disadvantage is particularly pertinent to characterization of key seal zones where drilling would be undesirable.

With respect to disturbed zone characterization, a further consideration is the direction of wave travel relative to the tunnel axis. Using radial boreholes, cross-hole waves are transmitted longitudinally along the excavation wall (Figure 5-3). The velocities (or other parameters) obtained will be influenced by fractures perpendicular to the excavation which in turn determine radial flow toward the excavation. With the refraction method, waves are transmitted partly in a radial direction and, depending on the source-geophone separation, partly in a longitudinal direction. Parameters measured by seismic refraction should be more sensitive to fractures parallel to the excavation than parameters measured by cross-hole methods.

As reported by Bieniawski (1978), recent developments have greatly improved seismic methods for use in underground excavations and boreholes. Improvements have been made in the methods used to generate shear waves, in signal enhancement techniques, and in understanding of the fundamental relationships between seismic parameters and rock properties. Seismic methods, using refraction (or *petite sismique*) and cross-hole in combination, appear particularly promising for disturbed zone evaluation.

### 5.1.3.2 Resistivity Methods

Resistivity measurements using a Wenner array appear to have potential application to disturbed zone investigations in shafts and tunnels. With this technique, four electrodes are evenly spaced in contact with the tunnel wall (Figure 5-5). A current is supplied to electrodes  $C_1$  and  $C_2$  while electric potential is measured at electrodes  $P_1$  and  $P_2$ . The apparent resistivity obtained is a function of the volume of rock sampled which is in turn determined by the electrode spacing. As the spacing is increased, a greater volume of rock (and a greater depth into the rock) is included in the measurement. By making a series of measurements at one location, using increasing electrode spacing, the true resistivity as a function of depth can be obtained.

Examples of the use of resistivity surveys for disturbed zone characterization were given in Section 3.2.3.2. Although there have been limited applications to date, the method appears to be potentially very useful. Because electrical resistivity is sensitive to the degree of fracturing in the rock and the moisture conditions, the method may be particularly appropriate for fractured media. Further development of the method is needed in order to establish relationships between resistivity and the parameters which influence hydraulic conductivity (e.g., fracture aperture and spacing). Application of the method to salt may be difficult due to the low resistivity of salt and the large amount of power required to make useful measurements.

### 5.1.3.3 Radar

Radar profiling has been used to detect fractures in mine walls in coal and hard rocks (Cook, 1975; Fowler, 1981). In salt, radar has been used to detect boreholes in mine pillars and is being investigated as a technique for locating waste packages after emplacement and backfilling (Cook, 1980). Radar is a promising technique for disturbed zone characterization although, as with resistivity methods, further development is required to establish whether the method is sensitive to the parameters which influence permeability (especially fracture aperture).

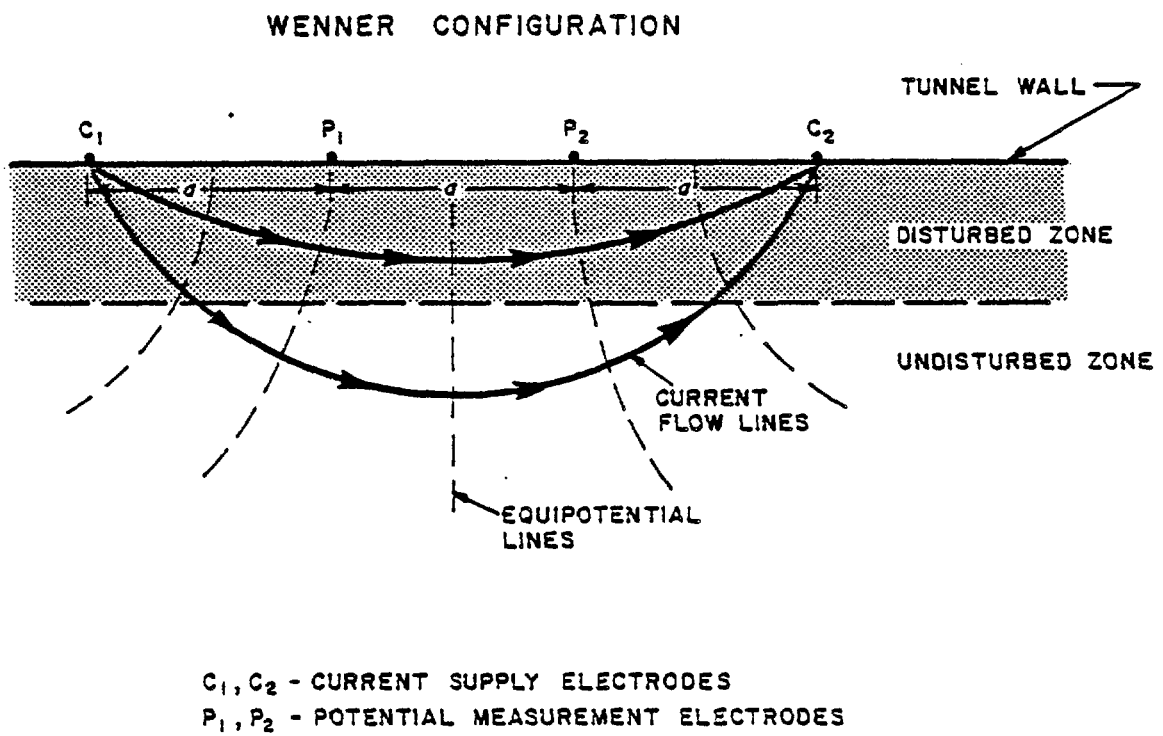


Figure 5-5. Resistivity Method for Delineating Disturbed Zone Extent

#### 5.1.3.4 Borehole Logs

Various geophysical logs can be used to detect fractures in boreholes. These methods have wide application in deep boreholes but they are not highly sensitive to isolated fractures and are more suited to detecting zones of intense fracturing within otherwise unfractured rock. Geophysical logs appear to have little application in shallow boreholes drilled from an excavation where other methods (such as core logging or the impression packer) have much better resolution.

#### 5.1.4 Mechanical Methods

A number of tests used to determine mechanical properties of the rock mass might be used to determine disturbed zone characteristics. Examples of the extent of the disturbed zone indicated by borehole jack, plate loading tests, and extensometers were given in Section 3.2.3.3. Extensometers are particularly useful for characterizing the rock mass deformation as elastic or plastic and for validating analytical predictions of rock mass behavior. Plate-loading tests are useful for determining the extent to which deformations within the disturbed zone are reversible. Extensive testing will be conducted at a repository site to determine mechanical properties required for mine design. These tests can be extended inexpensively to obtain data required for disturbed zone characterization. For example, borehole jack measurements can be repeated at various intervals away from the excavation. These tests would provide values for a parameter of direct interest to seal design, i.e., deformability, and might provide some indication of permeability changes.

#### 5.1.5 Test Program for Fractured Rock

A test program for disturbed zone characterization in fractured rock (such as basalt, granite or welded tuff) should include a combination of several of the tests described above. The test plan would include a comprehensive test program at one or more test locations representative of the geology and the excavation methods used in the repository. The intention would be to establish correlations among the various rock mass properties and select index tests that could be used rapidly and

inexpensively throughout the repository. A candidate index test is seismic refraction profiling, assuming that firm correlations can be established between seismic parameters and permeability.

Figures 5-6 and 5-7 outline a complete program for disturbed zone characterization divided into two major stages. Stage 1 includes scoping studies of the type presented in this report, conducted at the time of site characterization. This stage provides a preliminary disturbed zone model for use in schematic and conceptual seal design. Recommendations regarding repository construction and rock support methods are also made at this time. Stage 2 includes detailed in situ testing and model verification, conducted in an at-depth test facility in the repository formation. This stage provides an updated disturbed zone model for use in preliminary seal design and license application. Correlations between properties are established at this time and index tests to be used in the repository are developed.

A comprehensive test program intended specifically for disturbed zone characterization should include the following tests:

- macropermeability,
- piezometers installed in boreholes at varying distance from excavation,
- injection tests in boreholes,
- cross-hole tracer flow,
- integral sampling in boreholes, and borescope or impression packer logging,
- resistivity and radar profiling,
- seismic refraction (petite sismique) surveys,
- cross-hole acoustic surveys,
- borehole deformation jack,
- plate loading,
- multiple-point borehole extensometers.

STAGE I

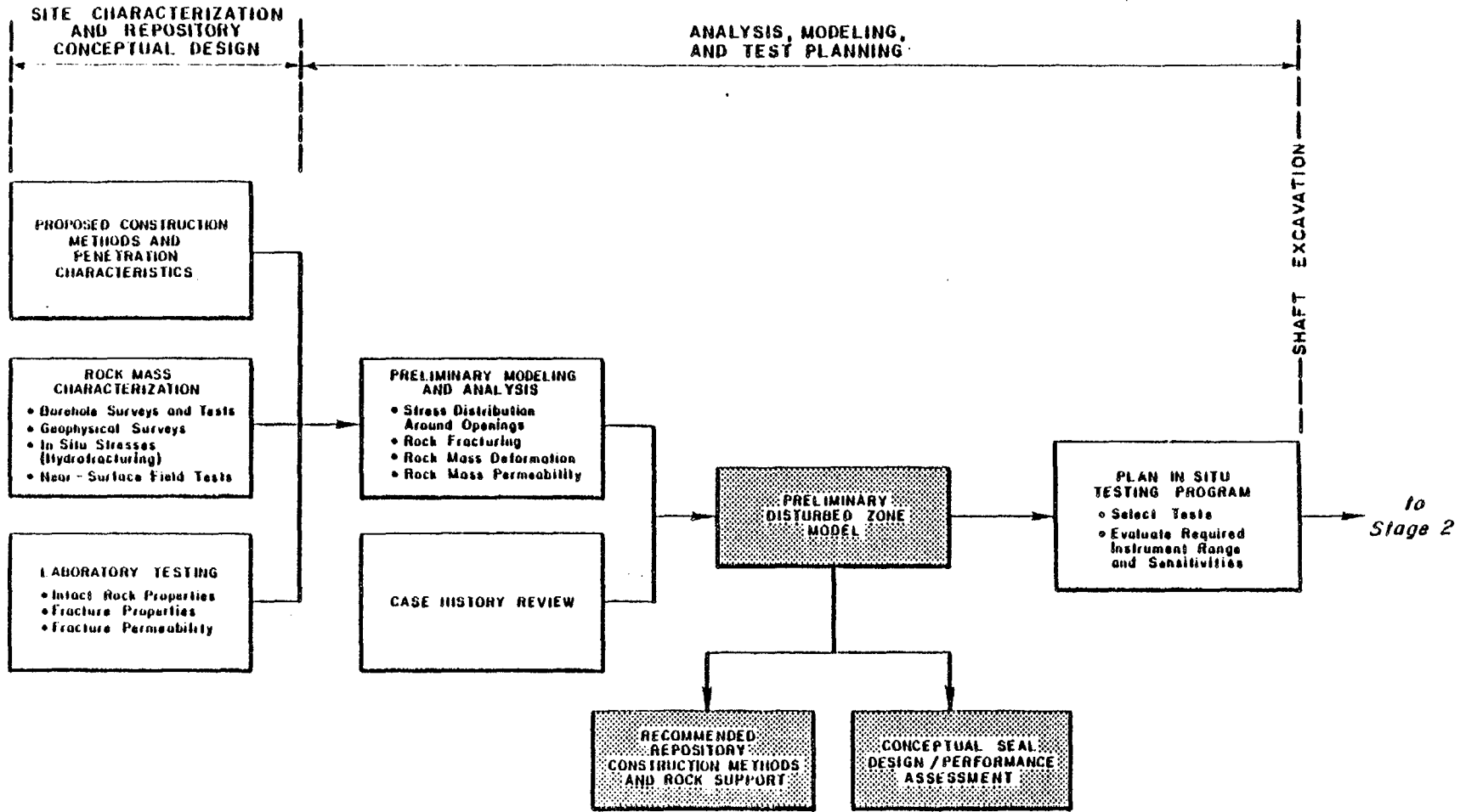


Figure 5-6. Approach for Disturbed Zone Characterization - Stage 1

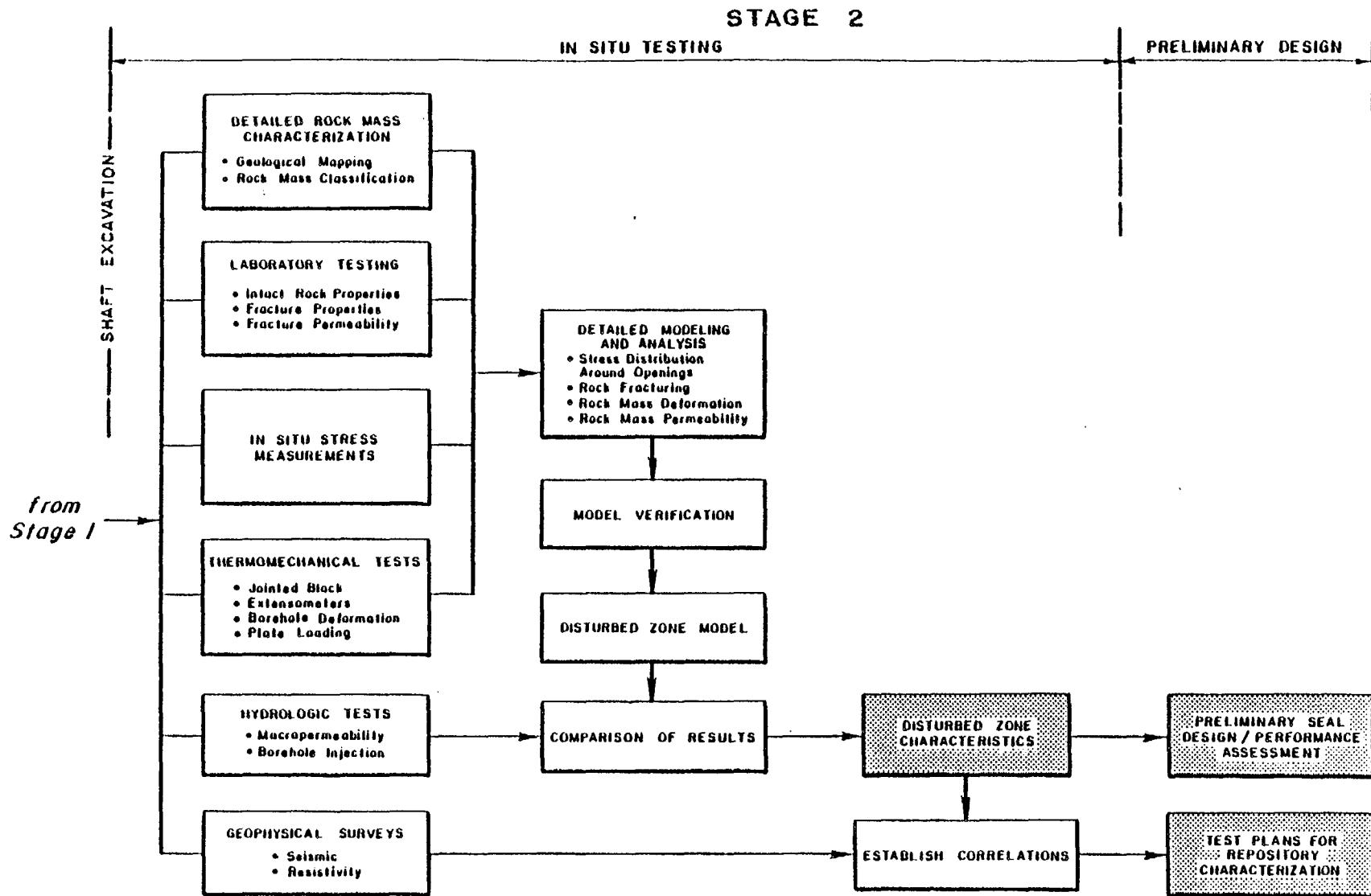


Figure 5-7. Approach for Disturbed Zone Characterization - Stage 2.

Most of these tests are fairly well established and do not require extensive development. Further planning and field testing are required to establish a suitable macropermeability test. When completed, the tests at Colorado School of Mines (Section 3.2.1) will provide a thorough evaluation of several of the recommended methods at one site, including injection tests, borescope logging, cross-hole seismic, and borehole deformation jacks. Depending on the results obtained it may be appropriate to conduct a macropermeability test and to run refraction surveys at the same site.

In addition to tests conducted specifically for disturbed zone characterization, other tests will be conducted in the same test facility to obtain rock mass characteristics required for mine design. Information of great value to the sealing program regarding coupled hydrologic, thermal and mechanical properties will be obtained from jointed block tests similar to that conducted at Colorado School of Mines. These tests, combined with laboratory testing of discrete fractures, will provide stress-permeability or aperture-permeability relationships for use in disturbed zone modeling.

#### 5.1.6 Test Program for Salt

With the exception of the deformability tests (which would be difficult to interpret), the test program described above may be applied to salt although on a more experimental basis. Either the borescope or integral sampling should be adequate for detecting fractures formed by blasting or creep rupture. Also, preliminary work by Thoms et al (1978) in a Gulf Coast salt mine has shown that a microfractured, destressed zone around a mine opening can be detected using seismic methods. Tests to evaluate the ability of radar to detect fractures in a tunnel wall in salt are in progress at the Waste Isolation Pilot Plant in New Mexico. A macropermeability test using gas, such as that developed by Systems, Science and Software (Section 5.1.1), may be particularly appropriate for salt.

## 5.2 TEST METHODS FOR DEEP BOREHOLES

Many of the test methods described above are inappropriate for boreholes because of the limited accessibility. Currently, a dual approach is being followed within the repository sealing program for assessing disturbance around boreholes, using laboratory tests and a guarded straddle packer system for field tests.

The laboratory tests conducted at Terra Tek and the University of Arizona have been reviewed in Section 2.0. Laboratory tests are favored because they are relatively inexpensive and allow direct examination of disturbance. Preliminary results indicate that the degree of disturbance associated with boreholes is so small that it very likely could not be detected by field tests.

The guarded straddle packer system under development by Systems, Science and Software (1981) employs a highly sensitive flow measurement system which should measure radial hydraulic conductivities as low as  $10^{-12}$  to  $10^{-13}$  cm/sec. Pressure monitors and tracer gas detectors are placed in the guard zones in order to detect flow through any disturbed zone that exists. Theoretically, a disturbed zone can be detected provided that the permeability contrast between the disturbed zone and the undisturbed rock is at least an order of magnitude. In practice the packer system may be used to demonstrate that a significant disturbed zone does not exist, as well as for wellbore characterization and plug testing.

Various geophysical logs may be considered for locating fractures and possibly detecting a disturbed zone. However, an evaluation of current methods (D'Appolonia, 1981) concluded that it is unlikely that geophysical logs can be used to detect either fine fractures or a relatively thin disturbed zone. Methods that can be used to evaluate sidewall characteristics and to locate major fractures include downhole television (Christensen & Petersen, 1980), the borehole televiewer (Zemanek et al, 1970; Keys et al, 1979; Wiley, 1981; Broding, 1982), and the impression packer (Section 5.1.2.2).

## 6.0 METHODS FOR TREATMENT OF THE DISTURBED ZONE

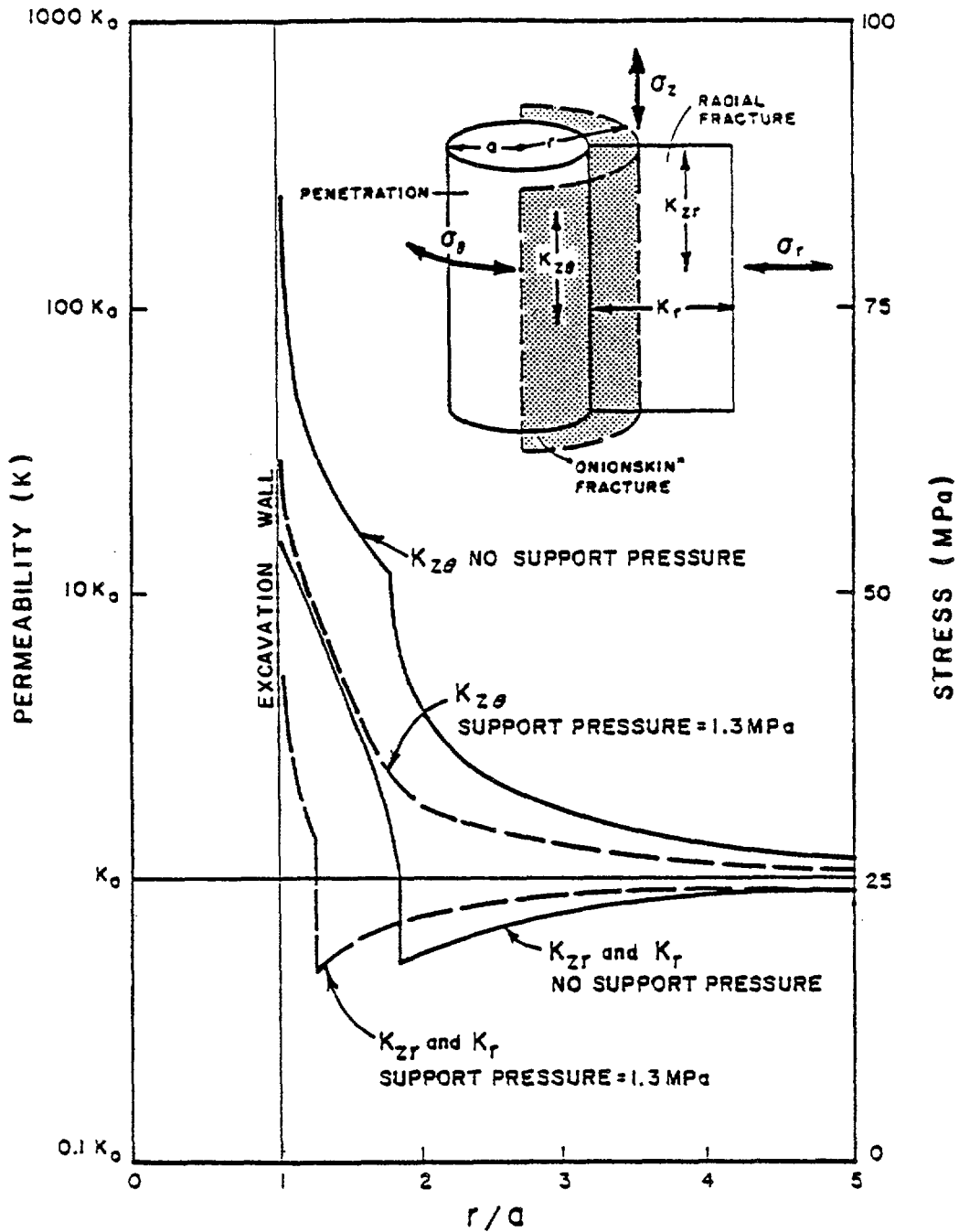
Section 1.2.1 showed that the disturbed zone may be a major component of flow for shafts and tunnels. This section considers possible means for eliminating the disturbed zone or at least reducing its impact. Consideration is given specifically to fractured rocks such as basalt or granite. Treatment methods appropriate to salt were reviewed in Section 4.0.

### 6.1 ROCK SUPPORT

The preferable means for "treating" the disturbed zone is to prevent the disturbance from occurring. Damage by the excavation process may be reduced by selecting an appropriate excavation method. Damage due to stress relaxation may be reduced by supporting the rock mass immediately following excavation. Support methods which might be considered include rock bolting, shotcrete, steel sets, and concrete arches, each of which can be modified to exert a particular level of support pressure. For this application, steel sets are probably not appropriate because they require blocking in order to apply a support pressure. It is unlikely that this blocking could be sufficiently effective to adequately limit rock deformation. Shotcrete appears preferable to rock bolting in key sealing locations because there is no drilling involved.

The effects of support pressure are shown analytically in Figure 6-1 which compares the predicted permeability distribution with and without support. The analysis uses the same elasto-plastic solution and assumptions described in Section 3.1.3.2. The effect of 1.3 MPa (200 psi) support pressure, which corresponds approximately to the upper limit achievable with shotcrete (Goodman, 1980), is to reduce the integrated permeability across the disturbed zone by about one half.

The effect shown in Figure 6-1 will occur in practice only if the support is applied immediately after excavation before irreversible deformations take place. In a typical repository (where rock quality should be good) such support probably will not be required to prevent major



$K_{zr}$  = PERMEABILITY OF RADIAL FRACTURES IN THE VERTICAL DIRECTION  
 $K_{z\theta}$  = PERMEABILITY OF ONIONSKIN FRACTURES IN THE VERTICAL DIRECTION  
 $K_z$  = TOTAL PERMEABILITY IN THE VERTICAL DIRECTION:  $K_{zr} + K_{z\theta}$   
 $K_r$  = PERMEABILITY IN THE RADIAL DIRECTION  
 $K_0$  = PERMEABILITY IN THE UNDISTURBED ROCK (ISOTROPIC)

Figure 6-1. Effect of Support Pressure on Predicted Extent of Disturbed Zone (Isotropic Initial Stress Condition-Elasto-Plastic Analysis)

failure but might be applied in main haulage ways as a precaution against minor rock fall. Supports installed at the time of excavation will be in place for a period of 50 to 100 years before the excavations are sealed. During this period the supports might relax or degrade allowing the rock to deform. It may then be necessary to remove the support before placing the seal in which case its value may be lost. In conclusion, the use of shotcrete in key seal zones (especially the tunnels connecting the shafts to the repository) may help to reduce long-term disturbance but this cannot be relied upon to significantly reduce disturbance effects.

## 6.2 GROUTING

Grouting might be considered either to prestress the rock mass prior to excavation or to reduce disturbed zone permeability after excavation. A preliminary evaluation of "groutability" shows that neither of these approaches is likely to be feasible.

In fractured rock, groutability is determined by fracture aperture (width). For cement grouts, values quoted in the literature for the minimum fracture aperture which can be penetrated vary considerably, with perhaps 0.2 mm most widely quoted (e.g., Hoek & Londe, 1974). Waterways Experiment Station (1956) conducted a series of laboratory tests using artificial joints in concrete blocks to investigate the factors which control grout penetration in fissures. These tests showed that fractures with thicknesses of 0.01 inch (0.25 mm) could be penetrated by cement grouts with relatively high water contents. The Waterways Experiment Station work showed that the ratio of crack thickness to grout particle size should be at least 1.7, and preferably 3.0 or more for adequate penetration.

The penetrability of particulate grouts may be improved by reducing the particle size. For most ordinary cements the maximum particle size (99% passing) is in the range 44-100  $\mu$  (Littlejohn, 1982). This maximum can be reduced by screening out the coarser particles or by using an especially fine grind. Shimoda & Ohmori (1982) describe a patented

"ultra fine grouting material" which has a maximum particle size of about 10  $\mu$ . Grout penetration may also be improved by increasing the water:cement ratio although this can lead to excessive bleeding, i.e., separation of water and cement particles (Houlsby, 1982). Bleeding can be reduced by adding a small proportion of bentonite (2-5% by weight of water), although there may be a tendency for the bentonite and cement to separate in fine fissures.

There is now available a wide variety of chemical grouts including inorganic varieties such as sodium silicate and organic varieties such as bitumen emulsions or resins (Karol, 1982). Generally, chemical grouts will penetrate finer soils and fissures than will cement grouts. For example, cracks in concrete as narrow as 0.05mm have been treated with chemical grout (Department of the Army, 1973). Theoretically, because chemical grouts are solutions rather than particulate suspensions, penetrability is determined by viscosity rather than particle size. In practice, solid particles may develop in chemical grouts as a result of incomplete mixing or early setting.

The penetrability of chemical grouts in rock fractures may be estimated and compared with the penetrability of cement and clay grouts by considering an effective particle size given by Cambefort (1977). This can be related to rock mass hydraulic conductivity using relationships among fracture aperture, spacing and hydraulic conductivity given by Hoek & Bray (1977). Table 6-1 assumes a fracture spacing in the range 0.1 to 1 m and is based on a ratio of fracture aperture to maximum grout particle size of 3.0.

An acceptable average hydraulic conductivity for a repository host rock might be in the range of  $10^{-8}$  to  $10^{-10}$  cm/sec. Hydraulic conductivities in a disturbed zone might be one to two orders of magnitude greater (Section 3.3), in the range  $10^{-6}$  to  $10^{-9}$  cm/sec. Thus, the table suggests that the disturbed zone might be grouted using bentonite, silicate, bitumen, or organic resin. In practice, however, groutability

TABLE 6-1

Groutability in Fractured Rock

<u>Grout Type</u>	<u>Mean diameter of grout particles (Microns)*</u>	<u>Groutability (Minimum Hydraulic Conductivity cm/sec)</u>
Cement	60	$10^{-2}$ - $10^{-4}$
Clay	17	$10^{-4}$ - $10^{-5}$
Bentonite	6	$10^{-6}$ - $10^{-7}$
Sodium silicate gel	5	$10^{-6}$ - $10^{-7}$
Very dilute silicate gel	2	$10^{-7}$ - $10^{-8}$
Bitumen emulsion	2	$10^{-7}$ - $10^{-8}$
Organic resins	0.6	$10^{-8}$ - $10^{-10}$

\*From Cambefort (1977)

and the effectiveness of grouting may be further reduced below the limits given above by factors such as the tortuosity of fractures, fracture infillings, and the practical problems of intersecting conducting fractures. Also, adequate grout penetration might require high injection pressures which could increase permeability by opening fractures. A further consideration is the doubtful long-term chemical stability of the grout. This concern applies particularly to organic materials used either as a basic grouting material or as an additive in silicate grouts. Although extensive testing has been conducted to demonstrate the short-term stability of organic materials in hot and hydrothermal environments, these tests cannot be extrapolated with confidence to periods of hundreds or thousands of years (Coons et al, 1982). In conclusion, it appears unlikely that grouting is a suitable technique for treating the disturbed zone, at least in repository formations. Grouting may have considerable application for sealing more permeable zones encountered in the shafts, or fractured zones encountered in the repository.

### 6.3 REDUCTION OF PERMEABILITY BY PRECIPITATION OF SECONDARY MINERALS

This section examines the possibility that the permeability in the disturbed zone (or in other parts of the rock mass) might be reduced by precipitation of secondary minerals. This precipitation might occur without inducement under the influence of temperature gradients generated by the waste. Further, it may be possible to deliberately induce precipitation. The potential for precipitation is examined by reference to basalt at the Hanford Site.

#### 6.3.1 Formation of Secondary Minerals

Secondary minerals are minerals which form in a rock subsequent to its initial lithification. The source for these minerals is commonly the fluids or ground water associated with the local geology. If these fluids are rich in the chemical components which form minerals, then changes in the state of the solution can cause precipitation of a secondary mineral. A common example of this process is the crystallization in veins of quartz and other polymorphs of silica ( $\text{SiO}_2$ ) which have prograde solubilities (i.e., they are more soluble at higher temperatures). If a high temperature solution becomes saturated in  $\text{SiO}_2$  and then travels to a lower temperature, there is a thermodynamic potential for a solid phase (e.g., quartz) to precipitate. Aiding this thermally driven process is a related but more subtle chemical concept, the activity of water.

The chemical activity of water (i.e., its chemically active concentration) is dependent on temperature, but is also dependent on the concentration of dissolved materials, and, because water is volatile, on pressure or pressure-related phenomena. For instance, the pressure of water can be decreased by allowing it to expand into a free volume, or by addition of another volatile species. Any process which decreases water pressure (i.e., activity) decreases the ability of water to retain dissolved material and increases the likelihood of precipitation. Thus, as silica-rich ground waters flow from small volume pores into larger volume fractures, the decrease in activity of water that attends expansion aids formation of quartz veins.

### 6.3.2 Secondary Mineralization at Hanford

The natural ground waters at Hanford are rich in mineral forming components, with the deepest ground waters (Grande Ronde) saturated in silica (Smith et al, 1980). The fractures and vugs at Hanford are already mineralized with phases such as smectite,  $\text{SiO}_2$ , calcite, barite and magnetite (Benson et al, 1979) reducing the permeability of these otherwise open areas. In some cases, mineralization is dense enough that fractures appear to be hydraulically tight (Rockwell Hanford, 1979). As a result, over the long-term, a repository at Hanford may have self-sealing potential. If this concept is to be utilized by seal designs, however, the kinetics for secondary mineral nucleation and growth must be understood, and mechanisms must be found for hastening the crystallization.

### 6.3.3 Concepts for Inducing Secondary Mineralization

Perhaps the most obvious way to induce secondary mineral crystallization in disturbed zones would be to utilize the high thermal gradient generated by the buried waste. Because of the relatively steep gradient, substances with prograde solubilities might be expected to precipitate as the transporting ground water travels through pores and fractures to lower temperature regions. In contrast, substances with retrograde solubilities might be used to seal pathways leading toward higher temperature. It should be emphasized, however, that these sealing substances must be selected from the natural secondary mineral assemblage in order to enhance the probability of long-term performance and to minimize the chemical effects of ground water acting on other parts of the barrier system. In addition, the solubilities of the sealing minerals must be sensitive to the thermal range anticipated for a nuclear waste repository.

#### 6.3.3.1 Candidate Sealing Phases

While at this time development of the proposed treatment is at a speculative stage, two promising sealing minerals appear to be  $\text{SiO}_2$  and calcite. Both of these phases occur naturally at Hanford, thereby fixing the chemical activity of their dissolved components. As a

result, their addition should not perturb the natural ground water chemistry. Furthermore, both phases crystallize densely enough to restrict fracture permeability within desirable limits. Finally, the solubilities of both change by more than an order of magnitude over the 100°C range that might be associated with a repository in basalt.

Amorphous silica is the natural, low temperature control on  $\text{SiO}_2$  solubility, and it is likely to govern the maximum concentrations of silica in ground waters circulating through a repository. The solubility is prograde so that crystallization would likely occur as ground water migrates from a hot to a cooler zone.

The efficiency of silica precipitation might be enhanced by treating the disturbed zone with a volatile silica solution such as tetraethylorthosilicate (TEOS) prior to repository closure. As envisioned, TEOS could be pumped under low pressure into the fractures of the disturbed zone. Close to the repository the ambient temperature, supplemented by radiogenic heating, should produce temperatures higher than 80°C before closure. The organic carrier would be volatilized by this heat and exhausted through the ventilation system, leaving a silica residue in the fractures. The residue would probably not be sufficient to reduce permeability significantly on its own. It would, however, provide ready nucleation sites for subsequent silica precipitation from supersaturated ground waters and increase the likelihood for forming a dense fracture filling in the disturbed zone.

In contrast to silica, calcite has a retrograde solubility, and although it is much more sensitive than silica to controls other than temperature (e.g., common ion effect, salting out process, pressure), it has the potential to dissolve at lower temperature and precipitate at higher temperature. Thus, if soluble carbonate [e.g.,  $\text{Na}_2\text{CO}_3$ ] and calcium [ $\text{Ca}(\text{OH})_2$ ] salts were dispersed in cool areas not critical to sealing, a potential for crystallization at higher temperatures in disturbed zones could be created. The relatively abundant  $\text{SO}_4^{=}$  in the ground water might also lead to secondary anhydrite accompanying carbonate

precipitation. In addition, spiking ground waters with carbonate may promote hydrothermal precipitation of silica. Silica saturated ground waters enriched in carbonate could precipitate quartz (or a polymorph) in high temperature regions because at elevated temperatures carbonate converts to  $\text{CO}_2$ . As a gas, the  $\text{CO}_2$  will depress the activity of water substantially and could decrease its ability to retain dissolved  $\text{SiO}_2$ . The result might be the precipitation of silica in high temperature, low pressure regions.

#### 6.3.4 Conclusions and Recommendations

The concept of secondary mineral crystallization (and its enhancement) as a potential treatment for disturbed zones in basalt repositories appears promising. At this stage, the illustrative examples have not been documented with rigorous theoretical calculations. Before the concept can be refined and seriously applied to repository sealing issues, these detailed thermodynamic computations will be required. In addition, site-specific data for estimating mineral nucleation and growth rates must be generated by experiment. These experiments should use site-derived materials and appropriate conditions, and the degree of undercooling should be scaled to expected water flow rates. Results from empirical experiments monitoring changes in fracture permeability as a function of time would also be very helpful.

In summary, a decrease in disturbed zone permeability is likely to result at Hanford from the precipitation of secondary minerals in fractures. The rate and efficiency with which the fracture filling might proceed is currently unknown. Experimental and theoretical investigations of precipitation phenomena (and mechanisms for their enhancement) appear warranted.

#### 6.4 BULKHEADS

A method incorporated in previous schematic designs for reducing disturbed zone flow consists of bulkheads with cutoff collars excavated into the walls of the excavation. Bulkheads may reduce disturbed zone flow in a number of ways:

- by replacing high-permeability rock close to the walls of the excavation with a low-permeability engineered material such as concrete or clay;
- by intercepting any continuous longitudinal fractures that may exist in the walls of the excavation, and thereby lengthening travel paths;
- by reducing the extent of the disturbed zone by virtue of very closely controlled, low-energy excavation methods in cutoff zones which produce less disturbance than the methods used to excavate the original shaft or tunnel;
- by restressing the rock mass by means of an expansive bulkhead material.

The validity of these possible benefits is considered in the remainder of this section. Regardless of the effectiveness of bulkheads for reducing disturbed zone flow, however, bulkheads may have other important functions in seal systems. For example, bulkheads provide structural support, and they reduce interface flow by intercepting the interface and by possibly increasing normal stresses acting across it. Also, bulkheads are relatively short sections of the seal in which there can be very stringent specifications for materials and placement methods. As relatively small seal components, bulkheads can be constructed and tested at full scale in order to demonstrate construction feasibility and performance.

Extending the theoretical analyses of disturbed zone characteristics presented in Section 3.1.3, it can be shown that bulkheads (not properly constructed) may tend to increase rather than reduce the extent of the disturbed zone. This arises, theoretically, because the extent of the disturbed zone is proportional to the radius of the excavation. If the radius is increased by excavation of a cutoff collar, the width of the disturbed zone will also be increased. Even if the linear extent of the disturbed zone around the cutoff is the same as that around the penetration, a greater impact occurs because the area of the disturbed zone annulus around the cutoff is much greater than that of the annulus around the penetration. For a cylindrical bulkhead with "square ends,"

the "total permeability" (permeability integrated over the area of the disturbed zone) would be increased by a factor of 4 or 5 times relative to that of the disturbed zone without a cutoff collar.

The effect described above will not occur, or will be reduced in practice, if the rock around the bulkhead can be prestressed in such a way, or excavated in such a way, that the disturbed zone is not propagated further into the rock mass. Methods that might be considered include:

- excavation in segments so that only a small volume of the rock is distressed at any particular time;
- immediate support of excavated segments using shotcrete or other means;
- sequencing excavation and support so that the entire cutoff area in the center of the bulkhead is protected by a compression arch -- conceptually this might be achieved by excavating above and below the cutoff (or on either side) and stressing the rock by means of expansive concrete;
- use of expansive seal materials to restress the rock mass and restore to some degree the original permeability;
- use of narrow cutoff slots extending beyond the main bulkhead structure (see Section 6.5).

Additional study is required to determine the effectiveness of bulkheads for reducing disturbed zone permeabilities. This should include detailed analyses to determine stresses in critical cutoff zones at all times during and after excavation and construction. Analyses should also examine the benefits of expansive materials and the stress changes that will occur during the repository thermal cycle. Other practical considerations may have an impact on detailed bulkhead design. These include the effects of heat of hydration on adjacent seal components, the potential for thermally-induced cracks within the concrete, and the effects of shrinkage during cooling. In practice, these problems are generally eliminated by pouring the concrete in small lifts.

### 6.5 DRILLED CUTOFFS

Many of the problems associated with bulkheads described in the previous section should be overcome by constructing a narrow cutoff as a series of overlapping boreholes (Figure 6-2). Each hole is drilled and grouted with a low permeability material prior to excavation of adjacent holes. In this way only a small volume of the rock mass is distressed at any one time. Further, the stress relief should not extend significantly beyond each hole in the longitudinal direction. As shown in the figure, two or more overlapping, horizontal (for a shaft) rings of holes would be drilled with the axes offset to achieve a complete overlap. Cutoffs excavated and filled in this manner will serve as barriers to water migration through the disturbed zone, but they are not intended to act as structural bulkheads. Clays might be considered in place of cement grouts in order to place a sorptive barrier in the disturbed zone. The holes would be as long as necessary to penetrate through the part of the disturbed zone in which the permeability is significantly increased, i.e., the lengths would probably be in the range 1 to 2 penetration radii, although there would be no limit on making the holes longer. Conceptually, considering 25-cm diameter holes and a 6-m diameter shaft, each horizontal ring would include about 75 holes, and a cutoff consisting of 3 overlapping rings would include about 200 holes. In further developing the scheme, consideration can be given to using larger holes.

### 6.6 CONCLUSIONS

Disturbed zone effects may be reduced by a combination of careful excavation and properly constructed cutoffs and bulkheads. It is essential that the rock mass in bulkhead cutoffs be supported immediately following excavation in order to avoid irreversible deformations. Properly sequenced construction procedures are required to maintain relatively high stresses in the zones adjacent to the cutoffs. Bulkhead materials should be sufficiently rigid to prevent rock mass deformation. Expansive materials are desirable in order to develop high normal stresses at the interface. An alternative method for restricting disturbed zone flow, which may be used in addition to conventional bulkheads, involves

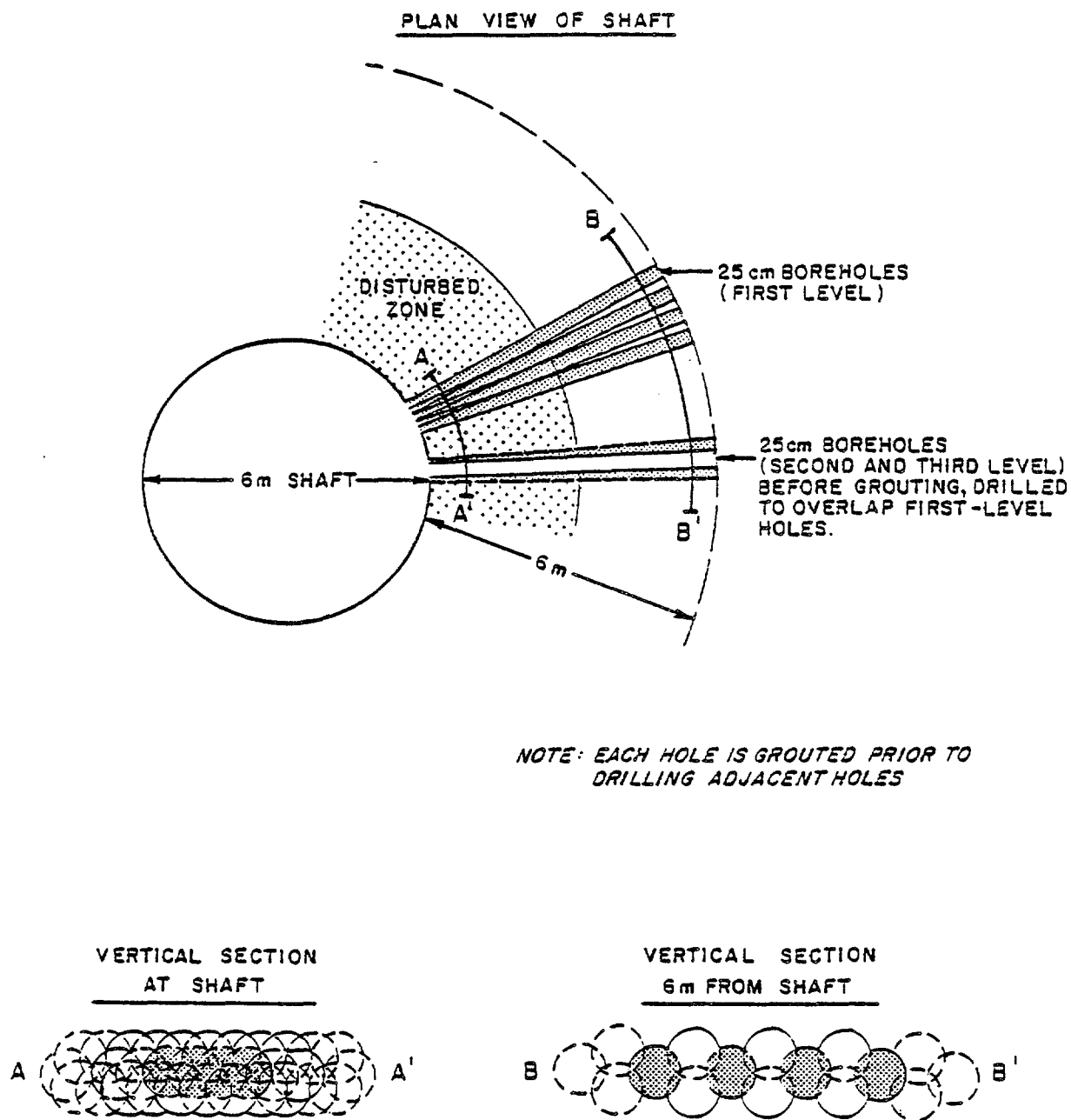


Figure 6-2. Concept for Forming Impermeable Barriers in the Disturbed Zone Using Overlapping Boreholes

cutoffs constructed as a series of overlapping boreholes. This is considered as the most promising method for engineering a disturbed zone barrier. It is noted that disturbed zone permeability may be reduced "naturally" in the repository environment by secondary precipitation of silica in fractures. It is doubtful, however, that such a passive treatment method used alone would be acceptable to licensing authorities.

## REFERENCES

- Acres, 1977. Weeks Island Mine Geotechnical Study, Acres American, Inc., Buffalo, NY.
- Acres, 1979. Weeks Island Mine Additional Geotechnical Studies, Acres American, Inc., Buffalo, NY.
- Andersson, B., and P. A. Halen. 1978. Mining Methods Used In the Underground Tunnels and Test Rooms at Stripa, LBL-7081, Lawrence Berkeley Laboratory, Berkeley, CA.
- Aufricht, W. R., and K. C. Howard. 1961. "Salt Characteristics as They Affect Storage Hydrocarbons," Journal of Petroleum Technology, Vol. 8, p. 730-738.
- Baar, M. V., and G. Hocking, 1976. "Borehole Structural Logging Employing a Pneumatically Inflatable Impression Packer," Symposium on Exploration for Rock Engineering Proceedings, ed., Z. T. Bienawski, (November, Johannesburg, S.Africa), pp. 29-34.
- Barron, K., 1978. "An Air Injection Technique for Investigating the Integrity of Pillars of Ribs in Coal Mines," International Journal of Rock Mechanics, Mining Sciences and Geomechanics Absts., 15:69-76.
- Barron, K., and N. A. Toews, 1963. "Deformation Around a Mine Shaft," Proceedings, Rock Mechanics Symposium, (Dec. 6-7, Queens University, Kingston, Ontario).
- Benson, L. V., L. S. Teague, C. A. Mouton, C. J. Frisch, R. A. Stoleman and D. J. Corrigan, 1979. A Study of Rock-Water-Waste Interactions in the Pasco Basin, Washington. Part I: Distribution and Composition of Primary and Secondary Mineral Phases in Basalts of the Pasco Basin, Washington, LPID-068, Lawrence Berkeley Laboratory, Berkeley, CA.
- Benson, R. P., D. K. Murphy, and D. R. McCreath. 1970. "Modulus Testing of Rock at the Churchill Falls Underground Powerhouse, Labrador," in Determination of the In Situ Modulus of Deformation of Rock, American Society for Testing and Materials, ASTM STP 477, pp. 89-116.
- Bieniawski, Z. T. 1978. "The 'Petite Sismique' Technique - A Review of Current Developments," Proceedings of the 2nd Conference on Acoustic Emission/Microseismic Activities in Geologic Structures and Materials, The Pennsylvania State University, State College, PA.
- Bray, J. W., 1967. "A Study of Jointed and Fractured Rock - Part II: Theory of Limiting Equilibrium," Rock Mechanics and Engineering Geology, Vol. V No.4, pp. 197-216.
- Brizzolari, E., 1981. "Miniseismic Investigations in Tunnels: Methodology and Results," Geoexploration, 18, pp. 259-267.

Broding, R. A., 1982. "Volumetric Scanning Allows 3-D Viewing of the Borehole," World Oil, June 1982, pp. 190-196/

Cambeport, H., 1977. "The Principles and Applications of Grouting," Quarterly Journal of Engineering Geology, 10:57-95.

Chabannes, C. R., 1982. An Evaluation of the Time-Dependent Behavior of Solution Mined Caverns in Salt for the Storage of Natural Gas, M.S. Thesis, Department of Mining, The Pennsylvania State University, State College, PA, 150 pp.

Chan, S. S. M., H. E. Thomas, and N. Bada, 1974. "Air Injection and Hot-Film Flow Logging for Evaluation of Roof Cracks in White Pine Mine," Society of Mining Engineers of AIME, Transactions, Vol 256, 131-137.

Christensen, C. L., and E. W. Petersen, 1980. Downhole Television Applications in Borehole Plugging, SAND80-0459, Sandia National Laboratories, Albuquerque, NM.

Christensen, C. S., and E. W. Peterson, 1981. The Bell Canyon Test Summary Report, SAND80-1375, Sandia National Laboratories, Albuquerque, NM.

Cook, J. C., 1975. "Radar Transparencies of Mine and Tunnel Rocks," Geophysics, 40, No. 5, pp. 865-885.

Cook, C. W., 1980. Impulse Radar Scanning of Intact Salt at the Avery Island Mine, SAND80-0632, Sandia National Laboratories, Albuquerque, NM.

Coons, W. E., D. Meyer, and P. C. Kelsall, 1982. An Evaluation of Polymer Concretes for Application to Repository Sealing, D'Appolonia Consulting Engineers, Inc., Albuquerque, NM.

Cording, E. J., A. J. Hendron, and D. U. Deere, 1971. "Rock Engineering for Underground Caverns," Underground Rock Chambers, ASCE, New York, NY, 567-600.

Costin, L. S., and W. R. Wawersik. 1980. Creep Healing of Fractures in Rock Salt, SAND80-0392, Sandia National Laboratories, Albuquerque, NM.

Daemen, J. J. K., S. L. Cobb, W. B. Green, R. G. Jeffrey, S. P. Mathis, and D. L. South. 1981. Nuclear Waste Management Research. Annual Report; Rock Mass Sealing, Nuclear Fuel Cycle Research Program, University of Arizona, Tuscon, AZ, Sponsored by the U.S. Nuclear Regulatory Commission.

D'Appolonia Consulting Engineers, Inc., 1981. Repository Sealing Field Testing Workshop - Proceedings, (September 18 and 19, 1980, Santa Fe, NM), ONWI-239, Office of Nuclear Waste Isolation, Battelle Memorial Institute, Columbus, OH.

Department of the Army, 1973. Engineer Manual, Engineering & Design, Chemical Grouting, EM 1110-2-3504, U.S. Department of the Army, Office of the Chief of Engineers.

Fisekci, M. Y., and K. Barron, 1975. "Methane Pressure and Flow Measurements in Coal and Surrounding Strata," CIM Bulletin (Canadian Institute of Mining and Metallurgy), 68:91-98.

Fowler, J. C., 1981. "Subsurface Reflection Profiling Using Ground-Probing Radar," Mining Engineering, August, 1981, pp. 1266-1270.

Gangi, A. F., 1978. "Variation of Whole and Fractured Porous Rock Permeability with Confining Pressure," International Journal of Rock Mechanics, Mining Science and Geomechanics Abstracts, 15, 249-257.

Golder, 1977. Geotechnical Study of Cote Blanche Island Salt Mine, Golder Associates, Kirtland, WA.

Goodman, R. E., 1976. Methods of Geological Engineering in Discontinuous Rocks, West Publishing Co., St. Paul, MN.

Goodman, R. E., 1980. Introduction to Rock Mechanics. John Wiley & Sons, New York, NY, 468 pp.

Harper, T. R., and D. V. Hinds, 1977. "Impression Packer: A Tool for Recovery of Rock Mass Fracture Geometry," Storage in Excavated Rock Caverns: Rockstore 77, 1st International Symposium, Ed. Magnus Bergman, Stockholm, Vol. 2, p. 245.

Herrmann, W., W. R. Wawersik, and H. S. Lauson, 1980. Analysis of Steady State Creep of Southeastern New Mexico Bedded Salt, SAND80-0558, Sandia National Laboratories, Albuquerque, NM, 43 pp.

Heuze, F. E., W. C. Patrick, R. V. De la Cruz and C. F. Voss, 1981a. In Situ Geomechanics Climax Granite, Nevada Test Site, UCRL-53076, Lawrence Livermore Laboratory, Livermore, CA.

Heuze, F. E., T. R. Butkovich, and J. C. Peterson, 1981b. An Analysis of the "Mine-By" Experiment, Climax Granite, Nevada Test Site, UCRL-53133, Lawrence Livermore Laboratory, Livermore, CA.

Hocking, G. and C. M. St. John, 1979. Annual Report - Fiscal Year 1979. Numerical Modeling of Rock Stresses Within a Basaltic Nuclear Waste Repository, RHO-BWI-C-58, Rockwell Hanford Operations, Richland, WA.

Hoek, E., and J. Bray, 1977. Rock Slope Engineering, Institution of Mining and Metallurgy, London, 134 pp.

Hoek, E., and E. T. Brown, 1980. Underground Excavations in Rock. Institution of Mining & Metallurgy, London, 527 pp.

- Hoek, E., and P. Londe, 1974. "The Design of Rock Slopes and Foundations," General Report for Third Congress of the International Society for Rock Mechanics, (September, Denver, CO), 40 pp.
- Holmberg, R., and P. A. Persson, 1980. "Design of Tunnel Perimeter Blasthole Patterns to Prevent Rock Damage," Institution of Mining and Metallurgy, Transactions, London, 89:A37-40.
- Hood, M., 1979. Some Results from a Field Investigation of Thermomechanical Loading of a Rock Mass When Heaters are Emplaced in the Rock, LBL-9392, Lawrence Berkeley Laboratory, Berkeley, CA.
- Houlsby, A. C., 1982. "Optimum Water: Cement Ratios for Rock Grouting," Proceedings of the Conference on Grouting in Geotechnical Engineering, (Feb., New Orleans, LA), ASCE, New York, NY, pp. 317-331
- Hustrulid, W., R. Cudnik, R. Trents, R. Holberg, P. E. Sperry, R. Hutchinson, and P. Rosasco, 1980. "Mining Technology Development for Hard Rock Excavation," Storage in Excavated Rock Caverns: Rockstore 80, Stockholm, Vol 2., pp. 919-926.
- Isherwood, D., 1981. Geoscience Data Base Handbook for Modeling a Nuclear Waste Repository, UCRL-52719, Lawrence Livermore Laboratory, Livermore, CA.
- Iwai, K., 1976. Fundamental Studies of Fluid Flow Through a Single Fracture, Ph.D. Dissertation, University of California, Berkeley, CA, 208 pp.
- Jaeger, J. C., and N. G. W. Cook, 1969. Fundamentals of Rock Mechanics, Methuen & Co Ltd, London.
- Karol, R. H., 1982. "Chemical Grouts and their Properties," Proceedings of the Conference on Grouting in Geotechnical Engineering, (Feb., New Orleans, LA), ASCE, New York, NY, pp. 359-377.
- Kelsall, P. C., J. B. Case, C.R. Chabannes, W. E. Coons, R. D. Ellison, D. Meyer, D. K. Shukla, and D. E. Stephenson, 1982. Schematic Designs for Penetration Seals for a Reference Repository in Bedded Salt, ONWI, Office of Nuclear Waste Isolation, Battelle Memorial Institute, Columbus, OH.
- Keys, W. S., D. E. Eggers, and T. A. Taylor, 1979. "Borehole Geophysics as Applied to the Management of Radioactive Waste, Site Selection and Monitoring," in Management of Low-Level Radioactive Waste, Ed. by Melvin W. Carter, et al., Pergamon Press, NY.
- Kranz, R. L., A. D. Frankel, T. Engelder and C. H. Scholz, 1979. "The Permeability of Whole and Jointed Barre Granite," International Journal of Rock Mechanics and Mining Science and Geomechanics Abstracts, 16, pp. 225-234.

Krebs, E., 1967. "Optical Surveying With a Borehole Periscope," Mining Magazine, 116:340-399.

Kujundzic, B., L. Joranovic and Z. Radosavljevic. 1970. "A Pressure Tunnel Lining Using High-Pressure Grouting," (in French) Proceedings of the 2nd Congress International Society for Rock Mechanics, Belgrade, 4-66, pp.867-881.

Lai, C. S., 1971. Fluid Flow Through Rock Salt Under Various Stress States, Ph.D. Dissertation, Michigan State University, East Lansing, MI.

Lingle, R., K. L. Standord, P. E. Peterson, and S. F. Woodhead, 1981. Technical Report on Wellbore Damage Zone Experimental Determination, Terra Tek, TR81-76 (Draft), Salt Lake City, UT.

Littlejohn, G. S., 1982. "Design of Cement Based Grouts," Proceedings of the Conference on Grouting in Geotechnical Engineering, (Feb., New Orleans, LA), ASCE, New York, NY, 35-48.

Miller, C. H., D. R. Cunningham, and M. J. Cunningham, 1974. "An Air-Injection Technique to Study Intensity of Fractures Around a Tunnel in Volcanic Rock," Association of Engineering Geologists, Bulletin, Vol. XI, No. 3, pp. 203-217.

Miller, C. H. and E. H. Skinner, 1980. "The Nature of Fracturing and Stress Distribution in Quartzite Around the 1128m (3700 ft.) Level of the Crescent Mine, Coeur d-Alene Mining District, Idaho," Engineering Geology, 16, 321-338.

Moak, D. J., and T. M. Wintzak, 1980. Near-Surface Test Facility Phase I Geologic Site Characterization Report, RHO-BWI-ST-4, Rockwell Hanford Operations, Richland, WA.

Montazer, P. M. and W. A. Hustrulid, 1981. An Investigation of Fracture Permeability Around an Underground Opening in Metamorphic Rocks, Topical Report No. 5, Colorado School of Mines, Golden, CO.

Murphy, V. J., 1972. "Seismic Velocity Measurements for Moduli Determinations in Tunnels," Proceedings of the First North American Rapid Excavation and Tunneling Conference, (June, Chicago, IL), 1:209-216.

Nair, K. and R. D. Singh, 1974. "Creep Rupture Criteria for Salt," Fourth Symposium on Salt, Northern Ohio Geological Society, 1,41-49.

Nelson, P., B. Paulsson, R. Raichiele, L. Andersson, T. Schrauf, W. Hustrulid, O. Duran, and K. A. Magnusson, 1979. Preliminary Report on Geophysical and Mechanical Borehole Measurements at Stripa, LBL-8280, Lawrence Berkeley Laboratories, Berkeley, CA.

Nelson, P., and C. Wilson, 1980. "Thermomechanical and Macropermeability Experiments in the Stripa Granite - Status Report," Proceedings, Workshop on Thermomechanical-Hydrochemical Modeling for a Hardrock Waste Repository, LBL-11204, Lawrence Berkeley Laboratory, Berkeley, CA.

New, B. M., and G. West, 1980. "The Transmission of Compressional Waves in Jointed Rock," Engineering Geology 15:151-161.

O'Donoghue, J. B., and R. M. O'Flaherty, 1974. "The Underground Works in Turlough Hill; Part I," Water Power, January, pp. 5-12.

Olkiewicz, A., J. E. Gale, R. Thorpe, and B. Paulsson, 1979. Geology and Fracture System at Stripa, LBL-8907, Lawrence Berkeley Laboratory, Berkeley, CA.

Olson, J. J., R. J. Willard, D. E. Fogelson, and K. E. Hjelmstad, 1973. Rock Damage from Small Charge Blasting in Granite, RI 7751, U. S. Bureau of Mines.

Ostrowski, W. J. S., 1972. "Design Considerations for Modern Shaft Linings," Transactions of the Canadian Institute of Mining and Metallurgy, 75: 184-198.

Paulsson, B. N. P., and M. S. King. 1980. "Between-Hole Acoustic Surveying and Monitoring of a Granitic Rock Mass," International Journal of Rock Mechanics, Mining Science and Geomechanics Abstracts, 17:371-376.

Peterson, E. W., and P. L. Lagus, 1980. Disturbed Region In Situ Characterization for Tunnel and Shaft Sealing Applications, Systems, Science and Software, La Jolla, CA.

Plichon, J. N., 1980. "Measurement of the Thickness of the Decompressed Zone in an Excavation Under High Overburden Cover," in Analysis of Tunnel Stability by the Convergence-Confinement Method, Underground Space, 4, (6):361-402.

Pratt, H. R., H. S. Swolfs, W. F. Brace, A. D. Black, and J. W. Handin, 1977. "Elastic and Transport Properties of an In Situ Jointed Granite," International Journal of Rock Mechanics, Mining Sciences and Geomechanics Abstracts, Vol. 14, pp. 35-45.

Reynolds, T. D., and E. F. Gloyna, 1960. Reactor Fuel Waste Disposal Project: Permeability of Rock Salt and Creep of Underground Salt Cavities, Final Report, AEC Contract AT-(11-1)-490.

Rocha, M., 1971. "A Method of Integral Sampling of Rock Masses," Rock Mechanics, 3:1-12.

Rocha, M., and F. Franciss, 1977. "Determination of Permeability in Anisotropic Rock Masses from Integral Samples," Rock Mechanics, 9:67-93.

Rockwell Hanford Operations, 1979. Hydrologic Studies within the Columbia Plateau, Washington - An Integration of Current Knowledge, October 1979. RHO-BWI-ST-5, Rockwell Hanford Operations, Richland, WA.

Rockwell Hanford Operations, 1981. Basalt Waste Isolation Project - Presentation to the National Academy of Sciences, June 11-13, 1981, Rockwell Hanford Operations, Richland, WA.

Schneider, B., 1967. "Contribution a' l'etude des massifs de fondations de barrages," Travaux du Laboratoire de Geologie de la Faculte de Sciences de Grenoble. Memoires No. 7, Grenoble, 241 pp.

Scott, J. H., F. T. Lee, R. D. Carroll, and C. S. Robinson, 1968. "The Relationship of Geophysical Measurements to Engineering and Construction Parameters in the Straight Creek Tunnel Pilot Bore, Colorado," International Journal of Rock Mechanics, Mining Sciences, and Geomechanics Abstracts, Vol. 5, 1-30.

Shimoda, M., and H. Ohmori, 1982. "Ultra-fine Grouting Material," Proceedings of the Conference on Grouting in Geotechnical Engineering, (Feb., New Orleans, LA), ASCE, New York, NY, pp. 77-91.

Siskind, D. E., and R. R. Fumanti, 1974. Blast-Produced Fractures in Lithonia Granite, RI 7901, U.S. Bureau of Mines.

Siskind, D. E., R. C. Steckley, and J. J. Olson, 1973. Fracturing in the Zone Around a Blasthole, White Pine, Michigan, RI 7753, U. S. Bureau of Mines.

Smith, M. J. (principal author), 1980. Engineered Barrier Development for a Nuclear Waste Repository in Basalt: An Integration of Current Knowledge, RHO-BWI-ST-7, Rockwell Hanford Operations, Richland, WA.

Stacy, T. R., 1976. "Seismic Assessment of Rock Masses," Proceedings of the Symposium on Exploraton for Rock Engineering, (November, Johannesburg, S. Africa), 2:113-117.

Sutherland, H. J. and S. P. Cave, 1980. "Argon Gas Permeability of New Mexico Rock Salt Under Hydrostatic Compression," International Journal of Rock Mechanics, Mining Sciences and Geomechanics Abstracts, 17, 281-288.

Systems, Science & Software, 1981. Guarded Straddle Packer System, SSS-R-81-4918, Systems Science & Software, La Jolla, CA, Report for Sandia Laboratories, Albuquerque, NM.

Thoms, R. I., R. L. Eidemiller, and R. K. Hilding, 1978. "A Preliminary Survey of Seismic Velocities through In Situ Rock Salt," American Society of Mechancial Engineers, Preprint, 78-Pet-79.

Tsang, Y. W. and P. A. Witherspoon, 1981. "Hydromechanical Behavior of a Deformable Fracture Subject to Normal Stress," Journal of Geophysical Research, 86, 9287-9298.

Voegele, M., E. Hardin, D. Lingle, M. Board, and N. Barton, 1981. "Site Characterization of Joint Permeability Using the Heated Block Test," Proceedings of the 22nd U. S. Symposium on Rock Mechanics, Massachusetts Institute of Technology, Cambridge, MA.

Wagner, R. A., 1980. Preliminary Investigation of the Thermal and Structural Influence of Crushed-Salt Backfill on Repository Disposal Rooms, ONWI-138, Office of Nuclear Waste Isolation, Battelle Memorial Institute, Columbus, OH.

Waterways Experiment Station, 1956. Pressure Grouting Fine Fissures. Technical Report No. 6-437, Waterways Experiment Station, U.S. Army Corps of Engineers, Vicksburg, MS.

Wiley, R., 1981. "The Borehole Televiewer: An Update on Application," World Oil, March 1981, 47-53.

Witherspoon, P. A., J. S. Y. Wang, K. Iwai, and J. E. Gale, 1980. "Validity of Cubic Law for Fluid Flow in a Deformable Rock Fracture," Water Resources Research, 16 (6), 1016-1024.

Witherspoon, P. A., 1981. "Effect of Size on Fluid Movement in Rock Fractures," Geophysical Research Letters, 8, No. 7, 659-661.

Witherspoon, P. A., N. G. W. Cook, and J. E. Gale, 1981. "Geologic Storage of Radioactive Waste: Field Studies in Sweden," Science, Vol. 211, 27 February 1981.

Zemanek, J., E. E. Glenn, L. J. Norton, and R. L. Caldwell, 1970. "Formation Evaluation by Inspection with the Borehole Televiewer," Geophysics, Vol. 35, No. 2, 254-269.

APPENDIX A  
FRACTURING OF INTACT ROCK

A.1 INTRODUCTION

This appendix summarizes calculations performed to assess the conditions in which fracturing of intact crystalline rock could occur around a shaft or borehole. The procedure is to calculate the state of stress throughout the region of interest assuming that the rock behaves elastically. The stress values are then compared with a Mohr-Coulomb failure criterion for fracturing of intact rock. Failure is assumed to occur at points where the value of the calculated major principal stress is greater than the maximum stress given by the failure criterion. Consideration is given to the stress conditions required for the onset of failure, and to the extent of the failure zone for the given stress condition.

A.2 STATE OF STRESS

A circular shaft or tunnel of arbitrary diameter is excavated in basalt. The material is assumed to be homogeneous, isotropic, and linearly elastic. Within a horizontal plane, the far field state of stress is assumed to be anisotropic (i.e.,  $P_2 > P_1$ ). The maximum tangential stress at point A (Figure A-1) on the shaft circumference is given (Goodman, 1980) as a special case of the Kirsch solution:

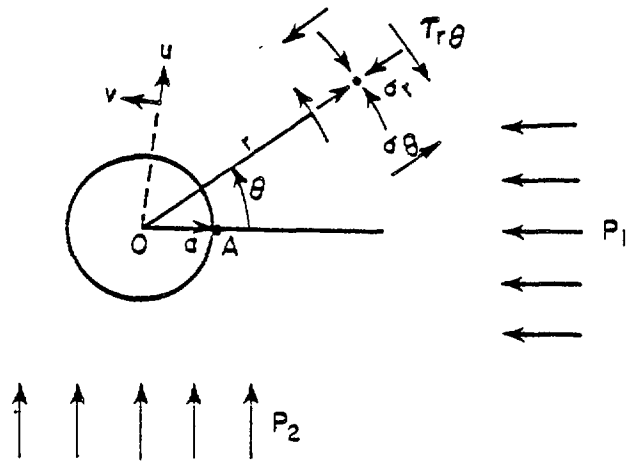
$$\sigma_r = 3P_2 - P_1 \quad (A-1)$$

where:

$\sigma_r$	=	maximum tangential boundary stress,
$P_1$	=	minimum horizontal stress far field, and
$P_2$	=	maximum horizontal stress far field.

This value occurs at point A shown in Figure A-1. If a factor  $k$  is defined as the ratio of the maximum horizontal far field stress to the minimum horizontal far field stress, then:

$$\sigma_r = (3k-1) P_1 \quad (A-2)$$



*After Goodman (1980)*

Figure A-1. Stress Analysis for a Circular Opening in a Homogeneous, Elastic Medium

This equation expresses the maximum boundary stress in terms of the stress ratio  $k$  and a reference stress  $P_1$  which is assumed equal to the overburden stress at some depth:

$$\begin{aligned} P_1 &= \gamma h \\ \gamma &= \text{unit weight of rock} \\ h &= \text{depth} \end{aligned}$$

The state of stress away from the most critical point A (Figure A-1) is determined by the general Kirsch solution:

$$\begin{aligned} \sigma_r &= \left[ \frac{P_1 + P_2}{2} \right] \left( 1 - \frac{a^2}{r^2} \right) + \left[ \frac{P_1 - P_2}{2} \right] \left( 1 - \frac{4a^2}{r^2} + \frac{3a^4}{r^4} \right) \cos 2\theta \\ \sigma_\theta &= \left[ \frac{P_1 + P_2}{2} \right] \left( 1 + \frac{a^2}{r^2} \right) - \left[ \frac{P_1 - P_2}{2} \right] \left( 1 + \frac{3a^4}{r^4} \right) \cos 2\theta \\ \tau_{r\theta} &= - \left[ \frac{P_1 - P_2}{2} \right] \left( 1 + \frac{2a^2}{r^2} - \frac{3a^4}{r^4} \right) \sin 2\theta \end{aligned} \quad (A-3)$$

where:

$$\begin{aligned} r, \theta &= \text{polar coordinates (Figure A-1)} \\ P_1, P_2 &= \text{horizontal far field stress,} \\ a &= \text{radius of opening,} \\ \sigma_r &= \text{radial stress} \\ \sigma_\theta &= \text{tangential stress, and} \\ \tau_{r\theta} &= \text{shearing stress} \end{aligned}$$

The principal stresses for the general biaxial stress state are given by:

$$\sigma_{P_1}, \sigma_{P_2} = \frac{\sigma_r - \sigma_\theta}{2} \pm \sqrt{\frac{(\sigma_r - \sigma_\theta)^2}{4} + \tau_{r\theta}^2} \quad (A-4)$$

Equations (A-4) are used to determine the state of stress at some point. Equation (A-5) transforms the stresses to principal stresses for comparison to the Mohr-Coulomb failure criterion.

### A.3 STRENGTH OF INTACT ROCK

The definition of intact rock strength for basalt refers to the strength of intact core (free from discernable discontinuities) measured at the laboratory scale. Goodman (1980) gives a range of 148 to 355 MPa for the unconfined compressive strength of basalt. In the analyses herein a conservative lower bound strength of 150 MPa is assumed.

The uniaxial compressive strength may be used as a criterion for rock failure in cases where the confining stress is zero, i.e., at the shaft perimeter. In cases where the rock is confined it is necessary to use a failure criterion expressed in terms of either the shear and normal stresses, or the principal stresses acting at a point. Hoek and Brown (1980) have proposed the following general criterion expressed in terms of principal stresses:

$$\frac{\sigma_1}{\sigma_c} = \frac{\sigma_3}{\sigma_c} + \sqrt{m \frac{\sigma_3}{\sigma_c} + s} \quad (\text{A-5})$$

where:

- $\sigma_c$  = unconfined compressive strength at the laboratory scale,
- $m, s$  = constants depending on rock quality, and
- $\sigma_1, \sigma_3$  = major and minor principal stresses at failure.

The values used for the constants  $m$  and  $s$  are those given by Hoek and Brown for intact, fine-grained, polymineralic igneous rocks ( $m = 17$ ,  $s = 1$ ).

### A.4 RESULTS

The possibility for failure of intact rock at some point on the shaft (or borehole) perimeter is evaluated by comparing the maximum boundary stress (for various depths and values of the in situ stress ratio,  $k$ ) against the intact unconfined compressive strength (Figure 3-3). For a depth of 1000m, and an unconfined compressive strength of 150 MPa, fracturing of intact rock can occur when the stress ratio is between 2 and 3. If the intact compressive strength is greater than 150 MPa, higher stress ratios are required to initiate fracturing of intact rock.

The extent of the fractured zone is calculated using the general Kirsch solution for a stress ratio ( $k$ ) equal to 2.5 (Figure A-2). At the rock surface, the radial stress is zero but, within a short distance from the shaft boundary, the radial stress increases the intact rock strength due to the effects of confinement. The analysis indicates that fracturing of rock occurs to a depth of only 15 cm for a 6.0 m diameter shaft and is localized within a small arc. For a borehole the extent of fracturing would be negligible.

In summary, the analysis indicates that fracturing of intact rock in basalt is only likely to occur where the ratio of maximum to minimum far field horizontal stresses at repository depth is significantly greater than 2. If fracturing were to occur, it would be limited to a thin zone, and would not extend far around the shaft from the direction of the minimum horizontal stress. This is attributed to the effects of confinement greatly increasing compressive strength.

#### References

- Goodman, R. E., 1980. Introduction to Rock Mechanics, John Wiley and Sons, New York, 478 p.
- Hoek, E., and E. T. Brown, 1980. Underground Excavations in Rock, Institution of Mining and Metallurgy, London, 527 p.

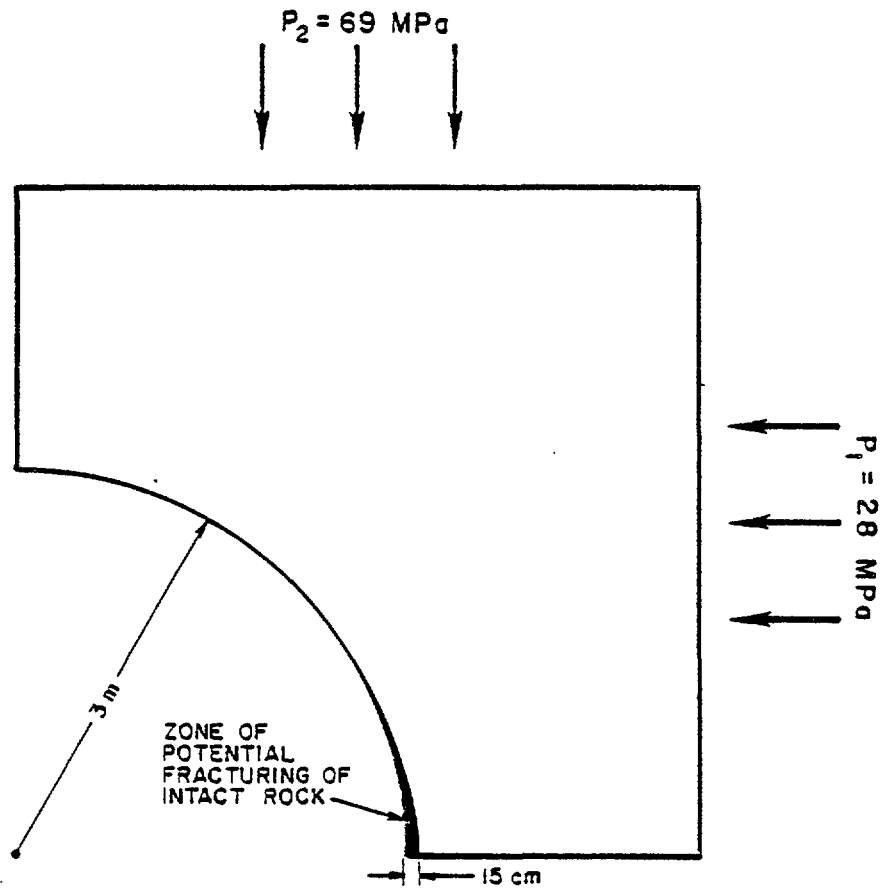


Figure A-2. Typical Analysis to Predict Extent of Fracturing of Intact Rock Around a Circular Opening for Given Stress Conditions and Rock Strength

APPENDIX B  
STRESS AND DISPLACEMENT ANALYSES

This Appendix describes closed-form and numerical solutions used to predict stresses and displacements around a shaft. Section B.1 describes the rock mass deformability and strength parameters used in the stress and displacement analyses. Closed-form solutions for stress distributions and displacements are presented in Sections B.2 and B.3 respectively.

B.1 ROCK MASS STRENGTH AND DEFORMABILITY

B.1.1 Strength

Rigorous analysis of rock mass response in jointed rock requires consideration of rock mass rather than intact rock properties. Hoek and Brown (1980) proposed a criterion for the strength of discontinuous rock masses. Laboratory and in situ strength data were compiled and interpreted according to the relation:

$$\frac{\sigma_1}{\sigma_c} = \frac{\sigma_3}{\sigma_c} + \sqrt{m \frac{\sigma_3}{\sigma_c} + s} \quad (\text{B-1})$$

where:

- $\sigma_c$  = unconfined compressive strength at the laboratory scale,
- $m, s$  = constants depending on rock quality, and
- $\sigma_1, \sigma_3$  = major and minor principal stresses at failure.

or alternatively

$$\tau_N = A(\sigma_N - \sigma_{tN})^B \quad (\text{B-2})$$

where:

- $\sigma_{tN}$  = tensile strength normalized to uniaxial compressive strength,
- $A, B$  = constants depending on rock quality,

$\tau_N, \sigma_N$  = shear and normal stress on the failure plane  
normalized to uniaxial compressive strength.

Hoek and Brown present a method of estimating the empirical constants used in the strength criteria on the basis of rock mass classifications such as the Q index (Barton et al, 1974) or the CSIR Rock Mass Rating (RMR) index (Bieniawski, 1979). This is perhaps an inexact method for predicting rock mass strength, but it is considered adequate for the purposes herein.

Typical rock mass characteristics for the Pomona basalt are obtained from Moak and Wintczak (1980). Fracture spacing ranges from 70-90 mm, and the fractures have slightly rough surfaces. The RQD ranges from 30 to 60. These data indicate an approximate RMR rating of 65, and a Q rating of 14. Analyses herein used a compressive strength of 276 MPa, an average value for basalt given by Isherwood (1981). (The average intact compressive strength reported for Pomona basalt is 313 MPa.) According to Hoek and Brown, for a fine-grained igneous rock with RMR = 65, A = 0.525 and B = 0.698, so that:

$$\tau_N = 0.525 (\sigma_N + .002)^{0.698} \quad (B-3)$$

This criterion is plotted in Figure B-1 as a "peak" strength envelope which is considered to apply to undisturbed rock. Also shown is a "residual" strength envelope which is considered to apply to rock within a disturbed zone where there has been some dilatancy and loss of apparent cohesion and friction. A small cohesion is assigned to the disturbed material because it seems likely that the walls of an excavation at 1000m depth would be self-supporting.

#### B.1.2 Deformability

The analysis of displacements requires an assessment of rock mass deformability in terms of the elastic constants for an equivalent continuous material representative of the rock mass. Bieniawski (1978) showed that

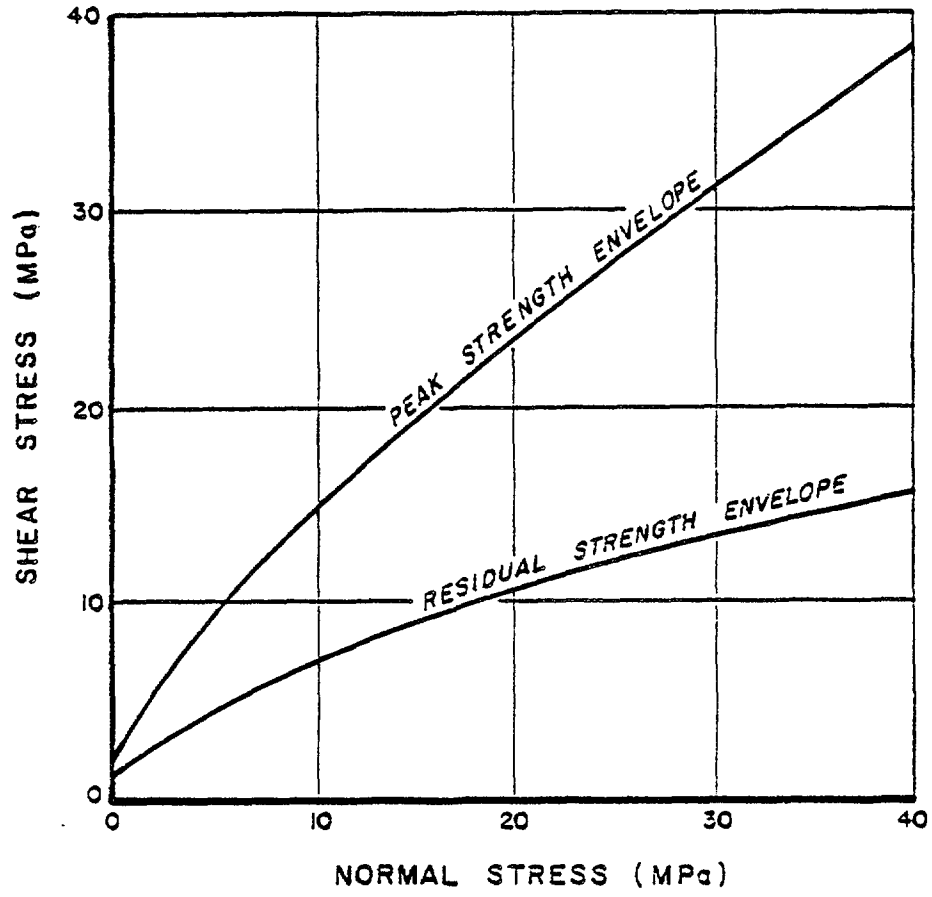


Figure B-1. Shear Strength of Fractured Basalt

a rock mass modulus could be estimated from the RMR index. For RMR greater than 55:

$$E = 2 (\text{RMR}) - 100 \quad (\text{B-4})$$

where:

E = equivalent Young's modulus (GPa) and  
RMR = rock mass rating

For RMR = 65 the deformation modulus is 30,000 MPa. The value of Poisson's ratio ( $\nu$ ) was selected at 0.2.

## B.2 CLOSED-FORM STRESS ANALYSIS

### B.2.1 Elastic Solution

Analysis of stresses within the elastic zone is based upon the Kirsch solution. For an elastic material that is unsupported the solution is:

$$\begin{aligned} \sigma_r &= p (1 - a^2/r^2) \\ \sigma_\theta &= p (1 + a^2/r^2) \end{aligned} \quad (\text{B-5})$$

where:

r = radius at point of stress calculation,  
a = radius of shaft,  
 $\sigma_r$  = radial stress,  
 $\sigma_\theta$  = tangential stress, and  
p = farfield hydrostatic stress.

This solution predicts that the radial stress is equal to zero at the shaft. The tangential stress at the shaft is twice the far field stress. These equations are used for elastic analysis of stress distribution around a shaft. If the tangential boundary stress ( $\sigma_\theta$ ) exceeds the unconfined compressive strength ( $\sigma_u$ ) of the rock mass, failure occurs and elasto-plastic analysis is applicable.

For an interior circular surface under internal support pressure from artificial support or from a failed annulus of rock:

$$\sigma_r = p - \frac{b}{r^2} \quad (B-6)$$

$$\sigma_\theta = p + \frac{b}{r^2}$$

where:

$b$  = constant (see below)

### B.2.2 Elasto-Plastic solution

Hoek and Brown (1980) present an elasto-plastic solution based upon the failure criterion in equation (B-1) for ultimate strength of the undisturbed rock. The form of the equation for residual strength of the plastic zone is similar with reduced  $m_r$  and  $s_r$  parameters replacing  $m$  and  $s$  in equation (B-1). Hoek and Brown express the elastic stresses as:

$$\sigma_r = p - (p - \sigma_{re}) (R/r)^2 \quad (B-7)$$

$$\sigma_\theta = p + (p - \sigma_{re}) (R/r)^2 \quad (B-8)$$

where:

$R$  = radius to the elastic boundary, and  
 $\sigma_{re}$  = constant.

$R$  is calculated as follows:

$$R = a e \left[ N - 2/m_r/\sigma_c (m_r \sigma_c p_i + s_r \sigma_c^2) \right]^{1/2} \quad (B-9)$$

where:

$$N = 2/(m_r \sigma_c) (m_r \sigma_c p + s_r \sigma_c^2 - m_r \sigma_c^2 M)^{1/2}$$

$m_r, s_r$  = residual strength parameter,  
 $p$  = farfield stress,  
 $\sigma_c$  = unconfined compressive strength, and  
 $p_i$  = internal support stress.

$$M = 1/2 \left[ (m/4)^2 + mp/\sigma_c + s \right]^{1/2} - (m/8)$$

The constant  $b$  (equation B-6) is given by:

$$b = p - \sigma_{re} \quad (B-10)$$

and the constant  $\sigma_{re}$  by:

$$\sigma_{re} = p - M\sigma_c \quad (B-11)$$

The radial and tangential stresses in the plastic zone are given by:

$$\sigma_r = (m_r \sigma_c / 4) \left[ \ln(r/a) \right]^2 + \left[ \ln(r/a) \right. \\ \left. (m_r \sigma_c p_i + s_r \sigma_c^2)^{1/2} \right] + p_i \quad (B-12)$$

$$\sigma_\theta = \sigma_r + (m_r \sigma_c \sigma_r + s_r \sigma_c^2)^{1/2} \quad (B-13)$$

Stress distributions predicted using the Hoek and Brown solution have been compared with stresses predicted using a solution developed by Bray (1967) and have been found to be in close agreement.

### B.3 CLOSED-FORM DISPLACEMENTS ANALYSIS

The analysis that follows assumes that the stress distribution and radius,  $R$ , to the elastic-plastic boundary is determined according to the Hoek and Brown (1980) solution. Let  $e_{av}$  be the average plastic volumetric strain associated with the passage from the original state to the failed state. By comparing volumes of the broken zone before and after, the following equation is obtained:

$$\pi (R^2 - r^2) = \pi \left[ (R + u_e)^2 - (r + u)^2 \right] (1 - e_{av}) \quad (B-14)$$

where:

- R = radius to elastic plastic boundary,  
 $u_e$  = displacement at elastic boundary R,  
 r = radius,  
 u = displacement at radius r, and  
 $e_{av}$  = average volumetric plastic strain.

Equation B-14 is a quadratic equation in u which can be solved. The elastic displacement is readily determined at the elastic boundary by substituting elastic stresses into the elastic constitutive relations of the rock mass:

$$u = \left[ -2a + \sqrt{(2a)^2 - 4Ta} \right] / 2 \quad (B-15)$$

where:

$$T = a \left[ \frac{-e_{av}}{1 - e_{av}} \right] + \frac{R^2}{a} \left[ \frac{e_{av}}{1 - e_{av}} \right] - 2 \left( \frac{R}{a} \right) u_e - \frac{u_e^2}{a} \quad (B-16)$$

To derive expressions for the radial and tangential components of strain, it is noted that:

$$\begin{aligned} \epsilon_{\theta} &= \frac{u}{r} \\ \epsilon_r &= \frac{du}{dr} \end{aligned} \quad (B-17)$$

The hoop strain is simply the radial displacement divided by r. The radial strain can be determined by setting the derivative of u to zero in Equation B-14:

$$2u + 2u + 2r \frac{du}{dr} + 2a \frac{-e_{av}}{1-e_{av}} = 0 \quad (\text{B-18})$$

From which the derivative,  $\frac{du}{dr}$  is obtained:

$$\epsilon_r = \frac{du}{dr} = \frac{-u - a \left[ \frac{e_{av}}{1 - e_{av}} \right]}{u + a} \quad (\text{B-19})$$

The distribution of displacement and strains for elasto-plastic analysis is illustrated in Figure B-2. The maximum displacement is calculated as 24 mm for a 3.7 m diameter shaft. This represents a displacement which is 1.33% of the shaft radius. The elastic displacement for a shaft which does not undergo plastic deformation is given by:

$$u = \frac{1 + \nu}{E} pa$$

Substituting in values for the elastic constants (Section B.1.2), a displacement of 2 mm is obtained. The ratio of predicted inelastic displacement to elastic displacement is thus approximately an order of magnitude. This ratio has practical significance as an indication that inelastic deformation has taken place. The radial strain in Figure B-2 exhibits a strain discontinuity at  $r = R$ , produced by the requirement that displacements at  $r = R$  are equal while tangential stress is discontinuous. The radial strain, equal to the derivative of the displacement is useful for assessing the extent of the disturbed zone.

#### References

- Barton, N., R. Lien and J. Lunde, 1974. "Engineering Classification of Rock Masses for the Design of Tunnel Supports," Rock Mechanics, 6, pp. 189-236.
- Bieniawski, Z. T., 1978, "Determining Rock Mass Deformability - Experience from Case Histories," Int. J. Rock Mech. Min. Sci., Vol. 15, No. 5, pp 237-248.
- Bieniawski, Z. T., 1979. The Geomechanics Classification in Rock Engineering Applications, 4th International Congress on Rock Mechanics, Vol. 2, 41-48, International Society for Rock Mechanics.

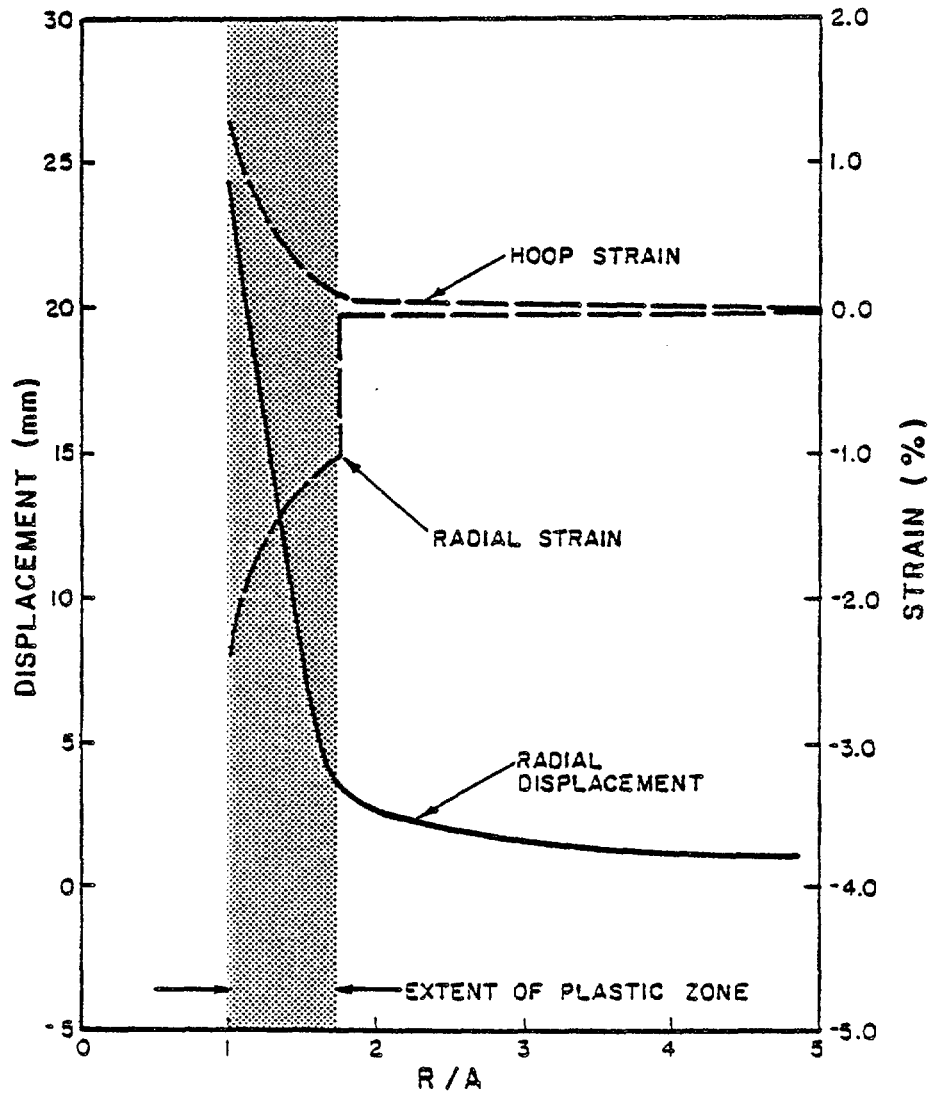


Figure B-2. Predicted Displacement and Strain for a 3.7m Diameter Shaft in Basalt at 1000m Depth - Elastoplastic Analysis

Bray, J. W., 1967. A Study of Jointed and Fractured Rock - Part II: Theory of Limiting Equilibrium," Rock Mechanics and Engineering Geology, Vol. V, No. 4, pp. 197-216.

Hoek, E., and E.T. Brown, 1980, Underground Excavations in Rock, Institution of Mining and Metallurgy, London, 527 pp.

Isherwood, D., 1981, Geoscience Data Base Handbook for Modeling a Nuclear Waste Repository, UCRL-52719, Lawrence Livermore Laboratories, Livermore, CA Vol. 2, p. 156.

Moak, D. J. and T. M. Wintczak, 1980. Near-Surface Test Facility Phase I Geologic Site Characterization Report, RHO-BWI-ST-8, Rockwell Hanford Operations, Richland, WA.

### 1.0 SCOPE

The purpose of this procedure is to provide the details for performing a down-hole tilt scale gyroscopic cluster-shot survey.

### 2.0 RESPONSIBILITIES

The NL Sperry-Sun personnel are responsible to carry out this procedure. Surveys will be performed at intervals of thirty feet (30') and as otherwise requested by the contractor.

### 3.0 PROCEDURE

#### 3.1 Instrument Preparation

##### A. Check 0° - 2° IOL (Inclinometer Oriented Line) in the test stand.

##### 1. Check alignment of scribe line and "T" slot

a. Place inclinometer "T" slot into the test stand jig.

b. Incline angle unit slowly at 30' intervals from 0° - 2° and observe that the scribe line remains centered over the bulls eye.

##### 2. Disengage "T" slot from test jig.

##### 3. Set test stand at 30' inclination.

##### 4. Place angle unit in the test stand, but do not clamp down.

##### 5. Gently rotate the angle unit through one complete revolution. DO NOT DISTURB THE TEST STAND!

##### 6. Observe that the angle unit reads the same as it is rotated.

##### 7. Set the test stand at inclinations of 1° 0', 1° 30' and repeat steps 3.1.a.5 - 3.1.a.6.

B. Check the gyro on the warm up power supply to assure that the drift (precession) rate is less than 6°/hour. Balance the gyro as necessary.

C. Check upper and lower solenoids for proper operation.

D. Check the lights in both inclinometer and gyro lens units.

PREPARED BY:

*S. E. Johnson* Date 2-16-83

APPROVED BY:

*S. E. Johnson* Date 2-17-83

QA CONCURRENCE BY:

*W. D. Small* Date 2-17-83

### 3.0 PROCEDURE (Cont.)

#### 3.1 Instrument Preparation (Cont.)

- E. Check programmer for proper operation.

#### 3.2 Rig-floor Preparation

- A. Check with the Driller and/or the Tool Pusher for the following:
  - 1. Verify that a landing crossbar is in the bit.
  - 2. Verify that the drilling assembly has a bit and top stabilizer of the same guage. (Cluster-shot surveys are invalid unless the drilling assembly meets this requirement.)
  - 3. Obtain a copy of Drilling Assembly drawing from Morrison-Knudsen or Geodril.
  - 4. Check the pipe talley and determine the bit depth prior to each survey.
  - 5. Bit depths shall be referenced to pad elevation as "Ground Zero", unless otherwise instructed by Morrison-Knudsen.
- B. Check wireline unit and wireline-rope socket compatibility.
- C. Check that a wireline swivel is in good condition and used for all surveys.
- D. Check instrument protective case, battery supply, and centralizers in accord with operator's manual.
- E. Make certain that a "Landing Foot" is installed on the bottom centralizer bar!
- F. Verify Foresight Direction of Reference Object supplied by Morrison-Knudsen.

#### 3.3 Conducting Cluster-Shot Surveys

- A. Assemble and orient gyro in accord with operator's manual.
- B. Position bottom of downhole assembly at the top of the drill pipe above the rotary table. Set wireline counter at (Zero - Length of pipe above Ground Zero).
- C. Restrict the wireline operator to a traverse speed of 200 ft/min or less.
- D. Make certain that the tool lands softly; stop the operator at least 60 feet above the predetermined bit depth and control the speed at a "crawl" rate until the tool has landed.

### 3.0 PROCEDURE (Cont.)

#### 3.3 Conducting Cluster-Shot Surveys (Cont.)

- E. Permit the wireline to have approximately 5 or 10 feet of slack.
- F. Be certain that the wireline remains slack and that the instrument is not disturbed during cluster-shot rotations.
- G. Proceed to take an eight-point, cluster shot survey.
  - 1. Delete drift checks; instead compute drift from initial orientation to final orientation and make a straight-line correction.
  - 2. After the instrument has landed inside the drilling assembly, subdivide the rotary bushings and table into eight points equally spaced at 45°.
  - 3. Obtain at least three still pictures at each point.
  - 4. Instruct the driller to rotate the pipe very slowly clockwise to the next point.
  - 5. If more than one depth is to be surveyed per trip in the hole, leave the instrument at rest in the bit, instruct the wireline operator to slack off as the Driller raises the bit to the next survey station.
  - 6. Repeat steps 3.3.G.1 - 3.3.G.5 as necessary.
  - 7. Four stations can be surveyed on one trip in the hole using three, 30-foot joints of drill pipe that are raised above the rotary table.
- H. Retrieve instrument and take final orientation in accord with operator's manual.
- I. Secure all equipment and leave the instruments in a state of readiness for the next job.

#### 3.4 Processing Survey Data

- A. Develop film and determine validity of survey immediately.
  - 1. In case of an instrument malfunction, notify the Engineer, Tool Pusher and/or the Driller immediately of the mis-run.
    - a. At the instruction of Morrison-Knudsen, the survey will be re-run immediately; or,
    - b. The missed survey station may be re-run along with the next survey station after the next 30 feet are drilled.

### 3.0 PROCEDURE (Cont.)

#### 3.4 Processing Survey Data (Cont.)

2. In case of a valid survey, results will be computed on location and posted in the M-K QA office.
  - a. The Survey Tabulation sheet will be updated for each subsequent survey.
  - b. A Horizontal Projection Map will be updated after each survey, and the map will be maintained in the M-K QA office.
  - c. Before leaving the location, the surveyor will report the survey results to the M-K QA office.

#### b. Computation Methods

Either of two methods of calculations may be used: 1) Monroe 1880 Calculator or 2) manual calculation.

1. Calculator method will be used at times when 110VAC/60HZ power is available and when the calculator is in an operating condition.
  - a. Compute survey data for each rotation shot in accord with operator's manual.
  - b. Determine observed inclination and corrected Surwel Hole Direction Azimuth (counter-clockwise Az.) for each rotation point.
  - c. Use the two-film New Center Program and enter the data as follows:
    1. Revert the Surwel Azimuth from counter-clockwise to Real-World (clockwise) Azimuth, i.e.  $(360^\circ - \text{Surwel Az.} = \text{Real-World Azimuth})$ .
    2. Use the "eight-point" New Center Program.
    3. Enter observed inclination for each rotation point in accord with the program.
    4. Enter the Hole Direction Real-World (clockwise) Azimuth as the inclination Azimuth for each rotation point.
    5. Enter corrected gyro data in accordance with program.

3.0 PROCEDURE (Cont.)

3.4 Processing Survey Data (Cont.)

B. Computation Methods (Cont.)

1. (Cont.)

c. (Cont.)

6. The True Inclination and Direction for the survey station will be printed out in an Inclination and Clockwise (Real-World) Azimuth.

7. Compute the Latitude, Departure, and Horizontal Displacement for the survey station in accord with the operator's manual.

2. Manual Calculation Method

a. Perform steps 3.4.A.1 and 3.4.A.2.

b. Using polar-coordinate paper, select a convenient scale for the amount of observed inclination for the eight points of the survey station.

c. Plot the inclination and the Surwel, Hole Direction Azimuth (Inclination Azimuth plus corrected Gyro Azimuth) counter-clockwise.

d. The true inclination and direction for the survey station is found at the "center" formed by the perpendicular bisectors of the cords of the circular, rotation points.

e. Perform step 3.4.B.1.c.7.

3.5 Cluster-Shot Survey Reports

A. The official Survey Tabulation sheet and Horizontal Plot for cluster-shots taken during drilling operations shall be maintained in the M-K QA office.

B. Each survey shall be assigned an NL Sperry-Sun job number and all copies of respective field data sheets, computation sheets, and field envelopes shall be properly identified with the following information:

1. Hole Number

2. Job Number

3. Contractor's Name

4. Depths Surveyed

5. Date

3.0 PROCEDURE (Cont.)

3.5 Cluster-Shot Survey Reports (Cont.)

- C. The survey reports will be submitted to Morrison-Knudsen QA department at the field operations office.

3.6 Reports for ~~Bottom~~<sup>t</sup>-Hole Location Surveys

- A. All surveys will be calculated on location, and the field reports will be submitted in accord with the operator's manual.
- B. The survey data will be forwarded to the nearest NL Sperry-Sun district office where it will be recalculated and a formal survey report complete with computer print-out and computerized plots will be prepared and mailed to:

Mr. F.C. Larvie  
Morrison-Knudsen Co., Inc.  
P.O. Box 1450  
Richland, WA 99352

Rockwell Hanford Operations

Total page count 132

<b>SUPPORTING DOCUMENT</b>		Number <b>SD- BWI-TI-113</b>	Rev. Ltr./ Chg. No. <b>0-0</b>	Page 1 of 95 <b>A1-A23 B1-B14</b>
PROGRAM: <b>Basalt Waste Isolation Project</b>		Baseline Document <input type="checkbox"/> Yes <input checked="" type="checkbox"/> No		
Document Title: <b>Principal Borehole Report Borehole RRL-2</b>		WBS No. or Work Package No. <b>LF422 CEI 004,003</b>		
Key Words:		Prepared by (Name and Dept. No.) <b>T. M. Wintczak</b> <i>T. M. Wintczak</i>		Date <b>1/20/83</b>
Abstract		* Distribution Name Mail Address		
<p>The Principal Borehole, RRL-2, was drilled to provide information required for shaft design, selection of porthole locations and site suitability studies.</p> <p>The borehole meets objective 1 of the Test Plan for Exploratory Shaft - Phase I and Phase II.</p> <p>The report presents the results of borehole drilling, the geological and geophysical logging, and the testing associated with Borehole RRL-2.</p>		<b>ROCKWELL HANFORD OPERATIONS</b>		
		<ul style="list-style-type: none"> <li>* S. M. Baker PBB/700</li> <li>* H. W. Brandt PBB/700</li> <li>* D. J. Brown PBB/700</li> <li>* R. W. Bryce PBB/700</li> <li>* R. A. Deju PBB/700</li> <li>* H. B. Dietz PBB/700</li> <li>* L. R. Fitch PBB/700</li> <li>* R. N. Gurley 1135 Jad/700</li> <li>* G. S. Hunt PBB/700</li> <li>* L. L. Johnson PBB/700</li> <li>* K. S. Kim PBB/700</li> <li>* J. H. LaRue PBB/700</li> <li>* P. E. Long PBB/700</li> <li>* R. K. Ledgerwood PBB/700</li> <li>* D. J. Moak MO-029/600</li> <li>* S. M. Price PBB/700</li> <li>* W. H. Price MO-029/600</li> <li>* P. J. Reder <i>(PP)</i> 1135 Jad/700</li> <li>* T. A. Rundle Gable Mtn/600</li> <li>* M. J. Smith 2101M/200E</li> <li>* F. A. Spane MO-029/600</li> <li>* S. R. Strait MO-029/600</li> <li>* W. R. Sublette Gable Mtn/600</li> <li>* D. A. Turner PBB/700</li> <li>* Rec. Ret. 1135 Jad/700</li> <li>* D&amp;T File MO-029/600</li> <li>* T. M. Wintczak(2) MO-029/600</li> <li>* R. M. Ybarra PBB/700</li> <li>* W. F. Todish (Orig &amp; 2) 1135J/1100</li> </ul> <p style="text-align: center;"><b>U. S. DEPARTMENT OF ENERGY</b></p> <ul style="list-style-type: none"> <li>* J. H. Anttonen FED/700</li> <li>* M. W. Frei DOE/HQ</li> <li>* A. G. Lassila PBB/700</li> <li>* O. L. Olson (2) PBB/700</li> </ul>		
<p>Initiated by: <b>ROCKWELL</b> Used by: <b>ROCKWELL</b></p> <p style="text-align: center;">*COMPLETE DOCUMENT (No asterisk, title page/ summary of revision page only)</p>		(May be continued on page 2)		
<div style="border: 2px solid black; padding: 5px; display: inline-block;"> <p><b>BASALT</b></p> <p>THIS DOCUMENT IS A ROCKWELL SUPPORTING DOCUMENT FOR USE BY ROCKWELL, ITS AUTHORIZED SUBCONTRACTORS, AND THE DEPARTMENT OF ENERGY</p> </div>		Initial Release Stamp		
		<div style="border: 1px solid black; padding: 10px; display: inline-block;"> <p style="font-size: 2em; border: 1px solid black; border-radius: 50%; width: 30px; height: 30px; display: flex; align-items: center; justify-content: center; margin: 0 auto;">10</p> <p style="margin: 5px 0;"><b>OFFICIALLY RELEASED</b></p> <p style="margin: 5px 0;"><b>1983 JAN 31 PM 2:32</b></p> </div>		

Rockwell Hanford Operations

SUPPORTING DOCUMENT	Number SD - BWI-TI-113	Page 2												
<p>Approvals</p> <p><input checked="" type="checkbox"/> <u><i>R. A. Deju</i></u> Program Office R. A. Deju</p> <p><input type="checkbox"/> _____ Research and Engineering</p> <p><input type="checkbox"/> _____ Plant Operations</p> <p><input type="checkbox"/> _____ Health, Safety and Environment</p> <p><input type="checkbox"/> _____ Quality Assurance</p> <p><input type="checkbox"/> _____ Training</p> <p><input checked="" type="checkbox"/> <u><i>E. R. Fitch</i></u> E. R. Fitch</p> <p><input checked="" type="checkbox"/> <u><i>H. B. Dietz</i></u> H. B. Dietz</p> <p><input checked="" type="checkbox"/> <u><i>D. A. Turner</i></u> D. A. Turner</p> <p><input checked="" type="checkbox"/> <u><i>G. S. Hunt</i></u> G. S. Hunt</p> <p><input checked="" type="checkbox"/> <u><i>W. H. Price</i></u> Approval Authority W. H. Price</p>	<table border="1" style="width:100%; border-collapse: collapse;"> <thead> <tr> <th style="width:10%;">* Distribution</th> <th style="width:60%;">Name</th> <th style="width:30%;">Mail Address</th> </tr> </thead> <tbody> <tr> <td>*</td> <td>P. E. Rasmussen</td> <td>FED/700</td> </tr> <tr> <td>*</td> <td>R. Stein (2)</td> <td>DOE/HQ</td> </tr> <tr> <td>*</td> <td>J. J. Sutey</td> <td>FED/700</td> </tr> </tbody> </table>		* Distribution	Name	Mail Address	*	P. E. Rasmussen	FED/700	*	R. Stein (2)	DOE/HQ	*	J. J. Sutey	FED/700
* Distribution	Name	Mail Address												
*	P. E. Rasmussen	FED/700												
*	R. Stein (2)	DOE/HQ												
*	J. J. Sutey	FED/700												

PRINCIPAL BOREHOLE REPORT  
BOREHOLE RRL-2  
STAFF  
BASALT WASTE ISOLATION PROJECT  
JANUARY 1983

## CONTENTS

Introduction . . . . .	7
Summary and Conclusions. . . . .	7
Selection of Reference Repository Location . . . . .	16
General Geology. . . . .	17
Borehole History . . . . .	20
Introduction. . . . .	20
Drilling. . . . .	20
Geologic Logging. . . . .	22
Geomechanical Logging . . . . .	30
Geophysical Logging . . . . .	30
Geologic Characterization. . . . .	37
Introduction. . . . .	37
Methodology . . . . .	37
Results . . . . .	39
Hydrologic Testing . . . . .	53
Introduction. . . . .	53
Methodology . . . . .	53
Results . . . . .	56
Hydrochemistry . . . . .	62
Introduction. . . . .	62
Methodology . . . . .	62
Results . . . . .	62
Geomechanics Laboratory Characterization . . . . .	72
Introduction. . . . .	72
Methodology . . . . .	72
Physical Property Tests . . . . .	73
Mechanical Property Tests . . . . .	73
Results . . . . .	74
In Situ Stress Measurements. . . . .	87
Introduction. . . . .	87
Methodology . . . . .	87
Results . . . . .	90
References . . . . .	94
Bibliography . . . . .	95
Appendices	
A. . . . .	A-1
B. . . . .	B-1

## FIGURES:

1.	Location Map of the Columbia Plateau, Pasco Basin and Hanford Site . . . . .	8
2.	Location of Candidate Sites in the Cold Creek Syncline . . . . .	9
3.	Stratigraphic Nomenclature, Columbia River Basalt Group, Pasco Basin. . . . .	18
4.	Informal Structural Subprovinces of the Pasco Basin Columbia Plateau . . . . .	19
5.	As-Built for Borehole RRL-2. . . . .	21
6.	Borehole RRL-2--Drill and Test Schedule. . . . .	23
7.	Borehole RRL-2--Deviation Survey Plan View . . . . .	25
8.	Borehole RRL-2--Deviation Survey Sectional View. . . . .	26
9.	Shift Report of Operations Form. . . . .	29
10.	Borehole RRL-2--Summary Geophysical Log, 0-1,400 Feet. . . . .	34
11.	Borehole RRL-2--Summary Geophysical Log, 1,400-2,800 Feet. . . . .	35
12.	Borehole RRL-2--Summary Geophysical Log, 2,800-3,973 Feet. . . . .	36
13.	Location Map--Columbia Plateau, Hanford Site, Cold Creek Syncline, Reference Repository Location, and Borehole RRL-2 . . . . .	38
14.	Lithology of the Cohasset Flow--Borehole RRL-2. . . . .	40
15.	Lithology of the McCoy Canyon Flow--Borehole RRL-2 . . . . .	41
16.	Lithology of the Umtanum Flow--Borehole RRL-2. . . . .	42
17.	Borehole RRL-2-- Geophysical Logs of Test Intervals, 1,300-2,700 Feet . . . . .	54
18.	Borehole RRL-2--Geophysical Logs of Test Intervals, 2,700-3,900 Feet . . . . .	55
19.	Comparison of Equivalent Conductivity Values Between Borehole RRL-2 Interflow Zones and Sedimentary Interbeds. . . . .	61
20.	Selected Stiff Diagrams for Columbia River Basalt in Groundwaters in Borehole RRL-2 . . . . .	65
21.	Strength Test Results Plotted in Linear Form of Empirical Failure Criteria . . . . .	85
22.	Disking in the Cohasset Flow in Borehole RRL-2 . . . . .	88
23.	Downhole Tools. . . . .	91
24.	Typical Pressure Versus Time Curve . . . . .	92
25.	Typical Fracture Impression. . . . .	93

## TABLES:

1.	Detailed Stratigraphy of Borehole RRL-2. . . . .	11
2.	Borehole RRL-2--Cementing Details. . . . .	24
3.	Borehole RRL-2--Deviation Survey . . . . .	27
4.	Borehole RRL-2--Geophysical Logging Intervals. . . . .	33
5.	Borehole RRL-2--Major Element Chemistry (vol%) . . . . .	44
6.	Means of Major and Minor Oxides for the Candidate Horizons . . . . .	48
7.	Borehole RRL-2--Estimated Inclination and Statistical Parameters for Paleomagnetic Samples . . . . .	49
8.	Model Mineralogy of Cohasset, McCoy Canyon, and Umtanum Flows from Borehole RRL-2 Core Samples . . . . .	50

9.	Borehole RRL-2--Predicted and Observed Stratigraphy. . . . .	52
10.	Hydrologic Properties from Borehole RRL-2. . . . .	57
11.	Predicted Versus Observed Hydrologic Characteristics in Borehole RRL-2. . . . .	59
12.	Borehole RRL-2--Groundwater Sample Intervals . . . . .	63
13.	Borehole RRL-2--Major Inorganic Constituents in Groundwater. . . . .	64
14.	Borehole RRL-2--Trace Element Concentrations in Groundwater. . . . .	66
15.	Borehole RRL-2--Distribution of Dissolved Gas Components in Grande Ronde Basalt Zones . . . . .	68
16.	Borehole RRL-2--Isotopic Data for Groundwater . . . . .	69
17.	Borehole RRL-2--pH, Eh, Temperature and Electrical Conductivity for Groundwater Samples. . . . .	71
18.	Summary of Borehole RRL-2--Basalt Physical and Mechanical Property Data--Flow Top/Vesicular Zones. . . . .	75
19.	Summary of Borehole RRL-2--Basalt Physical and Mechanical Property Data--Entablature . . . . .	77
20.	Summary of Borehole RRL-2--Basalt Physical and Mechanical Property Data--Colonnade . . . . .	79
21.	Thermomechanical Characteristics of the Columbia River Basalt Group. . . . .	82
22.	Linear Regression Analysis of Borehole RRL-2--Strength Test Results . . . . .	83
23.	Borehole RRL-2--Hydraulic Fracturing Data Analysis, October 1982. . . . .	89

## INTRODUCTION

The principal borehole, RRL-2, was drilled to provide information required for shaft design, selection of porthole locations and site suitability studies. The borehole meets the following objectives:

**Principal Borehole Tests:** Provide the design information required for design and selection of porthole locations and ascertain the overall suitability of the proposed location for an exploratory shaft at the reference repository location.

Examination of core, downhole tests and laboratory tests provided the site-specific data required for shaft design and selection of porthole locations in the shaft. The borehole serves to assure that the stratigraphic and hydrologic regime are consistent with the overall isolation requirements for a repository.

The initial choices for candidate horizons were the Umtanum and Cohasset\* flows. The testing in Borehole RRL-2 was based on these flows. Recently, a screening of candidate horizons was conducted. The results indicated that the Cohasset, McCoy Canyon, and Umtanum flows all met the screening criteria. Since the McCoy Canyon flow was recently identified as a candidate horizon, hydrology and in situ stress data for this flow, in borehole RRL-2, are not available.

Borehole RRL-2 is located on the Hanford Site in the western half of the A-H site (Fig. 1 and 2). The collar elevation is 633.9 ft (193.2 m) above mean sea level. The Washington State coordinates are N444,297.87, E2,211,184.57. The borehole is 300 ft (91.4 m) east of the exploratory shaft location.

This principal borehole report presents the results of borehole drilling, the geological and geophysical logging and the testing associated with borehole RRL-2. It includes the borehole history, geology, hydrology, geomechanics laboratory characterization, and in situ stress tests for borehole RRL-2.

---

\*Cohasset flow--previously called the Middle Sentinel Bluffs flow or Sentinel Bluffs "through runner."

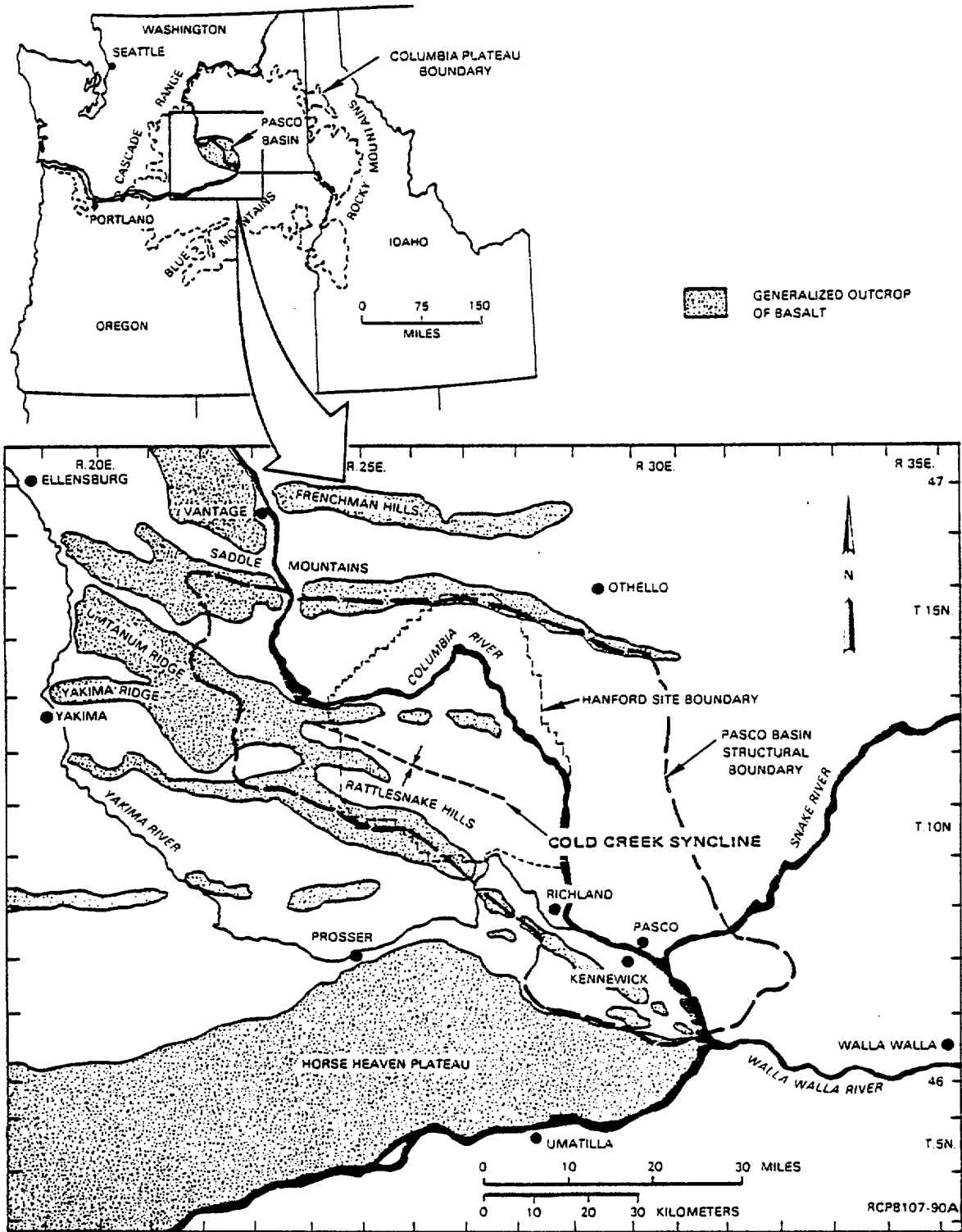


FIGURE 1. Location Map of the Columbia Plateau, Pasco Basin and Hanford Site.

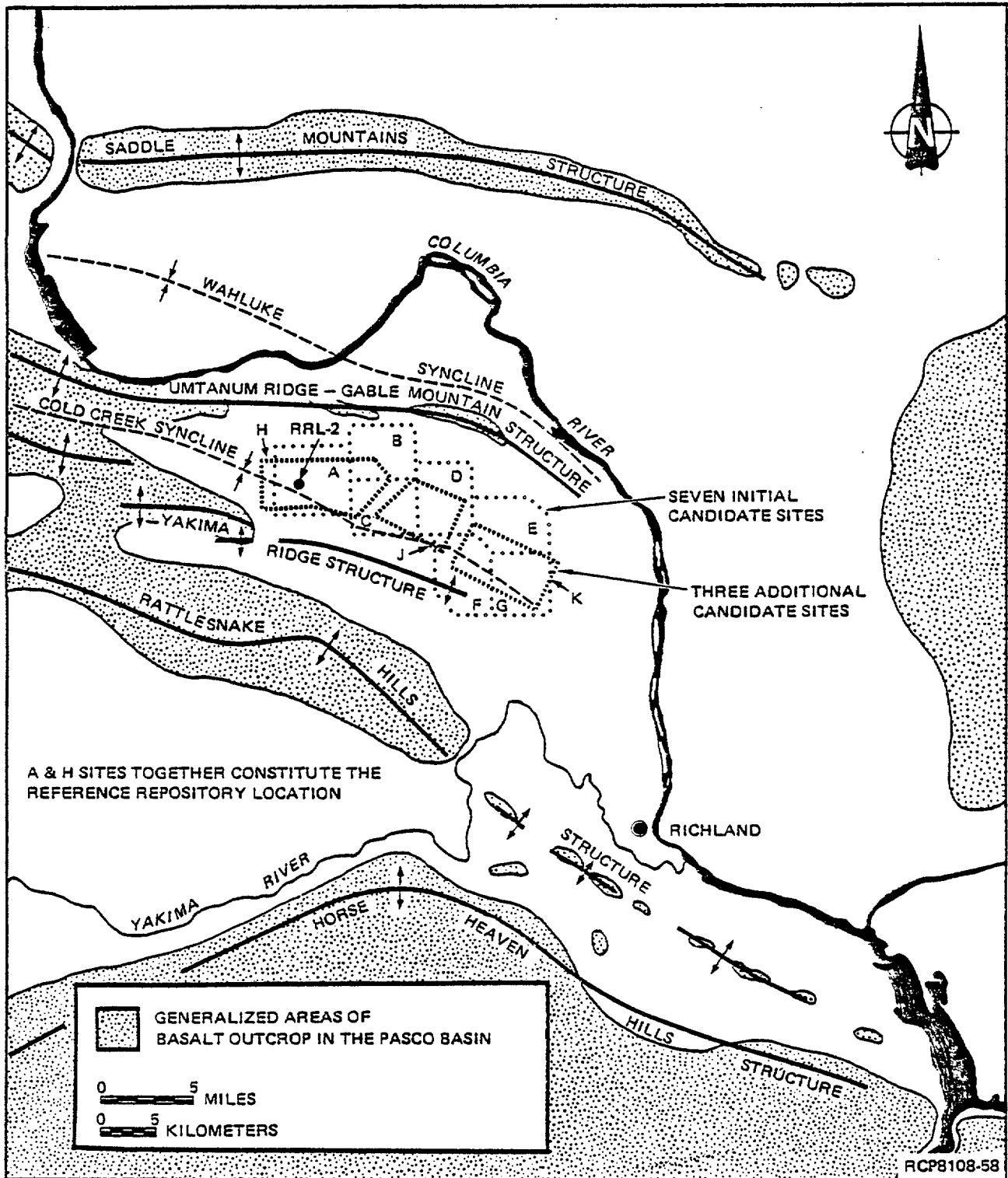


FIGURE 2. Location of Candidate Sites in the Cold Creek Syncline.

## SUMMARY AND CONCLUSIONS

The principal borehole, RRL-2, was drilled to provide the information required for shaft design, selection of porthole locations and to ascertain the overall suitability of the proposed location for an exploratory shaft at the reference repository location (RRL).

The information necessary for porthole design and location is the detailed stratigraphy (Table 1). The parameters on which site suitability is to be judged are the following:

- Depth to top of candidate repository horizon

The design basis maximum depth is 4,000 ft (1,219.2 m). The depths to the top of the candidate horizons are:

Cohasset	2,993 ft (912.3 m)
McCoy Canyon	3,475 ft (1,059.2 m)
Umtanum	3,607 ft (1,099.4 m)

- Thickness of candidate repository horizon interior

The design basis minimum thickness is 80 ft (24.4 m). The thickness of the interiors of the candidate horizons are:

Cohasset	245 ft (74.7 m)
McCoy Canyon	106 ft (32.3 m)
Umtanum	84 ft (25.6 m)

- In situ temperature of the candidate repository horizon

The design basis maximum temperature is 150°F (65°C). The temperatures of the interiors of the candidate horizons are:

Cohasset	124°F (51°C)
McCoy Canyon	131°F (55°C)
Umtanum	136°F (58°C)

- Maximum horizontal stress magnitude

The design basis maximum horizontal stress magnitude is 12,000 psi (81 MPa). The maximum average stress magnitude measured for the candidate horizons are:

Cohasset	7,780 psi (53 MPa)
McCoy Canyon	no data
Umtanum	9,730 psi (67 MPa)

TABLE 1. Detailed Stratigraphy of Borehole RRL-2. (Sheet 1 of 4)

Ground surface elevation = 633.9 ft.  
All numbers are drilled depths or thicknesses in feet.

Stratigraphic units*	Contact (top of unit)	Thickness	Interval of flow top or bottom rubble or breccia (B)	Vesicle zone	Vuggy zone	Disking
			Top - bottom	Top - bottom	Top - bottom	
Saddle Mountain Basalt						
Elephant Mountain	Start of core 605	81		613.5 - 662.5 618.0 - 686.0		
Rattlesnake Ridge Interbed	686	96				
Pomona	782	159.5	798.0 - 798.0 812.0 - 814.0 845.0 - 855.0	782.0 - 796.0 798.0 - 810.0 814.0 - 839.0 855.0 - 857.0	858.0 - 868.0	
Selah Interbed	941.5	44.5				
Esquatzel	986	118	986.0 - 1004.0 1103.0 - 1104.0	1005.0 - 1009.0 1016.0 - 1018.0	1020.0 - 1030.0	
Cold Creek Interbed	1104	64				
Umatilla	1168	231	1168.0 - 1185(b)		1199.0 - 1202.0	
Mabton Interbed	1399	124				

TABLE 1. Detailed Stratigraphy of Borehole RRL-2. (Sheet 2 of 4)

Ground surface elevation = 633.9 ft.  
 All numbers are drilled depths or thicknesses in feet.

Stratigraphic units*	Contact (top of unit)	Thickness	Interval of flow top or bottom rubble or breccia (B)	Vesicle zone	Vuggy zone	Disking
			Top - bottom	Top - bottom	Top - bottom	
Wanapum Basalt						
Priest Rapids (Lolo)	1523	166			1526.0 - 1531.0 1551.0 - 1555.0	
Priest Rapids (Rosalia)	1689	60	1689.0 - 1692.0	1692.0 - 1714.0		1692.0 - 1712.0
Unnamed Interbed	1749.4	0.6				
Roza (Lobe II)	1750	28	1750.0 - 1754.0 1774.0 - 1776.0	1754.0 - 1762.0 1776.0 - 1778.0		
Roza (Lobe I)	1778	144	1778.0 - 1786.0		1786.0 - 1790.0	
Frenchman Springs 1	1922	182		1922.0 - 1928.0 1931.0 - 1933.0 1938.0 - 1943.0 2006.0 - 2013.0 2022.0 - 2034.0 2102.0 - 2104.0	1051.0 - 1979.0	
Frenchman Springs 2	2104	113	2104.0 - 2110(b)	2111.0 - 2122.0	2127.0 - 2142.0	2145.0 - 2148.0 2171.0 - 2177.0 2190.0 - 2195.0 2197.0 - 2205.0
Frenchman Springs 3	2217	56	2223.0 - 2227.0	2216.0 - 2217.0 2217.0 - 2223.0	2227.0 - 2234.0	2239.0 2254.0 - 2255.0 2269.0
Frenchman Springs 4	2273	108	2271.0 - 2273(b) 2273.0 - 2275.0	2270.0 - 2273.0 2275.0 - 2318.0  2338.0 - 2340.0		2295.0 - 2299.0 2311.0 - 2312.0 2327.0 - 2329.0 2344.0 - 2353.0

TABLE 1. Detailed Stratigraphy of Borehole RRL-2. (Sheet 3 of 4)

Ground surface elevation = 633.9 ft.  
All numbers are drilled depths or thicknesses in feet.

Stratigraphic units*	Contact (top of unit)	Thickness	Interval of flow top or bottom rubble or breccia (B)	Vesicle zone	Vuggy zone	Disking
			Top - bottom	Top - bottom	Top - bottom	
Frenchman Springs 5	2381	108	2381.0 - 2409.0	2443.0 - 2445.0	2412.0 - 2443.0 2445.0 - 2453.0	2439.0 - 2450.0
Frenchman Springs 6	2489	128	2489.0 - 2500.0	2581.0 - 2525.0	2500.0 - 25.8.0	2527.0 - 2530.0 2573.0 - 2577.0 2586.0 - 2589.0 2594.0 - 2598.0
Frenchman Springs 7	2617	66	2617.0 - 2619(b) 2619.0 - 2623.0	2623.0 - 2628.0 2666.0 - 2669.0 2671.0 - 2677.0 2679.0 - 2683.0		2645.0 - 2651.0
Vantage Interbed	2683	4				
Grande Ronde Basalt						
Grande Ronde 1	2687	34		2687.0 - 2702.0		
Grande Ronde 2	2721	102		2721.0 - 2742.0	2746.0 - 2761.0	2816.0 - 2818.0
Grande Ronde 3	2823	170	2823.9 - 2840(b)	2851.0 - 2854.0 2858.0 - 2862.0	2871.0 - 2905.0	2857.0 - 2858.0 2865.0 - 2867.0 2911.0 - 2921.0 2933.0 - 2938.0 2969.0 - 2974.0 2979.0
Grande Ronde 4 Cohasset	2993	262	2993.0 - 2999.0	3095.0 - 3107.0	2999.0 - 3010.0 3083.0 - 3092.0	3011.0 - 3017.0 3021.0 - 3078.0 3105.0 - 3107.0 3183.0 - 3217.0

TABLE 1. Detailed Stratigraphy of Borehole RRL-2. (Sheet 4 of 4)

Ground surface elevation = 633.9 ft.  
All numbers are drilled depths or thicknesses in feet.

Stratigraphic units*	Contact (top of unit)	Thickness	Interval of flow top or bottom rubble or breccia (B)	Vesicle zone	Vuggy zone	Disking
			Top - bottom	Top - bottom	Top - bottom	
Grande Ronde 5	3255	133	3255.0 - 3277(b) 3280.0 - 3291.0	3301.0 - 3306.0 3312.0 - 3317.0 3320.0 - 3335.0	3294.0 - 3301.0 3306.0 - 3312.0 3317.0 - 3320.0	3341.0 - 3343.0 3353.0 - 3354.5 3364.0 - 3372.0
Grande Ronde 6	3388	30	3386.0 - 3388(b) 3388.0 - 3397.0	3416.5 - 3418.0		3404.0 - 3415.0
Grande Ronde 7	3418	57		3421.5 - 3428.0 3474.0 - 3475.0	3418.0 - 3421.5 3428.0 - 3442.0	
Grande Ronde 8	3475.0	132	3475.0 - 3493(b)	3525.0 - 3527.0  3599.0 - 3607.0	3493.0 - 3496.0 3527.0 - 3548.0	3523.0 - 3525.0 3533.0 - 3541.0 3544.0 - 3549.0 3553.0 - 3558.0 3571.0 - 3577.0 3583.0 3590.0 - 3593.0
Grande Ronde 9 Umtanum flow	3607	232	3607.0 - 3755(b)		3624.0 - 3626.0	3763.0 - 3802.0 3829.0 - 3834.0
Grande Ronde 10 very-high Mg flow	3839	64	3839.0 - 3865(b) 3891-3903(b)			
Grande Ronde 11	3903	70+	3903.0 - 3916.0		3916.0 - 3936.0 3937.0 - 3942.0 3947.0 - 3960.0	3944.0 - 3947.0
Total depth = 3,973.0						

\*Units include members, flows, flow lobes and sedimentary interbeds.  
NOTE: To convert feet to meters, multiply by 0.3048.

Therefore, the Cohasset and Umtanum flows are acceptable candidate horizons for all four design basis parameters. The McCoy Canyon flow is acceptable for the design basis parameters of depth, thickness and temperature, however, no stress data is available.

An additional parameter on which suitability of the site was judged was hydrologic long-term performance, which was reported in the Site Characterization Report for the Basalt Waste Isolation Project (Rockwell, 1982). The hydrology data presented in the section under "Hydrologic Testing" in this report provides the basis for the long-term performance analysis.

## SELECTION OF THE REFERENCE REPOSITORY LOCATION

The National Waste Terminal Storage siting process is a stepwise procedure involving several phases, beginning with site screening and ending with site selection. In 1979, available geologic and hydrologic data were combined with existing information on socioeconomics, land use and environment to identify the seven initial sites in the Cold Creek syncline in the Pasco Basin (see Fig. 1 and 2). Geologic information obtained subsequent to that presented in Myers, Price and others (1979) was used to identify three additional sites (H, J and K; see Fig. 2). All candidate repository sites were evaluated by a committee comprised of personnel from Rockwell Hanford Operations and Woodward-Clyde Consultants (WCC, 1981). One site, the combination of sites A and H, emerged as the highest ranked. This candidate site in the Cold Creek syncline is referred to as the RRL.

## GENERAL GEOLOGY

The Cold Creek syncline, in which the RRL is located, is in the western Pasco Basin, one of several structural and topographic basins within the western Columbia Plateau (see Fig. 1). The plateau is primarily underlain by a Miocene volcanic sequence termed the Columbia River Basalt Group (Fig. 3).

The bulk of the Columbia River Basalt Group is comprised of flows that belong to the Yakima Basalt Subgroup. The oldest formation of this subgroup, the Grande Ronde Basalt, was erupted between 16.5 and 14.5 million years before present (m.y.B.P.). The Grande Ronde Basalt is the most voluminous unit of the group ( 85 vol%) and underlies most of the Columbia Plateau. Grande Ronde Basalt is overlain by Wanapum Basalt. This is the second most voluminous formation of the group ( 5 vol%) and was erupted between 14.5 and 13.5 m.y.B.P. The Saddle Mountains Basalt, the youngest formation of this subgroup, comprises 1 vol% of the group and was erupted during a period of waning volcanism, 13.5 to 6 m.y.B.P.

In general, the Columbia Plateau can be subdivided into three informal structural subprovinces: the Yakima Fold Belt subprovince, Palouse subprovince and Blue Mountain subprovince (Fig. 4).

The Pasco Basin spans the area of transition between the Yakima Fold Belt subprovince and the Palouse subprovince. Anticlinal folds of the Yakima Fold Belt bound the basin on the north and south and plunge eastward into the basin from the west (see Fig. 2). Most of the anticlines are asymmetric and have second-order folds in their hinge zones. Drill holes and geophysical surveys reveal that most subsurface structures in the central Pasco Basin appear to be extensions of the Yakima folds and their associated second-order structures; however, a few subsurface structures might be related to northwest-trending structures that appear to crosscut the east-west-trending Yakima folds.

Synclines between the anticlines are generally broad, open folds that are sediment filled. Major synclines within the Pasco Basin include the Wahluke and Cold Creek synclines. The Wahluke syncline lies between the Saddle Mountains and Umtanum Ridge-Gable Mountain anticlinal structures (see Fig. 2). The Cold Creek syncline is the relatively low-relief, sediment-filled trough that is bounded by the Umtanum Ridge-Gable Mountain anticlinal structure and the Yakima Ridge anticlinal structure (see Fig. 2).



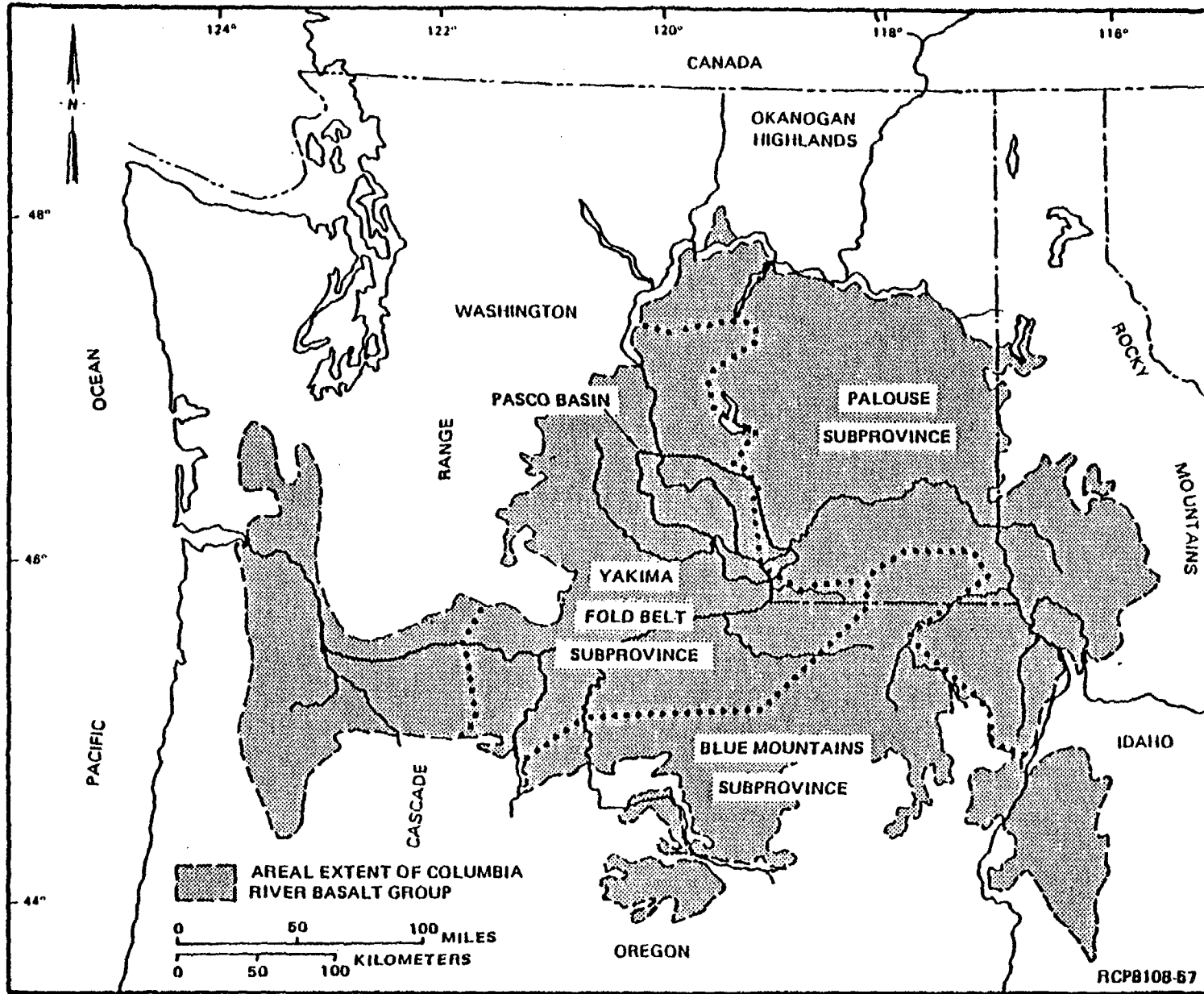


FIGURE 4. Informal Structural Subprovinces of the Columbia Plateau.

## BOREHOLE HISTORY

## INTRODUCTION

Borehole RRL-2 was completed in June 1982 by the Boyles Brothers Drilling Company, Salt Lake City, Utah, under subcontract to Rockwell Hanford Operations, Richland, Washington. Rockwell's Basalt Waste Isolation Project (BWIP) personnel furnished continuous supervision of the core drilling, geologic logging, geophysical logging and hydrologic testing activities for this borehole.

## DRILLING

The initial phase of drilling was performed between February and September of 1981 as part of a program of six boreholes to identify an exploratory shaft site. The work during this period included drilling borehole RRL-2 to a depth of 1,544 ft (470.6 m) and installing 16-in. (40.6-cm) casing to 18 ft (5.5 m), 12-in. (30.5-cm) casing to 103 ft (31.4 m), and 8-in. (20.3-cm) PVC casing and 5.5-in. (14.0-cm) casing to 615 ft (187.5 m) (Fig. 5).

The sediments overlying the basalt were drilled by cable tool and mud rotary methods to a depth of 615 ft (187.4 m). The top of basalt was encountered at a depth of 605 ft (184.0 m). A Chicago Pneumatic Model (CP) 50 core drill using a PQ 4.835-in.- (12.3-cm-) diameter diamond bit was used to drill the basalt sequence from 616 ft (187.8 m) to a depth of 1,544 ft (470.6 m). For this interval, the borehole penetrated the Saddle Mountains Basalt and was terminated in the interior of the Priest Rapids II flow of the Wanapum Basalt.

After completion of the six boreholes, the data were integrated with existing geological, geophysical, and hydrological data to select a site within the RRL for the principal borehole and exploratory shaft (BWIP, 1982). The data analysis showed that borehole RRL-2 was located in what was determined to be a suitable area for the exploratory shaft.

In January 1982, after selection of borehole RRL-2 as the principal borehole, drilling was resumed using a CP-50 core drill. Prior to drilling, a 4.5-in.- (11.4-cm-) steel casing was cemented to the total depth of 1,545 ft (470.9 m).

The borehole was then advanced using HQ 3.937-in.- (10-cm-) diameter diamond bits to a depth of 2,713 ft (826.9 m). After completion of hydrological testing and geophysical logging, 3.5-in. (8.9-cm) casing was cemented to the total depth. The borehole was then drilled using NQ 2.98-in.- (76-mm-) diameter diamond bits to the completed depth of 3,973 ft (1,211.0 m). All coring utilized triple tube core barrels. The core recovery for the borehole exceeded 99%. The zones of lost core were due to mechanical problems with the drilling equipment. A coring record, bit record, and mud loss record are included in Appendix A.

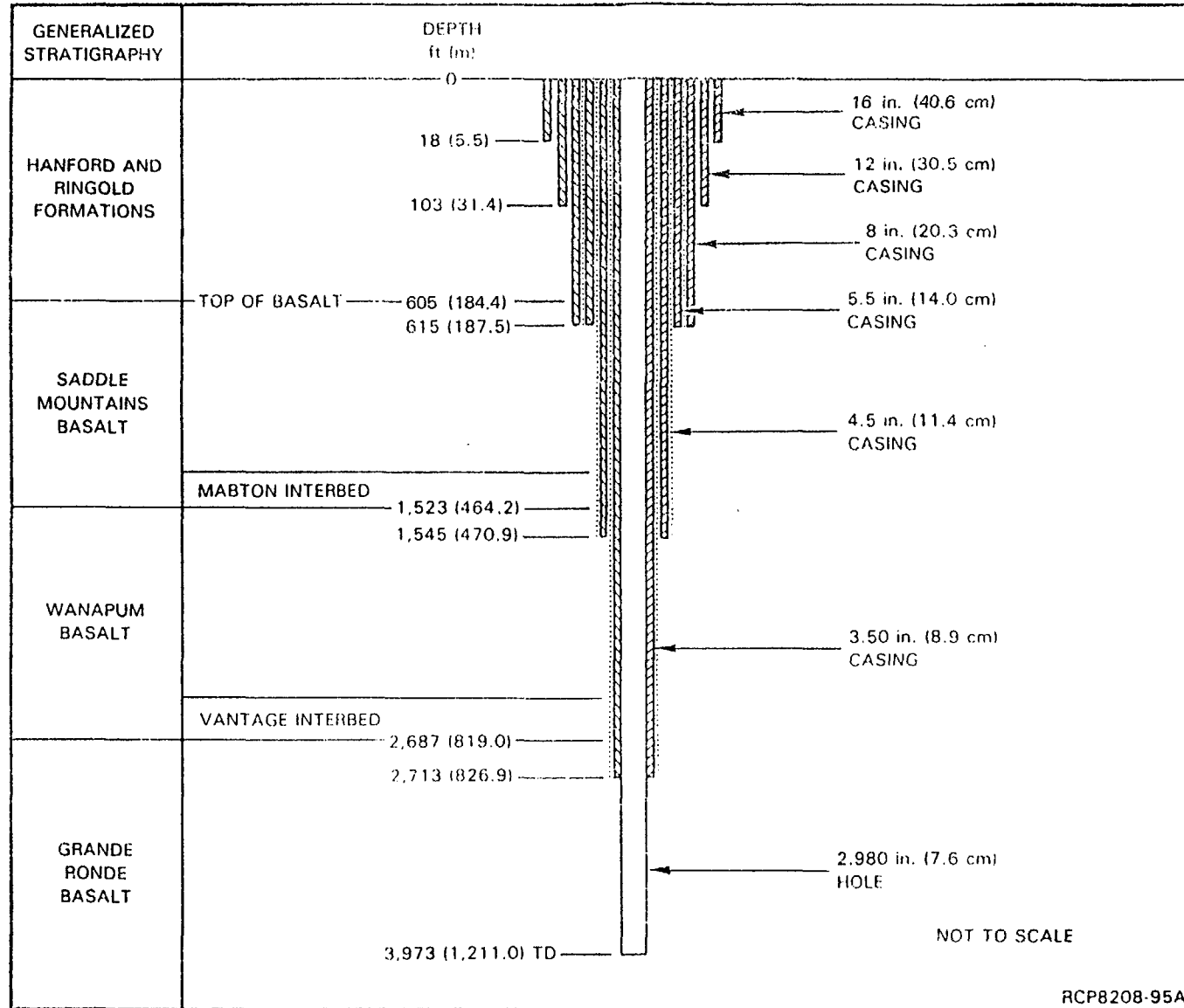


FIGURE 5. As-Built for Borehole RRL-2.

The proposed and actual drill and test schedules for Borehole RRL-2 are shown in Figure 6. Although drilling started 17 days behind schedule, the borehole was completed 38 days ahead of schedule.

Selected zones of relatively high permeability were hydrologically tested concurrent with drilling. Tested zones to a depth of 2,913 ft (887.8 m) were cemented at the conclusion of hydrologic testing to establish drilling fluid circulation and to prevent cross-flow interference with subsequent tests.

Two cementing methods were used; displacement through the casing and "squeeze" displacement. Neat Portland cement, Cal-Seal, and Portland cement with bentonite were used. The casing positive displacement method involved pumping the cement slurry through the existing casing. After the required volume of cement was pumped, a rubber wiper plug was released in the casing. A calculated volume of water was then used to displace the cement and wiper plug to the desired interval. The borehole was then capped to avoid further displacement and cement allowed to set before coring operations resumed. The "squeeze" displacement method utilized a packer to isolate the zone to be cemented between the packer and the bottom of the borehole. Cement was pumped through the rods and a predetermined amount of water was then pumped into rods displacing the cement. The packer was then released, the rods removed, and the cement was allowed to set before coring resumed. The intervals cemented and the cementing details are listed in Table 2.

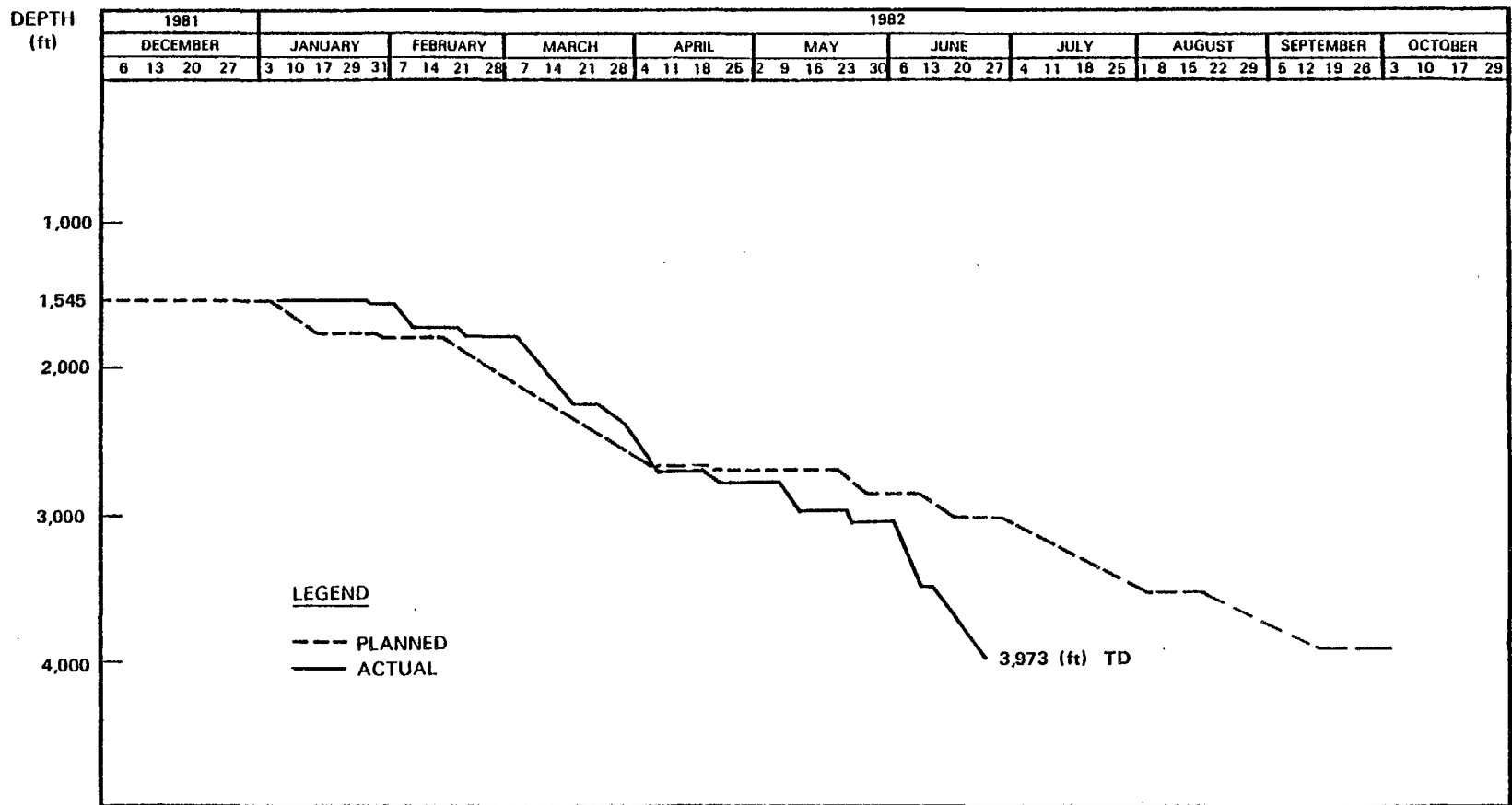
The borehole was surveyed for deviation, with a single-shot survey tool, at ~100-ft (30.5-m) intervals during drilling. After completion of the borehole, a multishot gyroscopic survey was run. Results of this survey appear in Figures 7 and 8, and Table 3.

All drilling, coring, cementing and testing activities were documented on Shift Report of Operations forms (Fig. 9). Copies of these forms are on file in Basalt Waste Isolation Project Records Retention Center, Richland, Washington.

#### GEOLOGIC LOGGING

The core from borehole RRL-2 was logged immediately after drilling. The geologic log consists of a description of the lithology, mineralogy and fracture patterns. Also recorded for each core run is fracture frequency, drill rate, percent recovery, and rock quality designation. A summary geologic log and rock quality designation summary table are presented in Appendix B.

Core is stored in the Hanford Geotechnical Sample Library, 2101M Building, 200 East Area, Hanford Site. Color photographs of the core are on file in the Basalt Waste Isolation Project Records Retention Center, Richland, Washington.



RCP8208-96A

FIGURE 6. Borehole RRL-2--Drill and Test Schedule.

TABLE 2. Borehole RRL-2--Cementing Details.

DATE	INTERVAL (ft)	CEMENT (sacks)	REMARKS
3-27-81	730-827	12 (Cal-Seal)	Lost Returns at 810' Tagged cement at 812' Lost circulation again at 810'
3-30-81	730-827	12 (Cal-Seal)	Tagged cement at 765' Soft cement from 765' - 827'
3-31-81	737-834	12 (Cal-Seal)	Tagged soft cement at 812' Partial Returns
4-1-81	680-841	20 (Cal-Seal)	Hard and soft cement 750' to 841' No returns
4-2-81	751-848	12 (Cal-Seal)	No returns
4-3-81	751-848	12 (Cal-Seal)	Soft cement 775' - 848' No returns
4-6-81	701-862	20 (Cal-Seal)	734' - 862' soft and hard cement, 65% returns
4-8-81	893-934	5 (Cal-Seal)	Washed soft cement from 932' - 943'
4-9-81	752-994	30 (Portland)	Tagged cement at 740', hung the PQ rods up at 704', drilled solid cement from 740' to 994'
12-16-82	1574-1714	30 (Portland)	Soft cement at 1580', solid cement at 1605', 100% returns
2-26-82	1735-1773	30 (Portland)	No cement, No returns.
3-1-82	1735-1773	30 (Portland)	Push plug to 1754', no returns
3-2-82	1735-1773	40 (Portland)	Push plug to 1754', soft cement to 1733', 100% returns
3-4-82	1773-1802	30 (Portland)	Push plug to 1752', 100% returns
3-10-82	1920-1980	19 (Portland) 1 (bentonite)	Push plug to 1980', 100% returns
3-24-82	2100-2239	17 (Portland) 1/2 (bentonite)	Push plug to 1960', 50% returns
3-29-82	2210-2342	30 (Portland) 1/2 (bentonite)	Push plug to 1900', 100% returns
4-14-82	2375-2644	29 (Portland) 1/2 (bentonite)	Push plug to 2351', 95% returns
4-30-82	0-2713	51 (Portland)	Casing
5-17-82	2715-2913	40 (Portland)	Push plug to 2613', 100% returns

NOTE: To convert feet to meters, multiply by 0.3048..

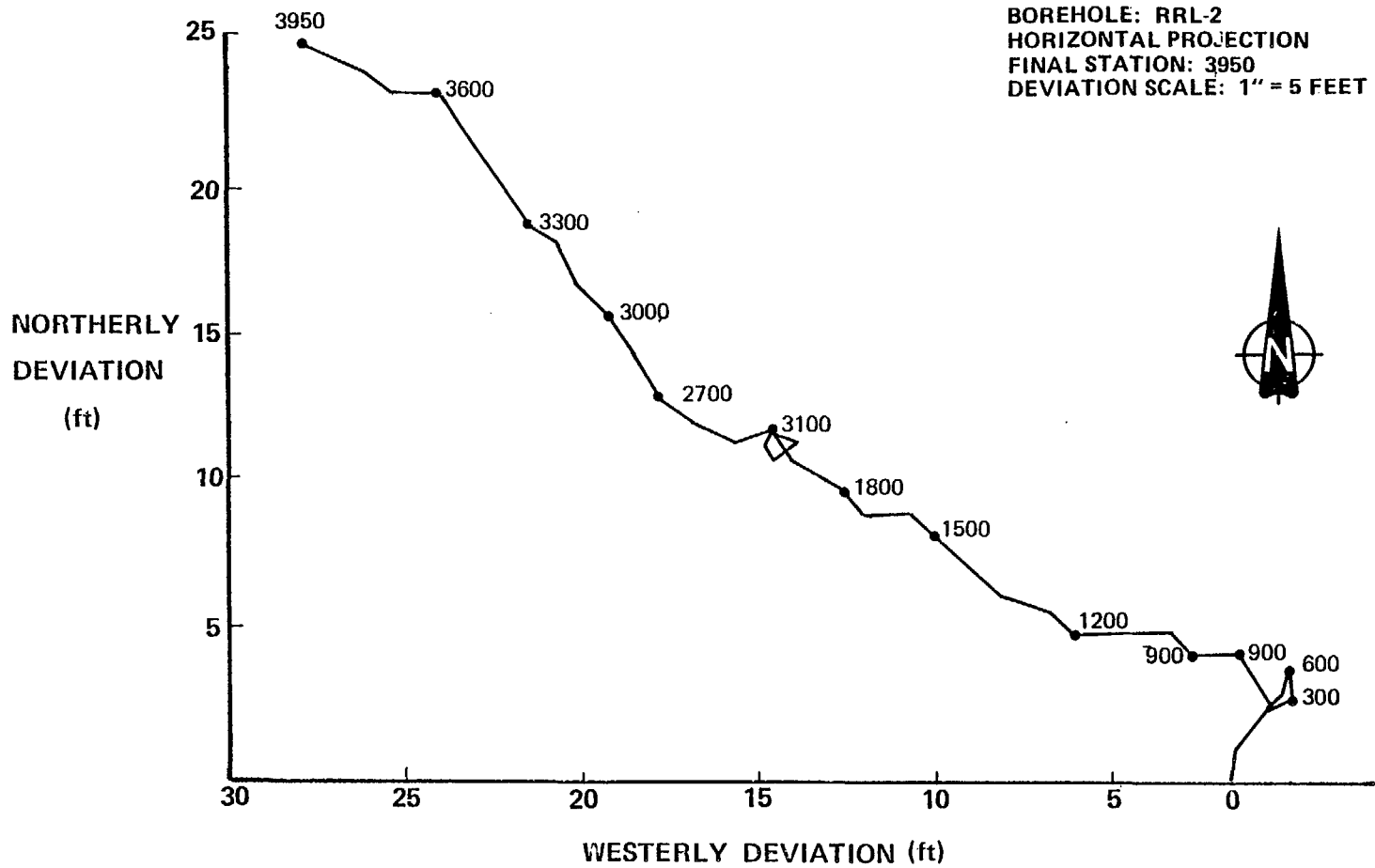


FIGURE 7. Borehole RRL-2--Deviation Survey Plan View.

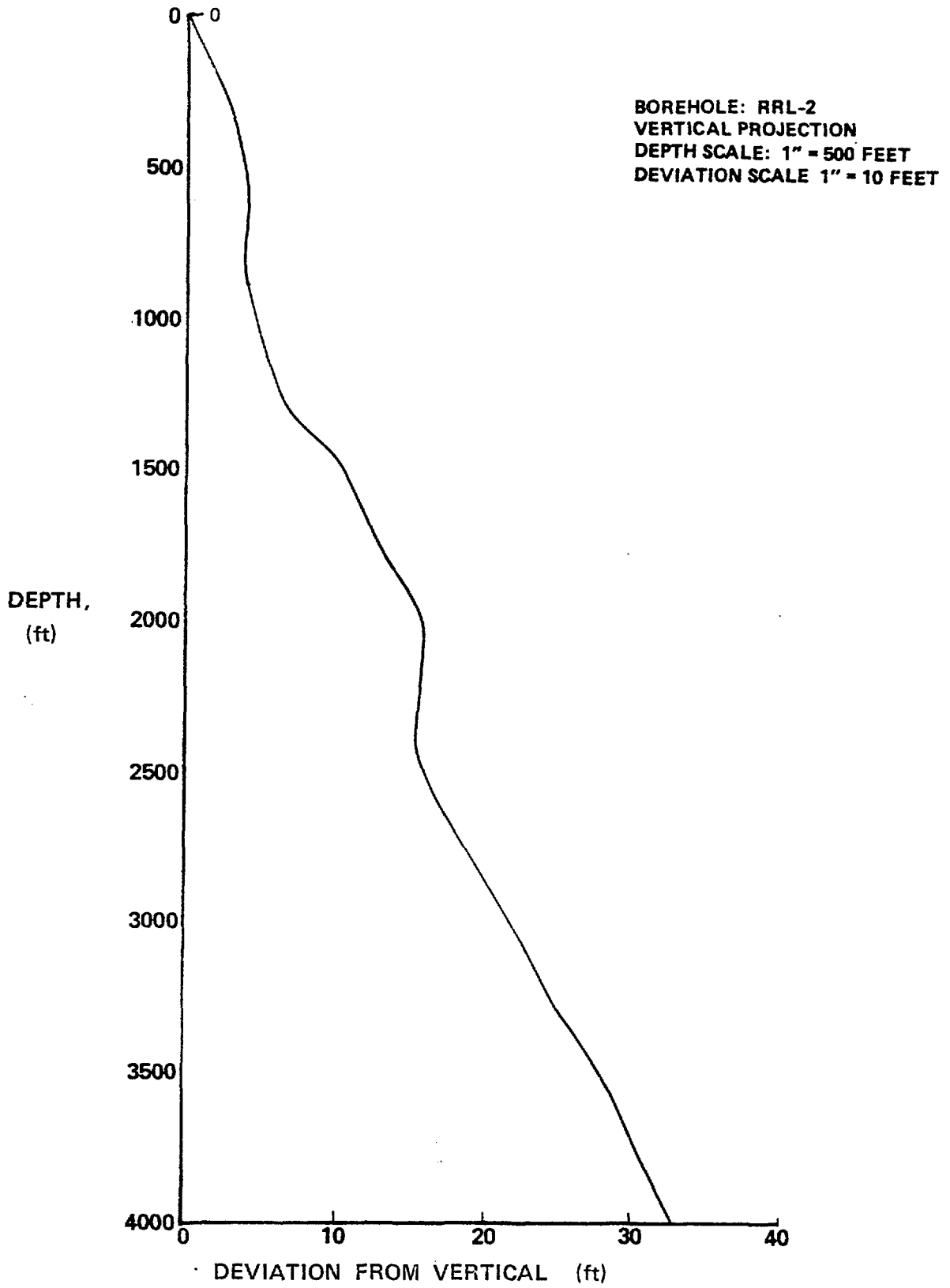


FIGURE 8. Borehole RRL-2--Deviation Survey Sectional View.

TABLE 3. Borehole RRL-2--Deviation Survey. (Sheet 1 of 2)

MEASURED DEPTH (ft)	TRUE VERTICAL DEPTH (ft)	VERTICAL SECTION (ft)	RECTANGULAR COORDINATES (ft)		CLOSURE	
					DISTANCE (ft)	DIRECTION
100	100.00	0.41	0.86 N	0.15 E	0.87	N 10 0 E
200	199.99	0.45	1.92 N	0.92 E	2.13	N 25 39 E
300	299.98	0.10	2.33 N	1.69 E	2.88	N 36 0 E
400	399.98	0.66	3.20 N	1.66 E	3.61	N 27 26 E
500	499.98	0.39	2.38 N	1.36 E	2.74	N 29 47 E
600	599.98	0.43	2.06 N	1.06 E	2.32	N 27 20 E
700	699.97	1.23	2.82 N	0.64 E	2.90	N 12 48 E
800	799.97	2.06	3.55 N	0.15 E	3.55	N 2 29 E
900	899.96	3.05	3.48 N	1.15 W	3.67	N 18 20 W
1000	999.96	3.91	4.12 N	1.75 W	4.47	N 23 0 W
1100	1099.95	4.90	4.05 N	3.06 W	5.07	N 37 2 W
1200	1199.94	5.95	4.07 N	4.36 W	5.97	N 46 59 W
1300	1299.93	6.82	4.66 N	5.01 W	6.84	N 47 7 W
1400	1399.92	8.49	5.28 N	6.64 W	8.49	N 51 31 W
1500	1499.90	10.66	6.74 N	8.26 W	10.66	N 50 48 W
1600	1599.89	11.53	7.34 N	8.90 W	11.53	N 50 30 W
1700	1699.88	12.53	7.29 N	10.21 W	12.55	N 54 28 W
1800	1799.88	13.38	7.97 N	10.76 W	13.39	N 53 28 W
1900	1899.86	15.11	8.84 N	12.27 W	15.12	N 54 14 W
2000	1999.86	15.95	9.56 N	12.77 W	15.95	N 53 12 W
2100	2099.86	15.95	9.56 N	12.77 W	15.95	N 53 12 W
2200	2199.86	15.87	9.17 N	12.98 W	15.89	N 54 45 W
2300	2299.86	15.47	8.79 N	12.76 W	15.49	N 55 25 W
2400	2399.85	15.29	9.35 N	12.09 W	15.29	N 52 16 W

TABLE 3, Borehole RRL-2--Deviation Survey. (Sheet 2 of 2)

MEASURED DEPTH (ft)	TRUE VERTICAL DEPTH (ft)	VERTICAL SECTION (ft)	RECTANGULAR COORDINATES (ft)		CLOSURE	
					DISTANCE (ft)	DIRECTION
2500	2499.85	16.08	9.55 N	12.94 W	16.08	N 53 34 W
2600	2599.85	16.56	9.28 N	13.77 W	16.60	N 56 1 W
2700	2699.84	17.84	9.83 N	14.96 W	17.90	N 56 40 W
2800	2799.83	19.15	10.60 N	16.01 W	19.21	N 56 30 W
2900	2899.82	20.34	11.76 N	16.63 W	20.37	N 54 44 W
3000	2999.81	21.60	12.83 N	17.38 W	21.60	N 53 34 W
3100	3099.80	22.88	13.80 N	18.26 W	22.89	N 52 54 W
3200	3199.80	24.11	14.93 N	18.93 W	24.11	N 51 45 W
3300	3299.79	24.97	15.39 N	19.67 W	24.97	N 51 58 W
3400	3399.78	26.20	16.51 N	20.34 W	26.20	N 50 56 W
3500	3499.77	27.89	17.89 N	21.42 W	27.90	N 50 8 W
3600	3599.76	29.15	18.93 N	22.21 W	29.18	N 49 33 W
3700	3699.75	30.17	18.91 N	23.52 W	30.17	N 51 12 W
3800	3799.75	31.04	19.47 N	24.18 W	31.05	N 51 10 W
3900	3899.74	32.33	20.06 N	25.35 W	32.33	N 51 38 W
3950	3949.73	32.94	20.27 N	25.97 W	32.94	N 52 2 W

NOTE: To convert feet to meters, multiply by 0.3048.



## GEOMECHANICAL LOGGING

Geomechanical logging of the core took place at the drill site prior to moving the core to storage. The geomechanical log records each fracture's location, aperture, dip, type, and a generalized description of the fracture filling mineralogy. Geomechanical logging was completed for the Grande Ronde Basalt section of the borehole. A summary of the fracture data is included in the section under "Geology Characterization."

## GEOPHYSICAL LOGGING

Borehole geophysical logs are utilized for determining stratigraphic relationships, selection of potential zones of high or low porosity and permeability, rock mechanics properties, and heat flow relationships. Geophysical logging was performed by Pacific Northwest Laboratory (PNL) and Birdwell Division of Seismograph Services. Log parameters determined are summarized as follows:

- Spontaneous potential log--records the difference in electric potential between a movable electrode in the borehole and a surface reference electrode. It is used to determine:
  - Interbed characteristics
  - Zone thicknesses and depths.
- Resistivity log--records apparent formation electric resistivity using a device having 16-in. short spacing and 64-in. long spacing. It is used to determine:
  - Stratigraphic correlations
  - Zone thickness and depths
  - Mud infiltrate zones.
- Fluid temperature log--records temperatures within the borehole, utilizing a temperature-sensitive element exposed to the borehole fluids. It is used to determine:
  - Sources of groundwater inflow into borehole
  - Direction of groundwater circulation in borehole
  - Pressure corrections for head measurements
  - Geothermal gradient.

- Flowmeter log (PNL only)--records flow of fluids past a flowmeter located within the borehole. It is used to determine:
  - Fluid flow velocity in borehole
  - Location of fluid gain and loss zones.
- Caliper log--records hole diameter using a tool that has three arms. It is used to determine:
  - Borehole breakouts
  - Changes in borehole diameter
  - Casing sections.
- Natural gamma log--records the natural formation radioactivity level. It is used to determine:
  - Lithology
  - Stratigraphic correlations.
- Neutron-epithermal neutron log--records a response related primarily to hydrogen ion concentration but is also affected by lithology and borehole effects. The tool contains a continuously emitting neutron source (Am-Be) and either a neutron or gamma-ray detector. It is used to determine:
  - Moisture content
  - Bulk porosity
  - Stratigraphic correlations.
- Gamma-gamma density log--records apparent formation density using a gamma-ray source (Cs-137) and at least one detector shielded from the source so that it records gamma rays backscattered from the formation. It is used to determine:
  - Bulk density.
- Sonic log--records the acoustic wave train propagated by an acoustic source. It is used to determine:
  - Cement bonding between rock and casing
  - Bulk porosity.

- Magnetometer log (PNL only)--records the magnetic properties (flux and polarity) of the formation rock surrounding the borehole. It is used to determine:
  - Stratigraphic correlations
  - Paleomagnetic record.

The various borehole geophysical logs, the interval logged and the dates logged for PNL and Birdwell are shown in Table 4. Digitized copies of the PNL logs are in Figures 10, 11, and 12.

The Pacific Northwest Laboratory has made fourteen temperature logging runs in borehole RRL-2. The data from 0 to 2,713 ft (0 - 826.9 m) are consistent and have a uniform temperature gradient.

The data from 2,713 ft (826.9 m) to 3,973 ft (1,211.0 m) are less reliable due to cross-hole flow. The data used to determine the temperature of the candidate horizons are a combination of the temperature log from 0 to 2,713 ft (823.2 m) and temperatures measured by downhole transducers during hydrologic testing. Using these data, the temperature for the interiors of the candidate horizons are:

Cohasset Flow	- 3,170 ft (966.2 m) - 124°F (51°C)
McCoy Canyon Flow	- 3,550 ft (1,082.0 m) - 131°F (55°C)
Umtanum Flow	- 3,800 ft (1,158.2 m) - 136°F (58°C)

TABLE 4. Borehole RRL-2--Geophysical Logging Intervals.

Performed by Pacific Northwest Laboratory

DATE	NEUTRON-NEUTRON (ft)	GAMMA GAMMA (ft)	NATURAL GAMMA (ft)	SONIC (ft)	FLUID TEMPERATURE (ft)	CALIPER (ft)	SPONTANEOUS POTENTIAL/RESISTIVITY (ft)	DENSITY (ft)	MAGNETOMETER (ft)
03-06-81	2-592		0-591	9-597	13-587			4-597	
06-09-81	3-1450		3-1450	569-1454	3-1450	3-1450	569-1454	3-1450	569-1454
10-21-81					160-1443				
12-31-81					50-552				
02-05-82				1400-1714	450-1714	1530-1712			1545-1712
02-18-82	1400-1772			1600-1772	1200-1772	1650-1771	1545-1770		
03-18-82	1740-2222				1700-2222	1740-2222			
04-07-82	2150-2642				2000-2642	2150-2642			
04-20-82	1400-2713	1400-2713	1400-2713		230-2713	2590-2713	1542-2713	1400-2713	1542-2713
04-26-82				1530-2712		1520-2712			
04-29-82					240-2713				
05-06-82	2650-2913				236-2913	2698-2913			
05-20-82	2850-3020				2600-3020	2850-3020			
06-21-82	2970-3851				220-3851				
06-25-82			2660-3972		2714-3972	3746-3972			2713-3972
06-30-82				2660-3972			2713-3972		
10-06-82		2650-3927							
10-07-82	3550-3951					2700-3951			

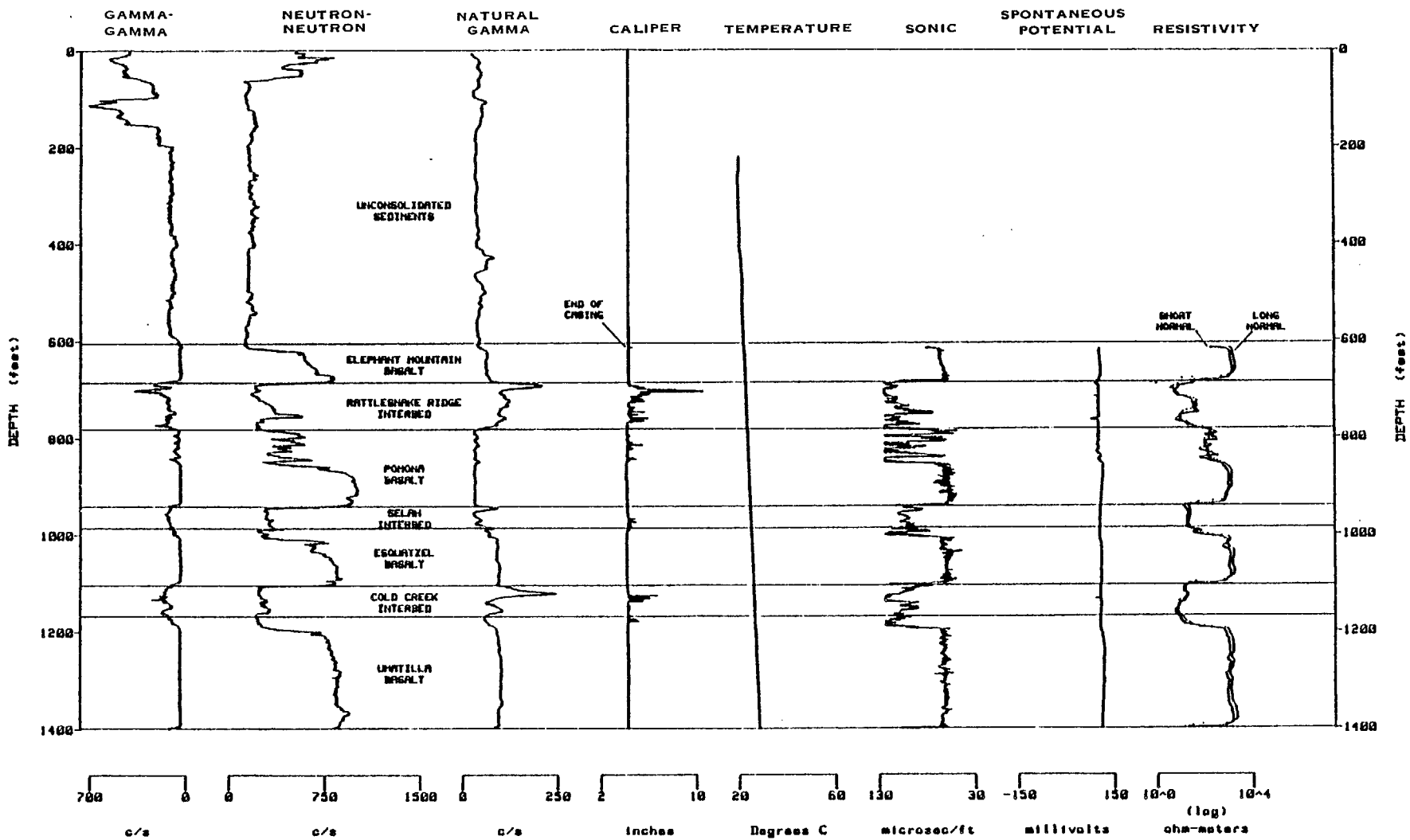
Performed by Birdwell

DATE	DENSITY	GAMMA RAY	NEUTRON	ELASTIC PROPERTIES	3-D VELOCITY	ELECTRIC	TEMPERATURE	CALIPER
04-27-82	1500-2712	0-2705	0-2705	1500-2700	1500-2695	1530-2713	0-2713	1500-2712
10-05-82	2650-3924	2700-3924	2700-3924	2700-3920	2700-3922	2710-3920		2650-3924

NOTE: To convert feet to meters, multiply by 0.3048.

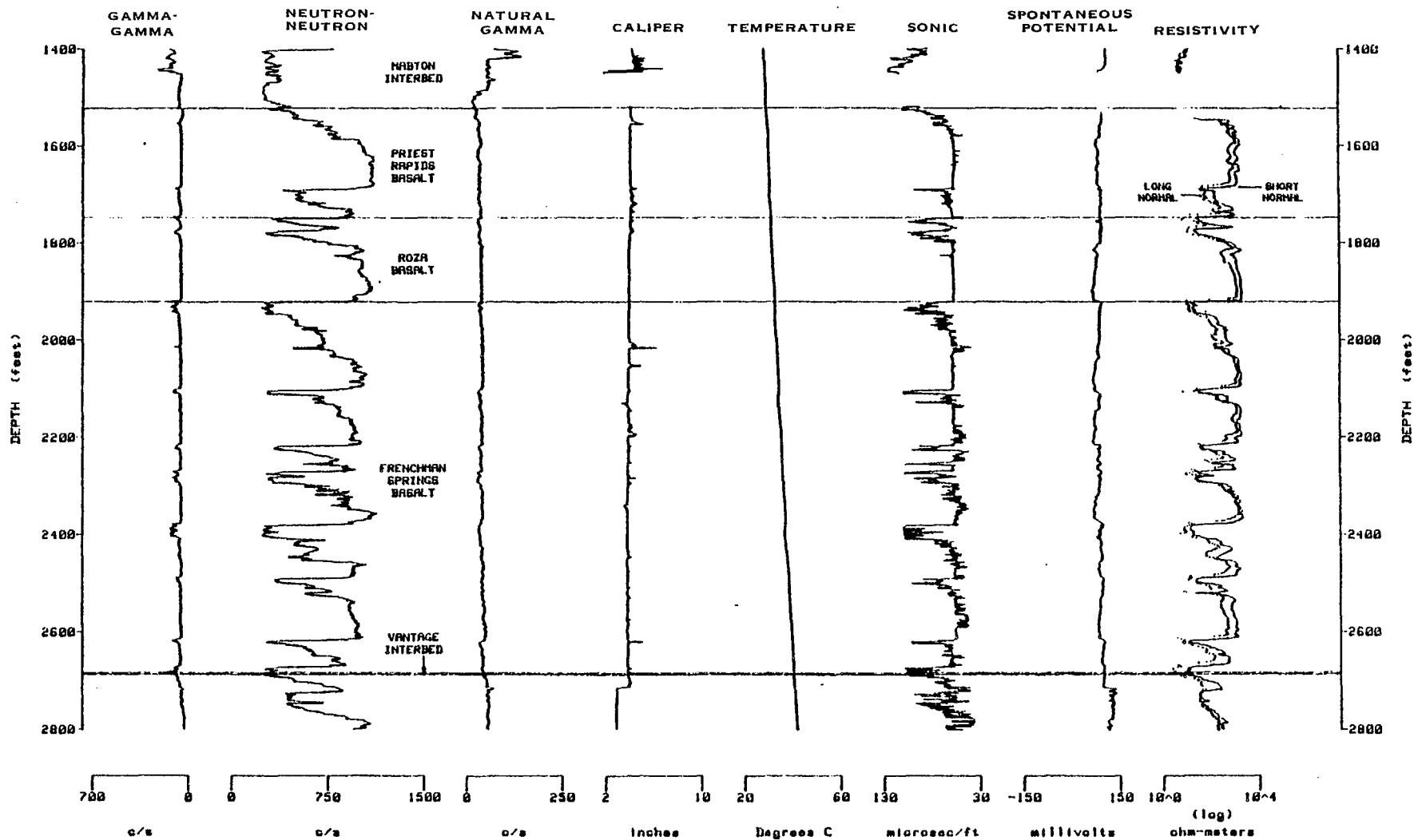
BEST AVAILABLE COPY

34



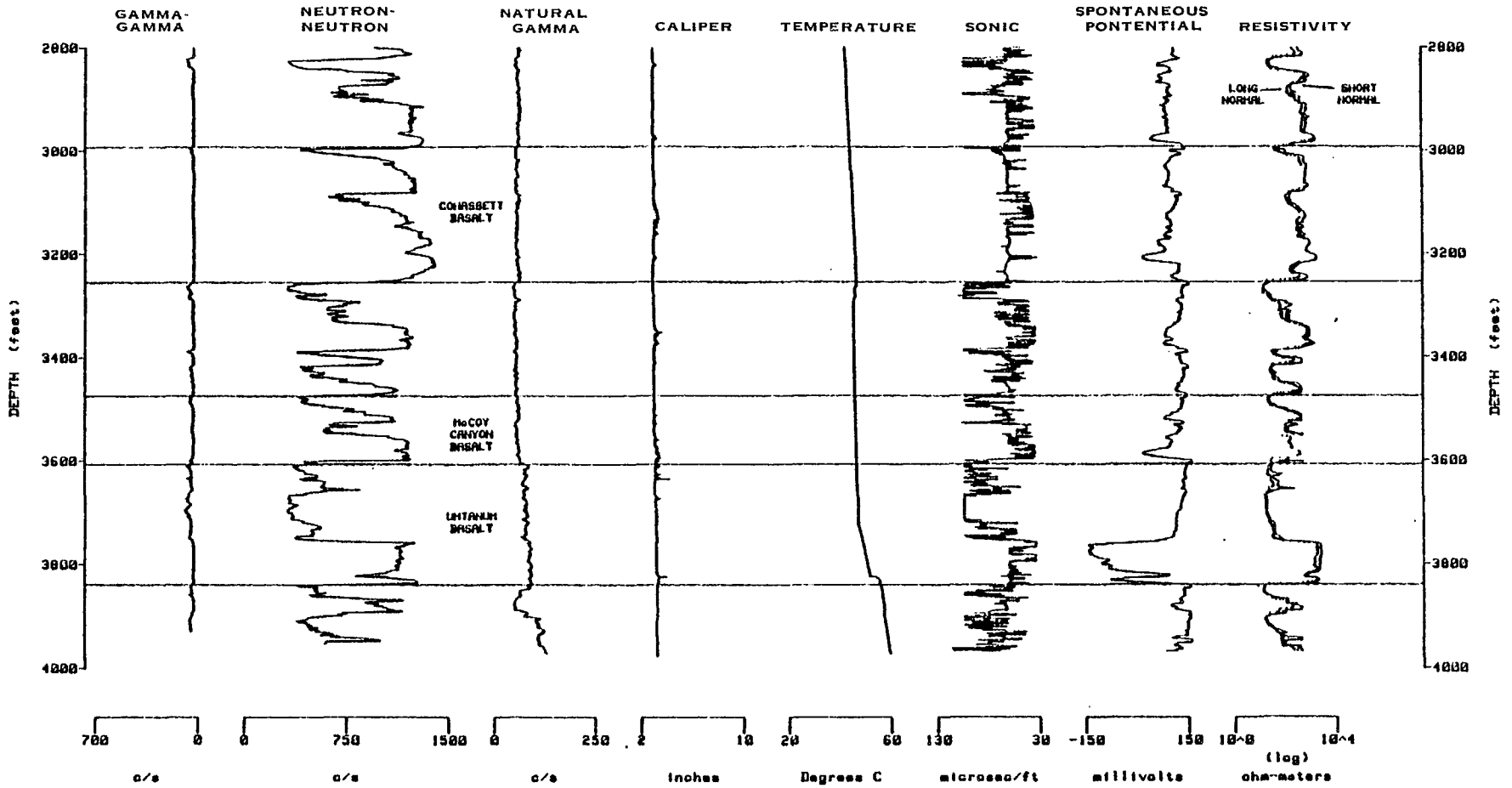
SD-BMI-TI-113

FIGURE 10. Borehole RRL-2--Summary Geophysical Log, 0-1,400 Feet.



SD-BWI-TI-113

FIGURE 11. Borehole RRL-2--Summary Geophysical Log, 1,400-2,800 Feet.



SD-BMI-TI-113

FIGURE 12. Borehole RRL-2--Summary Geophysical Log, 2,800-3,973 Feet.

## GEOLOGIC CHARACTERIZATION

## INTRODUCTION

The geology of borehole RRL-2 includes the stratigraphy, mineralogy and fracture characteristics. It will be used as input for shaft design, porthole locations and to assess the suitability of the RRL.

Borehole RRL-2 is located in the Pasco Basin near the axis of the Cold Creek syncline (Fig. 13). The Cold Creek syncline is asymmetrical, with a steeper south limb. The troughline is nearer the Yakima Ridge structure, which bounds it on the south, than the Umtanum Ridge-Gable Mountain structure, which bounds it on the north. The trough of the syncline is broad, open, and undulating with two minor depressions.

The bedrock of the Cold Creek syncline is comprised of flows belonging to all three formations of the Yakima Basalt Subgroup. The Wanapum and Saddle Mountains Basalts within the Cold Creek syncline are comprised of up to 20 flows with a maximum thickness of ~2,300 ft (~700 m). The basalt section is interbedded with sediments of the Ellensburg Formation (see Fig. 3) and is overlain by up to 720 ft (219.5 m) of fluvial-lacustrine, Miocene-Pliocene Ringold Formation and catastrophic flood deposits of the Pleistocene Hanford Formation. Holocene eolian deposits of loess and dune sand mantle much of the syncline.

Grande Ronde Basalt in the syncline consists of  $\geq 3,000$  ft ( $\geq 915$  m) of basalt, including at least 50 flows (see Fig. 3). Three basalt flows of this formation are considered the most likely candidates for a repository host rock.

## METHODOLOGY

Core logs, geophysical logs, major element chemistry, paleomagnetism, and thin sections are used to determine the geology of the borehole. Core logging and geophysical logging, which were previously discussed in the section under "Borehole History," were the preliminary methods used for identification of the stratigraphy. After the core was moved to permanent storage and photographed, samples were taken for chemical analysis, paleomagnetism, and thin sections. This sampling was done in conjunction with the sampling for rock mechanics testing to ensure the highest quality samples would be available for both purposes.

The samples for major and minor element analysis by X-ray fluorescence were taken from unaltered basalt, with three samples taken per flow. The paleomagnetic samples, which are taken at least 16 ft (5 m) below the upper contact, are 1-in. core samples, which are drilled in the existing core. Approximately eight samples are taken per flow. Since the original core is not oriented with respect to north, only paleomagnetic

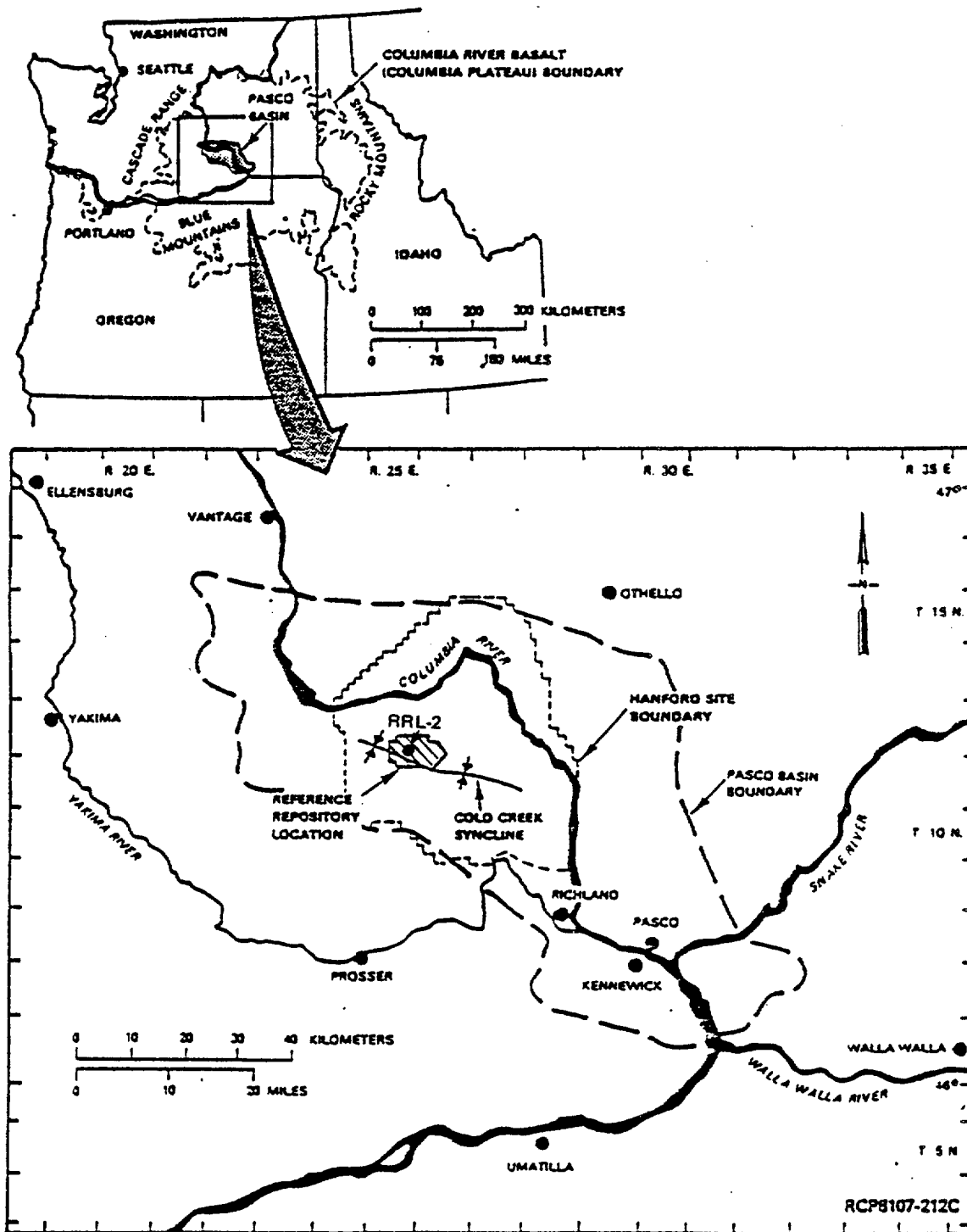


FIGURE 13. Location Map--Columbia Plateau, Hanford Site, Cold Creek Syncline, Reference Repository Location, and Borehole RRL-2.

inclination can be determined from the paleomagnetic samples. Normally, three thin section samples are taken per flow, one each in the flow top, entablature, and colonnade. In the case of a candidate horizon, additional samples are taken in order to define the contacts of intraflow structures.

Geomechanical logs (fracture logs) were completed for the Grande Ronde section of the borehole. These logs record each fracture's location, fracture filling width, dip, type, and generalized description of the fracture filling material. To aid in the measurement of fractures, a 7X ocular with 0.1-mm graduations was used. This allows accurate measurement to 0.1 mm so all fractures smaller than 0.1 mm are grouped under the 0.1-mm category.

Subsequent to the initial fracture logging, the filled widths of randomly selected fractures were measured with a binocular microscope. This provided an estimate of the distribution of fracture widths in the 0.01- to 0.3-mm range.

## RESULTS

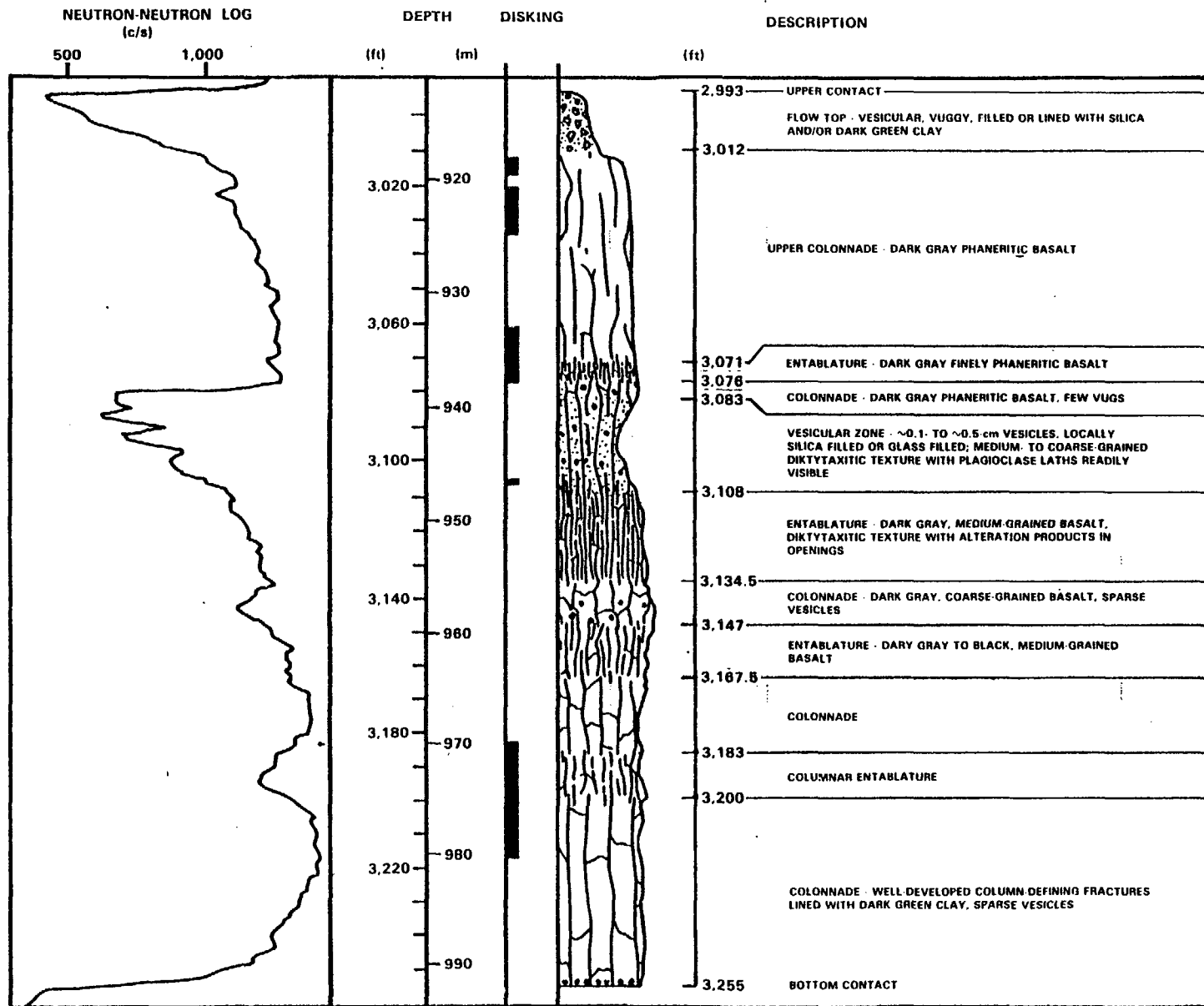
The lithology of the Cohasset, McCoy Canyon, and Umtanum flows in borehole RRL-2, as determined from core logs and geophysical logs, is illustrated in Figures 14, 15, and 16.

The lithology of the Cohasset flow in borehole RRL-2 is presented in Figure 14. The basic elements of this flow are:

- Thin, oxidized flow top containing both blocky "aa" zones and zones of welded pahoehoe
- Internal vesicular zone
- Dense interior with multiple zones of entablature and colonnade.

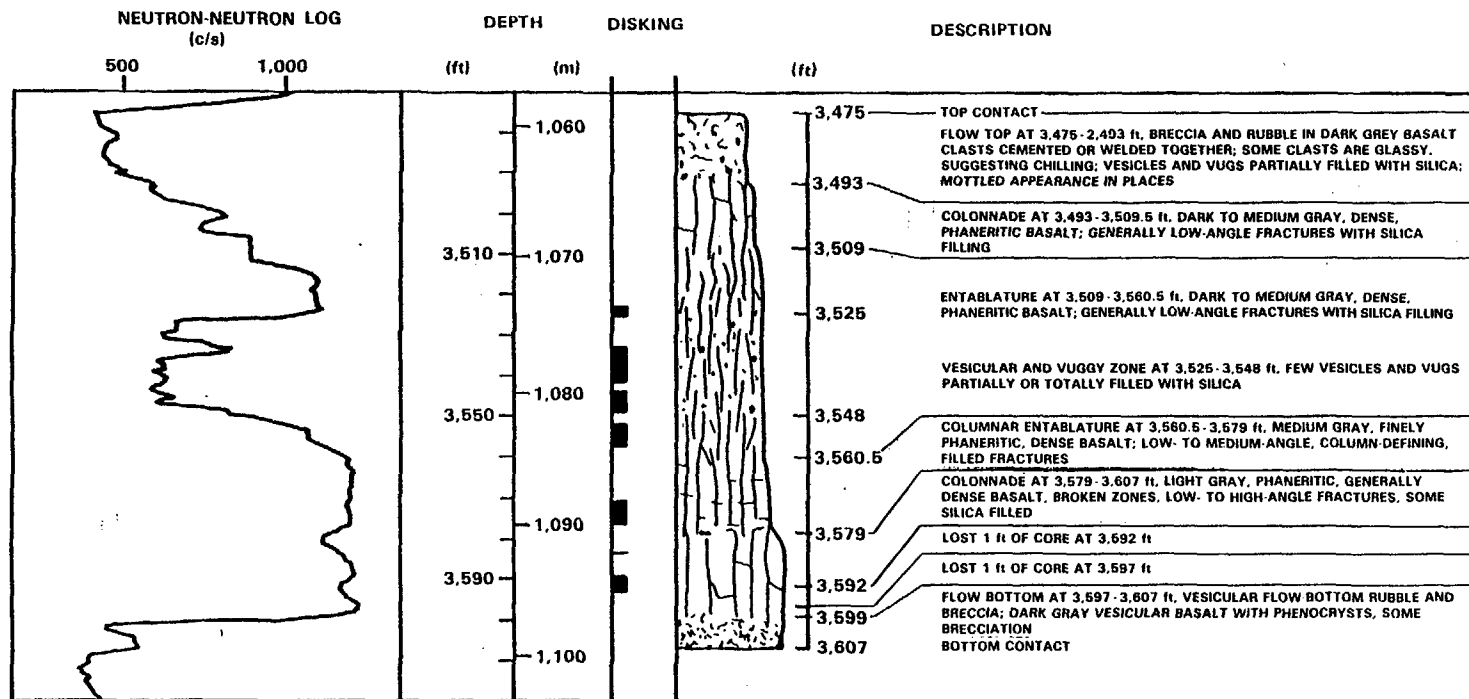
The thickness of the flow top is less than 20 ft (6.1 m) and is underlain by a relatively thick upper colonnade, thin entablature, and thin colonnade (70 ft (21.3 m) total). This section overlies the internal vesicular zone, which is ~30 ft (9 m) thick. This zone consists of intact basalt with as much as 20 vol% occupied by 0.1- to 0.5-cm-sized vesicles. The vesicles are commonly filled or partially filled with silica, clay, or glass. There is no evidence of brecciation in this zone. The vesicular zone is underlain by dense interior (140 ft (42.6 m) in thickness) consisting of alternating entablature and colonnade.

The lithology of the McCoy Canyon flow in borehole RRL-2 is presented in Figure 15. The brecciated flow top is ~20 ft (6.1 m) thick. The dense interior consists of ~15 ft (4.5 m) of upper colonnade, 50 ft (15.2 m) of entablature with a central vesicular zone of 15 ft (4.6 m), 20 ft (6.1 m) of columnar entablature, and a lower colonnade of ~25 ft (7.6 m). The bottom 10 ft (3 m) of the flow is a vesicular and brecciated flow bottom.



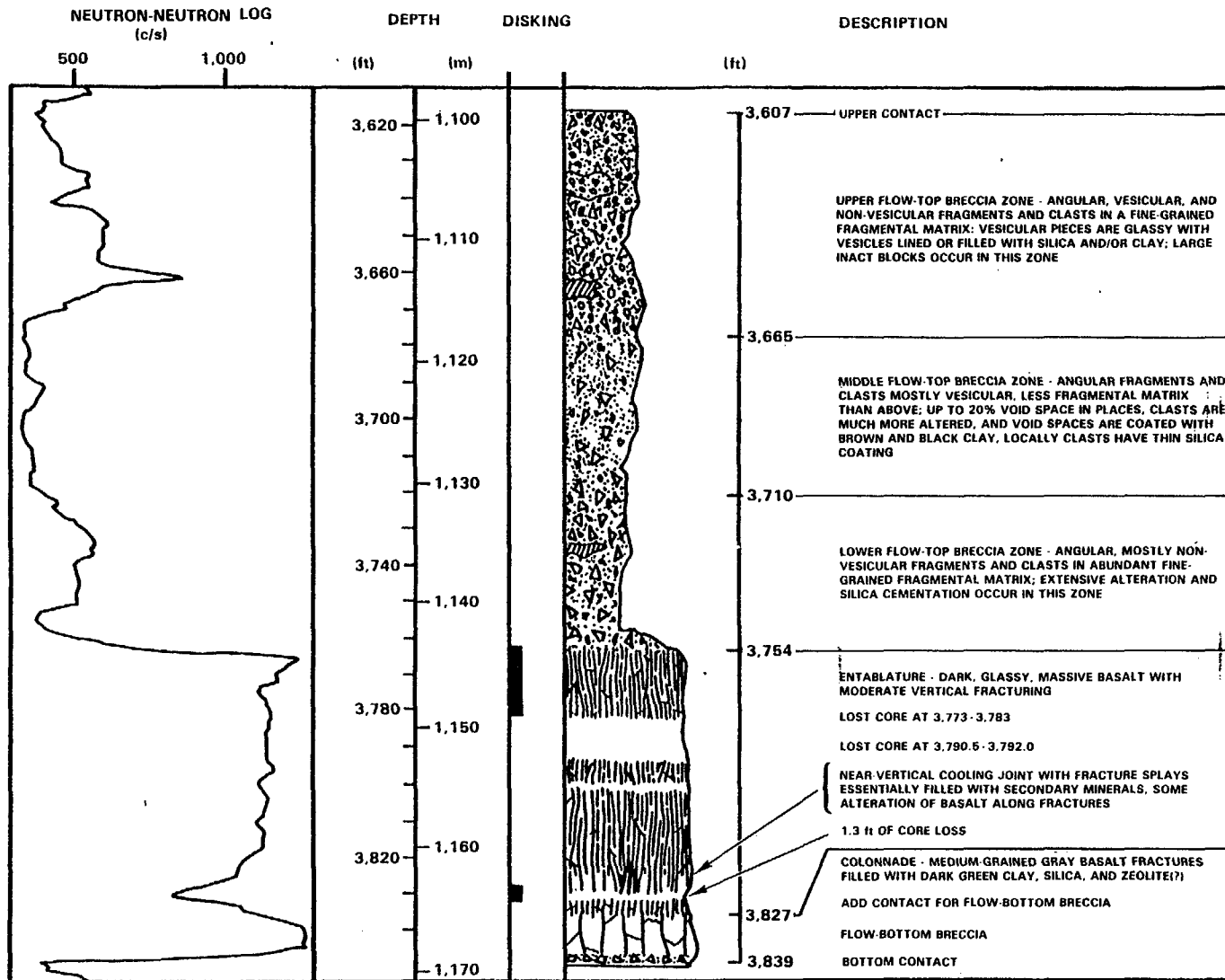
RCP8211-151

FIGURE 14. Lithology of the Cohasset Flow--Borehole RRL-2.



RCP8211-155

FIGURE 15. Lithology of the McCoy Canyon Flow--Borehole RRL-2.



RCP8211-159

FIGURE 16. Lithology of the Umtanum Flow--Borehole RRL-2.

The Umtanum flow in borehole RRL-2 (see Fig. 16) contains 148 ft (45.1 m) of flow-top breccia in the upper part of the flow and 84 ft (25.6 m) of dense interior in the lower part. The breccia can be divided into three parts as shown in Figure 16. In the upper zone, the breccia clasts, 2 to 50 cm in diameter, are cemented with a matrix of finer fragmental material and secondary minerals. In the middle part of the breccia zone, clasts are more vesicular, more altered, and there is significantly less matrix. Void spaces are coated with clay and silica. In the lower part of the breccia, clasts are largely nonvesicular and show a relatively high degree of cementation in a fragmental matrix.

The dense interior consists of ~69 ft (21 m) of entablature that overlies ~15 ft (4.6 m) of colonnade. Three zones of lost core occur in the colonnade. The neutron-neutron geophysical log indicates that the lowermost of the lost core zones apparently represents a narrow (~1.3-ft (.4-m)) zone of increased fracture abundance. Directly above this lost core zone are a few feet of core that contain prominent cooling joints essentially filled with secondary minerals. Texture of the core and the character of the cooling joints suggest this may be a zone of coarsely columnar entablature. The thin colonnade is typical of the Umtanum flow. It is underlain by a thin zone of flow-bottom breccia. A moderate amount of core diking occurs in the dense interior.

The major element chemistry of the basalt flows in borehole RRL-2 is listed in Table 5. If the major element chemistry of the candidate horizons in Table 5 is compared to the means for these flows presented in Table 6, it can be seen that the values from borehole RRL-2 fall within the range for these flows in the Pasco Basin.

The paleomagnetic data from borehole RRL-2 (Table 7) are consistent with previous data, but alone do not provide a basis for identification of individual flows.

The mineralogy of the candidate horizons, as determined from thin sections from the core, is presented in Table 8. The volume percent of mesostasis of a sample is a good indication of the intraflow structure. Generally, those samples with a higher relative volume percent of mesostasis within a flow are entablature, and those with lower relative volume percents are colonnade.

TABLE 5. Borehole RRL-2--Major Element Chemistry (vol%). (Sheet 1 of 4)

FLOW	DEPTH (ft)	SiO <sub>2</sub>	Al <sub>2</sub> O <sub>3</sub>	Fe <sub>2</sub> O <sub>3</sub>	FeO	MgO	CaO	K <sub>2</sub> O	TiO <sub>2</sub>	Na <sub>2</sub> O	P <sub>2</sub> O <sub>5</sub>	MnO
Elephant Mountain	0641.0	51.34	13.88	2	12.64	4.33	8.21	1.18	3.45	2.28	0.49	0.20
	0654.0	51.65	13.70	2	12.62	4.12	8.25	1.18	3.44	2.32	0.50	0.20
	0666.0	50.49	13.91	2	13.23	4.26	8.40	1.22	3.58	2.20	0.51	0.21
Pomona	0874.0	52.12	15.18	2	8.59	6.92	10.48	0.55	1.67	2.07	0.24	0.18
	0909.7	52.38	15.26	2	8.71	6.65	10.23	0.66	1.68	1.99	0.24	0.18
	0932.7	52.14	15.27	2	8.83	6.81	10.20	0.55	1.68	2.10	0.23	0.18
Esquatze1	1013.0	53.01	14.26	2	11.25	3.79	7.55	1.82	3.14	2.60	0.38	0.20
	1043.5	52.84	14.06	2	11.43	3.97	7.65	1.64	3.15	2.67	0.39	0.20
	1096.7	53.17	14.34	2	11.27	3.59	7.23	1.77	3.15	2.88	0.39	0.21
Umatilla	1197.8	53.68	14.81	2	10.27	3.16	6.69	2.63	3.13	2.71	0.70	0.23
	1227.4	54.89	14.63	2	10.38	2.46	6.08	2.63	2.83	3.14	0.78	0.16
	1265.5	55.12	14.72	2	10.33	2.59	5.80	2.78	2.69	2.91	0.87	0.18
	1309.7	54.27	15.12	2	10.46	2.85	5.97	2.71	2.65	2.91	0.86	0.21
	1359.5	54.20	14.60	2	10.16	3.05	6.27	2.62	2.92	3.15	0.80	0.22
	1393.8	53.78	14.62	2	11.22	3.02	6.14	2.40	3.09	2.81	0.70	0.21
Priest Rapids II	1543.5	50.62	14.15	2	12.19	4.83	8.85	0.94	3.13	2.40	0.65	0.24
	1593.7	49.80	14.14	2	11.92	5.07	9.17	1.00	3.36	2.63	0.69	0.22
	1680.6	50.52	14.13	2	11.70	5.30	8.77	1.11	3.23	2.36	0.66	0.23
Priest Rapids I	1718.6	50.66	13.59	2	12.75	4.62	8.55	0.82	3.66	2.48	0.64	0.24
	1746.0	51.71	13.87	2	12.44	3.47	7.96	1.31	3.65	2.71	0.69	0.20
Roza II	1763.0	51.62	14.21	2	11.49	4.64	9.03	0.95	3.22	2.06	0.58	0.22
	1771.5	51.35	14.44	2	11.56	4.60	8.68	0.96	3.16	2.50	0.55	0.21
Roza I	1839.7	51.02	14.27	2	11.44	4.77	8.49	1.24	3.11	2.89	0.55	0.22
	1859.8	50.51	13.99	2	11.76	4.76	8.78	1.24	3.26	2.90	0.57	0.23
	1919.5	51.22	14.54	2	11.17	4.57	8.61	1.23	3.06	2.81	0.56	0.24

TABLE 5. Borehole R-L-2--Major Element Chemistry (vol%). (Sheet 2 of 4)

FLOW	DEPTH (ft)	SiO <sub>2</sub>	Al <sub>2</sub> O <sub>3</sub>	Fe <sub>2</sub> O <sub>3</sub>	FeO	MgO	CaO	K <sub>2</sub> O	TiO <sub>2</sub>	Na <sub>2</sub> O	P <sub>2</sub> O <sub>5</sub>	MnO
Frenchman Springs 1	1971.8	51.92	14.01	2	11.53	4.01	8.23	1.20	3.15	3.16	0.55	0.24
	2045.0	50.63	13.47	2	13.29	4.22	8.00	1.40	3.19	3.05	0.54	0.22
	2094.0	51.68	14.14	2	11.79	4.32	7.93	1.34	3.10	2.93	0.54	0.22
Frenchman Springs 2	2133.6	51.79	14.30	2	11.53	4.42	8.31	1.29	2.96	2.69	0.49	0.22
	2169.7	51.18	14.31	2	11.67	4.32	8.40	1.33	3.09	2.95	0.53	0.21
	2212.6	51.75	14.03	2	12.18	4.47	7.77	1.34	2.95	2.77	0.52	0.22
Frenchman Springs 3	2238.8	51.68	14.38	2	11.49	4.29	8.31	1.29	3.02	2.83	0.49	0.22
	2265.0	51.58	14.09	2	11.84	4.58	8.35	1.17	3.01	2.65	0.49	0.24
Frenchman Springs 4	2317.8	51.66	14.51	2	11.40	4.11	8.38	1.23	3.17	2.76	0.55	0.21
	2350.7	50.40	13.74	2	12.80	4.31	8.32	1.36	3.28	2.99	0.55	0.24
	2377.7	51.57	14.11	2	11.73	4.11	8.24	1.30	3.16	2.99	0.56	0.23
Frenchman Springs 5	2434.0	50.96	13.81	2	12.70	4.07	8.21	1.32	3.27	2.87	0.59	0.22
	2456.0	51.48	13.94	2	12.63	4.27	7.71	1.28	3.12	2.81	0.55	0.22
	2486.8	50.63	13.95	2	12.48	4.12	8.40	1.24	3.24	3.07	0.62	0.23
Frenchman Springs 6	2508.5	52.16	13.81	2	12.70	3.75	7.45	1.61	2.97	2.66	0.65	0.23
	2534.8	50.76	13.72	2	13.04	4.10	8.14	1.34	3.15	2.89	0.62	0.24
	2594.0	50.39	14.15	2	12.60	4.33	8.38	1.24	3.15	2.91	0.62	0.23
	2610.8	50.36	14.13	2	12.73	4.30	8.08	1.28	3.11	3.14	0.63	0.23
Frenchman Springs 7	2618.2	54.52	16.36	2	11.82	1.54	7.89	1.83	2.57	1.21	0.10	0.17
	2641.2	56.67	16.06	2	11.69	4.84	0.96	0.91	3.06	3.02	0.56	0.23
	2660.3	50.03	14.19	2	13.12	4.39	8.46	1.00	3.22	2.80	0.53	0.25
	2669.3	50.79	14.18	2	12.60	4.01	8.35	1.15	3.14	2.99	0.54	0.23
Grande Ronde 1	2711.0	53.69	15.48	2	9.67	4.39	8.75	1.14	1.81	2.55	0.32	0.20
	2720.0	53.62	15.77	2	9.86	4.81	8.00	1.10	1.74	2.57	0.32	0.21

TABLE 5. Borehole RRL-2--Major Element Chemistry (vol%). (Sheet 3 of 4)

FLOW	DEPTH (ft)	SiO <sub>2</sub>	Al <sub>2</sub> O <sub>3</sub>	Fe <sub>2</sub> O <sub>3</sub>	FeO	MgO	CaO	K <sub>2</sub> O	TiO <sub>2</sub>	Na <sub>2</sub> O	P <sub>2</sub> O <sub>5</sub>	MnO
Grande Ronde 2	2720.7	53.97	15.97	2	9.08	4.36	8.12	1.21	1.81	2.98	0.31	0.18
	2774.0	53.46	15.81	2	9.28	4.88	8.52	0.93	1.76	2.88	0.29	0.20
	2780.3	54.00	16.09	2	9.22	4.95	7.63	1.00	1.75	2.85	0.30	0.19
	2819.4	53.61	15.66	2	9.36	4.86	8.53	1.10	1.69	2.72	0.28	0.19
Grande Ronde 3	2906.0	53.72	15.66	2	9.51	4.53	8.27	1.17	1.83	2.78	0.34	0.20
	2945.0	53.96	15.64	2	9.35	4.70	8.13	1.18	1.81	2.71	0.32	0.20
	2974.4	53.96	15.50	2	9.34	4.85	8.16	1.33	1.78	2.59	0.30	0.19
Cohassett	3035.0	53.46	15.79	2	9.61	5.13	8.08	1.01	1.81	2.62	0.29	0.19
	3050.5	52.98	15.57	2	9.77	4.92	8.54	1.01	1.85	2.88	0.29	0.19
	3070.0	52.33	15.50	2	10.07	5.10	8.76	1.14	1.91	2.69	0.29	0.21
	3175.5	53.12	15.52	2	9.66	5.07	8.69	1.03	1.81	2.64	0.27	0.20
	3210.8	53.12	15.60	2	9.85	5.04	8.58	1.10	1.84	2.38	0.29	0.20
	3253.0	52.92	15.21	2	10.23	4.62	8.58	1.21	1.93	2.70	0.39	0.21
Grande Ronde 5	3297.3	53.67	15.23	2	10.10	4.71	8.29	0.89	2.02	2.56	0.32	0.21
	3340.6	53.37	15.34	2	9.85	4.90	8.46	0.90	1.90	2.79	0.29	0.20
	3384.7	53.28	15.25	2	10.27	4.66	8.56	0.91	2.00	2.55	0.31	0.21
Grande Ronde 6	3397.8	52.54	15.06	2	10.78	4.68	8.34	1.19	2.06	2.80	0.33	0.22
	3404.2	53.23	15.15	2	10.51	4.47	8.51	0.93	2.04	2.64	0.32	0.20
	3413.0	53.62	15.09	2	10.34	4.71	8.11	0.84	2.00	2.76	0.32	0.20
Grande Ronde 7	3445.2	51.98	15.39	2	11.06	5.16	8.34	0.88	1.95	2.74	0.30	0.21
	3456.4	53.04	15.46	2	10.09	4.89	8.50	0.80	1.91	2.83	0.28	0.20
	3472.0	53.34	15.54	2	9.79	4.91	8.45	0.79	1.94	2.76	0.28	0.22
McCoy Canyon	3505.4	53.56	15.11	2	9.95	4.55	8.52	0.96	2.01	2.84	0.30	0.21
	3560.5	53.39	15.18	2	10.35	4.56	8.30	0.92	1.95	2.87	0.29	0.20
	3587.6	52.91	14.89	2	10.83	4.44	8.42	1.08	2.10	2.82	0.31	0.21
	3600.0	53.84	15.38	2	10.27	3.94	8.15	1.16	2.13	2.58	0.33	0.21
	3600.3	52.78	15.77	2	10.35	4.42	8.14	1.07	2.12	2.82	0.32	0.19
	3604.5	52.78	15.51	2	10.37	3.84	8.64	1.14	2.07	3.08	0.36	0.21

TABLE 5. Borehole RRL-2--Major Element Chemistry (vol%). (Sheet 4 of 4)

FLOW	DEPTH (ft)	SiO <sub>2</sub>	Al <sub>2</sub> O <sub>3</sub>	Fe <sub>2</sub> O <sub>3</sub>	FeO	MgO	CaO	K <sub>2</sub> O	TiO <sub>2</sub>	Na <sub>2</sub> O	P <sub>2</sub> O <sub>5</sub>	MnO
Umtanum	3627.2	52.37	15.11	2	11.55	3.59	7.36	2.22	2.42	2.77	0.38	0.23
	3756.8	52.70	14.41	2	11.65	3.42	8.57	1.41	2.42	2.83	0.38	0.22
	3771.0	54.84	14.60	2	10.90	3.43	6.94	1.36	2.19	3.18	0.36	0.21
	3799.0	54.64	14.93	2	10.82	3.35	6.97	1.39	2.21	3.10	0.38	0.21
	3832.5	54.86	15.03	2	10.83	3.54	6.84	1.35	2.29	2.70	0.36	0.21
Grande Ronde 10	3870.8	53.10	16.27	2	9.97	5.83	7.12	0.43	1.75	3.06	0.29	0.18
	3878.4	52.22	15.57	2	9.77	5.64	9.53	0.45	1.73	2.62	0.28	0.20
	3889.2	51.88	15.38	2	9.81	5.39	9.79	0.66	1.77	2.82	0.30	0.20
	3897.3	55.51	14.90	2	8.65	4.70	6.91	3.10	1.57	2.23	0.26	0.16
	3907.3	53.71	15.79	2	10.16	3.63	7.22	2.00	2.08	2.85	0.32	0.24
Grande Ronde 11	3947.0	55.31	15.63	2	9.79	3.46	7.00	1.41	1.96	2.93	0.32	0.19
	3971.4	54.31	15.45	2	10.13	3.42	7.28	1.63	2.01	3.26	0.32	0.20

NOTE: To convert feet to meters, multiply by 0.3048.

TABLE 6. Means of Major and Minor Oxides for the Candidate Horizons.

OXIDE	NUMBER OF SAMPLES	MEAN wt %	STANDARD DEVIATION	MINIMUM wt %	MAXIMUM wt %
COHASSETT					
SiO <sub>2</sub>	42	53.38	0.43	52.33	54.21
Al <sub>2</sub> O <sub>3</sub>	42	15.07	0.39	14.16	15.79
FeO	42	11.70	0.32	11.10	12.50
MgO	42	5.04	0.20	4.56	5.34
CaO	42	8.82	0.29	8.08	9.31
K <sub>2</sub> O	42	1.01	0.12	0.51	1.28
Na <sub>2</sub> O	42	2.49	0.32	1.44	2.92
TiO <sub>2</sub>	42	1.78	0.07	1.67	1.93
MnO	42	0.21	0.01	0.19	0.24
P <sub>2</sub> O <sub>5</sub>	42	0.28	0.03	0.24	0.39
McCOY CANYON					
SiO <sub>2</sub>	38	53.58	0.51	52.62	54.79
Al <sub>2</sub> O <sub>3</sub>	38	14.96	0.33	14.40	15.86
FeO	38	12.30	0.25	11.56	12.70
MgO	38	4.62	0.25	3.84	5.38
CaO	38	8.44	0.22	8.04	9.13
K <sub>2</sub> O	38	1.01	0.12	0.70	1.18
Na <sub>2</sub> O	38	2.45	0.39	1.43	3.08
TiO <sub>2</sub>	38	1.95	0.08	1.79	2.13
MnO	38	0.21	0.01	0.19	0.23
P <sub>2</sub> O <sub>5</sub>	38	0.29	0.02	0.25	0.36
UMTANUM					
SiO <sub>2</sub>	53	54.65	0.79	51.66	56.03
Al <sub>2</sub> O <sub>3</sub>	53	14.68	0.31	14.08	15.53
FeO	53	12.91	0.28	12.47	14.00
MgO	53	3.53	0.19	3.32	4.36
CaO	53	7.13	0.28	6.79	8.57
K <sub>2</sub> O	53	1.52	0.24	0.94	2.30
Na <sub>2</sub> O	53	2.55	0.40	1.53	3.22
TiO <sub>2</sub>	53	2.18	0.07	2.05	2.42
MnO	53	0.22	0.01	0.21	0.29
P <sub>2</sub> O <sub>5</sub>	53	0.35	0.01	0.33	0.38

TABLE 7. Borehole RRL-2--Estimated Inclination and Statistical Parameters for Paleomagnetic Samples.

FLOW	DEPTH (ft)	NUMBER OF SAMPLES	ESTIMATED INCLINATION	UNCERTAINTY (95% Level)
Frenchman Springs 5	2285-2300	6	39.7	±5.6
Frenchman Springs 5	2326-2366	7	56.3	±16.8
Frenchman Springs 6	2400-2454	7	35.7	±10.4
Frenchman Springs 7	2500-2604	6	42.1	±17.5
Frenchman Springs 8	2628-2666	7	15.0	±4.5
Grande Ronde 1	2694-2719	7	74.3	±4.9
Grande Ronde 2	2736-2791	6	73.0	±6.4
Grande Ronde 3	2851-2902	7	71.0	±5.7
Cohasset	3002-3233	7	66.4	±10.9
Grande Ronde 5	3278-3341	7	61.7	±8.0
Grande Ronde 6	3399-3413	7	58.3	±2.6
Grande Ronde 7	3428-3471	7	69.7	±3.8
McCoy Canyon	3491-3551	7	69.9	±5.0
Umtanum	3747-3838	6	34.6	±15.3
Grande Ronde 10	3851-3890	7	79.4	±5.9
Grande Ronde 11	3905-3939	7	75.6	±7.9

NOTE: To convert feet to meters, multiply by 0.3048.

TABLE 8. Model Mineralogy of Cohasset, McCoy Canyon, and Umtanum Flows from Borehole RRL-2 Core Samples (vol%).

MINERAL	Cohasset Flow									McCoy Canyon		Umtanum				
	Sample depth below surface in feet.															
	3040.0	3112.0	3132.2	3134.0	3142.2	3163.9	3173.0	3175.5	3210.8		3560.5	3587.6	3770.7	3816.9	3828.5	3832.5
Plagioclase	38.38	33.65	33.05	29.38	38.83	36.77	45.38	42.25	41.65		35.60	42.00	25.05	25.50	29.15	34.20
Microlites	36.85	30.72	30.92	24.95	33.00	34.35	41.53	39.10	38.10		32.75	40.40	24.78	25.23	28.60	33.78
Microphenocrysts	1.53	2.93	2.13	3.93	5.60	2.42	3.80	3.15	3.55		2.85	1.60	0.27	0.27	0.55	0.42
				0.45	0.25		0.05									
Pyroxene	23.80	13.65	14.40	13.10	23.50	19.50	27.13	28.28	26.48		17.65	23.68	7.30	8.88	14.40	14.73
Microlites	20.53	12.40	13.58	10.40	9.85	16.35	16.08	15.88	16.15		11.88	17.90	7.13	8.63	14.15	14.45
Microphenocrysts	3.27	1.25	0.82	2.70	13.65	2.15	11.05	12.40	10.33		5.77	5.78	0.17	0.25	0.25	0.28
Mesostasis	29.03	38.33	42.95	50.20	26.18	36.03	20.87	22.15	24.98		36.15	25.88	62.30	59.95	50.20	43.73
Glass	19.80	21.38	19.83	19.98	21.40	22.72	13.88	15.13	16.70		19.75	18.93	34.93	33.43	37.30	29.03
Polycrystalline inclusions	0.03	3.02	4.75	7.53	0.22	3.83	0.03	TR	TR		3.13	TR	6.13	6.43	0.15	TR
Pyroxene	4.88	8.27	10.15	12.63	3.05	6.08	4.15	3.90	4.40		8.08	4.90	13.93	13.05	7.65	9.75
Titaniferous-magnetite	0.30	0.48	0.38	0.80	0.03	0.15	0.23	0.05	0.08		0.40	0.13	0.65	0.93	0.03	0.05
Plagioclase	4.02	5.18	7.83	9.27	1.48	3.62	2.55	3.07	3.55		4.85	1.92	6.66	6.13	5.07	4.90
Titaniferous-magnetite	3.28	2.90	3.13	2.28	2.88	2.90	3.50	3.30	3.13		4.05	3.92	2.25	3.13	4.03	4.98
Apatite	0.75	TR	0.05	TR	1.05	0.05	0.45	1.13	0.78		TR	0.68	TR	TR	0.30	1.03
Alteration products	4.73	11.53	6.50	5.23	7.40	4.73	2.45	2.90	1.80		6.70	3.78	3.28	1.98	1.75	0.95
Clay	4.73	11.53	6.50	5.23	7.40	4.73	2.45	2.90	1.80		6.70	3.75	3.05	1.73	1.65	0.57
Zeolite	TR	TR	TR	TR	TR	TR	TR	TR	TR		TR	0.03	0.28	0.25	0.10	0.38
Silica	TR	TR	TR	TR	TR	TR	TR	TR	TR		TR	TR	TR	TR	TR	TR
*Other	0.78	0.03	0.05	TR	1.18	0.08	0.63	1.40	1.93		TR	0.93	0.08	0.63	0.70	1.75
Sulfide Blebs	0.03	TR	TR	TR	TR	0.03	0.18	0.13	TR		TR	0.25	0.03	TR	0.08	0.05
	Col	Ent	Ent	Ent	Col	Ent	Col	Col	Col		Ent	Col	Ent	Ent	Col	Col

Col = Colonnade; Ent = Entablature.

\*This category includes pits, vesicles, holes, diktytaxitic vesicles, sulfide blebs, apatite and fractures.

The geomechanical data for the candidate horizons from borehole RRL-2 were analyzed to determine the average fracture frequency, average fracture filling width, and percentage of fractures that remained intact after the core was retrieved. The fracture filling width was determined only on fractures that remained intact. Two sets of average width data are presented for the Cohasset and Umtanum flows. One set is based on the data gathered at the wellsite with the aid of a 7X lens, and the other set is based on 200 randomly selected fractures in each flow measured with a binocular microscope. The results are as follows:

#### Average Fracture Frequency

Cohasset	2.0 fractures/ft
McCoy Canyon	2.6 fractures/ft
Umtanum	2.6 fractures/ft

#### Average Fracture Filling Width

<u>Wellsite data using 7X lens</u>		<u>Data using binocular scope</u>	
Cohasset	0.23 mm	Cohasset	0.13 mm
McCoy Canyon	0.23 mm	Umtanum	0.13 mm
Umtanum	0.14 mm		

#### Percentage of Intact Fractures

<u>Percentage of intact fractures</u>	
Cohasset	34%
McCoy Canyon	59%
Umtanum	83%

These data indicate that the apparent increase in fracture filling width (wellsite data) in Cohasset and McCoy Canyon flows may also indicate a weakening of the joint strength as indicated by the lower percentage of intact joints in these flows. However, factors such as core handling, drilling conditions, and diskings could affect the percentage of intact fractures.

After analysis of the core logs, geophysical logs, major element chemistry, thin sections and paleomagnetic data, the final lithology of borehole RRL-2 was determined (see Table 1). The observed depths of all major flows and formation contacts varied <1% from the depths predicted prior to drilling (Table 9).

TABLE 9. Borehole RRL-2--Predicted and Observed Stratigraphy (BWIPa, 1982).

FLOW OR INTERBED	PREDICTED DEPTH (ft below ground surface)	PREDICTED THICKNESS (ft)	OBSERVED DEPTH (ft below ground surface)	OBSERVED THICKNESS (ft)
SADDLE MOUNTAINS BASALT				
Elephant Mountain		85	603 - 686	83
Rattlesnake Ridge interbed		100	686 - 782	97
Pomona		135	782 - 941	158
Selah interbed		50	941 - 986	45
Esquatze!l		125	986 - 1,104	118
Cold Creek interbed		70	1,104 - 1,168	63
Umatilla		225	1,168 - 1,399	232
Mabton interbed		140	1,399 - 1,523	124
WANAPUM BASALT				
Priest Rapids II	1,523 - 1,685	162	1,523 - 1,689	166
Priest Rapids I	1,685 - 1,755	70	1,689 - 1,749	60
Roza	1,755 - 1,925	170	1,749 - 1,922	173
Frenchman Springs 1	1,925 - 2,105	180	1,922 - 2,104	182
Frenchman Springs 2	2,105 - 2,205	100	2,104 - 2,217	113
Frenchman Springs 3	2,205 - 2,250	45	2,217 - 2,273	54
Frenchman Springs 4	2,250 - 2,290	40		
Frenchman Springs 5	2,290 - 2,355	65	2,273 - 2,381	110
Frenchman Springs 6	2,355 - 2,470	115	2,381 - 2,489	108
Frenchman Springs 7	2,470 - 2,595	125	2,489 - 2,617	128
Frenchman Springs 8	2,595 - 2,665	70	2,617 - 2,683	66
Vantage interbed	2,665 - 2,680	15	2,683 - 2,687	4
GRANDE RONDE BASALT				
Grande Ronde 1	2,680 - 2,745	65	2,687 - 2,721	33
Grande Ronde 2	2,745 - 2,800	55	2,721 - 2,823	103
Grande Ronde 3	2,800 - 2,970	170	2,823 - 2,993	170
Cohasset 4	2,970 - 3,235	265	2,993 - 3,255	262
Grande Ronde 5	3,235 - 3,350	115	3,255 - 3,388	133
Grande Ronde 6	3,350 - 3,395	45	3,388 - 3,418	29
Grande Ronde 7	3,395 - 3,465	70	3,418 - 3,475	58
McCoy Canyon 8	3,465 - 3,610	145	3,475 - 3,607	132
Umtanum 9	3,610 - 3,825	215	3,607 - 3,839	232
Flow top	3,610 - 3,675	65	3,607 - 3,755	148
Interior	3,675 - 3,825	150	3,755 - 3,839	84
Very High Mg 10	3,825 - 3,875	50	3,839 - 3,903	64
Low Mg 11	3,875		3,903 - 3,973 TD	70

NOTE: To convert feet to meters, multiply by 0.3048.

## HYDROLOGIC TESTING

## INTRODUCTION

In order to evaluate the groundwater systems within the RRL, hydrologic testing was conducted at selected intervals within borehole RRL-2. The effort was directed toward characterizing the vertical hydraulic head distribution, hydraulic properties, and hydrochemistry within the Columbia River basalts. Data obtained from these studies provide input for numerical modeling of groundwater flow and solute transport. These models are then used for evaluating potential waste migration from a nuclear waste repository in basalt.

Hydrologic property data were obtained from selected high and low permeability intervals. Each test interval was isolated by a single inflatable packer and the hole bottom or, in the case when the drilling was completed, by an inflatable bridge plug packer seated at the base of the test interval. The location of each test interval and an associated neutron-epithermal neutron log for the lower Saddle Mountains, Wanapum, and Grande Ronde Basalt are shown in Figures 17 and 18.

## METHODOLOGY

Hydrologic parameters determined from analysis of hydrologic test data include:

- Hydraulic head
- Transmissivity
- Equivalent hydraulic conductivity.

The hydrologic tests conducted to determine these parameters are:

- Constant discharge
- Constant drawdown
- Slug injection/withdrawal
- Over-pressure pulse
- Constant head injection test.

Tests utilized are based upon interval hydraulic characteristics. A brief description of each test is presented in the following paragraphs.

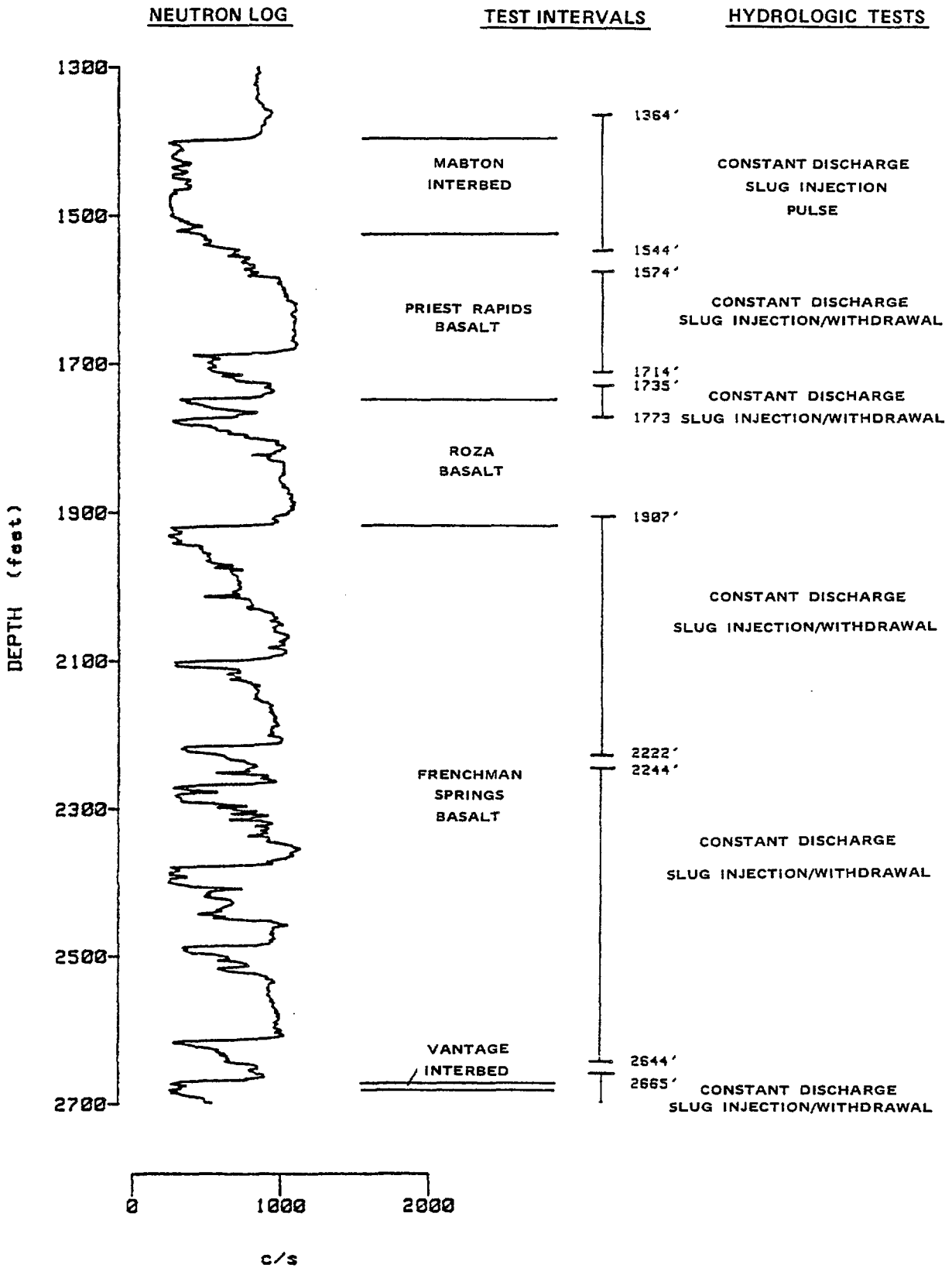


FIGURE 17. Borehole RRL-2--Geophysical Logs of Test Intervals, 1,300-2,700 Feet.

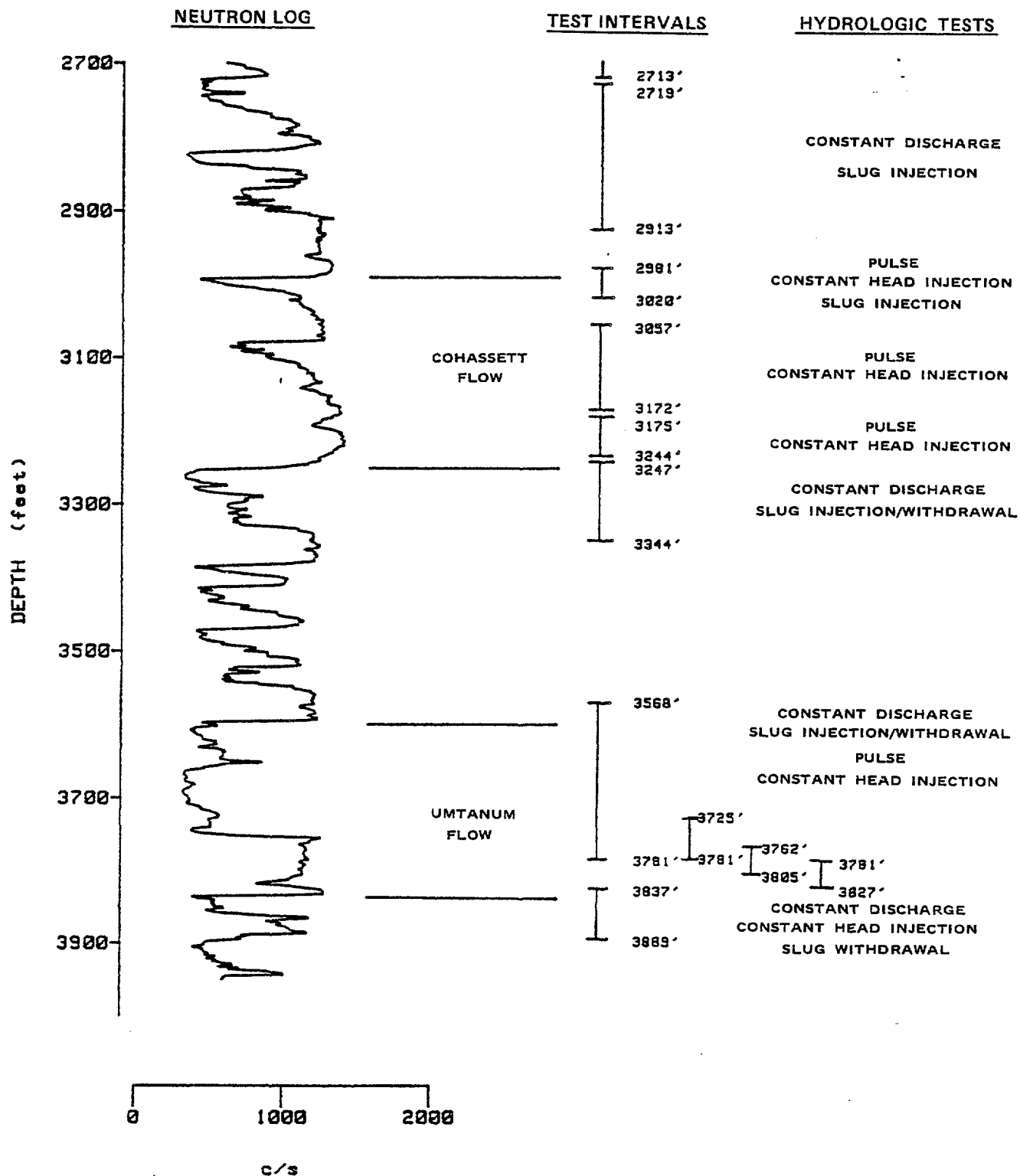


FIGURE 18. Borehole RRL-2--Geophysical Logs of Test Intervals, 2,700-3,900 Feet.

### Constant Discharge Test

The constant discharge test is conducted using air-lift or submersible pumping methods. The objective of the constant discharge test is to determine hydraulic properties and to obtain groundwater samples for hydrochemical analysis.

### Constant Drawdown Test

This test is performed by air-lift pumping in moderately low permeability horizons where the water level can be lowered at or near the base of the air line. The primary purpose of this test is to obtain hydraulic properties of the test interval.

### Slug Injection/Withdrawal Test

This test is conducted by inducing an instantaneous pressure reduction or increase in hydraulic head within the tested zone followed by observation of the associated hydraulic response. The purpose of these tests is to provide corroborative data on the hydrologic characteristics of the test interval.

### Over-Pressure Pulse Test

The over-pressure pulse test is conducted by inducing an instantaneous over pressure to the test interval followed by observation of the associated hydraulic response. The purpose of this test is to provide hydraulic properties in low permeability horizons.

### Constant Head Injection Test

This test is conducted by injecting water for an extended period of time at a constant over pressure into a test interval. The purpose of this test is to provide corroborative data on the hydrologic characteristics in low permeability zones.

## RESULTS

The transmissivities, equivalent hydraulic conductivities, and observed hydraulic heads for each test interval in borehole RRL-2 are listed in Table 10. Also presented are the test depths and an estimate of the effective test interval, based upon examination of core and borehole geophysical logs (e.g., neutron-epithermal neutron and sonic). The comparison of observed and predicted values is shown in Table 11.

TABLE 10. Hydrologic Properties from Borehole RRL-2. (Sheet 1 of 2)

STRATIGRAPHIC INTERVAL	TYPE OF ROCK TESTED	DEPTH INTERVAL FOR FIELD TEST (ft)	EFFECTIVE THICKNESS INTERVAL (ft)	TRANSMISSIVITY (ft <sup>2</sup> /day)	EQUIVALENT HYDRAULIC CONDUCTIVITY (ft/sec)	OBSERVED HYDRAULIC HEAD (Feet Above Mean Sea Level)*
Mabton	Interbed	1304-1544	1399-1449	$10^{-2} - 10^{-1}$	$10^{-9} - 10^{-8}$	418
Priest Rapids	Flow top	1574-1714	1689-1714	$10^2 - 10^3$	$10^{-5} - 10^{-4}$	401
Roza	Flow top	1735-1773	1749-1759	$10^3 - 10^4$	$10^{-4} - 10^{-3}$	404
Upper Frenchman Springs	Flow tops	1907-2222	1922-1947 2104-2112 2217-2222	$10^2 - 10^3$	$10^{-5} - 10^{-4}$	402
Lower Frenchman Springs	Flow tops	2244-2644	2270-2294 2380-2410 2490-2502 2618-2624	$10^3 - 10^4$	$10^{-4} - 10^{-3}$	400
Vantage	Interbed	2665-2713	2672-2690	$10^0 - 10^1$	$10^{-7} - 10^{-6}$	399
Upper Grande Ronde	Flow tops	2719-2913	2720-2760 2823-2840	$10^2 - 10^3$	$10^{-5} - 10^{-4}$	397
Cohasset	Flow top (Composite)	2981-3020	2993-3010	$10^{-1} - 10^0$	$10^{-8} - 10^{-7}$	399
Cohasset	Vesicular Zone	3057-3172	3083-3099	$10^{-4} - 10^{-3}$	$10^{-11} - 10^{-10}$	No Data
Cohasset	Colonnade/Entablature	3175-3244	3175-3244	$10^{-6} - 10^{-5}$	$10^{-13} - 10^{-12}$	No Data
Cohasset	Flow Bottom (Composite)	3247-3344	3255.5-3333	$10^2 - 10^3$	$10^{-5} - 10^{-4}$	406
Umtanum	Flow top (Composite)	3568-3781	3597-3754	$10^2 - 10^3$	$10^{-5} - 10^{-4}$	406
Umtanum	Flow top (Lower portion of composite)	3725-3781	3741-3749	$10^0 - 10^1$	$10^{-7} - 10^{-6}$	407

TABLE 10. Hydrologic Properties from Borehole RRL-2. (Sheet 2 of 2)

STRATIGRAPHIC INTERVAL	TYPE OF ROCK TESTED	DEPTH INTERVAL FOR FIELD TEST (ft)	EFFECTIVE THICKNESS INTERVAL (ft)	TRANSMISSIVITY (ft <sup>2</sup> /day)	EQUIVALENT HYDRAULIC CONDUCTIVITY (ft/sec)	OBSERVED HYDRAULIC HEAD (Feet Above Mean Sea Level)*
Untanum	Entablature	3762-3805	3762-3805	10 <sup>-5</sup> - 10 <sup>-4</sup>	10 <sup>-12</sup> - 10 <sup>-11</sup>	No Data
Untanum	Fracture Zone	3781-3827	3818-3824	10 <sup>1</sup> - 10 <sup>3</sup>	10 <sup>-4</sup> - 10 <sup>-3</sup>	407
Untanum	Flow Bottom (Composite)	3837-3889	3839-3862	10 <sup>2</sup> - 10 <sup>3</sup>	10 <sup>-5</sup> - 10 <sup>-4</sup>	407

\*Surface datum elevation = 633.9 feet MSL.

NOTE: To convert feet to meters, multiply by 0.3048.

TABLE 11. Predicted Versus Observed Hydrologic Characteristics  
in Borehole RRL-2 (BWIPa, 1982).

STRATIGRAPHIC HORIZON	PREDICTED HEAD *	ACTUAL HEAD *	PREDICTED TRANSMISSIVITY (ft <sup>2</sup> /day)	ACTUAL TRANSMISSIVITY (ft <sup>2</sup> /day)
Mabton Interbed	420	418	10 <sup>-1</sup> - 10 <sup>0</sup>	10 <sup>-2</sup> - 10 <sup>-1</sup>
Priest Rapids flow top	400	401	10 <sup>-1</sup> - 10 <sup>+1</sup>	10 <sup>2</sup> - 10 <sup>3</sup>
Roza flow top	400	404	10 <sup>3</sup> - 10 <sup>4</sup>	10 <sup>3</sup> - 10 <sup>4</sup>
Frenchman Springs (composite)	400	402	10 <sup>2</sup> - 10 <sup>3</sup>	10 <sup>3</sup> - 10 <sup>4</sup>
Vantage Interbed	400	399	10 <sup>-1</sup> - 10 <sup>0</sup>	10 <sup>0</sup> - 10 <sup>1</sup>
Upper Grande Ronde (composite)	395	397	10 <sup>1</sup> - 10 <sup>2</sup>	10 <sup>2</sup> - 10 <sup>3</sup>
Cohasset flow top	395	397	10 <sup>-2</sup> - 10 <sup>1</sup>	10 <sup>-1</sup> - 10 <sup>0</sup>
Cohasset Colonnade/Entablature	n/a	n/a	10 <sup>-6</sup> - 10 <sup>-5</sup>	10 <sup>-6</sup> - 10 <sup>-5</sup>
Cohasset flow bottom	400	407		10 <sup>2</sup> - 10 <sup>3</sup>
Middle Grande Ronde (composite)	400		10 <sup>-1</sup> - 10 <sup>1</sup>	
McCoy Canyon flow top	400		10 <sup>-1</sup> - 10 <sup>1</sup>	
Umtanum flow top	400	406	10 <sup>0</sup> - 10 <sup>1</sup>	10 <sup>2</sup> - 10 <sup>3</sup>
Umtanum interior	n/a	n/a	10 <sup>-6</sup> - 10 <sup>-5</sup>	10 <sup>-5</sup> - 10 <sup>-4</sup>
Very High Mg flow top	400	407	10 <sup>-1</sup> - 10 <sup>1</sup>	10 <sup>2</sup> - 10 <sup>3</sup>

\* Feet above MSL

NOTE: To convert feet to meters, multiply by 0.3048.

Observed hydraulic head measurements in borehole RRL-2 indicate a slight upward head gradient across the Grande Ronde Basalt. Most of this head increase appears to occur between the Cohasset and Umtanum flows. Within the Wanapum Basalt, a slight downward gradient exists between the Roza and lower Frenchman Springs basalt. These small gradients, centered around a hydraulic head of ~400 ft (121.9 m) above mean sea level are typical of that expected at borehole RRL-2.

A comparison of equivalent hydraulic conductivity values obtained at borehole RRL-2 with values calculated from other interflow and interbeds within the Columbia River Basalts, is shown in Figure 19. The equivalent hydraulic conductivity values within the Grande Ronde Basalt at borehole RRL-2 are generally slightly higher than the mean equivalent hydraulic conductivity for other boreholes.

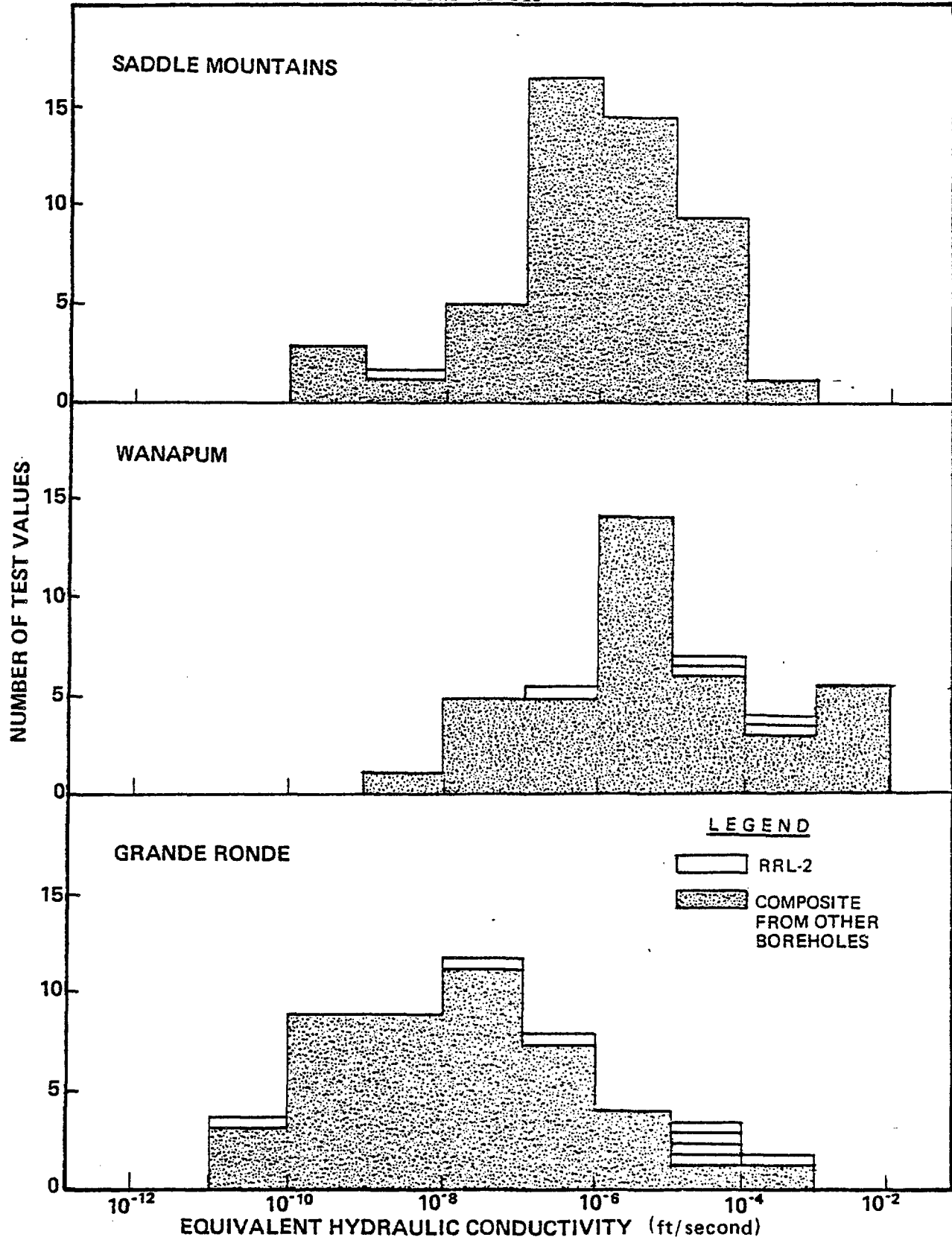


FIGURE 19. Comparison of Equivalent Conductivity Values Between Borehole RRL-2 Interflow Zones and Sedimentary Interbeds (Strait, 1982).

## HYDROCHEMISTRY

## INTRODUCTION

Groundwater samples were collected and analyzed to determine the chemical composition of the groundwater at selected sites. Chemical analyses provide information concerning geochemical and hydrological relationships in and between aquifers.

Eight intervals within the Wanapum and Grande Ronde Basalts were sampled for hydrochemical analyses in borehole RRL-2 (Table 12). Parameters analyzed include major cations and anions, trace elements, fluid temperature, pH, Eh, electrical conductivity, and major dissolved gas components. Isotopic analyses generally included tritium, deuterium, oxygen-18, carbon-13, carbon-14, uranium, sulfur-34, and chlorine-36.

## METHODOLOGY

The hydrologist assigned to the borehole determined where and when groundwater was suitable for sampling. Fluorescein dye, which was placed in the drilling fluid, was used to determine when a sample was representative of the aquifer source. The zone to be sampled was isolated by the use of inflatable or mechanical packers, then developed by air lifting until the fluorescein level was low enough to obtain a representative sample.

## RESULTS

Major Inorganic Constituents

Major inorganic constituents for groundwater samples collected at borehole RRL-2 are listed in Table 13. Groundwater within the interflow zones adjacent to the Priest Rapids and Roza basalts are of a sodium chloride-bicarbonate chemical type. Groundwaters in the Frenchman Springs and Grande Ronde Basalt are of a sodium chloride chemical type and have increased total dissolved solids content. This is shown graphically in Figure 20. In other boreholes on the Hanford Site, the change in groundwater type from sodium chloride-bicarbonate to sodium chloride generally takes place stratigraphically deeper, at the contact between the Frenchman Springs and Grande Ronde Basalts.

Anion-cation balances (anion equivalents-cation equivalents/cation equivalents) for samples collected from borehole RRL-2 are presented in Table 14. Balances generally fall within the range required for sample acceptance (5%). Some caution should be used in quantitative evaluation of sample data for which the anion-cation balance exceeds 5%. Tritium concentration in groundwater samples also provides a measure of sample quality. These measurements are discussed in the section under "Isotopic Chemistry."

TABLE 12. Borehole RRL-2--Groundwater Sample Intervals.

STRATIGRAPHIC INTERVAL	PACKER SETTING DEPTH BELOW LAND SURFACE (ft)	SAMPLE COLLECTION DATE
Priest Rapids Interflow	1574 - 1714	02/12/82
Roza Flow Top	1735 - 1773	02/24/82
Frenchman Springs Interflow	2244 - 2644	04/14/82
Upper Grande Ronde	2719 - 2913	05/17/82
Cohasset Flow Bottom	3247 - 3344	08/16/82
Umtanum Flow Top	3568 - 3781	07/21/82
Very High Magnesium Flow Top	3837 - 3889	09/29/82

NOTE: To convert feet to meters, multiply by 0.3048.

TABLE 13. Borehole RRL-2--Major Inorganic Constituents in Groundwater.

INTERVAL	SAMPLE NUMBER	DEPTH INTERVAL (ft)	(Units are mg/l)												TOTAL DISSOLVED SOLIDS	ANION-CATION BAL.*
			HCO <sub>3</sub>	CO <sub>3</sub> <sup>2-</sup>	OH <sup>-</sup>	H <sub>3</sub> SiO <sub>4</sub> <sup>-</sup>	Cl <sup>-</sup>	SO <sub>4</sub> <sup>2-</sup>	F <sup>-</sup>	Na <sup>+</sup>	K <sup>+</sup>	Ca <sup>2+</sup>	Mg <sup>2+</sup>	H <sub>4</sub> SiO <sub>4</sub>		
Priest Rapids Interflow	82-68	1574-1714	188.7	7.74	0.10	9.1	133.0	1.60	8.5	161.6	20.9	2.0	0.19	93.0	588	0
Roza Flow Top	82-65	1735-1773	143.6	13.96	0.23	23.1	122.0	2.0	8.6	141.1	15.5	1.9	0.10	93.4	522	3
Frenchman Springs Interflow	82-170	224-2644	106.9	1.08	0.02	3.6	344.0	21.0	15.0	282.2	35.10	9.4	0.23	87.6	874	6
Upper Grande Ronde	82-122	2719-2913	86.9	2.64	0.05	11.7	507.0	1.40	20.0	373.8	25.3	2.9	0.10	106.8	1094	0
Cohassett Flow Bottom	82-401	3247-3844	98.3	17.76	0.29	63.7	403.9	4.2	20.0	336.8	13.8	2.2	0.10	88.9	993	5
Umtanum Flow Top	82-364	3568-3781	89.3	9.76	0.18	55.0	451.0	1.7	18.2	354.9	9.4	1.6	0.10	107.9	1038	4
Umtanum Fracture Zone	82-309	3781-3827	110.1	8.24	0.13	35.5	384.5	3.5	17.3	335.5	8.5	2.8	0.14	87.9	948	3
Very High Magnesium Flow Top	82-456	3837-3889	73.4	11.76	0.27	55.7	455.3	2.4	20.1	363.5	5.9	1.83	0.10	71.62	1014	5

64

SD-BWI-TI-113

$$*Anion - cation balance = \frac{\sum anion\ equivalents - \sum cation\ equivalents}{\sum Cation\ equivalents} \times 100 \text{ (expressed as percent).}$$

NOTE: To convert feet to meters, multiply by 0.3048

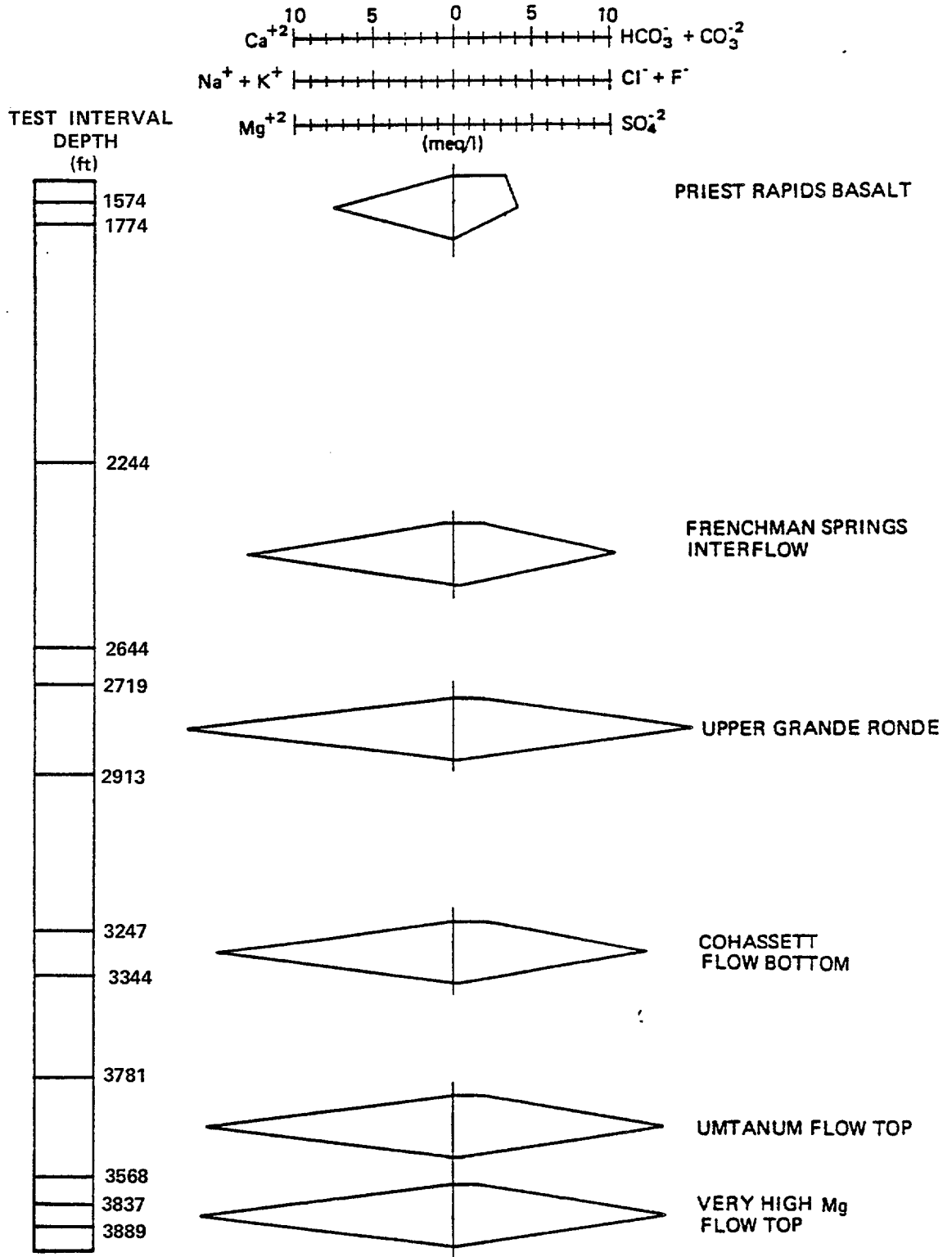


FIGURE 20. Selected Stiff Diagrams for Columbia River Basalt Groundwaters in Borehole RRL-2.

TABLE 14. Borehole RRL-2--Trace Element Concentrations in Groundwater.

INTERVAL	SAMPLE NUMBER	(Units are mg/l)												
		A1	Ba	B	Co	Cr	Cu	Fe	Li	Mn	Mo	Ni	Pb	Zn
Priest Rapids Interflow	82-68	<0.08	0.019	0.38	0.10	0.04	<0.006	6.60	0.10	0.08	0.10	<0.03	<0.15	0.05
Roza Flow Top	82-65	<0.08	0.005	0.36	<0.10	<0.03	<0.006	0.39	0.007	0.01	0.12	<0.02	<0.15	0.02
Frenchman Springs Interflow	82-170	<0.08	0.024	1.09	<0.10	<0.03	<0.006	0.11	0.017	0.015	0.05	0.02	<0.15	<0.01
Upper Grande Ronde	82-122	<0.08	0.004	2.60	<0.10	<0.03	<0.006	0.82	0.02	0.032	0.13	<0.02	<0.15	<0.01
Cohasset Flow Bottom	82-401	0.41	0.002	3.50	<0.10	<0.03	<0.006	0.13	0.03	0.004	0.28	<0.02	<0.15	<0.01
Umtanum Flow Top	82-364	<0.07	0.004	3.44	<0.10	<0.03	<0.006	0.048	0.04	<0.003	0.27	<0.02	<0.15	<0.01
Umtanum Fracture Zone	82-309	0.11	0.003	3.14	<0.10	<0.03	0.006	0.14	0.03	0.007	0.24	<0.02	<0.15	0.02
Very High Magnesium Flow	82-456	0.33	0.005	3.50	<0.01	<0.03	<0.006	0.05	0.04	<0.004	0.26	<0.02	<0.15	<0.01

TABLE 14. Borehole RRL-2--Trace Element Concentrations in Groundwater.

A comparison of groundwater hydrochemical data from borehole RRL-2 with data presented by Spane and others (1982) indicates Grande Ronde groundwater in RRL-2 is generally:

- Higher in chloride concentration
- Lower in fluoride concentration
- Lower in sulfate concentration than the average for other boreholes on the Hanford Site.

The significance of these differences is not completely understood and is currently under investigation.

### Trace Elements

Trace element concentrations in groundwater from borehole RRL-2 are listed in Table 14. The main trace elements found are boron and iron. Elevated iron concentrations are attributed to the iron drill pipe through which the samples are collected.

### Dissolved Gas

Dissolved gas information available for sampled intervals within borehole RRL-2 is presented in Table 15. Methane is the major gas component, with nitrogen generally making up the remaining percentage. Gas data are not available for Wanapum Basalt zones due to the use of air-lift pumping techniques to collect samples from those zones.

Also presented in Table 15 are concentrations of methane in groundwater. Comparison of these data with methane solubility (Bonham, 1978) at formation conditions indicates groundwaters are ~50% saturated with methane in borehole RRL-2.

### Isotopic Chemistry

Groundwater samples for both stable and radioactive isotopic analysis were also collected from borehole RRL-2. Available data are shown in Table 16. In examining Table 16, the following should be noted:

- All samples contain measureable tritium concentrations
- Carbon-13 values are zero or greater.

Tritium's primary use in basalt hydrological studies at the Hanford Site has been as a natural tracer in drilling fluids. Drilling fluids used in borehole RRL-2 were made up using Columbia River water. This water has a high level of tritium that serves as a natural tracer for evaluating drilling-fluid contamination groundwater sampled from test intervals. This procedure has been used to provide information concerning the groundwater's representativeness following final sample collection.

TABLE 15. Borehole RRL-2--Distribution of Dissolved Gas Components  
in Grande Ronde Basalt Zones.

STRATIGRAPHIC INTERVAL	SAMPLE NUMBER	CARBON DIOXIDE	ARGON	OXYGEN	NITROGEN	VOLUME PERCENT				METHANE CONCENTRATION (mg/l)
						CARBON MONOXIDE	HELIUM	HYDROGEN	METHANE	
Cohasset Flow Bottom	82-401	0.04	0.04	0.01	2.36	0.10	0.01	0.01	97.6	620
Umatanum Flow Top	82-364	0.01	0.03	0.01	1.87	0.5	0.01	0.15	97.9	702
Umatanum Fracture Zone	82-370	0.01	0.05	0.03	3.11	0.10	0.01	0.11	96.7	527
Very High Magnesium Flow	82-456	0.01	0.03	0.03	2.43	0.10	0.02	0.03	97.5	661

TABLE 16. Borehole RRL-2--Isotopic Data for Groundwater.

STRATIGRAPHIC UNIT	STABLE ISOTOPES				RADIOACTIVE ISOTOPES					
	$\delta^{18}\text{O}$ (A)	$\delta^2\text{H}$ (A)	$\delta^{13}\text{C}$ (A)	$\delta^{34}\text{S}$ (A)	$^3\text{H}$ (B)	$^{14}\text{C}$	RELATIVE AGE (C)	$^{234}\text{U}/^{238}\text{U}$	TOTAL U ng/ml	$^{36}\text{Cl}$
Priest Rapids Interflow	-17.0	-134	----	----	$1.19 \pm 0.08$	----		---	----	----
Rosa Flow Top	-16.0	-136	8.50	*	$0.98 \pm 0.09$	----	$36000 \pm 4000$	---	----	----
Frenchman Springs Interflow	-13.2	-120	-0.30	+2.5	$6.43 \pm 0.22$	----	$12300 \pm 1800$	---	----	----
Upper Grande Ronde	-11.5	-114	15.4	----	$0.90 \pm 0.10$	----		---	----	----
Cohasset	----	----	----	----	----	----	----	---	----	----
Umtanum Flow Top	----	----	+16.9	----	$0.86 \pm 0.11$	----		---	----	----
Umtanum Fracture Zone	----	----	----	----	----	----		---	----	----
Very High Mg Flow Top	----	----	----	----	----	----		---	----	----

\* Too small for analysis

(A)  $\delta$  units (0/00) = parts per thousand

(B) Tritium units

(C) Elevated tritium indicates C-14 age dates are incorrect

Samples for which tritium concentration is less than one tritium unit are generally considered to be acceptable for analysis of major inorganic constituents. Samples with a measureable amount of tritium (two standard deviations), however, indicate some drilling fluid remained in the groundwater and the sample may be unsuitable for carbon-14, chlorine-36, and uranium analyses. Due to the presence of tritium in groundwater sampled at borehole RRL-2, caution should be used in interpreting these data. Resampling of contaminated zones for age dating purposes is currently being evaluated.

Carbon-13 values range between -31.5 and +20.7 with a mean value of -9.85 in Columbia River basalt groundwaters. As shown in Table 16, carbon-13 in groundwater sampled at borehole RRL-2 is generally positive. This has previously been attributed to the occurrence of methane in groundwater at borehole RRL-2.

#### Fluid Temperature, pH, Eh, Electrical Conductivity

Fluid temperatures for groundwater measured at ground surface are listed in Table 17. Downhole measurements are considered to be more representative of in situ formation temperatures. Fluid temperature increases with depth and is reflective of the local geothermal gradient, which is about 1.14°C per 100 ft (30.5 m) depth, based upon temperature measurements in several deep boreholes.

The pH measurements are routinely performed at the sample site at the time of collection. Several problems are associated with surface measurements of pH. Formation waters can cool and may degas during transport from depth to the point of collection. Groundwater pH measured at the ground surface, however, can be corrected to formation temperature conditions.

While fluid temperatures and pH can be measured directly with reasonable accuracy, surface measurement of Eh is generally not suitable for quantitative interpretations (Stumm and Morgan, 1981; Langmuir, 1971); however, such measurements may be useful as a qualitative tool to indicate the general oxidizing or reducing conditions. Potentiometric measurements of Eh on Columbia River basalt groundwaters in borehole RRL-2 indicate Eh may range from near zero to -0.165 volts. Mineral assemblages and redox couples evaluated in other boreholes suggest conditions may be more strongly reducing than indicated by potentiometric measurements (Rockwell, 1982).

Electrical conductivity data for groundwater at borehole RRL-2 are presented in Table 17. Electrical conductivity may be used as an estimate of total dissolved solids in surface waters and some groundwaters.

TABLE 17. Borehole RRL-2--pH, Eh, Temperature and Electrical Conductivity for Groundwater Samples.

STRATIGRAPHIC INTERVAL	pH	Eh	FLUID TEMPERATURE °C	ELECTRICAL CONDUCTIVITY Micromhos/cm
Priest Rapids Interflow	9.14	---	6.5	810
Roza Flow Top	9.30	---	21.8	683
Frenchman Springs Interflow	8.30	---	29.1	1408
Upper Grande Ronde	8.77	-0.165	26.9	1856
Cohasset Flow bottom	9.71	-0.048	23.4	1616
Umtanum Flow Top	9.45	0.018	29.4	1740
Umtanum Fracture Zone	9.34	---	25.9	---
Very High Magnesium Flow top	9.78	-0.057	22.3	1747

## GEOMECHANICS LABORATORY CHARACTERIZATION

## INTRODUCTION

A series of laboratory tests were conducted on the core from borehole RRL-2 in the BWIP Rock Mechanics laboratory. The purpose of this testing was to characterize the core with respect to its physical and mechanical properties. Subsequently, these rock characterization properties will be used in designing the exploratory shaft, evaluating the rock drillability, assist in the selection of the repository's breakout horizon, and help establish or verify a preliminary design for the repository's underground openings.

The following flows were tested from borehole RRL-2:

- Grande Ronde 3
- Cohasset
- McCoy Canyon
- Umtanum.

Each flow was further subdivided into the following three types of intraflow structures:

- Flow top
- Entablature
- Colonnade.

Samples were selected for laboratory testing from each of the previously mentioned intraflow structures.

## METHODOLOGY

After visually examining the rock core, and selecting the samples from each intraflow structure, the samples were characterized, then cut and ground to the appropriate specimen size. Every attempt was made to select rock core samples with no apparent flaws or fractures. This became very difficult in some portions of the core due to the presence of diking and preexisting fractures.

## PHYSICAL PROPERTY TESTS

A series of physical and mechanical property tests were conducted on specimens from each of the intraflow structures. The physical tests were as follows:

- Grain density--the mass of a unit volume of the grains of the rock
- Bulk density--is the dry bulk density, where bulk volume is equal to grain volume plus pore volume
- Total and apparent porosity--porosity of rock is defined as the ratio of the volume of internal open spaces (also referred to as pores or voids) to the bulk volume of the rock. If the volumes above are experimentally determined and the sample is not a powdered sample, thus making the pore volume measured that of the interconnected pores, the value calculated is the apparent porosity.

## MECHANICAL PROPERTY TESTS

The mechanical property tests are divided into strength tests and elastic property tests. The elastic property testing can be further segregated into static and dynamic testing. Strength and elastic parameter tests are as follows:

- Uniaxial compression--a measure of a rock's compressive strength under conditions where the sample is axially loaded and not confined in a lateral direction
- Triaxial compression--a measure of a rock's compressive strength under conditions of varying confining pressure applied in the lateral direction while the specimen is axially loaded
- Brazilian tensile strength--an indirect method of determining a rock's tensile strength by measuring the pressure a disk-shaped rock sample can withstand when pressure is applied across its diameter
- Modulus of rupture--a measure of the outer fiber tensile strength of a rock sample during bending.

The mechanical elastic properties are determined from data obtained via strain gauges that are attached to the circumferential surface of the rock core to measure the stress-strain behavior of the specimen when tested in either a uniaxial or triaxial compressive strength test. Dynamic elastic properties are determined from the velocity measurements of pulse-generated compression and shear waves and are defined as follows:

- Young's modulus--a linear factor of proportionality between normal stress and normal strain

- Poisson's ratio--a ratio of the transverse lateral strain (perpendicular to the applied stress), with respect to the normal strain (parallel to the applied stress)
- Shear modulus--a factor of proportionality between shear stress and shear strain
- Bulk modulus--a factor of proportionality between a hydrostatic pressure (stress), applied to the sample and the resulting volumetric strain.

## RESULTS

A statistical summary of all the test results is provided in Tables 18 through 20. These tables are separated according to the following intraflow structure groupings:

- Flow top
- Entablature
- Colonnade.

Within each table there is a further segregation according to flow:

- Grande Ronde 3
- Cohasset
- McCoy Canyon
- Umtanum.

Only data from tests on intact specimens were utilized to develop the elastic and strength statistical summaries in Tables 18 through 20.

From the physical property (bulk density, grain density, apparent porosity, and total porosity) statistical summarization presented in Tables 18 through 20, it is apparent that there is very little variation in grain density within the four flows tested. Values of bulk density were essentially the same in all four flows in the entablature and colonnade intraflow structures, but were notably less in flow tops (references to the flow-top intraflow structure will include both the vesicular and brecciated rock). The most obvious dissimilarity in apparent and total porosity data was that the flow-top values were greater than those in the entablature and colonnade.

TABLE 18. Summary of Borehole RRL-2--Basalt Physical and Mechanical Property Data--Flow Top/Vesicular Zones. (Sheet 1 of 2)

FLOW	TEST INTERVAL (ft)	UNIAXIAL COMPRESSIVE STRENGTH MPa	BULK DENSITY g/cc	YOUNG'S MODULUS (Static) GPa	POISSON'S RATIO (Static)	BRAZILIAN TENSILE STRENGTH MPa	MODULUS OF RUPTURE MPa
Cohassett Flow Top No. of Samples Mean Standard Deviation Range Confidence Limits*	2993 - 3006	5 69.88 20.10 43.42-97.60 56.10-83.66	14 2.29 0.10 2.13-2.47	—	—	8 7.90 2.04 5.86-12.10	—
Vesicular No. of Samples Mean Standard Deviation Range Confidence Limits*	3083 - 3108 3254 - 3256	3 155.77 34.44 123.94-192.34 118.27-193.27	6 2.71 0.01 2.69-2.73	3 52.40 6.39 45.02 - 56.13	3 0.27 0.06 0.21-0.33	3 13.05 1.96 10.81-14.43	—
McCoy Canyon Flow Top No. of samples Mean Standard Deviation Range Confidence Limits*	3478 - 3489	9 37.80 14.04 27.32-70.94 31.26-44.34	19 2.14 0.16 1.88-2.42	1 14.0	1 0.16	9 4.39 1.2 2.70-6.34	—
Vesicular No. of samples Mean Standard Deviation Range Confidence Limits*	3525 - 3543	5 96.84 13.33 84.16-117.78 87.70-105.98	16 2.50 0.15 2.27-2.74	—	—	11 11.77 5.49 7.16-26.82	—
Untanum Breccia No. of Samples Mean Standard Deviation Range Confidence Limits*	3607 - 3755	19 67.68 53.20 13.83-201.55 51.45-83.91	48 2.27 0.18 1.79-2.64	4 30.34 12.99 14.69-44.0	3 0.24 0.08 0.17-0.32	23 5.92 2.4 2.18-11.81	—

\* 80% Confidence Level

NOTE: To convert feet to meters, multiply by 0.3048

TABLE 18. Summary of Borehole RRL-2--Basalt Physical and Mechanical Property Data--Flow Top/Vesicular Zones. (Sheet 2 of 2)

FLOW	YOUNG'S MODULUS (Dynamic) GPa	SHEAR MODULUS (Dynamic) GPa	BULK MODULUS (Dynamic) GPa	POISSON'S RATIO (Dynamic)	GRAIN DENSITY g/cc	APPARENT POROSITY %	TOTAL POROSITY %
Cohasset Flow Top							
No. of samples	2	2	2	2	3	14	3
Mean	53.9	21.8	34.3	0.24	2.88	12.6	23.0
Standard Deviation	4.5	1.9	1.8	0.01	0.01	2.4	4.9
Range	50.7-57.0	20.4-23.1	33.0-35.6	0.23-0.24	2.88-2.89	9.7-17.4	17.3-26.0
Vesicular							
No. of samples	3	3	3	3	1	6	1
Mean	62.6	24.1	52.7	0.30	2.90	2.7	7.2
Standard Deviation	2.0	0.6	3.1	0.01		0.7	
Range	60.4-64.0	23.4-24.6	49.5-55.6	0.30-0.31		1.6-3.4	
McCoy Canyon Flow Top							
No. of samples	4	4	4	4	3	19	3
Mean	25.2	11.3	16.1	0.22	2.89	21.6	27.7
Standard Deviation	6.0	2.4	2.8	0.04	0.08	3.8	4.5
Range	20.7-33.8	8.94-14.0	12.6-19.0	0.18-0.27	2.85-2.98	13.5-26.9	22.5-30.5
Vesicular							
No. of samples	9	9	9	9	1	16	1
Mean	55.0	21.7	40.0	0.28	2.88	8.5	6.6
Standard Deviation	12.7	4.9	11.8	0.05		3.9	
Range	39.8-75.7	15.9-29.7	23.8-56.1	0.22-0.38		3.6-17.0	
Umtanum Breccia							
No. of samples	15	15	15	15	8	39	7
Mean	35.9	14.9	20.7	0.20	2.84	18.1	19.4
Standard Deviation	7.6	3.2	5.0	0.04	0.07	6.5	5.4
Range	26.3-50.0	10.3-20.7	13.7-29.0	0.13-0.32	2.68-2.94	7.0-34.6	12.6-27.0

TABLE 19. Summary of Borehole RRL-2--Basalt Physical and Mechanical Property Data--Entablature. (Sheet 1 of 2)

FLOW	TEST INTERVAL (ft)	UNIAXIAL COMPRESSIVE STRENGTH MPa	BULK DENSITY g/cc	YOUNG'S MODULUS (Static) GPa	POISSON'S RATIO (Static)	BRAZILIAN TENSILE STRENGTH MPa	MODULUS OF RUPTURE MPa
Grande Ronde 3 No. of samples Mean Standard Deviation Range Confidence Limits*	2952 - 2967	1 382.40	9 2.83 0.02 2.80-2.85	2 83.60 1.70 82.40-84.80	2 0.28 0.01 .027-.029	1 9.08 1.57 6.77-9.77	—
Cohasset No. of samples Mean Standard Deviation Range Confidence Limits*	3071 - 3076 3108 - 3135 3147 - 3168 3183 - 3200	7 255.78 19.18 214.74-271.53 245.34-266.52	21 2.84 0.03 2.76-2.87	10 75.56 4.94 69.36-85.74	10 0.27 0.01 0.24-0.29	8 13.03 4.16 8.73-19.42	1 42.09
McCoy Canyon Entablature No. of samples Mean Standard Deviation Range Confidence Limits*	3500 - 3525 3543 - 3575	8 351.55 27.24 365.57-404.49 337.92-365.18	28 2.83 0.03 2.76-2.87	11 78.30 5.08 68.12-84.26	10 0.26 0.02 0.23-0.29	10 18.31 3.62 10.08-23.93	—
Entablature/Colonnade No. of samples Mean Standard Deviation Range Confidence Limits*	3575 - 3607	7 305.63 64.25 176.08-368.90 270.60-340.60	20 2.81 0.09 2.59-2.88	6 69.07 14.6 41.37-80.40	6 0.26 0.02 0.24-0.28	10 20.38 4.36 11.59-26.50	—
Umtanum No. of samples Mean Standard Deviation Range Confidence Limits*	3755 - 3824	3 413.47 47.75 390.17-468.40 361.48-465.46	20 2.81 0.02 2.78-2.83	5 82.47 1.55 80.95-84.41	6 0.26 0.01 0.24-0.28	5 14.06 2.30 10.56-16.67	—

\* 80% Confidence Level

NOTE: To convert feet to meters, multiply by 0.3048.

77

SD-BWI-TI-113

TABLE 19. Summary of Borehole RRL-2--Basalt Physical and Mechanical Property Data--Entablature. (Sheet 2 of 2)

FLOW	YOUNG'S MODULUS (Dynamic) GPa	SHEAR MODULUS (Dynamic) GPa	BULK MODULUS (Dynamic) GPa	POISSON'S RATIO	GRAIN DENSITY g/cc	APPARENT POROSITY %	TOTAL POROSITY %
Grande Ronde 3							
No. of samples	3	3	3	3	4	9	4
Mean	84.1	33.1	61.6	0.27	2.88	1.2	1.9
Standard Deviation	3.7	1.9	3.3	0.02	0.01	0.7	0.7
Range	79.8-86.8	30.9-34.2	57.8-63.5	0.25-0.29	2.87-2.90	0.2-1.9	1.0-2.8
Cohasset							
No. of samples	19	19	19	19	3	21	4
Mean	74.3	31.0	44.3	0.24	2.89	1.0	2.1
Standard Deviation	6.4	4.0	12.8	0.03	0.02	0.4	0.6
Range	62.8-85.8	24.0-45.1	13.1-59.5	0.17-0.31	2.87-2.91	0.1-1.8	1.4-2.8
McCoy Canyon Entablature							
No. of samples	27	27	27	27	8	29	7
Mean	72.8	29.7	45.2	0.23	2.89	2.1	2.4
Standard Deviation	8.2	3.1	7.9	0.03	0.02	1.1	1.2
Range	49.0-83.7	20.5-34.8	26.9-59.4	0.19-0.28	2.86-2.91	0.9-4.8	1.0-4.1
Entablature/Colonnade							
No. of samples	20	20	20	20	3	20	3
Mean	68.9	28.0	43.2	0.23	2.90	2.8	2.7
Standard Deviation	10.2	4.5	8.7	0.05	0.01	1.8	2.7
Range	49.6-80.5	20.1-34.5	28.8-55.9	0.13-0.31	2.89-2.91	1.4-7.4	1.0-5.8
Untanun							
No. of samples	11	11	11	11	4	20	3
Mean	76.9	31.1	49.3	0.24	2.85	1.1	1.3
Standard Deviation	4.6	1.7	7.2	0.03	0.02	0.4	0.5
Range	70.6-82.4	27.3-32.9	37.8-58.4	0.19-0.29	2.82-2.87	0.5-1.9	0.7-1.7

NOTE: To convert feet to meters, multiply by 0.3048.

TABLE 20. Summary of Borehole RRL-2--Basalt Physical and Mechanical Property Data--Colonnade. (Sheet 1 of 2)

FLOW	TEST INTERVAL	UNIAXIAL COMPRESSIVE STRENGTH	BULK DENSITY	YOUNG'S MODULUS (Static)	POISSON'S RATIO (Static)	BRAZILIAN TENSILE STRENGTH	MODULUS OF RUPTURE
	(ft)	MPa	g/cc	GPa		MPa	MPa
Grande Ronde 3	2850 - 2866						
No of samples		1	13	2	2	3	
Mean	2974 - 2986	171.49	2.81	86.68	0.27	10.41	—
Standard Deviation			0.06	11.60	0.01	1.06	
Range			2.71-2.87	78.47-94.88	0.26-0.28	9.72-11.63	
Confidence Limits*							
Cohassett	3006 - 3071						
No. of samples	3076 - 3083	4	17	8	8	8	2
Mean	3135 - 3147	287.10	2.82	76.82	0.26	16.05	39.40
Standard Deviation	3168 - 3183	32.73	0.07	6.56	0.01	2.45	4.45
Range	3200 - 3254	262.71-332.26	2.65-2.88	66.40-86.67	0.24-0.28	12.01-20.62	36.24-42.54
Confidence Limits*		260.29-313.91					
McCoy Canyon	3494 - 3500						
No of samples		2	7	3	3	3	
Mean		103.71	2.62	36.89	0.23	11.59	—
Standard Deviation		5.83	0.06	6.17	0.05	1.91	
Range		99.58-107.83	2.55-2.72	32.89-43.99	0.17-0.27	9.40-12.88	
Confidence Limits*		91.02-116.40					
Umtanum	3824 - 3839						
No. of samples		2	13	5	5	4	
Mean		405.99	2.81	70.58	0.25	22.79	—
Standard Deviation		4.08	0.12	3.24	0.02	2.12	
Range		403.10-408.87	2.78-2.83	67.10-75.71	0.23-0.28	20.10-24.59	
Confidence Limits*		397.11-414.87					

\* 80% Confidence Level

NOTE: To convert feet to meters, multiply by 0.3048.

TABLE 20. Summary of Borehole RRL-2--Basalt Physical and Mechanical Property Data--Colonnade. (Sheet 2 of 2)

FLOW	YOUNG'S MODULUS (Dynamic) GPa	SHEAR MODULUS (Dynamic) GPa	BULK MODULUS (Dynamic) GPa	POISSON'S RATIO (Dynamic)	GRAIN DENSITY g/cc	APPARENT POROSITY %	TOTAL POROSITY %
Grande Ronde 3							
No. of samples	5	5	5	5	4	11	4
Mean	80.2	32.6	50.3	0.23	2.90	1.1	3.1
Standard Deviation	5.1	1.6	7.4	0.02	0.02	0.6	2.0
Range	75.8-89.0	31.4-35.3	43.2-61.3	0.21-0.26	2.87-2.92	0.3-2.5	1.0-5.6
Cohasset							
No. of samples	15	15	15	15	6	17	5
Mean	74.0	29.5	51.6	0.26	2.94	1.8	2.2
Standard Deviation	7.7	3.1	8.6	0.04	0.03	1.5	0.8
Range	60.6-82.4	23.3-33.0	33.3-63.8	0.15-0.30	2.89-2.00	0.1-5.6	1.7-3.7
McCoy Canyon							
No. of samples	4	4	4	4	1	7	1
Mean	53.2	21.7	32.6	0.23	2.99	8.2	13.0
Standard Deviation	8.3	3.4	5.1	0.01		3.0	
Range	45.7-64.8	18.7-26.5	27.4-38.7	0.22-0.24		4.3-12.4	
Umanum							
No. of samples	9	9	9	9	4	13	4
Mean	72.3	29.4	45.4	0.24	2.87	2.1	2.3
Standard Deviation	6.3	1.9	9.0	0.04	0.03	0.8	0.6
Range	61.0-81.0	23.5-31.6	31.2-61.4	0.17-0.28	2.84-2.91	1.1-3.9	1.9-3.1

NOTE: To convert feet to meters, multiply by 0.3048.

In regard to mechanical strength properties, the uniaxial compressive strength results showed the greatest variability with respect to flows as well as intraflow structures. The Umtanum entablature and colonnade had the highest uniaxial compressive strengths, with confidence limits at an 80% level of 361.48 to 465.46 MPa, and 397.11 to 414.87 MPa, respectively. The McCoy Canyon flow top and colonnade had the lowest uniaxial compressive strengths with confidence limits at an 80% level of 31.26 to 44.34 MPa, and 84.00 to 167.32 MPa, respectively. Flow-top uniaxial compressive strengths were on the average 70% less than the entablature and colonnade intraflow structures. The very low bulk density, Young's modulus, and Poisson's ratio values of the McCoy Canyon's flow top and colonnade correlate very well with the previously mentioned low uniaxial compressive strengths in the McCoy Canyon's flow top and colonnade.

When comparing the conceptual designs uniaxial compressive strength and the Brazilian tensile strength (Table 21) with borehole RRL-2's Umtanum entablature (see Table 19), it was noted that borehole RRL-2's uniaxial compressive strength is 95% greater than the conceptual design strength, and borehole RRL-2 Brazilian tensile strength is 18% greater than the conceptual design strength.

The strength test results are shown in Table 22. Included in Table 22 are the mean Brazilian tensile strength results, mean compressive strength results, and linear regression slope and intercept values. The major principal stress ( $\sigma_1$ ) is assumed to be three times the minor principal Brazilian tensile strength ( $\sigma_3$ ) (Goodman, 1980).

A linear regression analysis was conducted on the major and minor principal failure stress results ( $\sigma_1$  and  $\sigma_3$ ) from the uniaxial, triaxial, and Brazilian tensile strength testing. An empirical failure criteria developed by Hoek and Brown (1980) was used to relate  $\sigma_1$  and  $\sigma_3$  at failure.

From Table 22 the correlation coefficient ( $r$ ), which is an indication of the concordance of fit between the empirical failure criteria relationship and the strength data, showed good concordance of fit for all the intraflow structures. All the intraflow structures had correlation coefficients at the 99% level or greater except for the McCoy Canyon colonnade at 97.5%. For purposes of curve fitting and linear regression analysis, only those intraflow structures with five or more pairs of data were used.

The linear form of the empirical failure criteria was used to plot the results of the linear regression analysis of the strength data. These failure envelopes are illustrated in Figure 21. It is evident that the Umtanum colonnade and McCoy Canyon entablature/cornnade have the highest strengths, while the McCoy Canyon colonnade has the lowest strengths. The square root of the ordinate axis intercept ( $\sigma_c$ ) in Figure 21 is the uniaxial compressive strength as determined from the linear regression analysis of the triaxial results. These uniaxial compressive strengths compared very favorably with the uniaxial compressive strength as

TABLE 21. Thermomechanical Characteristics of the Columbia River Basalt Group (KE/PB, 1980).

PRELIMINARY THERMOMECHANICAL VALUES	UNITS	MEAN VALUES	RANGE
Specific Heat (at 75°C)	cal/g°C	0.225	0.225 + 0.005 standard deviation
Thermal Conductivity (at 50°C)	W/m°C	2.17	2.17 + 0.26 standard deviation
Bulk Density	g/cm <sup>3</sup>	2.78	2.41 - 3.01
Grain Density	g/cm <sup>3</sup>	2.90	2.78 - 3.10
Water Content	wt%	TBD	
Thermal Expansion Coefficient	°C	8.81	8.81 + 1.78 standard deviation
Young's Modulus (static)	ksi (MPa)	10.300 (71.0)	7.900 - 13.700 (54.5 - 94.5)
Poisson's Ratio (static)		0.27	0.15 - 0.32
Young's Modulus (dynamic)	ksi (MPa)	11.600 (80.0)	9.700 - 14.800 (66.9 - 102.0)
Poisson's Ratio (dynamic)		0.24	0.15 - 0.32
Compressional Wave Velocity	m/sec	5.860	5.360 - 6.430
Shear-wave Velocity	m/sec	3.420	3.080 - 3.900
Angle of Internal friction (at 20°C)	degrees	44	
Brazilian Tensile Strength	ksi (MPa)	1.7 (11.9)	0.2 - 3.4 (1.4 - 23.7)
Cohesion	ksi (MPa)	4.6 (32)	2.2 - 5.5 (15 - 38)
Compressive Strength Unconfined	ksi (MPa)	30.5 (212)	11.6 - 53.0 (81 - 369)
Confined at 51.7 MPa	ksi (MPa)	66.3 (461)	51.3 - 96.5 (357 - 671)

\*Based on testing of samples from the Umtanum flow.

TABLE 22. Linear Regression Analysis of Borehole RRL-2--Strength Test Results. (Sheet 1 of 2)

FLOW	INTRAFLOW STRUCTURE	MEAN MAJOR PRINCIPAL FAILURE STRESS $\sigma_1$ (MPa)	MINOR PRINCIPAL FAILURE STRESS $\sigma_3$ (MPa) (# of specimens tested)	BRAZILIAN TENSILE STRENGTH		CORRELATION COEFFICIENT (r)
				$\sigma_3$ (MPa)	$\sigma_1$ (MPa)	
Grande Ronde 3	Entablature	382.40 493.45	0. (1) 6.90 (1)	- 9.08	27.24	—
	Colonnade	171.49 465.65 478.15	0. (1) 6.90 (1) 13.79 (1)	-10.41	31.23	—
Cohasset	Entablature	255.78 431.23 385.64 481.36	0. (7) 10.34 (1) 13.79 (1) 17.24 (1)	-12.29 -19.42 -10.98 - 8.37 - 9.53 -12.66 -11.64 -19.33	36.87 58.26 32.94 25.11 28.59 37.98 34.92 57.99	0.94 (A)
	Colonnade	287.10 339.79 431.20	0. (4) 3.45 (2) 6.90 (2)	-15.58 -20.62 -16.22 -17.43 -14.77 -16.60 -12.01 -15.19	46.74 61.86 48.66 52.29 44.31 49.80 36.03 45.57	0.95 (A)
McCoy Canyon	Entablature	351.55 443.03 461.71	0. (8) 6.90 (6) 13.80 (2)	-16.57 -17.19 -16.75 -20.23 -19.57 -20.67 -19.40 -18.72 -10.08 -23.93	49.71 51.57 50.25 60.69 58.71 62.01 58.20 56.16 30.24 71.79	0.96 (A)

TABLE 22. Linear Regression Analysis of Borehole RRL-2--Strength Test Results. (Sheet 2 of 2)

FLOW	INTRAFL <small>OW</small> STRUCTURE	MEAN MAJOR PRINCIPAL FAILURE STRESS $\sigma_1$ (MPa)	MINOR PRINCIPAL FAILURE STRESS $\sigma_3$ (MPa) (# of specimens tested)	BRAZILIAN TENSILE STRENGTH		CORRELATION COEFFICIENT (r)
				$\sigma_3$ (MPa)	$\sigma_1$ (MPa)	
	Entablature/ Colonnade	305.63 493.65 478.16 594.92	0. (7) 6.90 (1) 10.34 (1) 13.80 (1)	-19.93 -26.50 -11.59 -23.68 -23.64 -22.59 -19.85 -22.36 -17.09 -16.59	59.79 79.50 34.77 71.04 70.92 67.77 59.55 67.08 51.27 49.77	0.91 (A)
	Colonnade	103.71 222.40	0. (2) 6.90 (1)	- 9.40 -12.49 -12.88	28.20 37.47 38.64	0.89 (B)
Umtanum	Entablature	413.47 311.36 371.13	0. (3) 6.90 (1) 13.80 (2)	-10.56 -15.26 -16.67 -14.43 -13.36	31.68 45.78 50.01 43.29 40.08	0.80 (A)
	Colonnade	405.99 474.24 485.11	0. (2) 6.90 (1) 13.80 (2)	-20.10 -24.59 -24.38 -22.09	60.30 73.77 73.14 66.27	0.99 (A)

NOTES:

(A) Correlation coefficient (r) is significant at the 99.0% confidence level or greater.

(B) Correlation coefficient (r) is significant at the 97.5% confidence level or greater.

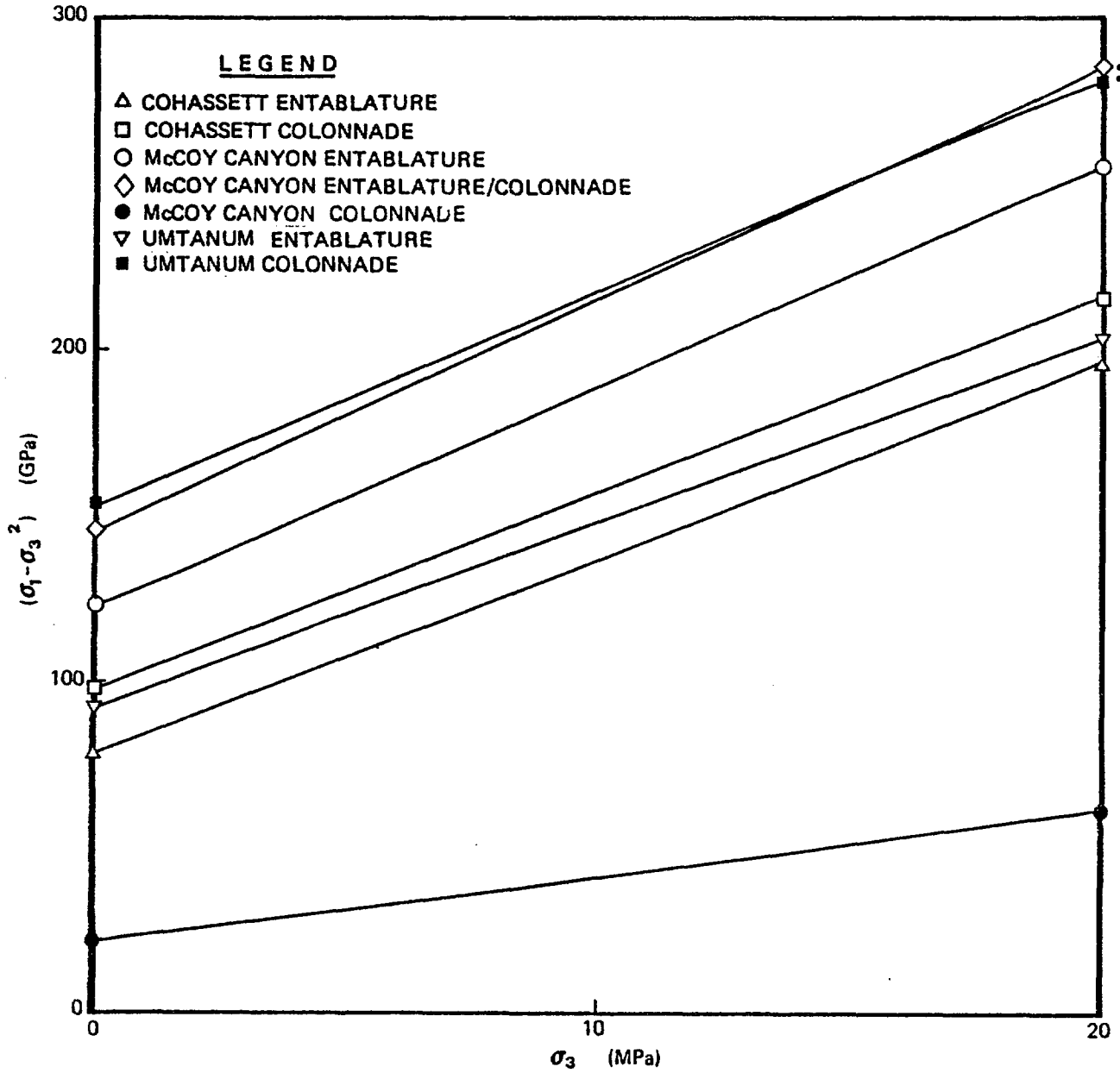


FIGURE 21. Strength Test Results Plotted in Linear Form of Empirical Failure Criteria.

determined in the laboratory. The laboratory uniaxial compressive strengths are all slightly less than the uniaxial compressive strengths determined from the regression analysis except for the Umtanum entablature and colonnade, which has higher laboratory uniaxial compressive strengths.

The elastic properties showed compatible results between the static and dynamic testing of Young's modulus and Poisson's ratio. The flow top elastic properties were all noticeably less than the entablature and colonnade. In addition, there is a much wider range of elastic property values between various flow tops than between the various entablatures and colonnades.

A comparison of the conceptual design elastic properties (see Table 21) with the borehole RRL-2 Umtanum entablature elastic properties (see Table 19), does not show any significant variations. The Umtanum entablature's static Young's modulus is 16% greater, the static Poisson's ratio is 4% less and the dynamic Young's modulus is 4% less than the design elastic properties. The dynamic Poisson's ratio for borehole RRL-2's Umtanum entablature and the conceptual design are both 0.24.

When the results of the borehole RRL-2 laboratory testing are compared with previous tests conducted on the Umtanum flow (see Table 21), Grande Ronde Basalt, and Pomona member, it was apparent the mechanical strength and elastic properties of borehole RRL-2 were in almost all cases higher than those previously reported for other boreholes. This was especially true for the uniaxial compressive strength in which the borehole RRL-2 results were in most cases 50 to 100% greater. This can be explained by the fact that extraordinary care was taken in choosing intact samples with no apparent fractures. In addition, if preexisting fractures were found after breaking the specimen, then this specimen was not considered in the statistical summary. Earlier testing had identified the need to improve procedures for choosing samples as well as for post-failure characterization.

In reviewing the borehole RRL-2 physical property results, the differences in bulk density, apparent porosity, and total porosity between flow top, entablature, and colonnade can be explained by the more vesicular and brecciated nature of the flow top. This results in the lower bulk densities and high apparent and total porosities of the flow top.

No explanation is given for the significant variation in uniaxial compressive strengths between flows. However, the test results are considered valid. The lower strength values of the flow top, vesicular and brecciated rock can be attributed to its lower bulk density and higher porosity. These same physical characteristics can also explain the lower elastic properties of the flow top vesicular and brecciated rock. Few static elastic property tests were conducted due to the very vesicular or brecciated characteristics of the flow top intraflow structure. The presence of the vesicles and breccia clasts made it difficult to attach strain gauges. In addition, the data would be suspect due to the possible development of abnormal stress concentrations in the vicinity of the vesicles or breccia clasts.

## IN SITU STRESS MEASUREMENTS

## INTRODUCTION

In situ stress and rock mass strength are the two most critical rock mechanics parameters affecting the stability of underground structures in hard rock. The stress generally increases with depth while rock strength is independent of depth. Accurate assessment of the in situ stress state of the candidate horizons in advance of excavation is necessary for design of tunnel structures and selection of support methods.

The Pasco Basin, a subdivision of the Columbia Plateau, spans the area between the Yakima Fold Belt subprovince and the Palouse subprovince (see Fig. 4). Structural features bound the Pasco Basin on the north and south, plunging eastward into the basin. Primary folds are oriented in an east-west direction. Most of this folding occurred during deposition of the younger basalt flows and sedimentary interbeds. The folding is considered the result of tectonic compression in a north-south direction. Seismic monitoring of events in the Pasco Basin tends to corroborate the north-south orientation of the principal tectonically induced stress.

Numerous deep boreholes have been cored in the Pasco Basin to support geological and hydrological site characterization. Some cores obtained from borehole RRL-2, and most of the other deep boreholes, exhibit a type of fracturing known as diskings (Fig. 22). Core diskings in hard rock is considered to be indicative of a high horizontal to vertical in situ stress ratio.

Due to the effect of the in situ stress on design, it was decided to conduct hydraulic fracturing stress measurements in the candidate horizons in borehole RRL-2 after completion of the hydrologic testing.

## METHODOLOGY

Hydraulic fracturing was selected because it is the only available developed method for measuring in situ stress in a borehole at the required depths of 3,000 to 4,000 ft (914.4 to 1,219.2 m).

The Umtanum flow and Cohasset flow were selected as the flows for the testing. The intervals (Table 23) were selected using color photographs of the core in conjunction with geophysical logs of the borehole.

A conventional test method described in American Society for Testing and Material, Special Technical Publication 554 was used as a guideline (Haimson, 1974).



FIGURE 22. Disking in the Cohasset Flow in Borehole RRL-2.

TABLE 23. Borehole RRL-2--Hydraulic Fracturing  
Data Analysis, October 1982.

	TEST #	DEPTH (ft)	$P_{isi}$ (A) (psi)	$P_f$ (B) (psi)	$P_{f2}$ (C) (psi)	$P_H$ (D) (psi)	$P_o^*$ (E) (psi)	$\sigma_{Hmin}$ (F) (psi)	$\sigma_{Hmax}$ (G) (psi)	$\sigma_v$ (H) (psi)	$\frac{\sigma_{Hmax}}{\sigma_{Hmin}}$ (psi)	$\frac{\sigma_{Hmax}}{\sigma_v}$ (psi)
Cohasset	11-B	3053	3500	4950	4500	1323	1219	4823	8750	3371	1.81	2.60
Cohasset	9-B	3181	2100	2650	2350	1378	1274	3478	6811	3517	1.96	1.94
Grande Ronde #7	6-B	3457.5	4100	4600	4300	1498	1394	5598	11100	3833	1.98	2.90
	5-B	3471	3400	3800	3500	1504	1400	4904	9812	3849	2.00	2.55
Umtanum	4-B	3768	2350	3400	3000	1632	1528	3982	7418	4188	1.86	1.77
Umtanum	3-A	3782	4250	5300	4800	1640	1536	5890	11334	4208	1.92	2.69
Umtanum	2-B	3806.5	3650	4250	3900	1649	1545	5300	10453	4233	1.97	2.47
Umtanum	1-A	3827	3400	4150	3900	1660	1556	5060	9720	4260	1.92	2.28

\*Water level 240' below ground level.

NOTE: To convert feet to meters, multiply by 0.3048.

- (A)  $P_{isi}$  = Instantaneous Shut-In Pressure
- (B)  $P_f$  = Breakdown Pressure
- (C)  $P_{f2}$  = Secondary Breakdown Pressure
- (D)  $P_H$  = Head
- (E)  $P_o$  = Pore Pressure
- (F)  $\sigma_{Hmin}$  = Minimum Horizontal Stress
- (G)  $\sigma_{Hmax}$  = Maximum Horizontal Stress
- (H)  $\sigma_v$  = Vertical Stress

In borehole RRL-2 hydrofracturing tests, a 2-ft (0.6-m) section of the borehole was isolated with a straddle packer (Fig. 23). Once the straddle packer had isolated the test interval, water was injected into the isolated zone yielding a typical pressure-time record (Fig. 24).

The pressure first rises to a maximum value called the breakdown pressure ( $P_f$ ), then, as injection proceeds at a constant flow rate, the pressure drops and stabilizes at the value known as the fracture propagation pressure ( $P_{fj}$ ). The difference between the fracture propagation pressure and the breakdown pressure can be considered to be the in situ rupture strength of the borehole ( $T$ ).

After the hydraulically induced fractures propagate a sufficient distance away from the borehole, the injection fluid is ceased abruptly to obtain the instantaneous shut in pressure ( $P_{jsi}$ ). This pressure at the moment of shut in is considered to be equivalent to the in situ stress acting normal to the plane of the induced vertical fracture. In most cases, the borehole is subjected to repressurization cycles to verify the so called shut-in pressure.

Under the assumption that the borehole is parallel to one of the principal stress directions, and the rock is linear elastic and isotropic, the breakdown pressure and the shut-in pressure can be used to determine the components of the local stress tensor in a plane perpendicular to the borehole axis. The vertical stress component is assumed to be equal to the overburden pressure.

Strike and dip of the induced fractures in the borehole wall were determined by the use of an oriented impression packer (see Figure 23). An impression packer consists of a 3-ft-long (0.9-m-) inflatable packer covered with a thin layer of uncured rubber. The fractures recorded by the impression rubber were traced on to clear mylar, which can be unrolled. The packer was oriented using a downhole gyroscopic survey tool. A typical fracture impression is shown in Figure 25.

## RESULTS

An analysis of data obtained from borehole RRL-2 is shown in Table 23. It must be emphasized that these results are preliminary and only those intervals in which a vertical fracture was verified by an impression packer have been listed.

Some of the tests that show a high horizontal to vertical stress ratio may be due to poorly defined vertical fractures. Conversely, tests with low stress ratios may be due to the presence of inclined joints intersecting the test interval.

Using the data from Table 23, the average horizontal to vertical stress ratios for the candidate horizons are:

- Cohasset--2.27:1
- Umtanum--2.30:1.

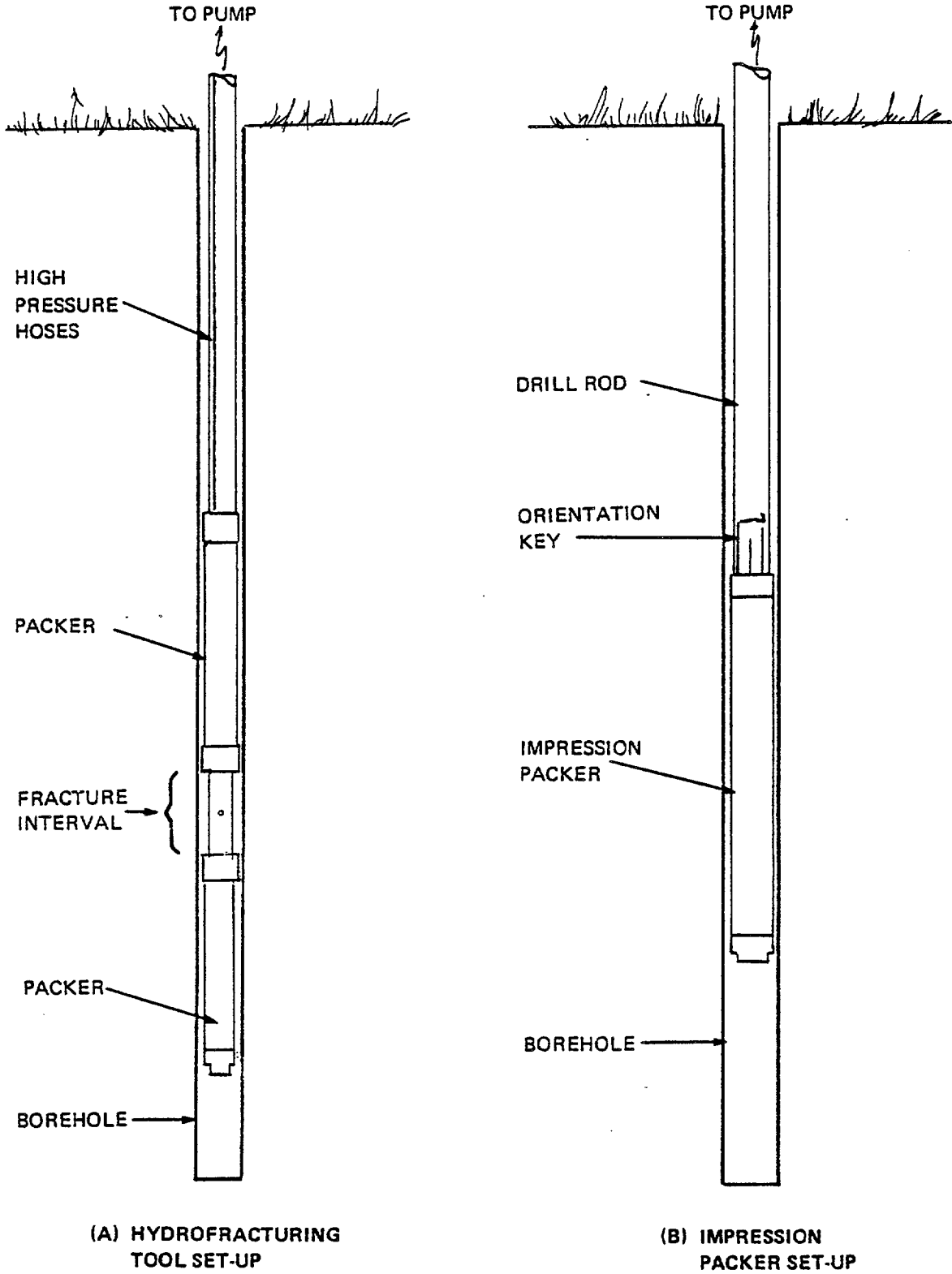


FIGURE 23. Downhole Tools.

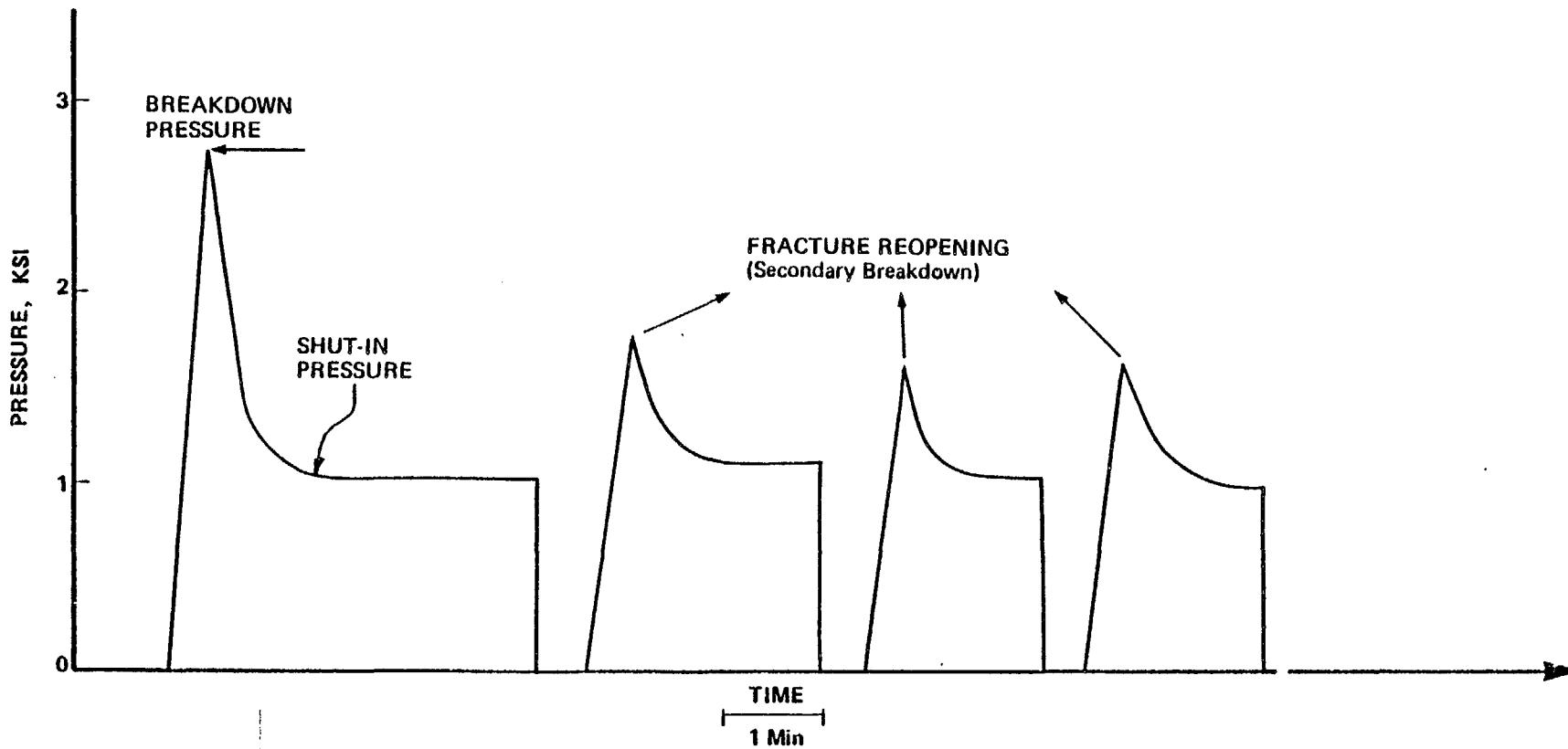


FIGURE 24. Typical Pressure Versus Time Curve.

SD-BWI-TI-113

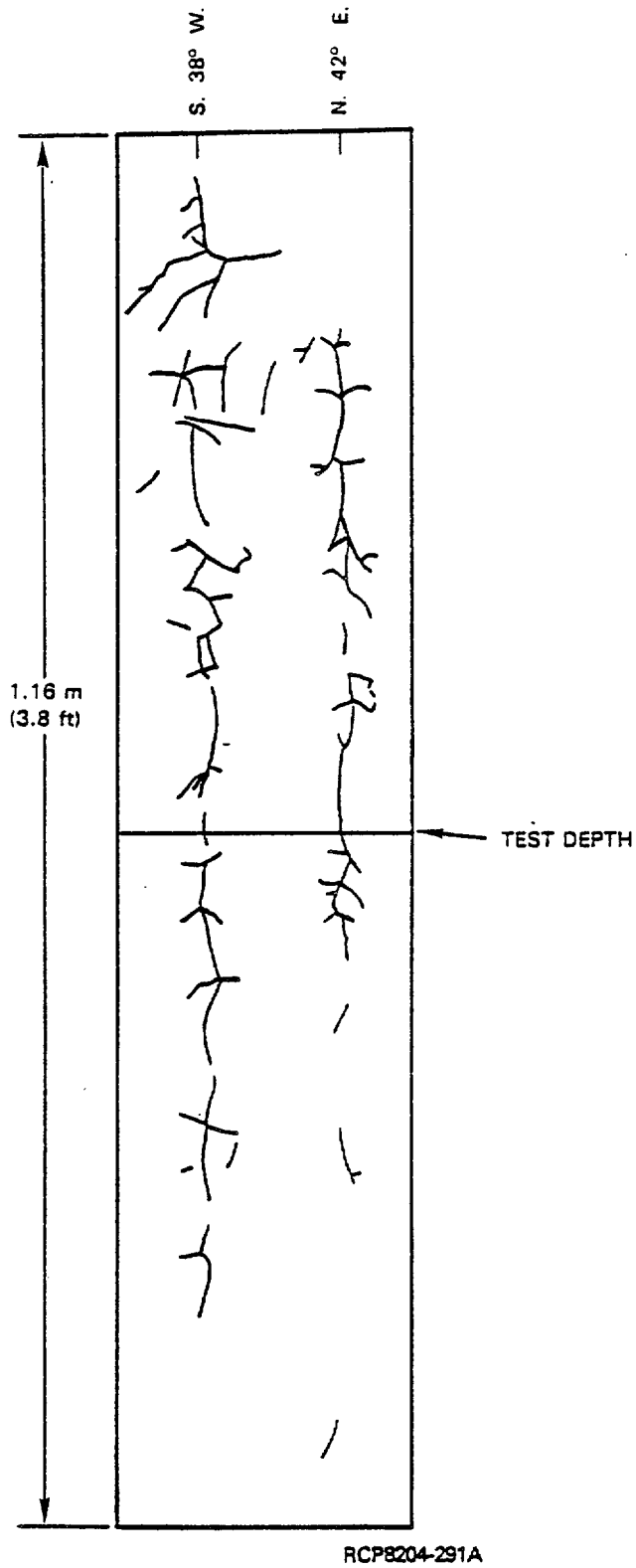


FIGURE 25. Typical Fracture Impression.

## REFERENCES

- Bonham, L. D. 1978, "Solubility of Methane in Water at Elevated Temperatures and Pressures," The American Association of Petroleum Geologists Bulletin, Vol. 62, No. 12, pp. 2478-2488.
- BWIP, 1982, The Identification of a Preferred Site for the Exploratory Shaft Within the Reference Repository Location: Hanford Site, RHO-BWI-ST-16, Rockwell Hanford Operations, Richland, Washington, January 1982.
- BWIPa, 1982, Test Procedure for the Principal Borehole RRL-2 SD-BWI-TC-001, Basalt Waste Isolation Project, Rockwell Hanford Operations, Richland, Washington.
- Goodman, R. E., 1980, Introduction to Rock Mechanics, John Wiley & Sons, New York.
- Haimson, B. C., 1974, "A Simple Method for Estimated In Situ Stresses at Great Depth, Field Testing and Instruments of Rock," ASTM STP 554, 156-182.
- Hoek, E. and Brown, E. T., 1980, Underground Excavation in Rock, The Institute of Mining and Metallurgy, London.
- KE/PB, 1980, Nuclear Waste Repository in Basalt, Project B-301, Functional Design Criteria, RHO-BWI-CD-38 REV 3, Kaiser Engineers, Inc. and Parsons Brinckerhoff Quade & Douglas, Inc. for Rockwell Hanford Operations, Richland, Washington.
- Langmuir, D., 1971, "Eh-pH Determination," in Procedures in Sedimentary Petrology, Carver, R. E., ed., Wiley Interscience, New York, pp. 597-635.
- Rockwell, 1982, Site Characterization Report for the Basalt Waste Isolation Project, DOE/RL 82-3, Rockwell Hanford Operations, Richland, Washington.
- Spane, F. A. Jr., Graham, D. L. and Bryce, R. W., 1982, Hydrochemical and Isotopic Content of Basalt Groundwaters Beneath the Hanford Site, Washington, RHO-BW-SA-190 P, Rockwell Hanford Operations, Richland, Washington.
- Strait, S. R., Spane, F. A., Jackson, R. L., and Pidcoe, W. W., 1982, Hydrologic Testing Methodology and Results from Deep Basalt Boreholes, RHO-BW-SA-189, Rockwell Hanford Operations, Richland, Washington.
- Stumm, W. and Morgan, J. J., 1981, Aquatic Chemistry, 2nd ed., John Wiley & Sons, New York.
- WCC, 1981, Study to Identify a Reference Repository Location for a Nuclear Waste Repository on the Hanford Site, Vol. I: Text; Vol. II: Appendixes, RHO-BWI-C-107, Woodward-Clyde Consultants for Rockwell Hanford Operations, Richland, Washington, May 1981.

BIBLIOGRAPHY

Bieniawski, Z. T. 1973, "Engineering Classification of Jointed Rock Masses," The Civil Engineer in South Africa, December 1973, pp. 335-343.

BWIP, 1982, Basalt Waste Isolation Project Drill and Testing Quarterly Report, RHO-BW-SR-82-2 2Q P, Basalt Waste Isolation Project, Rockwell Hanford Operations, Richland, Washington.

FSI, 1981, Thermal/Mechanical Properties of Umtanum Basalt-Borehole DC-3, RHO-BWI-C-92, Foundation Sciences, Inc. for Rockwell Hanford Operations, Richland, Washington.

Lama, R. D. and Vutukuri, V. S., 1978, "Handbook on Mechanical Properties of Rock, Volume II," Transactions, Technical Publications, pp. 323-327.

Myers, C. W./Price, S. M., Ault, T. D, Cochran, M. P., Davidson, N. J., Fecht, K. R., Holmes, G. E., Kunk, J. R., Landon, R. D., Lillie, J. T., Long, P. E., Mitchell, T. H., Price, E. H., Reidel, S. P., and Tallman, A. M., 1979, Geologic Studies of the Columbia Plateau, a Status Report, RHO-BWI-ST-4, Rockwell Hanford Operations, Richland, Washinton.

Myers, C. W. and Price, S. M., eds., 1981, Subsurface Geology of the Cold Creek Syncline, RHO-BWI-ST-14, Rockwell Hanford Operations. Richland, Washington.

Schmidt, B., Daly, W. F., Bradley, S. W., Squire, P. R., and Hulstrom, L. C., 1980, Thermal and Mechanical Properties of Hanford Basalts, Compilation and Analysis, RHO-BWI-C-90, Kaiser Engineers, Inc. and Parsons Brinckerhoff Quade & Douglas, Inc. for Rockwell Hanford Operations, Richland, Washington.

APPENDIX A

CORING RECORD

BIT RECORD

MUD LOSS SUMMARY



# Rockwell International

Rockwell Hanford Operations  
Energy Systems Group

## CORING RECORD

Hole: RRL-2

Contractor: Continental Drilling Co.

Core Size: 4.828" PQ3-1

Sheet 1 of 5

Date	Shift	Core No.	Interval		Core Recovered			Core Time Min.	Accumulative			Remarks
			From	To	Ft.	%	Longest Piece		Ft. Drilled	Core Recovered	%	
3/16/81	N/A	1	613.5	616.5	3	100	N/A	30	3	3	100	
3/18/81		2	616.5	617.5	1	100		10	4	4	100	
		3	617.5	624	6.5	100		86	10.5	10.5	100	
3/19/81		4	624	634	10	100		127	20.5	20.5	100	
		5	634	644	10	100		120	30.5	30.5	100	
		6	644	645	1	100		15	31.5	31.5	100	
3/20/81		7	645	654	9	100		106	40.5	40.5	100	
		8	654	664	10	100		112	50.5	50.5	100	
		9	664	674	10	100		150	60.5	60.5	100	
3/23/81		10	674	684	10	100		120	70.5	70.5	100	
		11	684	694	10	100		30	80.5	80.5	100	
		12	694	704	10	100		100	90.5	90.5	100	
		13	704	714	10	100		70	100.5	100.5	100	
3/24/81		14	714	724	9.5	9.5		67	110.5	110	99	Lost .5'
		15	724	734	9.5	95		30	120.5	119.5	99	Lost .5'
		16	734	744	9	90		30	130.5	128.5	98	Lost 1'
		17	744	750	3.5	56		40	136.5	132	97	Lost 2.5'
		18	750	753.5	3.5	100		66	140	135.5	97	
3/25/81		19	753.5	763.5	9	90		78	150	144.5	96	Lost 1'
		20	763.5	772.5	10	110		81	159	154.5	97	Recovered 1' of lost core
		21	772.5	782.5	10	100		82	169	164.5	97	
		22	782.5	792.5	10	100		60	179	174.5	97	

A-2

SD-BMI-TI-113



# Rockwell International

Rockwell Hanford Operations  
Energy Systems Group

## CORING RECORD

Hole: RRL=2

Contractor: Continental Drilling Co.

Core Size: 4.828" PQ3-1

Sheet 2 of 5

Date	Shift	Core No.	Interval		Core Recovered			Core Time Min.	Accumulative			Remarks
			From	To	Ft.	%	Longest Piece		Ft. Drilled	Core Recovered	%	
3/26/81	N/A	23	792.5	802.5	9.5	95	N/A	65	189	184	97	Flow Breccia/Lost .5'
		24	805.6	812.5	10	100		75	199	194	97	
		25	812.5	822	9.5	100		77	208.5	203.5	97	
		26	822	827.5	4.5	82		38	214	208	97	Lost 1'
3/31/81		27	827.5	829	1.5	100		30	215.5	209.5	97	
		28	829	831	2	100		23	217.5	211.5	97	
		29	831	834	3	100		25	220.5	214.5	97	
		30	834	841.5	7.5	100		150	228	222	97	
4/2/81		31	841.5	844	2.5	100		10	230.5	224.5	97	
		32	844	848	3.5	88		23	234.5	228	97	Lost .5'
4/3/81		33	848	852	4	100		60	238.5	232	97	
4/4/81		34	852	862	10	100		180	248.5	242	97	
4/7/81		35	862	868	6	100		54	254.5	248	97	
		36	868	874	6	100		60	260.5	254	97	
		37	874	882	8	100		102	268.5	262	98	
		38	882	892	10	100		114	278.5	272	98	
		39	892	899	7	100		70	285.5	279	98	
		40	899	907.5	8.5	100		90	294	287.5	98	
		41	907.5	914	6.5	100		70	300.5	294	98	
4/8/81		42	914	924	10	100		125	310.5	304	98	
		43	924	934	10	100		90	320.5	314	98	
4/9/81		44	934	941.5	7.5	100		120	328	321.5		

A-3

SD-BMI-TI-113



# Rockwell International

Rockwell Hanford Operations  
Energy Systems Group

## CORING RECORD

Hole: RRL-2

Contractor: Continental Drilling Co.

Core Size: 4.828" PQ3-1

Sheet 3 of 5

Date	Shift	Core No.	Interval		Core Recovered			Core Time Min.	Accumulative			Remarks
			From	To	Ft.	%	Longest Piece		Ft. Drilled	Core Recovered	%	
	N/A	45	941.5	951.5	10	100	N/A	80	338	331.5	98	
4/9/81		46	951.5	961.5	10	100		60	348	341.5	98	
		47	961.5	971.5	10	100		31	358	351.5	98	
		48	971.5	978	6.5	100		30	364.5	358	98	
		49	978	986	8	100		40	372.5	366	98	
		50	986	994	8	100		80	380.5	374	98	
4/22/81		51	994	1004	10	10		60	390.5	384	98	
		52	1004	1014	10	100		88	400.5	394	98	
		53	1014	1024	10	100		90	410.5	404	98	
		54	1024	1034	10	100		100	420.5	414	98	
4/23/81		55	1034	1044	10	100		110	430.5	424	98	
		56	1044	1054	10	100		110	440.5	434	99	
		57	1054	1064	10	100		110	450.5	444	99	
4/24/81		58	1064	1074	10	100		120	460.5	454	99	
		59	1074	1084	10	100		125	470.5	464	99	
		60	1084	1094	10	100		105	480.5	474	99	
4/27/81		61	1094	1104	10	100		120	490.5	484	99	
4/28/81		62	1104	1114	10	100		185	500.5	494	99	
4/29/81		63	1114	1124	10	100		77	510.5	504	99	
		64	1124	1134	10	100		40	520.5	514	99	
		65	1134	1144	10	100		43	530.5	524	99	
		66	1144	1154	10	100		80	540.5	534	99	

A-4

SD-BMI-TI-113



# Rockwell International

Rockwell Hanford Operations  
Energy Systems Group

## CORING RECORD

Hole: RRL-2

Contractor: Continental Drilling Co.

Core Size: 4.828" PQ

Sheet 4 of 5

Date	Shift	Core No.	Interval		Core Recovered			Core Time Min.	Accumulative			Remarks
			From	To	Ft.	%	Longest Piece		Ft. Drilled	Core Recovered	%	
	N/A	67	1154	1164	10	100	N/A	60	550.5	544	99	
4/30/81		68	1164	1174	10	100		120	560.5	554	99	
		69	1174	1184	10	100		126	570.5	564	99	
		70	1184	1194	10	100		105	580.5	574	99	
5/1/81		71	1194	1204	10	100		90	590.5	584	99	
		72	1204	1214	10	100		105	600.5	594	99	
		73	1214	1224	10	100		110	610.5	604	99	
5/4/81		74	1224	1234	6.5	65		90	620.5	610.5	98	
5/5/81		75	1234	1244	10	100		90	630.5	620.5	98	
		76	1244	1254	10	100		108	640.5	630.5	98	
		77	1254	1264	10	100		120	650.5	640.5	98	
5/6/81		78	1264	1274	10	100		143	660.5	650.5	98	
		79	1274	1284	10	100		128	670.5	660.5	99	
		80	1284	1294	10	100		180	680.5	670.5	99	
5/7/81		81	1294	1304	10	100		180	690.5	680.5	99	
		82	1304	1314	10	100		150	700.5	690.5	99	
5/8/81		83	1314	1324	10	100		149	710.5	700.5	99	
		84	1324	1334	10	100		120	720.5	710.5	99	
5/11/81		85	1334	1344	10	100		164	730.5	720.5	99	
		86	1344	1354	10	100		150	740.5	730.5	99	
5/12/81		87	1354	1364	10	100		180	750.5	740.5	99	
		88	1364	1374	10	100		175	760.5	750.5	99	

A-5

SD-BMI-TI-113



# Rockwell International

Rockwell Hanford Operations  
Energy Systems Group

## CORING RECORD

Hole: RRL-2

Contractor: Continental Drilling Co.

Core Size: 4.828" PQ

Sheet 5 of 5

Date	Shift	Core No.	Interval		Core Recovered			Core Time Min.	Accumulative			Remarks
			From	To	Ft.	%	Longest Piece		Ft. Drilled	Core Recovered	%	
5/13/81	N/A	89	1374	1384	10	100	N/A	72	770.5	760.5	99	
		90	1384	1394	10	100		80	780.5	770.5	99	
		91	1394	1404	10	100		120	790.5	780.5	99	
5/18/81		92	1404	1414	8.5	85		110	800.5	789	99	Lost 1.5'
		93	1414	1423	10	110		130	809.5	799	99	Recovered 1'
5/19/81		94	1423	1432	9	100		120	818.5	808	99	
		95	1432	1442	10	100		192	828.5	818	99	
		96	1442	1448	1	17		120	834.5	819	98	Lost 5'
5/20/81		97	1448	1453	10	183		120	839.5	829	99	Recovered 5'
		98	1453	1463	10	100		100	849.5	839	99	
		99	1463	1473	10	100		104	859.5	849	99	
5/21/81		100	1473	1489	5	50		205	869.5	854	89	Lost 5'
5/22/81		101	1483	1485.5	1.5	100		60	872	859.5	90	Recovered 4'
5/26/81		102	1485.5	1494	8.5	112		240	880.5	869	99	
5/27/81		103	1494	1504	10	100		333	890.5	879	99	
5/28/81		104	1504	1506.5	2.5	100		60	893	881.5	99	
		105	1506.5	1514	5.5	73		196	900.5	889	99	
5/29/81		106	1514	1520	6	127		120	906.5	897	99	Recovered 2'
		107	1520	1530	10	100		104	916	907	99	
6/1/81		108	1530	1534	4	100		20	920.5	911	99	
		109	1534	1544	10	10		72	930.5	921	99	

A-6

SD-BWI-TI-113



# Rockwell International

Rockwell Hanford Operations  
Energy Systems Group

## CORING RECORD

Hole: RRL-2

Contractor: Boyles Brothers

Core Size: 3.937"

Sheet 1 Of 14

Date	Shift	Core No.	Interval		Core Recovered			Core Time Min.	Accumulative			Remarks
			From	To	Ft.	%	Longest Piece		Ft. Drilled	Core Recovered	%	
1/25/82	N/A	110	1545	1547	2	100	N/A	15	2	2	100	
1/26/82		111	1547	1554	6	86		60	9	8	89	
		112	1554	1564	10	100		120	19	18	95	
2/3/82		113	1564	1574	10	100		60	29	28	97	
		114	1574	1584	10	100		70	39	38	97	
		115	1584	1594	10	100		65	49	48	98	
		116	1594	1604	10	100		65	59	58	98	
		117	1604	1614	10	100		105	69	68	99	
		118	1614	1624	10	100		110	79	78	99	
2/14/82		119	1624	1632	8	100		105	87	86	99	
		120	1632	1642	10	100		120	97	96	99	
		121	1642	1652	10	100		120	107	106	99	
		122	1652	1661	9	100		110	116	115	99	
		123	1661	1671	10	100		120	126	125	99	
		124	1671	1681	10	100		120	136	135	99	
		125	1681	1689	8	100		90	144	143	99	
2/15/82		126	1689	1690	1	100		15	145	144	99	
		127	1690	1694	4	100		30	149	148	99	
		128	1694	1704	10	100		100	159	158	99	
		129	1704	1714	10	100		105	169	168	99	
2/17/82		130	1714	1716	1.1	55		30	171	169.1	99	
		131	1716	1725	8.8	98		150	180	177.9	99	

A-7

SD-BMI-TI-113



# Rockwell International

Rockwell Hanford Operations  
Energy Systems Group

## CORING RECORD

Hole: RRL-2

Contractor: Boyles Brothers

Core Size: 3.937"

Sheet 2 Of 14

Date	Shift	Core No.	Interval		Core Recovered			Core Time Min.	Accumulative			Remarks
			From	To	Ft.	%	Longest Piece		Ft. Drilled	Core Recovered	%	
2/17/82	N/A	132	1725	1734	9	100	N/A	85	189	186.9	99	
2/18/82		133	1734	1744	10	100		90	199	196.9	99	
		134	1744	1754	9.8	98		105	209	206.7	99	
		135	1754	1764	10	100		80	219	216.7	99	
		136	1764	1773	8	89		130	228	224.7	99	
3/4/82		137	1773	1783	9	90		122	238	233.7	98	
		138	1783	1793	10	100		110	248	243.7	98	
		139	1793	1802	9	100		110	257	252.7	98	
3/5/82		140	1802	1806	4	100		60	261	256.7	98	
		141	1807	1814	6.2	78		90	269	262.7	98	
		142	1814	1820	7.8	122		70	275	270.7	98	
3/6/82		143	1820	1830	10	100		180	285	280.7	98	
3/8/82		144	1830	1840	10	100		130	295	290.7	99	
		145	1840	1850	10	100		130	305	300.7	99	
		146	1850	1860	10	100		130	315	310.7	99	
		147	1860	1870	10	100		135	125	320.7	99	
		148	1870	1880	10	100		120	335	330.7	99	
		149	1880	1888	8	100		70	343	338.7	99	
		150	1888	1894	6	100		40	349	344.7	99	
3/9/82		151	1894	1904	10	100		90	359	354.7	99	
		152	1904	1914	10	100		100	369	364.7	99	
		153	1914	1924	10	100		135	379	374.7	99	

A-8

SD-BMI-TI-113



# Rockwell International

Rockwell Hanford Operations  
Energy Systems Group

## CORING RECORD

Hole: RRL-2

Contractor: Boyles Brothers

Core Size: 3.937"

Sheet 3 of 14

Date	Shift	Core No.	Interval		Core Recovered			Core Time Min.	Accumulative			Remarks
			From	To	Ft.	%	Longest Piece		Ft. Drilled	Core Recovered	%	
3/9/82	N/A	154	1924	1925	0.5	100	N/A	15	379.5	375.2	99	
		155	1925	1926	0.8	100		15	380.3	377	99	
		156	1926	1934	.7	100		90	389	385.7	99	
		157	1934	1936	2	100		15	391	387.7	99	
		158	1936	1946	10	100		75	401	397.7	99	
		159	1946	1954	8	100		60	409	405.7	99	
3/10/82		160	1954	1964	10	100		95	419	415.7	99	
		161	1964	1974	9.6	96		130	429	425.3	99	
		162	1974	1980	6	100		100	435	431.3	99	
3/11/82		163	1980	1980.5	0.5	100		5	435.5	431.8	99	
		164	1980.5	1990.5	10	100		90	445.5	441.8	99	
		165	1990.5	1995.5	5	100		60	450.5	446.8	99	
		166	1995.5	1996	0.5	100		10	451	447.8	99	
3/12/82		167	1996	2006	10	100		110	461	457.8	99	
		168	2006	2014	8	100		90	469	465.3	99	
		169	2014	2020	5	83		75	475	470.3	99	
		170	2020	2030	10	100		180	485	480.3	99	
		171	2030	2040	10	100		180	495	490.8	99	
		172	2040	2045	5	100		60	500	495.3	99	
		173	2045	2052	7	100		105	507	502.3	99	
		174	2052	2062	7	70		150	517	509.3	99	
		175	2062	2068	9	150		120	523	518.3	99	

A-9

SD-BWI-TI-113



# Rockwell International

Rockwell Hanford Operations  
Energy Systems Group

## CORING RECORD

Hole: RRL-2

Contractor: Boyles Brothers

Core Size: 3.973"

Sheet 4 Of 14

Date	Shift	Core No.	Interval		Core Recovered			Core Time Min.	Accumulative			Remarks
			From	To	Ft.	%	Longest Piece		Ft. Drilled	Core Recovered	%	
3/15/82	N/A	176	2068	2074	5.5	92	N/A	60	529	523.8	99	
		177	2074	2083	10	100		120	539	533.8	99	
		178	2084	2094	10	100		120	549	543.8	99	
		179	2094	2104	10	100		110	559	553.8	99	
		180	2104	2107	3	100		45	562	556.8	99	
		181	2107	2110	3	100		45	565	559.8	99	
		182	2110	2114	2.4	60		60	569	562.2	99	
		183	2114	2122	9.6	120		210	577	571.8	99	
3/16/82		184	2122	2127	5	100		60	582	576.8	99	
		185	2127	2134	7	100		85	589	583.8	99	
		186	2134	2144	10	100		120	599	593.8	99	
		187	2144	2154	10	100		130	609	603.8	99	
		188	2154	2164	10	100		150	619	613.8	99	
		189	2164	2174	10	100		120	629	623.8	99	
		190	2174	2184	10	100		120	639	633.8	99	
3/17/82		191	2184	2194	10	100		90	649	643.8	99	
		192	2194	2204	10	100		90	659	653.8	99	
		193	2204	2214	10	100		75	669	663.8	99	
		194	2214	2219.5	5.5	100		60	674.5	669.3	99	
		195	2219.5	2222	.5	20		30	677	669.8	99	
3/23/82		196	2222	2223	1	100		15	678	670.8	99	
3/24/82		197	2223	2233	10	100		120	688	680.8	99	

A-10

SD-BWI-TI-113



# Rockwell International

Rockwell Hanford Operations  
Energy Systems Group

## CORING RECORD

Hole: RRL-2

Contractor: Boyles Brothers

Core Size: 3.937"

Sheet 5 of 14

Date	Shift	Core No.	Interval		Core Recovered			Core Time Min.	Accumulative			Remarks
			From	To	Ft.	%	Longest Piece		Ft. Drilled	Core Recovered	%	
3/24/82	N/A	198	2233	2239	6	100	N/A	100	694	686.8	99	
3/25/82		199	2239	2249	10	100		120	704	696.8	99	
		200	2249	2259	10	100		105	714	706.8	99	
		201	2259	2269	10	100		75	724	716.8	99	
		202	2269	2270	1	100		15	725	717.8	99	
		203	2270	2274	4	100		60	729	721.8	99	
		204	2274	2284	10	100		60	739	731.8	99	
3/26/82		205	2284	2294	10	100		90	749	741.8	99	
		206	2294	2304	10	100		100	759	751.8	99	
		207	2304	2312	8	100		90	767	759.8	99	
		208	2312	2322	10	100		120	777	769.8	99	
		209	2322	2332	10	100		120	787	779.8	99	
3/27/82		210	2332	2343	10	100		180	797	789.8	99	
3/31/82		211	2342	2347	5	100		60	802	794.8	99	
		212	2347	2347.5	.1	20		10	807.5	794.9	99	
		213	2347.5	2354	7	180		90	809	801.9	99	
		214	2354	2357	3	100		45	812	804.9	99	
		215	2357	2367	10	100		120	822	814.9	99	
		216	2367	2382	8	100		120	837	829.9	99	
		217	2374	2382	8	100		120	837	829.9	99	
		218	2382	2387	5	100		70	842	834.9	99	
		219	2387	2394	6.5	93		90	849	841.4	99	

A-11

SD-BMI-TI-113



# Rockwell International

Rockwell Hanford Operations  
Energy Systems Group

## CORING RECORD

Hole: RRL-2

Contractor: Boyles Brothers

Core Size: 3.937"

Sheet 6 of 14

Date	Shift	Core No.	Interval		Core Recovered			Core Time Min.	Accumulative			Remarks
			From	To	Ft.	%	Longest Piece		Ft. Drilled	Core Recovered	%	
4/1/82	N/A	220	2394	2404	10	100	N/A	90	859	851.4	99	
		221	2404	2414	10	100		100	869	861.4	99	
		222	2414	2424	10	100		120	879	871.4	99	
		223	2424	2434	10	100		120	889	881.4	99	
		224	2434	2444	10	100		150	899	891.4	99	
		225	2444	2448	4	100		60	903	895.4	99	
		226	2448	2454	6	100		90	909	901.4	99	
		227	2454	2464	10	100		120	919	911.4	99	
4/2/82		228	2464	2474	10	100		120	929	921.4	99	
		229	2474	2484	10	100		120	939	931.4	99	
		230	2484	2487	3	100		18	942	934.4	99	
		231	2487	2494	7	100		90	949	941.4	99	
		232	2494	2499	5	100		45	954	946.4	99	
		233	2499	2509	10	100		120	964	956.4	99	
		234	2509	2519	10	100		165	974	966.5	99	
4/3/82		235	2519	2529	10	100		120	984	976.4	99	
		236	2529	2538	8.3	92		110	993	985.7	99	
4/5/82		237	2538	2544	6	100		90	999	991.7	99	
		238	2544	2553	9	100		120	1008	100.7	99	
		239	2553	2563	10	100		180	1027	1019.7	99	
		240	2563	2572	9	100		180	1027	1019.7	99	
		241	2572	2578	6	100		120	1033	1025.7	99	

A-12

SD-BWI-TI-113



# Rockwell International

Rockwell Hanford Operations  
Energy Systems Group

## CORING RECORD

Hole: RRL-2  
Contractor: Boyles Brothers  
Core Size: 3.937"

Sheet 7 of 14

Date	Shift	Core No.	Interval		Core Recovered			Core Time Min.	Accumulative			Remarks
			From	To	Ft.	%	Longest Piece		Ft. Drilled	Core Recovered	%	
4/6/82	N/A	242	2578	2584	6	100	N/A	120	1039	1031.7	99	
		243	2584	2594	10	100		180	1049	1041.7	99	
		244	2594	2604	10	100		150	1059	1051.7	99	
		245	2604	2614	10	100		180	1069	1061.7	99	
		246	2614	2624	10	100		180	1079	1071.7	99	
4/7/82		247	2624	2634	10	100		180	1089	1081.7	99	
		248	2634	2644	10	100		120	1099	1091.7	99	
4/16/82		249	2644	2654	10	100		120	1109	1101.7	99	
		250	2654	2663	9	100		105	1118	1110.7	99	
		251	2663	2673	10	100		120	1128	1120.7	99	
4/17/82		252	2673	2683	10	100		130	1138	1130.7	99	
		253	2683	2693	10	100		135	1148	1140.7	99	
4/19/82		254	2693	2703	10	100		85	1158	1150.7	99	
		255	2703	2713	10	100		120	1168	1160.7	99	
5/4/82		256	2713	2723	7	70		75	1178	1167.7	99	
		257	1723	2731	10	125		50	1186	1177.7	99	
		258	2731	2741	9	90		40	1196	1186.7	99	
		259	2741	2750	10	110		60	1205	1196.7	99	
		260	2750	2759	9	100		60	1214	1205.7	99	
		261	2759	2769	10	100		80	1224	1215.7	99	
		262	2769	2779	10	100		120	1234	1225.7	99	
		263	2779	283	4	100		50	1238	1229.7	99	

A-13

SD-BMI-TI-113



# Rockwell International

Rockwell Hanford Operations  
Energy Systems Group

## CORING RECORD

Hole: RRL-2  
Contractor: Boyles Brothers  
Core Size: 2.980"

8 14  
Sheet \_\_\_ Of \_\_\_

Date	Shift	Core No.	Interval		Core Recovered			Core Time Min.	Accumulative			Remarks
			From	To	Ft.	%	Longest Piece		Ft. Drilled	Core Recovered	%	
5/5/82	N/A	264	2783	2793	10	100	N/A	120	1248	1239.7	99	
		265	2793	2803	9	90		120	1258	1248.9	99	
		266	2803	2813	10	100		120	1268	1258.7	99	
		267	2813	2823	10	100		130	1278	1268.7	99	
		268	2823	2833	10	100		45	1288	1278.7	99	
		269	2833	2843	10	100		60	1298	1288.7	99	
		270	2843	2853	10	100		90	1308	1298.7	99	
		271	2853	2863	10	100		120	1318	1308.7	99	
		272	2863	2864	1	100		10	1319	1309.7	99	
		273	2864	2873	9	100		100	1328	1318.7	99	
5/6/82		274	2873	2883	10	100		40	1338	1328.7	99	
		275	2883	2893	10	100		40	1348	1338.7	99	
		276	2893	2903	10	100		60	1358	1348.7	99	
		277	2903	2913	10	100		50	1368	1358.7	99	
5/19/82		278	2913	2923	10	100		80	1378	1368.7	99	
		279	2923	2933	10	100		76	1388	1378.7	99	
		280	2933	2943	10	100		60	1398	1388.7	99	
		281	2943	2951	8	100		60	1406	1396.7	99	
		282	2951	2961	10	100		60	1416	1406.7	99	
		283	2961	2969	8	100		75	1424	1414.7	99	
		284	2969	2979	10	100		60	1434	1424.7	99	
		285	2979	2984.5	5.5	100		50	1439.5	1430.2	99	

A-14

SD-BWI-TI-113



# Rockwell International

Rockwell Hanford Operations  
Energy Systems Group

## CORING RECORD

Hole: RRL-2

Contractor: Boyles Brothers

Core Size: 2.980"

Sheet 9 Of 14

Date	Shift	Core No.	Interval		Core Recovered			Core Time Min.	Accumulative			Remarks
			From	To	Ft.	%	Longest Piece		Ft. Drilled	Core Recovered	%	
5/20/82	N/A	286	2984.5	2994	9.5	100	N/A	70	1449	1439.7	99	
		287	2994	3003	9	100		50	1458	1448.7	99	
		288	3003	3013	10	100		70	1468	1458.7	99	
		289	313	3020	7	100		60	1475	1465.7	99	
6/1/82		290	3020	3030	10	100		120	1485	1475.7	99	
		291	3030	3040	10	100		60	1495	1485.7	99	
		292	3040	3050	10	100		120	1505	1495.7	99	
		293	3050	3060	10	100		75	1515	1505.7	99	
		294	3060	3070	10	100		75	1525	1515.7	99	
6/2/82		295	3070	3079	9	100		60	1534	1524.7	99	
		296	3079	3089	10	100		60	1544	1534.7	99	
		297	3089	3089	10	100		50	1554	1544.7	99	
		298	3099	3109	10	100		50	1564	1554.7	99	
		299	3109	3116	7	100		45	1571	1561.7	99	
		300	3116	3126	10	100		60	1581	1591.7	99	
		301	3126	3133	7	100		59	1588	1578.7	99	
		302	3133	3142	9	100		65	1597	1587.7	99	
		303	3142	3144	2	100		20	1599	1589.7	99	
		304	3144	3151	7	100		80	1606	1596.7	99	
		305	3151	1352	1	100		20	1607	1597.7	99	
6/3/82		306	3152	3162	10	100		84	1617	1607.7	99	
		307	3162	3164	2	100		55	1619	1609.7	99	

A-15

SD-BMI-TI-113



# Rockwell International

Rockwell Hanford Operations  
Energy Systems Group

## CORING RECORD

Hole: RRL-2

Contractor: Boyles Brothers

Core Size: 2.980"

Sheet 10 of 14

A-16

SD-BMI-TI-113

Date	Shift	Core No.	Interval		Core Recovered			Core Time Min.	Accumulative			Remarks
			From	To	Ft.	%	Longest Piece		Ft. Drilled	Core Recovered	%	
6/3/82	N/A	308	3164	3165	10	0	N/A	20	1620	1609.7	99	
		309	3165	3167	2	100		40	1622	1611.7	99	
		310	3167	3175	8	100		120	1630	1619.7	99	
		311	3175	3183	8	100		90	1638	1627.7	99	
		312	3183	3193	10	100		120	1648	1637.7	99	
		313	3193	3194	0.2	20		20	1649	1637.9	99	
		314	3194	3195	0.2	20		20	1650	1638.1	99	
6/4/82		315	3195	3203	9.3	116		150	1658	1647.4	99	
		316	3203	3211	7	88		95	1666	1654.4	99	
		317	3211	3217	5.5	92		75	1672	1659.9	99	
		318	3217	3224	7.5	106		100	1679	1667.4	99	
		319	3224	3233	9	100		120	1688	1676.4	99	
		320	3233	3243	10	100		120	1698	1686.4	99	
		321	3243	3253	10	100		60	1708	1696.4	99	
		322	3253	3263	10	100		60	1718	1706.4	99	
		323	3263	3273	10	100		60	1728	1716.4	99	
		324	3273	3283	10	100		40	1738	1726.4	99	
		325	3283	3293	10	100		40	1748	1736.4	99	
6/5/82		326	3293	3303	10	100		45	1758	1746.4	99	
		327	3303	3313	10	100		50	1768	1756.4	99	
		328	3313	3323	10	100		65	1778	1766.4	99	
6/7/82		329	3323	3333	9.5	95		70	1788	1776.9	99	



# Rockwell International

Rockwell Hanford Operations  
Energy Systems Group

## CORING RECORD

Hole: RRL-2

Contractor: Boyles Brothers

Core Size: 2.980"

Sheet 11 of 14

Date	Shift	Core No.	Interval		Core Recovered			Core Time Min.	Accumulative			Remarks
			From	To	Ft.	%	Longest Piece		Ft. Drilled	Core Recovered	%	
6/7/82	N/A	330	3333	3343	10	100	N/A	60	1798	1786.9	99	
		331	3343	3343	9	100		60	1807	1795.9	99	
		332	3352	3353	0	0		20	1808	1795.9	99	
		333	3353	3354.5	1.5	100		90	1809.5	1797.4	99	
		334	3354.5	3363	7	82		105	1818	1804.4	99	
6/8/82		335	3363	3367	4	100		45	1822	1808.4	99	
		336	3367	3370	3	100		55	1825	1811.4	99	
		337	3370	3372	2	100		40	1827	1813.4	99	
		338	3372	3373	1	100		25	1828	1814.4	99	
		339	3373	3377	4	100		38	1832	1818.4	99	
		340	3377	3383	6	100		46	1838	1824.4	99	
		341	3383	3393	9	100		70	1847	1833.4	99	
		342	3393	3402	10	100		60	1857	1843.4	99	
		343	3402	3412	10	100		120	1867	1853.4	99	
		344	3412	3422	10	100		90	1877	1863.4	99	
		345	3422	3432	10	100		105	1887	1873.4	99	
6/9/82		346	3432	3442	10	100		120	1897	1883.4	99	
		347	3442	3452	10	100		120	1907	1893.4	99	
		348	3452	3462	10	100		120	1917	1903.4	99	
		349	3462	3472	10	100		120	1927	1913.4	99	
		350	3472	3475	3	100		40	1930	1916.4	99	
6/11/82		351	3475	3483	8	100		90	1938	1924.4	99	

A-17

SD-BMI-TI-113



# Rockwell International

Rockwell Hanford Operations  
Energy Systems Group

## CORING RECORD

Hole: RRL-2

Contractor: Boyles Brothers

Core Size: 2.980"

Sheet 12 of 14

Date	Shift	Core No.	Interval		Core Recovered			Core Time Min.	Accumulative			Remarks
			From	To	Ft.	%	Longest Piece		Ft. Drilled	Core Recovered	%	
6/11/82	N/A	352	3483	3493	10	100	N/A	125	1948	1934.4	99	
6/12/82		353	3493	3503	10	100		90	1958	1944.4	99	
		354	3503	3513	10	100		115	1968	1954.4	99	
6/14/82		355	3513	3523	10	100		90	1978	1964.4	99	
		356	3523	3533	10	100		108	1988	1974.4	99	
		357	3533	3543	10	100		75	1998	1984.4	99	
		358	3543	3553	10	100		80	2008	1994.4	99	
		359	3553	3555.5	2.5	100		20	2010.5	1996.9	99	
		360	3555.5	3563	7.5	100		75	2018	2004.4	99	
6/15/82		361	3563	3573	10	100		110	2028	2014.4	99	
		362	3573	3583	10	100		145	2038	2024.4	99	
		363	3583	3593	9	90		120	2048	2033.4	99	
		364	3593	3598	4	80		90	2053	2037.4	99	
		365	3598	3608	10	100		120	2063	2047.4	99	
		366	3608	3618	10	100		60	2073	2057.4	99	
		367	3618	3628	10	100		90	2083	2067.4	99	
		368	3628	3638	9	90		120	2093	2076.4	99	
		369	3638	3643	4.5	90		60	2098	2080.9	99	
6/16/82		370	3643	3653	9.5	95		120	2108	2090.4	99	
		371	3653	3663	10	100		120	2118	2100.4	99	
		372	3663	3673	10	100		120	2128	2110.4	99	
		373	3673	3683	10	100		100	2138	2120.4	99	

A-18

SD-BMI-TI-113



# Rockwell International

Rockwell Hanford Operations  
Energy Systems Group

## CORING RECORD

Hole: RRL-2

Contractor: Boyles Brothers

Core Size: 2.980"

Sheet 13 of 14

Date	Shift	Core No.	Interval		Core Recovered			Core Time Min.	Accumulative			Remarks
			From	To	Ft.	%	Longest Piece		Ft. Drilled	Core Recovered	%	
6/16/82	N/A	374	3683	3691	8	100	N/A	90	2146	2128.4	99	
		375	3691	3701	8	80		100	2156	2136.4	99	
		376	3701	3711	10	100		120	2166	2146.4	99	
		377	3711	3720	9	100		120	2175	2155.4	99	
		378	3720	3730	10	100		120	2185	2165.4	99	
6/17/82		379	3730	3740	10	100		90	2195	2175.4	99	
		380	3740	3750	10	100		60	2205	2185.4	99	
		381	3750	3756	5	83		60	2211	2190.4	99	
		382	3756	3763	7	100		75	2218	2197.4	99	
		383	3763	3773	10	100		90	2228	2207.4	99	
		384	3773	3774	0	0		40	229	2207.4	99	
		385	3774	3775.5	0	0		90	2230.5	2207.4	99	
		386	3775.5	3782	0	0		120	2237	2207.4	99	
6/18/82		387	3782	3783	0	0			2238	2207.4	99	
		388	3783	3792	7.5	82		120	2247	2214.9	99	
		389	3792	3802	10	100		120	2257	2224.9	99	
6/19/82		390	3802	3812	10	100		120	2267	2234.9	99	
		391	3812	3822	10	100		120	2277	2244.9	99	
		392	3822	3823	0.5	50		20	2278	2245.4	99	
		393	3823	3824	0.2	20		20	2279	2245.6	99	
		394	3824	3832	8	100		75	2287	2253.6	99	
		395	3832	3842	10	100		80	2297	2263.6	99	

A-19

SD-BMI-TI-113







## BOREHOLE RRL-2, MUD LOSS SUMMARY

<u>FLOW</u>	<u>ESTIMATED LOSS IN GALLONS</u>
Mabton	None
Priest Rapids	4,000
Roza	11,000
Upper Frenchman Springs	16,000
Lower Frenchman Springs	100,000
Vantage	None
Upper Grande Ronde	16,500
Cohasset Vesicular Zone	None
Cohasset Interior	None
Cohasset Flow Top	None
Cohasset Flow Bottom	21,000
Umtanum Flow Top	103,950
Umtanum Interior	None
Umtanum Fracture Zone	25,000
Umtanum Flow Bottom	3,000

APPENDIX B

SUMMARY GEOLOGIC LOG--The summary geologic log is based on both the geologic logs and geophysical logs of the boreholes.

SUMMARY TABLE OF RQD VALUES FOR FLOW INTERIORS

FORMATION	MEMBER (ft)	FLOW OR BED (ft)	FOOTAGE	LITHOLOGY
HANFORD AND RINGOLD Undifferentiated			0-605	Overburden; alluvium, eolian sediments and including the Hanford and Ringold Formations.
SADDLE MOUNTAINS BASALT	ELEPHANT MOUNTAIN 605-686	ONE FLOW 605-686	605-618	Basalt, vesicular to 20%, 1-2 cm. in size. Aphanitic, diktytaxitic in places. Some secondary mineralization.
			618-640	Basalt, dark gray, aphanitic. Vesicles decreasing in size to 2 mm. Fractures 2/ft. with green clay filling fractures to 3 mm width.
			640-682	Basalt, dark gray, dense, aphanitic to finely phaneritic. Vertical fractures to 4 mm filled with green clay. Abundant pyritization on fracture surfaces.
			682-686	Basalt, dark gray with scattered flow bottom vesicles, some vesicles partially filled with clay
	RATTLESNAKE RIDGE INTERBED 686-782		686-688	Tuffaceous sandstone, black to gray. Baked or welded in upper portion. Scattered basalt clasts.
			688-720	Clayey siltstone, dark gray to light green. well consolidated with some possible iron staining. One foot of dark gray clay at 717-718 feet. Some cross bedding and lensing.
			720-755	Sandstone, gray. Unconsolidated with lenses of untemented pebble-cobble gravel 728-728.5, 738-738.5, 744-744.5, 748-755
			755-782	Clay, green. Tuffaceous and sandy. Hard to vitric. Some altered basalt clasts 776-782 with a hard clay matrix.

FORMATION	MEMBER (ft)	FLOW OR BED (ft)	FOOTAGE	LITHOLOGY
SADDLE MOUNTAINS BASALT	POMONA 782-941	ONE FLOW 782-941	782-796	Basalt, black. Vesicular flowtop to 25%. Vesicles lined with dark clay, iron oxidation stain in places
			796-800	Basalt flow rubble. Angular vesicular clasts in an oxidized red to light brown clay matrix.
			800-813	Basalt, gray phaneritic. Vesicular to 25% with green clay lining vesicles.
			813-856	Basalt flow rubble. Highly fractured with alternating pods of highly vesicular basalt and oxidized flow rubble.
			856-941.5	Basalt, gray, phaneritic. Scattered phenocrysts of plagioclase to 3 mm. Fractures decreasing to 1/ft. Fractures have alteration rims and surface pyritization.
	SELAH INTERBED 941-986		941.5-948	Clay, green. Tuffaceous, well indurated.
			948-984	Sandstone gray to dark green. Tuffaceous, moderately consolidated. Scattered very coarse pebbles. Bedding at 968 feet dipping 10-15°. Becomes more consolidated grading to bottom.
			984-986	Conglomerate, pebble-cobble. Moderately indurated, well-rounded. Matrix of well cemented sand and clay.
	ESQUATZEL 986-1,104	ONE FLOW 986-1,104	986-992	Basalt flow breccia. Angular, vesicular slightly oxidized clasts up to 4 cm in a hard green clay matrix. Well indurated.
			992-1,010	Basalt, dark gray. Vesicular to 10%. Oxidation and alteration in places with some iron staining. Pods of flow rubble with clay filling voids.
			1,010-1,051	Basalt, gray, aphanitic. Scattered phenocrysts of plagioclase to 3x5 mm. Occasional scattered vesicles.
			1,051-1,104	Basalt, dark gray, aphanitic to finely phaneritic. Diktytaxitic in places

FORMATION	MEMBER (ft)	FLOW OR BED (ft)	FOOTAGE	LITHOLOGY	
SADDLE MOUNTAINS BASALT		COLD CREEK INTERBED 1,104-1,168	1,104-1,111	Clay, gray, baked. Contains oxidized altered basalt clasts. Some apparent slickensides in clay.	
			1,111-1,125	Clay, green. Hard, well consolidated. Contains low angle bedding planes.	
			1,125-1,141	Sandstone, white to green. Coarse, clean, well sorted. Contains occasional bedding planes.	
			1,141-1,151	Tuff. Brecciated vitric tuff in a hard green clay matrix. Clasts range from 1 mm to 10 cm.	
			1,151-1,168	Clay, green with sand lenses. Some bedding planes evident.	
	UMATILLA BASALT 1,168-1,399	ONE FLOW 1,168-1,399	1,168-1,188	Basalt, vesicular clasts (1-4 cm) in an indurated black to green clay matrix. Clasts are sub-angular to angular, partially altered and oxidized,	
			1,188-1,247	Basalt, black, aphanitic. Dense with scattered vesicles. Slightly dikty-taxitic in places. Irregular to vertical well healed fractures up to 4 mm with green clay filling. Some fractures have alteration margins. Slightly phyrlic with phenocrysts of plagioclase to 1 mm.	
				1,247-1,399	Basalt, black, medium phaneritic. High angle, well healed fractures up to 3 mm, typically filled with hard green clay
		MABTON INTERBED 1,399-1,523	1,399-1,407	Lapilli tuff, baked, gray. Altered tuff and clay zones.	
			1,407-1,423	Sandstone, green, micaceous. Well sorted with intermixed clay layers.	
			1,423-1,426	Clay, gray to green.	
			1,426-1,433	Sand, green, quartzitic. Coarse, well sorted.	

FORMATION	MEMBER (ft)	FLOW OR BED (ft)	FOOTAGE	LITHOLOGY
SADDLE MOUNTAINS BASALT		MABTON INTERBED 1,399-1,523	1,433-1,450	Sand and clay, green to gray. Alternating varves or layers. Micaceous.
			1,450-1,463	Sandstone, gray to green, quartzitic. Subrounded to angular, coarse. Bedding planes 30-35° and 3-5 mm in width. Uncemented.
			1,463-1,518	Clay, green, hard with some apparent slickensides. Occasional lenses of sand, tuff and sideromelane.
			1,518-1,523	Clay, brown and green. Scattered non-petrified wood fragments. Vitrified silica at 1,519 feet followed by soft brown to green platy clay.
WANAPUM BASALT	PRIEST RAPIDS 1,523-1,749.4	UPPER FLOW (LOLO TYPE) 1,523-1,689	1,523-1,524	Basalt flow breccia, gray-brown. Oxidized clast to 10 cm with a hard green clay matrix.
			1,524-1,544	Basalt, gray. Finely phaneritic with occasional phenocrysts. Large open vugs or fissures up to 20 cm long. Zeolites as secondary mineralization. Irregular fracturing to 4/foot.
			1,544-1,564	Basalt, dark gray. Medium to coarsely phaneritic, slightly diktytaxitic in places with scattered vugs.
			1,564-1,688	Basalt, dark gray. medium to coarsely phaneritic, dense, 1-2 fractures foot. Fractures mostly clay filled. Horizontal layers of open matrix coarse grained minerals having a very high apparent intergranular porosity at 1,573,1,576, 1,583 and 1,595 feet. Disking 1,603-1,604, 1,630-1,640.
			1,688-1,689	Basalt flow-bottom breccia. Fractures healed and mineralized.

FORMATION	MEMBER (ft)	FLOW OR BED (ft)	FOOTAGE	LITHOLOGY
WANAPUM BASALT	PRIEST RAPIDS 1,523-1,749.4	LOWER FLOW (ROSALIA TYPE) 1,689-1,749.4	1,689-1,690	Basalt flow breccia, black, vesicular.
			1,690-1,728	Basalt, dark gray, vesicular. Grades from coarsely vesicular to finely vesicular and diktytaxitic. A few scattered vesicle sheets. Finely phaneritic. Disked 1,693-1,714.
			1,728-1,749	Basalt, dark gray, dense, finely phaneritic.
			1,749-1749.4	Basalt, black, glassy, finely vesicular.
		UNNAMED INTERBED	1,749.4-1,750	Clay, vitric, probable welded or altered tuff. Dark gray.
	ROZA 1,750-1,922	UPPER FLOW 1,750-1,778	1,750-1,761	Basalt, vesicular, black. Highly phyric, tabular plagioclase phenocrysts to 10%. Matrix finely phaneritic and diktytaxitic.
			1,761-1,775	Basalt, dark gray, dense. Moderately phaneritic, profusely phyric, tabular plagioclase phenocrysts to 15%.
			1,775-1,778	Basalt, brown gray, vesicular with inclined flow bottom vesicles, phyric.
		LOWER FLOW 1,778-1,922	1,778-1,785	Basalt flow rubble, black. Highly altered clasts in a clay ash matrix. Clasts are phyric with tabular plagioclase phenocrysts.
			1,785-1,798	Basalt, gray, vesicular and vuggy. Grades to scattered vugs. Moderately phaneritic, phyric with plagioclase phenocrysts.
1,798-1,922			Basalt, dark gray, dense. Moderately phaneritic, phyric to 10%. Tabular plagioclase phenocrysts. 0.2 foot glass chill zone 1921.8-1,922.	

FORMATION	MEMBER (ft)	FLOW OR BED (ft)	FOOTAGE	LITHOLOGY
WANAPUM BASALT	FRENCHMAN SPRINGS 1,922-2,683	FRENCHMAN SPRINGS 1 1,922-2,104	1,922-1,948	Basalt flow rubble, black. Highly altered vesicular clasts in a dark green and black clay matrix.
			1,948-2,014	Basalt, dark gray, finely phaneritic. Vesicular and vuggy grading to scattered vugs. Aphyric. Moderately fractured; (3-4 foot) becoming highly fractured
			2,014-2,018	Basalt, dark gray, aphyric. Highly fractured with some apparent gouge and slickensides on fracture surfaces.
			2,018-2,104	Basalt, dark gray, aphyric, moderate to finely phaneritic. Mostly low to medium angle fracturing 2-3 foot. Flow bottom vesicles 2,103-2,104.
		FRENCHMAN SPRINGS 2 2,104-2,217	2,104-2,111	Basalt flow rubble, black. Angular vesicular clasts, little cementation. Finely phaneritic, aphyric.
			2,111-2,128	Basalt, black, moderately vesicular with scattered vugs. Finely phaneritic, aphyric.
			2,128-2,217	Basalt, dark gray, moderately fractured. Finely phaneritic, aphyric. Scattered amygdules mostly filled with green clay. Disking; 2,146-2,149, intermittent-2,158-2,205.
		FRENCHMAN SPRINGS 3 2,217-2,273	2,217-2,228	Basalt flow rubble, black, vesicular.
			2,228-2,236	Basalt, dark gray. Scattered vesicle sheets, small vugs to 1 cm and clay filled amygdules. Finely phaneritic, aphyric.
			2,236-2,273	Basalt, dark gray to black. Finely phaneritic, aphyric, finely diktytaxitic, moderately fractured. Disking; 2,239-2,240, 2,253-2,255, 2,268-2,270. Flow-bottom breccia, 2,270-2,273. Glass, inclined vesicles in breccia clasts.

FORMATION	MEMBER (ft)	FLOW OR BED (ft)	FOOTAGE	LITHOLOGY
WANAPIUM BASALT	FRENCHMAN SPRINGS 1,922-2,683	FRENCHMAN SPRINGS 4 2,273-2,381	2,273-2,318	Basalt flow-top, black to gray, vesicular. Some glass or sideromelane near contact. Finely phaneritic, phyric scattered plagioclase phenocrysts, mostly tabular with sub-horizontal orientation. Alternating zones of vesicular basalt and lobes of denser material. Disking; 2,277-2,285, 2,294-2,299.
			2,318-2,381	Basalt, dark gray, diktytaxitic. Finely phaneritic, phyric, scattered plagioclase phenocrysts to 5%, phenocrysts oriented sub-horizontally. Moderate fracturing, most with alteration borders. Disking intermittent 2,318-2,354.
		FRENCHMAN SPRINGS 5 2,381-2,489	2,381-2,409	Basalt, black, vesicular flow rubble. Scoriaceous and vesicular clasts in a green and black clay matrix. Phyric with glomerophenocrysts of plagioclase, less than 5%.
			2,409-2,454	Basalt, dark gray, vesicular and vuggy. Finely phaneritic. Phyric, scattered phenocrysts of plagioclase. Intermittant diskings; 2,409-2,454.
			2,454-2,489	Basalt, dark gray. Finely phaneritic, slightly phyric- a few scattered phenocrysts of plagioclase. Fracturing moderate with some high and medium angle filled fractures. Some intermittent non-continuous diskings.
			FRENCHMAN SPRINGS 6 2,489-2,617	2,489-2,500
	2,500-2,525	Basalt, dark gray. Scattered vesicles, vugs and amygdules. Phyric, plagioclase phenocrysts less than 5%. Irregularly fractured.		
	FRENCHMAN SPRINGS 6 2,489-2,617	2,525-2,617	Basalt, black, dense. Finely phaneritic, phyric to 5%. Disked; 2,527-2,532, Intermittant - 2,560-2,600.	

FORMATION	MEMBER (ft)	FLOW OR BED (ft)	FOOTAGE	LITHOLOGY	
WANAPUM BASALT	FRENCHMAN SPRINGS 1,922-2,683	FRENCHMAN SPRINGS 7 2,617-2,683	2,617-2,624	Basalt flow-top breccia, dark gray. Vesicular clasts in a black sideromelane matrix. Aphyric, finely phaneritic.	
			2,624-2,644	Basalt, dark gray. Grading from vesicular to highly diktytaxitic with sheet vesicles. Medium to coarsely phaneritic with a few scattered plagioclase phenocrysts. Moderately fractured 1-2/foot.	
			2,644-2,670	Basalt, dark gray. Coarsely phaneritic with scattered plagioclase phenocrysts. Finely diktytaxitic. Moderately fractured, mostly irregular filled with dark green clay. Disked; 2,646-2,650.	
			2,670-2,683	Basalt flow-bottom breccia. Black and highly altered. Probable poorly developed pillow structure. Highly vesicular clasts with palagonitic margins.	
GRANDE RONDE BASALT	SENTINEL BLUFFS SEQUENCE 2,687-3,607	VANTAGE INTERBED 2,683-2,687	2,683-2,687	Claystone, green-brown. Indurated at contact, grades into massive gray siltstone then into black and brown bedded claystone. Bedding planes horizontal.	
			GRANDE RONDE 1 2,687-2,721	2,687-2,711	Basalt, dark gray. Vesicular and vuggy grading to scattered vesicles and diktytaxitic. Finely phaneritic, aphyric.
				2,711-2,721	Basalt, dark gray. Moderately fractured, 1-2/foot. Diktytaxitic with a few scattered vesicles. Aphyric, finely phaneritic.
			GRANDE RONDE 2 2,721-2,823	2,721-2,767	Basalt, dark gray. Vesicular and vuggy. diktytaxitic matrix. Some vugs up to 5 cm. Medium phaneritic, aphyric. Relatively few fractures.
				2,767-2,823	Basalt, dark gray. Diktytaxitic, finely phaneritic, aphyric. Moderately fractured, disked; 2,810-2,818.

FORMATION	MEMBER (ft)	FLOW OR BED (ft)	FOOTAGE	LITHOLOGY	
GRANDE RONDE BASALT	SENTINEL BLUFFS SEQUENCE 2,687-3,607	GRANDE RONDE 3 2,823-2,993	2,823-2,842	Basalt vesicular flow-top, dark gray. Flow breccia at 2,830,2,836 and 2,838 feet. Vesicular clasts in an oxidized clay matrix. Aphanitic, aphyric.	
			2,842-2,872	Basalt, dark gray. Aphanitic, aphyric. Intraflow vesicular zones 2,849-2855, 2,856-2,862 feet. Moderately fractured, mostly low angle. Disked; 2,853-2,858, 2,862-2,866.	
			2,872-2,904	Basalt, dark gray. Vuggy, mostly unfilled, some partially quartz filled, vugs are sub-horizontally elongated. Basalt shows flow banding striations. Finely phaneritic, aphyric. Intermittant diskings.	
			2,904-2,993	Basalt, dark gray. Finely phaneritic, aphyric, dense. Mostly medium to high angle fractures. Disking: 2,910-2,931, 2,934-2,939,2,967-2,982.	
	GRANDE RONDE 4 (COHASSET FLOW) 2,993-3,255		2,993-3,012	Basalt, gray. Vesicular and amygdaloidal, cavity fillings and linings are silica, dark green clay and zeolites. Some low angle clay and silica filled fractures. Some vesicles and vugs may be connected. Disked; 3,011-3,012.	
			3,012-3,083	Basalt, dark gray. Phaneritic, aphyric, diktytaxitic. A few scattered vugs and vesicles. Mostly high angle fractures and diskings; 3,012-3,054, 3,060-3,083.	
			3,083-3,108	Basalt, dark gray. Vesicular and amygdaloidal to 40%. Finely phaneritic, aphyric, diktytaxitic. Cavity fillings and linings silica and clay. Grades to scattered vesicles and small amygdules. Disked intermittantly.	
			3,108-3,255	Basalt, dark gray. Finely phaneritic, aphyric. High and low angle clay filled fractures. Scattered amygdules. Disked; 3,175-3,217.	

FORMATION	MEMBER (ft)	FLOW OR BED (ft)	FOOTAGE	LITHOLOGY
GRANDE RONDE BASALT	SENTINEL BLUFFS SEQUENCE 2,687-3,607	GRANDE RONDE 5 3,255-3,388	3,255-3,292	Basalt flow breccia, gray. Vesicular and altered. Several examples of missing matrix between breccia clasts. Breccia also oxidized to brown or tan. Alternating pods of vesicular basalt and breccia.
			3,292-3,335	Basalt, dark gray. Vuggy grading to vesicular and amygdaloidal. Filling of silica and green clay. Vugs sub-horizontally elongated. Finely phaneritic, aphyric. Some diskings; 3,297-3,298, 3,316-3,317
			3,335-3,388	Basalt, dark gray. Finely phaneritic, aphyric. Scattered vugs and amygdules, slightly diktytaxitic. Mostly high angle fractures, diskings; 3,335-3,380.
	SENTINEL BLUFFS SEQUENCE 2,687-3,607	GRANDE RONDE 6 3,388-3417.5	3,388-3,402	Basalt, dark gray. Vesicular flow-top with some brecciation. Some missing matrix in breccia with alteration areas yellow-brown in color. Much silica filling in voids.
			3,402-3,417	Basalt, dark gray. Finely phaneritic, aphyric. Scattered vesicles. High angle fractures with diskings; 3,402-3,414.
	SENTINEL BLUFFS SEQUENCE 2,687-3,607	GRANDE RONDE 7 3,417.5-3,475	3,417-3,448	Basalt vesicular flow-top, dark gray. Vuggy, vesicular and amygdaloidal. Finely phaneritic, aphyric. Many cavities filled with silica and dark green clay.
			3,448-3,475	Basalt, dark gray. Finely phaneritic, aphyric, slightly diktytaxitic. Dense, a few high angle fractures, no diskings.

FORMATION	MEMBER (ft)	FLOW OR BED (ft)	FOOTAGE	LITHOLOGY	
GRANDE RONDE BASALT	SENTINEL BLUFFS SEQUENCE 2,687-3,607	GRANDE RONDE 8 (MCCOY CANYON FLOW) 3,475-3,607	3,475-3,491	Basalt flow breccia, dark gray. Vesicular clasts in a tight matrix of green clay, occasional missing matrix fissuring. Some cavities filled with silica and green clay.	
			3,491-3,508	Basalt, dark gray. Vuggy, vugs to 3 cm and 20%. Mostly unfilled grading to silica filled. Sub-horizontally oriented. A few high angle fractures, no disking.	
			3,508-3,525	Basalt, dark gray. Dense, aphanitic, aphyric. A few scattered filled vugs (large amygdules). Disked; 3,516-3,525.	
			3,525-3,551	Basalt, dark gray. Vesicular and vuggy, some filled with silica and pyrite. Finely phaneritic, aphyric, diktytaxitic. Disked; 3,527-3,550.	
			3,551-3,599	Basalt, dark gray. Finely phaneritic, aphyric, slightly diktytaxitic. Dense with some healed high and low angle fractures, disking; 3,553-3,561, 3,571-3,593.	
				3,599-3,607	Basalt, dark gray. Vesicular and vuggy, some flattened, mostly unfilled.
	SCHWANA SEQUENCE 3,607-3,973+	GRANDE RONDE 9 (UMTANUM FLOW) 3,607-3,839	3,607-3,755	Basalt flow breccia, dark gray. Vesicular and vuggy clasts in a tight matrix of clay cemented angular rubble fragments. Matrix occasionally missing leaving fissures which are highly mineralized. An intercalated lens of denser competent basalt occurs at 3,653-3,658. Section from 3,666-3,717 becomes very poorly consolidated with much open matrix between clasts.	
			3,755-3,839	Basalt, dark gray. Finely phaneritic, aphyric. Dense, a few high angle and irregular fractures. Some near vertical high angle fractures occur at 3,818-3,824 - fractures appear to be open and have alteration borders. Disking; 3,758-3,806, 3,829-3,838.	

FORMATION	MEMBER (ft)	FLOW OR BED (ft)	FOOTAGE	LITHOLOGY
GRANDE RONDE BASALT	SCHWANA SEQUENCE 3,607-3,973+	GRANDE RONDE 10 (VERY HIGH MG FLOW) 3,839-3,903	3,839-3,864	Basalt flow rubble, dark gray. Clasts of amygdaloidal and vesicular basalt in a tight clay matrix. Some matrix consists of silica, some is missing and fissures are partially mineralized.
			3,864-3,891	Basalt, dark gray. Relatively competent. Finely phaneritic, aphyric. Mostly high angle fractures. Scattered amygdules 3,870-3,888.
			3,891-3,903	Basalt vesicular flow bottom, dark gray. Tight vesicular flow breccia with some open matrix fissures. Some reddish oxidation and silica filling vesicles.
		GRANDE RONDE 11 3,903-3,973+	3,903-3,970	Basalt vesicular flow-top. Red-gray to gray. Vesicles and vugs, most sub-horizontally elongated. Many filled with silica and green clay. Moderately fractured, no diskings.
			3,970-3,973	Basalt, dark gray. Dense, aphanitic, aphyric. A few low angle fractures
		Total Depth		

## SUMMARY TABLE OF RQD VALUES FOR FLOW INTERIORS

FLOW	DEPTH (ft)	RQD	CORE SIZE	COMMENTS
Elephant Mountain	613-684	96.5	PQ	
Pomona	863-941	91.5	PQ	
Esquatze1	1024-1104	97.5	PQ	
Umatilla	1194-1399	95.9	PQ	
Priest Rapids II	1534-1689	96.8	PQ, HQ	
Priest Rapids I	1716-1748	95.5	HQ	
Roza	1794-1922	99.1	HQ	
Frenchman Springs 1	1954-2104	72.0	HQ	
Frenchman Springs 2	2114-2217	77.8	HQ	Minor Disking
Frenchman Springs 3	2230-2272	82.7	HQ	
Frenchman Springs 4	2313-2381	86.9	HQ	Minor Disking
Frenchman Springs 5	2414-2489	80.5	HQ	Minor Disking
Frenchman Springs 6	2499-2617	53.5	HQ	Minor Disking
Frenchman Springs 7	2634-2671	79.2	HQ	
Grande Ronde 1	2693-2721	94.3	HQ, NQ	
Grande Ronde 2	2759-2823	90.5	NQ	
Grande Ronde 3	2903-2993	63.2	NQ	Moderate Disking
Cohasset	3010-3255	53.1	NQ	Disking
Grande Ronde 5	3293-3338	63.1	NQ	Disking
Grande Ronde 6	3402-3417	76.1	NQ	Disking
Grande Ronde 7	3432-3475	100	NQ	
McCoy Canyon	3493-3596	53.1	NQ	Disking
Umtanum	3757-3839	43.1	NQ	Disking
Grande Ronde 10	3861-3891	92.3	NQ	
Grande Ronde 11	3923-3973	87.4	NQ	

Rockwell Hanford Operations

SUPPORTING DOCUMENT		Number	Rev. Ltr./ Chg. No.	Page 1 of																																										
PROGRAM: Exploratory Shaft - Phase I		SD- BWI-AR-003	0-0	10																																										
Document Title: Morrison-Knudsen Company, Inc. Basalt Waste Isolation Project/Exploratory Shaft Phase I Drilling Program for 144" Surface Hole		Baseline Document <input type="checkbox"/> Yes <input checked="" type="checkbox"/> No																																												
Key Words: Drilling Program - 144-Inch Surface Hole		WBS No. or Work Package No. LF24 CEI 014		Date 2/11/83																																										
Abstract		Prepared by (Name and Dept. No.) <i>M. J. Lauterbach</i> M. J. Lauterbach See Page 2 for Approvals																																												
<p>This document outlines the drilling program procedure for the 144-inch surface hole.</p> <div data-bbox="277 1172 753 1449" data-label="Text" style="border: 1px solid black; padding: 5px; text-align: center;"> <p><b>INFORMATION COPY</b></p> <p>THIS COPY WILL NOT BE REPLACED AND MAY BE CHANGED WITHOUT NOTICE</p> </div> <p>*Initiated by M-K used by Rockwell.</p>		<table border="1"> <thead> <tr> <th>* Distribution</th> <th>Name</th> <th>Mail Address</th> </tr> </thead> <tbody> <tr> <td></td> <td>Rockwell</td> <td></td> </tr> <tr> <td>*</td> <td>M. T. Black</td> <td>PBB/700</td> </tr> <tr> <td>*</td> <td>H. W. Brandt</td> <td>PBB/700</td> </tr> <tr> <td>*</td> <td>R. W. Carlson</td> <td>PBB/700</td> </tr> <tr> <td>*</td> <td>M. F. Nicol</td> <td>PBB/700</td> </tr> <tr> <td>*</td> <td>J. V. Mohatt</td> <td>PBB/700</td> </tr> <tr> <td>*</td> <td>P. J. Reder (PP)</td> <td>PBB/700</td> </tr> <tr> <td>*</td> <td>W. F. Todish</td> <td>PBB/700</td> </tr> <tr> <td></td> <td>DOE</td> <td></td> </tr> <tr> <td>*</td> <td>R. D. Hudson</td> <td>PBB/700</td> </tr> <tr> <td></td> <td>M-K</td> <td></td> </tr> <tr> <td>*</td> <td>F. C. Larvie</td> <td>PBB/700</td> </tr> <tr> <td>*</td> <td>Records Retention</td> <td></td> </tr> </tbody> </table>			* Distribution	Name	Mail Address		Rockwell		*	M. T. Black	PBB/700	*	H. W. Brandt	PBB/700	*	R. W. Carlson	PBB/700	*	M. F. Nicol	PBB/700	*	J. V. Mohatt	PBB/700	*	P. J. Reder (PP)	PBB/700	*	W. F. Todish	PBB/700		DOE		*	R. D. Hudson	PBB/700		M-K		*	F. C. Larvie	PBB/700	*	Records Retention	
		* Distribution	Name	Mail Address																																										
	Rockwell																																													
*	M. T. Black	PBB/700																																												
*	H. W. Brandt	PBB/700																																												
*	R. W. Carlson	PBB/700																																												
*	M. F. Nicol	PBB/700																																												
*	J. V. Mohatt	PBB/700																																												
*	P. J. Reder (PP)	PBB/700																																												
*	W. F. Todish	PBB/700																																												
	DOE																																													
*	R. D. Hudson	PBB/700																																												
	M-K																																													
*	F. C. Larvie	PBB/700																																												
*	Records Retention																																													
		<p>*COMPLETE DOCUMENT (No asterisk, title page/summary of revision page only)</p> <p>(May be continued on page 2)</p>																																												
<div data-bbox="153 1768 612 1981" data-label="Text" style="border: 1px solid black; padding: 5px;"> <p>THIS DOCUMENT IS A ROCKWELL SUPPORTING DOCUMENT FOR USE BY ROCKWELL, ITS AUTHORIZED SUBCONTRACTORS, AND THE DEPARTMENT OF ENERGY</p> </div>		<div data-bbox="657 1832 987 1938" data-label="Text" style="font-size: 2em; font-weight: bold; text-align: center;"> <p>BASALT</p> </div>																																												
		<div data-bbox="1037 1708 1120 1783" data-label="Image" style="text-align: center;"> </div> <p>OFFICIALLY RELEASED</p> <p>1983 FEB 11 PM 3:48</p>																																												

SUPPORTING DOCUMENT

Number  
SD - BWI-AR-003

Page  
2

Approvals

\* Distribution Name Mail Address

\_\_\_\_\_  
Program Office

\_\_\_\_\_  
Research and Engineering

\_\_\_\_\_  
Plant Operations

\_\_\_\_\_  
Health, Safety and Environment

Harry Murphy 3/11/83  
Quality Assurance

\_\_\_\_\_  
Training

J.T. WEBSTER B.M. Hanford  
End Function CONSTR. (NOT AVAILABLE FOR SIGNATURE)

\_\_\_\_\_  
End Function

Sheldon A. Blum  
Blum 2/11/83

B. K. Schroeder  
Approval Authority



Basalt Waste Isolation Project  
Exploratory Shaft - Phase I  
DRILLING PROGRAM  
For 144 Inch Surface Hole

I. Activities Prior to Commencement of Drilling Operations

- A. Pick up Government furnished tools and drilling assembly, consisting of the following:
1. Mandrel with integral reamer-stabilizer, dressed with:
    - a.) 144 inch bit body w/cutters (bolted on after mandrel is dressed).
      - (1). A crows-foot will be installed in the bit per the attached sketch (Exhibit 1).
    - b.) Reamer-stabilizer rollers with brackets and spacers to full hole size.
    - c.) 21-22 ea. 60" diameter donuts.
    - d.) Top (spool type) stabilizer dressed with stabilizers, rollers and brackets to 1/2" under hole diameter.
    - e.) 3-4 ea. 60" diameter donuts on top of top stabilizer.
    - f.) Donut hold-down clamp, bolted and safety-cabled.
  2. One joint of drill pipe. It may be necessary to use 1 or 2 pup joints in lieu of a 30 ft. joint.
  3. Air string (Exhibit 2). Air line joints will be locked.

4. Kelly w/saversub.
5. Steel line measurements of all of the above will be made and recorded. (All drill pipe used during the drilling operation will be measured as above as it is picked up for use).

General Notes: All bolts (bit body, stabilizer brackets and rollers) shall be made up to Drilco-specified torques, and nuts locked with bar stock. (Drilco representative on site during initial installation).

Tool joints will be made up to Drilco-specified torques, using Varco power tong.

All of the above will be verified by the Drilling Advisor and recorded.

- B. Physically check bottom of existing hole for junk. Remove same.
- C. Run drilling assembly to bottom of dry hole. Stop at intervals and slowly (manually) rotate assembly to check corrugated metal pipe liner for alignment, clearances, out-of-roundness, etc.  
Trip out.
- D. If pre-existing 100 ft. shaft is satisfactory, fill hole with mud.
- E. Go in hole with assembly, run Sperry-Sun surveys as directed.
- F. Check all pertinent rig instrumentation (weight indicators, etc.).

G. Continue rig-up of G.F.E. (swivel, rotary hoses, etc.). Timing of this is coincident with dead time in above-listed operations.

H. Break circulation and condition mud.

II. Drilling Operation, -100 ft ± to -180 ft ± (-180 ft. is anticipated static water level).

A. Employing reverse circulation with air assist, pattern bit slowly and carefully as hole conditions warrant.

1. While patterning bit, bit RPM shall not exceed 2-8 RPM and weight on bit held from 10,000 lb. to not exceed 30,000 lb.

2. Continue drilling with light weights on bit and slow RPM until mandrel is buried in new formation.

a.) Check drilling condition and fluid returns for presence of cement (which would indicate sluffing of cement from around bottom of CMP liner).

b.) After drilling approximately 15 ft. of new hole, pull drilling assembly up into CMP casing; shut down circulation for approximately 2 hours; trip in, check hole bottom for slough.

c.) Repeat above after drilling 35-40 ft. <sup>perry Sun</sup> Surveys at bottom of casing and <sup>every</sup> 30 ft. ± below casing <sup>to total depth</sup>

d.) RPM and weights will be varied as formation changes dictate. Although not anticipated, careful watch will be maintained for the presence of large boulders that may affect hole alignment.

3. Continue drilling to -180 feet.
4. After approximately 100 rotating hours, unless earlier as dictated by surface indications, the drilling assembly will be pulled out of the hole and completely checked. This includes, but is not limited to, the bit body, cutters, stabilizers, dowel pins, bolts, etc. At this time, and each time the assembly is tripped, all bolts will be visually <sup>physically</sup> checked for integrity. All bolts in the assembly will be magnafluxed before re-using.

### III. Drilling -180 ft to -640 ± ft.

- A. Drilling will continue as outlined under 'A' above. Weight on bit and RPM may be varied as hole condition permits. However, the weight on the bit shall not exceed 60% of the combined buoyed weight of the drilling assembly, and rotary torque shall not exceed 60,000 ft. lbs.
- B. Upon completion of drilling with 144" bit, condition mud for running casing.

- C. Run round-trip Sperry-Sun survey.
- D. Trip out of hole.
- E. Run caliper logs and other logs as directed.
- F. Lay down tools, rig up to run casing.

IV. General Notes:

1. Should, at any time during drilling operations, severe loss of circulation occur that does not respond to lost circulation material treatment as outlined in the Mud Program, it will be necessary to pull the drilling assembly from the hole and set a cement plug. Details of this operation are covered under the cementing program.
2. Records and Submittals  
Records and observations will be kept and submitted in accordance with the approved Construction Specifications.



JOB TITLE M& BWIP CONTRACT NO. 3056  
 DESCRIPTION 3 1/2" INNER AIR STRING  
 SHEET NO. 1/1  
 MADE BY [Signature] CHECKED BY \_\_\_\_\_ DATE 1-26-83

# EXHIBIT 2

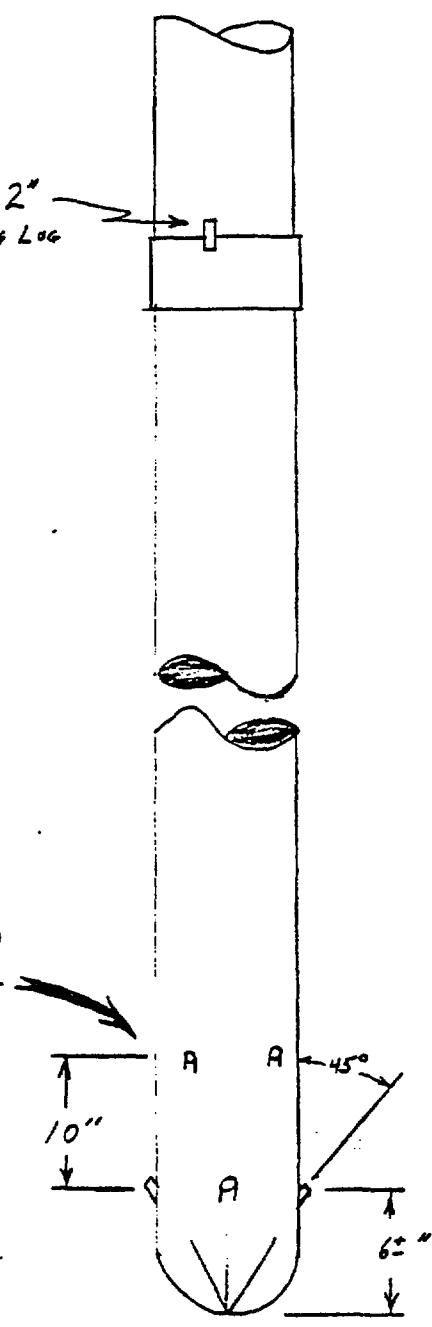
## MATERIALS:

3 1/2" O.D. LINER PIPE  
 7.7 lb/ft  
 3.068" ID

REQUIRED:  
 52 - 7/16" I.D. JETS  
 TO EQUAL AREA AND  
 MINIMIZE FRICTION LOSSES

1/4" x 1" x 2"  
 LOCKING LOG

4 - 7/16" JETS/ROW @ 90° SPACING  
 10" TYP. BETWEEN ROWS  
 OFFSET JETS 45° BETWEEN ROWS  
 JETS ORIENTED 45° TOWARD  
 ANNULUS



PIPE SLOTTED AND  
 WELDED CLOSED

NOT TO SCALE

MAY BE MODIFIED AS FIELD CONDITIONS REQUIRE



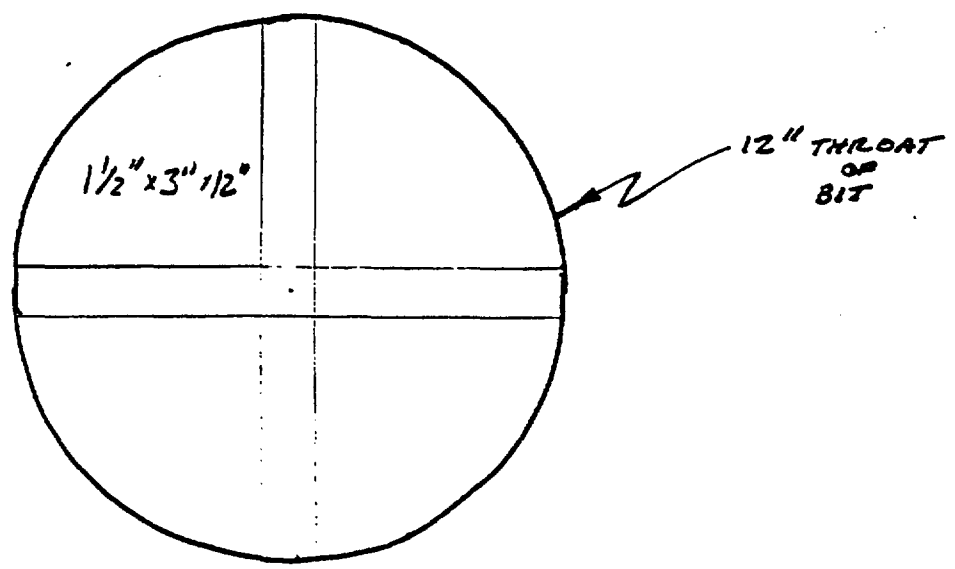
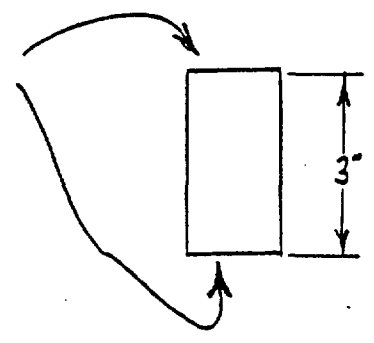
JOB TITLE M-K BWIP CONTRACT NO. 3055  
 DESCRIPTION LANDING BAFFLE FOR SPERRY-SUN INSTRUMENT (CROWS-FOOT WELDED IN THROAT OF BITS) SHEET NO. 1/1  
 MADE BY R CHECKED BY \_\_\_\_\_ DATE 1-26-83

MATERIAL:

EXHIBIT 1

MILD STEEL STRIPS 12" x 1/2" x 3" (±)

HARD SURFACE MATERIAL ON TOP AND BOTTOM



CROWS FOOT TO BE WELDED  
LEVEL IN THROAT OF BIT TO MEET  
REQUIREMENTS OF  
SPERRY-SUN TOOL

NOT TO SCALE

MAY BE MODIFIED AS FIELD CONDITIONS REQUIRE

# Rockwell Hanford Operations

<b>SUPPORTING DOCUMENT</b>		Number	Rev. Ltr./ Chg. No.	Page 1 of 20																																											
PROGRAM: Exploratory Shaft - Phase I		SD-BWI-AR-002	0-0																																												
Document Title: Morrison-Knudsen Co., Inc. Basalt Waste Isolation Project Exploratory Shaft Phase I Drilling Mud Program for 144-Inch Surface Hole		Baseline Document <input type="checkbox"/> Yes <input checked="" type="checkbox"/> No																																													
Key Words: Drilling Mud Program - 144' Inch Surface Hole		WBS No. or Work Package No. LF24 CEI 014		Date 2/11/83																																											
Abstract		Prepared by (Name and Dept. No.) <i>M. J. Lauterbach</i> M. J. Lauterbach																																													
<p>This document outlines the drilling mud program project.</p> <div style="border: 1px solid black; padding: 5px; text-align: center;"> <p><b>INFORMATION COPY</b></p> <p>THIS COPY WILL NOT BE REPLACED AND MAY BE CHANGED WITHOUT NOTICE</p> </div> <p>*Initiated by Morrison-Knudsen Co., Inc., used by Rockwell.</p>		See Page 2 for Approvals																																													
		<table border="1"> <thead> <tr> <th>* Distribution</th> <th>Name</th> <th>Mail Address</th> </tr> </thead> <tbody> <tr> <td>*</td> <td>Rockwell</td> <td></td> </tr> <tr> <td>*</td> <td>M. T. Black</td> <td>PBB/700</td> </tr> <tr> <td>*</td> <td>H. W. Brandt</td> <td>PBB/700</td> </tr> <tr> <td>*</td> <td>R. W. Carlson</td> <td>PBB/700</td> </tr> <tr> <td>*</td> <td>M. F. Nicol</td> <td>PBB/700</td> </tr> <tr> <td>*</td> <td>J. V. Mohatt</td> <td>PBB/700</td> </tr> <tr> <td>*</td> <td>P. J. Reder <i>PR</i></td> <td>PBB/700</td> </tr> <tr> <td>*</td> <td>W. F. Todish</td> <td>PBB/700</td> </tr> <tr> <td colspan="3"> </td> </tr> <tr> <td>*</td> <td>DOE R. D. Hudson</td> <td>PBB/700</td> </tr> <tr> <td colspan="3"> </td> </tr> <tr> <td>*</td> <td>M-K F. C. Larvie</td> <td>PBB/700</td> </tr> <tr> <td colspan="3"> </td> </tr> <tr> <td>*</td> <td>Records Retention (2)</td> <td></td> </tr> </tbody> </table>			* Distribution	Name	Mail Address	*	Rockwell		*	M. T. Black	PBB/700	*	H. W. Brandt	PBB/700	*	R. W. Carlson	PBB/700	*	M. F. Nicol	PBB/700	*	J. V. Mohatt	PBB/700	*	P. J. Reder <i>PR</i>	PBB/700	*	W. F. Todish	PBB/700				*	DOE R. D. Hudson	PBB/700				*	M-K F. C. Larvie	PBB/700				*
* Distribution	Name	Mail Address																																													
*	Rockwell																																														
*	M. T. Black	PBB/700																																													
*	H. W. Brandt	PBB/700																																													
*	R. W. Carlson	PBB/700																																													
*	M. F. Nicol	PBB/700																																													
*	J. V. Mohatt	PBB/700																																													
*	P. J. Reder <i>PR</i>	PBB/700																																													
*	W. F. Todish	PBB/700																																													
*	DOE R. D. Hudson	PBB/700																																													
*	M-K F. C. Larvie	PBB/700																																													
*	Records Retention (2)																																														
<div style="border: 1px solid black; padding: 5px;"> <p>THIS DOCUMENT IS A ROCKWELL SUPPORTING DOCUMENT FOR USE BY ROCKWELL, ITS AUTHORIZED SUBCONTRACTORS, AND THE DEPARTMENT OF ENERGY</p> </div> <p style="font-size: 2em; font-weight: bold; margin-left: 20px;">BASALT</p>		<p>Initial Release Stamp</p> <div style="border: 1px solid black; border-radius: 50%; width: 40px; height: 40px; display: flex; align-items: center; justify-content: center; margin: 0 auto;">10</div> <p style="font-size: 1.2em; font-weight: bold; margin: 5px 0;">OFFICIALLY RELEASED</p> <p style="font-size: 1.2em; margin: 5px 0;">1983 FEB. 11 PM 3:47</p>																																													

Rockwell Hanford Operations

SUPPORTING DOCUMENT

Number  
SD - BWI - AR - 002

Page  
2

Approvals

\* Distribution Name Mail Address

\_\_\_\_\_  
Program Office

\_\_\_\_\_  
Research and Engineering

\_\_\_\_\_  
Plant Operations

\_\_\_\_\_  
Health, Safety and Environment

*J.T. Murphy* 2/11/83  
Quality Assurance

\_\_\_\_\_  
Training

*J.T. WEBSTER* *Rmyhana for*  
End Function *CONSTR.* *NOT AVAILABLE FOR SIGNATURE*

\_\_\_\_\_  
End Function

\_\_\_\_\_

*Shirley A. Blehm*  
*B. K. Schroeder* 2/11/83

B. K. Schroeder  
Approval Authority

February 8, 1983

REV. 0-0

MORRISON-KNUDSEN COMPANY, INC.

BASALT WASTE ISOLATION PROJECT

EXPLORATORY SHAFT PHASE I

DRILLING MUD PROGRAM

FOR 144 INCH SURFACE HOLE

Robert R. Rommel  
ENGINEERING MANAGER

Feb 8, 1983  
DATE

J. J. ...  
CONSTRUCTION MANAGER

Feb 8 1983  
DATE

W. D. Small  
QA MANAGER

Feb 8, 1983  
DATE

Orville Jones  
SAFETY MANAGER

Feb 9, 1983  
DATE

ROCKWELL HANFORD OPERATIONS:

B. Schwandt

2/11/83  
DATE

Basalt Waste Isolation Project  
Exploratory Shaft Phase I  
DRILLING MUD PROGRAM  
For 144 Inch Surface Hole

I. GENERAL STATEMENTS

- A. Trained mud engineering personnel with large diameter hole experience will be provided to furnish mud analyses and recommendations each day. At least two mud checks daily will be posted <sup>by the mudman</sup> on the rig floor, in the drilling advisor's trailer, and in the M-K office on location. All recommendations for mud treatments conducted each tour for drilling fluids system makeup and maintenance will be written on each mud report (see attached Drill Mud Report form, Testing Procedures and Mud Program Specifications - exhibits 1, 2 and 3). This information will also be conveyed verbally to the M-K drilling advisor, and Geodril's rig pusher and rig crews.
- B. All mixing of mud and materials will be supervised by the mud engineer on location. He will advise the M-K drilling advisor verbally, and in writing, as to the procedures to be followed and the quantities of material to be mixed. The drilling advisor will convey this information to the rig personnel *for execution*.
- C. The M-K safety program and procedures will be strictly observed, with particular emphasis on those operations involving the handling

of caustic *material*.

- D. Upon request of M-K, a qualified Mud Engineer shall be on site 24 hours a day during surface hole drilling and on call during casing installation and cementing.
- E. A Corrosion Coupon will be attached to the air lift tube stinger, and onto the bit body. These will be removed and replaced with new Corrosion Coupons after approximately each 100 operating hours or at bit changes. The removed coupons will be evaluated, and if corrosion rates prove excessive, then based on the degree of scale or damage, a blend of materials will be recommended for the specific problem.
- F. Desanders will be utilized while tripping and/or while circulating to aid in conditioning mud, or as a subsidiary mud cleaning tool when mud conditions dictate.
- G. A dragline will be utilized to remove cuttings from pit bottoms. This will be the primary cuttings removal system. *the cuttings will be disposed of in the trash pit.*
- H. A water line will be an adjunct to the blooie line and fresh water will be used to help reduce mud viscosity to facilitate cuttings

settling. This water line can and will be utilized in any or each pit segment as required.

II. ACTIVITIES BEFORE COMMENCEMENT OF DRILLING OPERATIONS

A. Line Ponds With Bentonite.

1. Start with pit #2.
2. Will require use of approximately 93-2400# bags to line ponds (lining both pits is estimated to require approximately 3-4 days).

B. Commence Mud Mixing

1. Mix in 600 bbl batches.
2. Mix first 4,000 bbls at approximately 50 viscosity to help seal ponds (use gel and caustic).
3. Next mix approximately 30,000  $\pm$  bbl's at approximately 40 viscosity (use gel, caustic and lost circulation materials - L.C.M.). This operation is estimated to require 6-10 days.

III. DRILLING INTERVAL 104 FT. TO 180 FT. (180 FT. IS ANTICIPATED TOP OF WATER TABLE).

- A. Mix 40 viscosity mud to attached specification, using gel, caustic and L.C.M. (Exhibit 3).
- B. Mix mud additives to maintain proper specifications.
- C. Mud specifications can and will be varied if hole conditions dictate.

IV. DRILLING INTERVAL 180 FT. TO 640 FT.

- A. Continue maintaining mud system and properties as per above interval.
- B. Additional water dilution may be required to maintain proper weight ranges.
- C. Mud specifications can and will be varied if hole conditions dictate.

V. CONDITIONING MUD FOR RUNNING CASING

- A. Maintain mud specifications as per previous interval.
- B. Circulate approximately 5 hours at total depth.
- C. Short trip drill pipe and assembly and check for fill.
- D. If hole conditions are satisfactory, trip drilling assembly from

hole and run logs.

- E. If downhole problems become evident under (C) above, mud properties may be adjusted to provide additional wall support.

Should minor seepage occur while drilling surface hole, additional L.C.M. will be carried in mud system. Should total loss circulation occur, pull out of hole and run in with 4½ inch drill pipe and set cement plug as described in the cementing program. When drilling out cement plugs, additions of calcium sequesters, lignite and water will be needed to maintain proper mud properties.



P. O. BOX 6504  
HOUSTON, TEXAS 77005



MAGCOBAR GROUP  
Dresser Industries, Inc.

DRILLING MUD REPORT NO.	
DATE _____ 19__	DEPTH _____
PRESENT ACTIVITY _____	
SPUD DATE _____	

OPERATOR _____	CONTRACTOR _____	RIG NO. _____
REPORT FOR _____	REPORT FOR _____	SECTION, TOWNSHIP, RANGE _____
WELL NAME AND NO. _____	FIELD OR BLOCK NO. _____	COUNTY, PARISH OR OFFSHORE AREA _____
		STATE / PROVINCE _____

DRILLING ASSEMBLY			CASING		MUD VOLUME (BBL)		CIRCULATION DATA			
BIT SIZE	TYPE	JET SIZE	SURFACE SET @	FT.	HOLE	PITS	PUMP SIZE	X	IN.	ANNULAR VEL. (FT/MIN)
DRILL PIPE SIZE	TYPE	LENGTH	INTERMEDIATE SET @	FT.	TOTAL CIRCULATING VOLUME		PUMP MAKE, MODEL	ASSUMED EFF. %		CIRCULATION PRESSURE (PSI)
DRILL PIPE SIZE	TYPE	LENGTH	INTERMEDIATE SET @	FT.	IN STORAGE	WEIGHT	BBL/STK	STK/MIN		BOTTOMS UP (MIN)
DRILL COLLAR SIZE		LENGTH	PRODUCTION OR LINER SET @	FT.	MUD TYPE		BBL/MIN	GAL/MIN		TOTAL CIRC. TIME (MIN)

MUD PROPERTIES			MUD PROPERTY SPECIFICATIONS				
☞ SAMPLE FROM (1)	<input type="checkbox"/> F.L.	<input type="checkbox"/> PIT	<input type="checkbox"/> F.L.	<input type="checkbox"/> PIT	WEIGHT	VISCOSITY	FILTRATE
☞ TIME SAMPLE TAKEN (2)					☞ RECOMMENDED TOUR TREATMENT ☞		
☞ FLOWLINE TEMPERATURE °F (3)					MUD CONTAINS	TOUR TREATMENT	
☞ DEPTH (ft) (4)					<input type="checkbox"/> Magcobar	SX	
☞ WEIGHT <input type="checkbox"/> (Ppg) <input type="checkbox"/> (lb/cu.ft) <input type="checkbox"/> Sp. G (5)					<input type="checkbox"/> Magcogel	SX	
☞ FUNNEL VISCOSITY (SEC/qt) API @ °F (6)					<input type="checkbox"/> Salt Gel	SX	
☞ PLASTIC VISCOSITY cP @ °F (7)					<input type="checkbox"/> Spersene	SX	
☞ YIELD POINT (lb/100ft²) (8)					<input type="checkbox"/> XP-20	SX	
☞ STRENGTH (lb/100ft²) 10 SEC/10 MIN. (9)					<input type="checkbox"/> TannAlthin	SX	
☞ FILTRATE API (CM³/30 MIN) (10)					<input type="checkbox"/> Caustic Soda	SX	
API HTHP FILTRATE (CM³/30 MIN) @ °F (11)					<input type="checkbox"/> My-Lo-Jel	SX	
☞ CAKE THICKNESS (32nd IN. API/HTHP) (12)					<input type="checkbox"/>		
☞ SOLIDS CONTENT (% BY VOL) <input type="checkbox"/> CALCULATED <input type="checkbox"/> RETORT (13)					<input type="checkbox"/>		
☞ LIQUID CONTENT (% BY VOL) OIL/WATER (14)					<input type="checkbox"/>		
☞ SAND CONTENT (% BY VOL) (15)					<input type="checkbox"/>		
☞ METHYLENE BLUE CAPACITY (lb/bbl EQUIV CM³/CM³ MUD) (16)					<input type="checkbox"/>		
☞ PH <input type="checkbox"/> STRIP <input type="checkbox"/> METER @ °F (17)					<input type="checkbox"/>		
☞ ALKALINITY MUD (PM) (18)					<input type="checkbox"/>		
☞ ALKALINITY FILTRATE (P1/M) (19)					REMARKS—GIVE OPERATION, DEPTH, AND NATURE OF ANY PROBLEM ENCOUNTERED		
ALTERNATE ALKALINITY FILTRATE (P1/P2) (20)							
☞ CHLORIDE (Mg/L) (21)							
☞ TOTAL HARDNESS AS CALCIUM (Mg/L) (22)							

PRODUCT INVENTORY	STARTING INVENTORY	RECEIVED	LAST 24 HR.	CLOSING INVENTORY	COST LAST 24 HR.

EQUIPMENT			
SIZE	HRS./TOUR	SIZE	HRS./TOUR
Centrifuge		Desilter	
Degasser		Shaker	
Desander		Other	
DAILY COST		CUMULATIVE COST	

MAGCOBAR ENGINEER _____	HOME ADDRESS _____	PHONE _____
MOBILE UNIT _____	WAREHOUSE LOCATION _____	PHONE _____

Exhibit 2

TESTING PROCEDURES  
FROM MAGCOBAR DRILLING FLUIDS HANDBOOK

5. Page 1-1 - 1.1.1, 1.1.1.1, 1.1.1.2 - DENSITY (MUD WEIGHT)  
Calibrate mud scales filled with fresh water should balance @ 8.33 #/gal. @ 70<sup>o</sup>F. If not adjust screw or lead shot at end of graduated arm as required. Weigh the drilling fluid and record as ppg, #/ft<sup>3</sup>, or SG.  
For conversions to Specific Gravity refer to 1.1.1.2.
  
6. See Glossary - Page 15-14 - MARSH FUNNEL VISCOSITY IN CENTIPOISE
  
7. Page 1-8 - 1.1.3.2 - PLASTIC VISCOSITY IN CENTIPOISE  
Take the 600 RPM reading - 300 RPM reading on the V.G. meter at 115<sup>o</sup>F.  
See Glossary - Page 15-17 - Plastic Viscosity definition.
  
8. Page 1-8 - 1.1.3.2 - YIELD POINT IN LBS. PER 100 FT<sup>2</sup> =  
300 RPM reading - Plastic Viscosity  
See Glossary - Page 15-25 - Yield Value definition.
  
9. Page 1-8 - 1.1.3.1 - GEL STRENGTH DETERMINATION  
PROCEDURE:
  1. Stir sample at 600 RPM for approximately 15 seconds.
  2. Wait 10 seconds.

3. Read maximum deflection of dial by turning knob counter clockwise slowly and steadily (for 2 speed) or using 3 RPM (for 6 speed). This is the 10 sec. gel strength in lbs. per 100 ft<sup>2</sup>.
4. Wait 10 minutes.
5. Repeat step 3. This is the 10 mins. gel strength, lbs per 100 ft<sup>2</sup>.

See Glossary - Page 15-10 - Gel Strength definition.

10. Page 1-13 - 1.1.5.1 - FILTRATE API SPECIFICATIONS

Filter loss is conducted at surface temp @100 psi pressure and recorded as the cc's lost in 30 min. or double the cc's lost in 7½ min.

See Glossary - Page 15-9 - Definition of Fluid Loss.

12. FILTER CAKE THICKNESS - measured in 1/32nds of an inch.

13 &14 Page 1-93 - 1.1.9.1 - SOLIDS AND LIQUID CONTENT

PROCEDURE

1. Disassemble retort assembly and fill sample cup almost level full of the fluid to be tested. Put sample cup cover in place firmly, squeezing out excess fluid to obtain the exact 20 cc volume required. Clean spillover from cover and threads. (If threads are coated with silicone grease, it will prevent sticking).

2. Lift cover slightly and slide off so that fluid adhering to bottom surface will be scraped back into the sample cup.
3. To prevent boil over, put 5 to 10 drops of the "liquid steel wool" on top of the mud and attach the expansion chamber.
4. Select correct heater assembly for the available voltage and screw into top of expansion chamber. Keep assembly upright so that mud does not slosh into the drain tube.
5. Insert drain tube into hole at end of condenser, seating firmly. Percentage graduated cylinder should be clipped in place to catch condenser.
6. Plug in the correct condenser cord to the power supply and keep power on until distillation stops, which should occur in 15 to 25 minutes depending on the characteristics of oil content, solids content and atmosphere around the unit.
7. Read the percentage of water, oil and solids directly from the graduate. A drop or two of aerosol solution will help define the oil-water interface.
8. At end of test, grasp rubber covered connector just above heater and separate retort assembly from condenser. Handling the hot retort by means of the connector cord, dip in water to cool. (Plug is waterproof and may be immersed completely).
9. Most of the solids remaining in retort will adhere to the heater where removal is easy. Use spatula to scrape out cup and expansion chamber. Run short length of pipe cleaner through condenser hole and retort drain tube to remove oil residue.

See Glossary - Page 15-21 - Definition of Solids Concentration or Content.

15. Page 1-93 - 1.1.8 - SAND CONTENT

PROCEDURE

1. Fill the glass measuring tube to the indicated mark with mud. Add water to the next mark. Close the mouth of the tube and shake vigorously.
2. Pour the mixture onto the screen, add more water to the tube, shake, and again pour onto the screen. Repeat until the wash water is clear. Wash the sand retained on the screen to free it of any remaining mud.
3. Fit the funnel down over the top of the sieve. Invert slowly and insert the tip of the funnel into the mouth of the glass tube. Wash the sand into the tube by means of a fine spray of water. Allow the sand to settle. From the graduations on the tube, read the percent by volume of sand.

See Glossary - Page 15-19 - Definition of Sand Content.

16. Page 1-96 - 1.1.10.1 - METHYLENE BLUE CAPACITY

PROCEDURE

1. Add 1 ml of mud (or suitable volume of mud to require 2 to 10 ml of reagent) to 10 ml of water in the Erlenmeyer flask. Add 15 ml of 3% hydrogen peroxide and 0.5 ml of 5 N sulfuric acid solution and mix by swirling before heating. Boil gently for 10 minutes. Dilute to about 50 ml with water.

2. Add methylene blue solution, 0.5 ml at a time, from the buret or pipet to the flask. After each addition, insert rubber stopper and shake contents of the flask for about 30 seconds. While the solids are still suspended, remove a drop from the flask with a glass rod and place on filter paper. The endpoint of the titration is reached when the dye appears as a greenish-blue ring surrounding the dyed solids.
3. When the greenish-blue tint spreading from the spot is detected, shake the flask an additional 2 minutes and place another drop on the filter paper. If the greenish-blue ring is again evident, the endpoint has been reached. If the ring does not appear, continue as before until a drop taken after shaking 2 minutes shows the greenish-blue tint.
4. Record the ml of methylene blue solution used.

Page 1-97 - 1.1.10.2 - CALCULATION

$$\text{Cation exchange capacity} = \frac{\text{ml of methylene blue}}{\text{ml of mud}}$$

$$\text{Methylene blue capacity (Bentonite equiv.), lb/bbl} = \text{CEC} \times 5$$

17. Page 1-13 - 1.1.4 - pH PROCEDURE

PROCEDURE

1. Follow instructions on the instrument to put the amplifier into operation and standardize the meter with the proper buffer solution.
2. Wash the tips of the electrodes, gently wipe dry, and insert them

into the mud. Stir the mud about the electrodes by rotating the container. CAUTION: Do not allow the electrodes to rub the side of the container.

3. Measure the pH of the mud according to the directions. After the meter reading becomes constant, which may require from 30 seconds to several minutes, record the pH.
4. Report the pH of the mud to the nearest 0.1 unit.

See Glossary - Page 15-16 - Definition of pH.

18. Page 1-21 - 1.1.7.1 - MUD ALKALINITY

PROCEDURE:

1. Measure 1 ml of mud into the titration vessel using the syringe or the serological pipet.
2. Dilute the mud sample with 25 to 50 ml deionized water.
3. Add 4 or 5 drops of phenolphthalein indicator.
4. While stirring, titrate rapidly with 0.02 N acid or 0.1 N acid until the pink color disappears.

NOTE: If the sample is so colored that the color change of the indicator is masked, the endpoint is taken when the pH drops to 8.3 as measured with the glass electrode pH meter.

5. Report the phenolphthalein alkalinity of the mud,  $P_m$  as the number of milliliters of 0.02 N (N/50) acid required per milliliter of mud.

NOTE: If 0.1 N acid is used,  $P = 5 \times$  (milliliters of 0.1 N acid per milliliter of mud).

19. Page 1-20 - 1.1.7.1 - FILTRATE ALKALINITY

PROCEDURE

1. Measure one or more millileters of filtrate into the titration vessel using the syringe or seriological pipet.
2. Add two or three drops of phenolphthalein indicator solution.
3. If the indicator turns pink, add 0.02 N acid, drop by drop using a graduated pipet with stirring, until the pink color just disappears.

NOTE: If the sample is so colored that the color change of the indicator is masked, the endpoint is taken when the pH drops to 8.3 as measured with the glass electrode pH meter.

4. Report the phenolphthalein alkalinity of the filtrate,  $P_f$ , as the number of ml of 0.02 N (N/50) acid required per ml of filtrate.

21. Page 1-43 - 1.1.7.8 - CHLORIDE DETERMINATION

PROCEDURE

1. Measure one or more milliliters of filtrate into the titration vessel. Add 2 or 3 drops of phenolphthalein. If the indicator turns pink, add acid drop by drop from a pipet, with stirring, until the color is discharged. If the filtrate is deeply colored, add an additional 2 ml of 0.02 N sulfuric or nitric acid and stir. Then add 1 g of calcium carbonate and stir.
2. Add 25 to 50 ml deionized water and 5 to 10 drops of potassium chromate indicator. While stirring continuously, add the silver nitrate solution drop by drop from a pipet, until the color changes

from yellow to orange-red and persists for 30 seconds.

3. Record the milliliters of silver nitrate solution required to reach the endpoint. If over 10 ml of silver nitrate solution are used, repeat the test with a smaller sample of filtrate.

CALCULATION:

$$\text{mg/l Cl} = \frac{\text{ml of 0.0282 N silver nitrate} \times 1000}{\text{ml of filtrate}}$$

22. Page 1-36 - 1.1.7.6 - TOTAL HARDNESS AS CALCIUM

PROCEDURE

1. Add approximately 20 ml of deionized water to titration vessel.
2. Add 1 or 2 ml of the water or filtrate to be tested.

NOTE: The endpoint is occasionally difficult to see in the dark colored filtrates. Reduce the sample size to ½ ml if the endpoint cannot be seen with a 1 ml sample or follow procedure listed under determination of total hardness, calcium and magnesium in dark filtrates.

3. Add 1 ml of Strong Buffer solution.
4. Add 3 drops of Manver Indicator and mix with a stirring rod. A wine red color will develop if hardness is present.
5. Using a pipet, titrate with Standard Versenate Solution, stirring continuously, until the sample turns to blue (or green for dark colored filtrates) with no under tint or red remaining. Record the number of ml of Standard Versenate Solution used.

CALCULATION

$$\text{Total Hardness as calcium, mg/liter} = \frac{\text{ml of Standard Versenate} \times 400}{\text{ml of sample}}$$

## Exhibit 3

MUD PROGRAM SPECIFICATIONS

INTERVAL: FLUID TYPE: Non-dispersed Magcogel system.

0'-640'

144" Bit

PROPERTIES:\*

Weight:	8.7-9.5 ppg
Viscosity:	36-44
PV/YP:	10-15/4-12
Gels:	2-4/8-12
pH:	11-11.5
Solids:	3-5%
Fluid Loss:	N/C

PROCEDURE:

Build a system using 10-15 #/bbl Magcogel and 1-2 #/bbl Caustic Soda or Lime/Caustic combination as needed to maintain specified properties. Lost circulation material will be carried in the system.

POTENTIAL PROBLEMS:

(with recommendations)

1. Solids Buildup - Control by adding water to flowline. The use of a desander would be very beneficial. If the solids and/or weight exceed recommended limits, 1-3 #/bbl Tannathin may be

INTERVAL:            POTENTIAL PROBLEMS (cont'd)

0'-640'

added to maintain mud properties.

144" Bit

2. Lost Circulation - Maintain mud weight as low as possible compatible with hole condition. Maintain viscosity to control seepages. Lost circulation material in active system as required. If this fails, set cement plug.
3. Unconsolidated Formations - (Caving)  
Maintain viscosity necessary to stabilize hole. If running sands become a serious problem, raise viscosity as needed with additions of Magcogel. If this is unsuccessful, set a cement plug.
4. Tight Hole - Introduce fluid loss control with Magco-Ploy Pac or a Magco-Poly Pac and Tannathin combination to build a thin tough wall cake. Concentrations of 1/2 to 1#/bbl Poly Pac and 1 to 3 #/bbl Tannathin will be required if it becomes necessary to control fluid loss.

\* All properties and product concentrations are preconstruction parameters.  
Hole conditions may dictate changes in these ranges.

DATE: 2/17/83

Morrison-Knudsen Company, Inc.  
Peoples Bank Building  
1100 Jadwin Avenue  
Richland, Washington 99352

- For Information
- For Comment
- For Approval
- As Noted

TO:

Mr. O. L. Olson  
Project Manager BWIPO  
U. S. Department of Energy  
Peoples Bank Building  
Richland, WA 99352

TO:

Mr. H. B. Dietz  
Rockwell Hanford Operations  
Peoples Bank Building  
1100 Jadwin Ave.  
P. O. Box 800  
Richland, WA 99352

TO:

Mr. S. C. Paul  
U. S. Department of Energy  
Richland Operations Office  
825 Jadwin Ave.  
P. O. Box 550  
Richland, WA 99352

SUBJECT: BASALT WASTE ISOLATION PROJECT, CONTRACT DE-AC06-83RL10343  
TRANSMITTAL OF INFORMATION EXPLORATORY SHAFT CONSTRUCTION PHASE I  
TRANSMITTAL NO. XM-102

Transmitted herewith is the below listed document(s)

Telecon Record No. \_\_\_\_\_

Meeting Minutes No. \_\_\_\_\_

Report \_\_\_\_\_

Other Quality Assurance Plan for 144" Diameter Surface Hole Drilling(Updated)  
Please refer to XM-87, dated 2/11/83, additions E & F have been made to  
Page 1

DISTRIBUTION

Rockwell

H.W. Brandt	1 w/att
C.C. Bohrn	1 w/att
J.A. Hoogendoorn	1 w/att
M.F. Nicol	1 w/att
Rec. Ret.	2 w/atts

DOE

R.D. Hudson 1 w/att

M-K

J.A. Curl	1 w/att
R.R. Rommel	1 w/att
W.D. Small	1 w/att
<del>file</del>	1 w/att

Transmitted by: \_\_\_\_\_

*F.C. Larvie*  
F.C. Larvie  
Project Director

Geodril

G. Alleman  
w/att

Sperry-Sun

R. Johnson  
w/att

Magcobar

V. Hendrix  
w/att

## QUALITY ASSURANCE PLAN

### 144" DIAMETER SURFACE HOLE DRILLING

#### I. Purpose

This document describes the data to be accumulated in the Quality Assurance files during the drilling of the 144" diameter surface hole. This hole drilling is Quality Level II and III.

#### II. Responsibilities

- A. The M-K BWIP QA Manager is responsible to maintain the files of required accumulated data covering the drilling of the 144" diameter surface hole. This information shall be as required in the Drilling Program for the 144 inch surface hole.
- B. The Mud Engineer is responsible to provide the M-K BWIP QA Manager with the mud test data on a daily basis.
- C. The Drilling Field Manager is responsible to provide the M-K BWIP QA Manager with copies of the daily records of the drill rig operation.
- D. The Sperry-Sun Manager is responsible to provide the M-K BWIP QA Manager with the records of the down-hole surveys.
- E. The M-K BWIP QA Manager shall verify, by initials and dates, all submitted records are complete and legible.
- F. The M-K BWIP QA Manager shall perform and document periodic surveillances of the drilling operations to assure that specific requirements are being carried out.

#### III. Information Required

- A. Drill Rig Information

1. The IADC Daily Drilling Report form shall be kept as the standard daily report. The original and two copies shall be submitted daily to the Owner. The general remarks section shall contain an accurate record of work conditions, work performed and time required for all work to nearest quarter hour. Safety related activities and events shall also be reported on a daily basis.
2. Automatic drilling recorders shall be used to measure the rate of penetration, drilling weight, rpm and torque. All rig operations such as depth, round trip time, lost circulation intervals, equipment breakdown, mud conditioning time, and other important drilling data shall be clearly identified on the recorder charts. An original and one copy of the drilling recorder charts shall be submitted daily to the Owner.
3. Bit and cutter records shall be maintained daily and filed in the field office. A complete record shall be furnished to the Owner weekly. Records shall show bit type and serial number, footages, depths, rotary speeds, bit weights, cutter serial numbers, replacements, repairs, etc.
4. Accurate pipe tallies, including type, usage, measurements, etc., shall be provided by the Subcontractor and be available at the drill site for inspection at all times. Copies of steel line measurements of pipe and casing shall be furnished as directed by the Contractor.

The Contractor shall keep an accurate record of the total number of joints of all drill pipe, drill collars and tubing on location at all times.

5. The Contractor will be responsible for the inventory control of all Owner-furnished and reimbursable items.
6. Compressor records showing operating hours, discharge pressures, and air volumes on a continuous record shall be submitted to the Owner with the daily drilling report.
7. Accurate records of water volumes and mud consumed or lost shall be submitted with the daily drilling reports.

B. Mud Information

1. Trade name where applicable, and published performance characteristics for all drilling fluid additives supplied to the worksite.
2. A complete inventory control list of all drilling fluid additives delivered, used and returned.
3. Complete daily records of job site examinations shall be maintained and submitted containing all of the data obtained from the measurements and tests listed herein as well as an inventory of additives used. See Exhibit I.
4. A program of expected additives used.
5. The testing procedures to be employed are described in the 'Drilling Mud Program for the 144 Inch Surface Hole'.

C. Directional Survey Information

1. The results of the directional surveys to be run every 30 feet of hole advanced shall be provided by the Sperry-Sun Manager as delineated in the Directional Survey Procedure.

QA Surveillance Activities

Drilling 144" Surface Hole

Check items under surveillance:

A. All pen recorders in drill rig operational.

Note Exceptions:

B. Drill rig log up to date.

C. Observed Sperry-Sun survey.

D. Observed mud analysis.

E. M-K check list up to date.

Surveillance by \_\_\_\_\_ Date \_\_\_\_\_

Time \_\_\_\_\_



P. O. BOX 8504 HOUSTON, TEXAS 77005



MAGCOBAR GROUP Dresser Industries, Inc.

DRILLING MUD REPORT NO. DATE 19 DEPTH PRESENT ACTIVITY SPUD DATE

OPERATOR CONTRACTOR RIG NO. REPORT FOR REPORT FOR SECTION, TOWNSHIP. WELL NAME AND NO. FIELD OR BLOCK NO. COUNTY, PARISH OR OFFSHORE AREA STATE / PROVINCE

Table with columns: DRILLING ASSEMBLY (BIT SIZE, TYPE, JET SIZE), CASING (SURFACE, INTERMEDIATE, PRODUCTION OR LINER), MUD VOLUME (HOLE, TOTAL CIRCULATING VOLUME, IN STORAGE, WEIGHT), CIRCULATION DATA (PUMP SIZE, PUMP MAKE, MODEL, ASSUMED EFF., CIRCULATION PRESSURE, BOTTOMS UP, TOTAL CIRC. TIME)

MUD PROPERTIES and MUD PROPERTY SPECIFICATIONS. Includes sections for MUD PROPERTIES (SAMPLE FROM, TIME SAMPLE TAKEN, FLOWLINE TEMPERATURE, DEPTH, WEIGHT, FUNNEL VISCOSITY, PLASTIC VISCOSITY, YIELD POINT, STRENGTH, FILTRATE, API HTHP, CAKE THICKNESS, SOLIDS CONTENT, LIQUID CONTENT, SAND CONTENT, METHYLENE BLUE CAPACITY, PH, ALKALINITY MUD, ALKALINITY FILTRATE, ALTERNATE ALKALINITY FILTRATE, CHLORIDE, TOTAL HARDNESS) and MUD PROPERTY SPECIFICATIONS (WEIGHT, VISCOSITY, FILTRATE, RECOMMENDED TOUR TREATMENT).

Inventory table with columns: PRODUCT INVENTORY, STARTING INVENTORY, RECEIVED, LAST 24 HR, CLOSING INVENTORY, COST LAST 24 HR

EQUIPMENT table with columns: EQUIPMENT, SIZE, HRS./TOUR, CUMULATIVE COST

MAGCOBAR ENGINEER HOME ADDRESS 6 PHONE MOBILE UNIT WAREHOUSE LOCATION PHONE

Item/Title : 144" SHAFT DRILLING ACTIVITIES	Drawing / Spec No. : B-314-P-X28018	Rev. : 0
	Item Description : GENERAL DRILLING ACTIVITIES	
	Supplier : MORRISON-KNUDSEN CO., INC.	Inspection No. : N/A
	P.O., Subcontract or W.O. No. : N/A	
Prepared by: W. A. HERBER <i>[Signature]</i> Date: 2/17/83	Item No. : N/A Qty. : N/A Inspected by: N/A	Date:
Approved by: M. F. NICOL <i>[Signature]</i> Date: 2/17/83	Reference:	

CHAR. NO.	INSPECTION CHARACTERISTICS	INSPECTION STATUS					REMARKS
		Acc	Hld Tag	Rej	NCR	Cond. Acc	
1.	Verify M-K QA Manager maintains files of required accumulated data on drilling activities of the 144" shaft. (bi-monthly)						
2.	Verify that the Mud Engineer provides M-K QA Manager completed daily mud test data sheets. (weekly)						
3.	Verify that drilling field manager provides M-K QA Manager completed daily records of drill rig operations. (weekly)						
4.	Verify that the directional hole survey is performed by Sperry-Sun at specified intervals. (each occurrence)						
5.	Verify that Sperry-Sun manager provides M-K QA Manager completed records of the down hole survey results. (each occurrence)						
6.	Verify that approved drilling report form is being used to record drilling information and kept on file as the standard daily report. (weekly)						



